From the Institute of Lung Biology and Disease (ILBD) / Comprehensive Pneumology Center (CPC),

Helmholtz Zentrum München

Schriftliche Habilitationsleistung an der Medizinischen Fakultät der Ludwig-Maximilians-Universität zu München

KRAS Mutationen im Genom von Adenokarzinomzellen der Lunge und deren Einfluß auf Inflammation

KRAS mutations of the lung adenocarcinoma genome and their impact on inflammation

vorgelegt von:

Dr. Georgios T. Stathopoulos MD PhD

aus:

Patras, Achaia, Greece

Jahr: *2021*

Abbreviations

AE17	mouse pleural mesothelioma cells
B16F10	mouse skin melanoma cells
CCL2	C-C-motif chemokine ligand 2
CXCL	C-X-C motif chemokine ligand
CXCR	C-X-C motif chemokine receptor
EΘ	endothelial
ELISA	enzyme-linked immunosorbent assay
HLL	HIV.LTR.luc
IκBαDN	dominant negative inhibitor of NF-κB alpha
IKK	inhibitor of NF-κB kinase
IL	interleukin
IL1R1	interleukin 1 receptor 1
KRAS	KRAS proto-oncogene GTPase
LLC	mouse Lewis lung carcinoma cells
MC38	mouse colon adenocarcinoma cells
MΦ	macrophage
MPE	malignant pleural effusion
NF-κB	nuclear factor kappa B
NΦ	neutrophil
NGL	NF-κB.GFP.luc
NIK	NF-κB-inducing kinase
qPCR	quantitative real-time reverse transcriptase polymerase chain reaction
RNAi	RNA interference
SPP1	secreted phosphoprotein 1 also known as osteopontin
TBK1	TANK-binding kinase 1
TNF	tumor necrosis factor
TPSAB1	tryptase AB1
shRNA	short hairpin RNA
VCAN	versican
WT	wild-type

List of publications

I: Giannou AD, Marazioti A, Spella M, Kanellakis NI, Apostolopoulou H, Psallidas I, Prijovich ZM, Vreka M, Zazara DE, Lilis I, Papaleonidopoulos V, Kairi CA, Patmanidi AL, Giopanou I, Spiropoulou N, Harokopos V, Aidinis V, Spyratos D, Teliousi S, Papadaki H, Taraviras S, Snyder LA, Eickelberg O, Kardamakis D, Iwakura Y, Feyerabend TB, Rodewald HR, Kalomenidis I, Blackwell TS, Agalioti T, Stathopoulos GT. Mast cells mediate malignant pleural effusion formation. **J Clin Invest.** 2015 Jun;125(6):2317-34. doi: 10.1172/JCI79840. Epub 2015 Apr 27. PMID: 25915587; PMCID: PMC4497757.

II: Agalioti T, Giannou AD, Krontira AC, Kanellakis NI, Kati D, Vreka M, Pepe M, Spella M, Lilis I, Zazara DE, Nikolouli E, Spiropoulou N, Papadakis A, Papadia K, Voulgaridis A, Harokopos V, Stamou P, Meiners S, Eickelberg O, Snyder LA, Antimisiaris SG, Kardamakis D, Psallidas I, Marazioti A, Stathopoulos GT. Mutant KRAS promotes malignant pleural effusion formation. **Nat Commun.** 2017 May 16;8:15205. doi: 10.1038/ncomms15205. PMID: 28508873; PMCID: PMC5440809.

III: Marazioti A, Lilis I, Vreka M, Apostolopoulou H, Kalogeropoulou A, Giopanou I, Giotopoulou GA, Krontira AC, Iliopoulou M, Kanellakis NI, Agalioti T, Giannou AD, Jones-Paris C, Iwakura Y, Kardamakis D, Blackwell TS, Taraviras S, Spella M, Stathopoulos GT. Myeloid-derived interleukin-1β drives oncogenic KRAS-NF-κB addiction in malignant pleural effusion. **Nat Commun.** 2018 Feb 14;9(1):672. doi: 10.1038/s41467-018-03051-z. PMID: 29445180; PMCID: PMC5813197.

Summary

Malignant pleural effusion (MPE) is a significant clinical problem commonly caused by adenocarcinomas. Although different pleural tumors vary widely in their ability to produce MPE, the critical pathways that determine MPE formation are poorly defined. Improved understanding of tumor-host interactions that lead to MPE could lead to novel treatments for the condition. In this work, novel mouse models of MPE are put forth, which are subsequently employed to discover that carcinoma cells harboring KRAS mutations produce MPE while cells without such do not. To this end, Lewis lung carcinoma (LLC), colon adenocarcinoma (MC38), and malignant pleural mesothelioma (AE17) cells that are potent inducers of MPE displayed mutant *Kras* alleles, non-canonical nuclear factor (NF)-κB activation mediated via inhibitor of NF-κB kinase α (IKKα), overexpression of proinflammatory chemokines, and capability for the recruitment of specific myeloid cell subsets to the pleural space, including mast cells, macrophages, and neutrophils. In contrast, mouse skin melanoma (B16F10) and pancreatic adenocarcinoma (PANO2) cells did not have *Kras* mutations, lacked alternative NF-κB signaling and chemokine expression, and were incapable of attracting myeloid cells and of forming MPE in syngeneic mice. RNAi-mediated silencing of *Kras* or IKKα in MPE-competent cells abrogated MPE formation and alternative NF-κB activation, while these phenomena were reconstituted in MPE-defective cells after mutant *Kras* overexpression. MPE-contained myeloid cells fed the pleural tumor milieu with interleukin-1β (IL-1β), which peprpetuated IKKα activity and chemokine secretion by tumor cells, thereby sustaining MPE-associated inflammation. Treatment of mice with deltarasin, a novel KRAS blocker, imatinib mesylate, a mast cell and cKIT signaling inhibitor, or with 17-DMAG (alvespimycin), a dual IKKα/IKKβ inhibitor, limited MPE development. This work established experimental tools that can be used to better understand the pathophysiology of MPE, identified an inflammatory loop initiated by tumor cells and the KRAS oncogene and perpetuated by immune cells and IL-1β, and set the foundations for future targeted therapeutics of the condition.

Zusammenfassung

Der maligne Pleuraerguss (MPE) ist ein bedeutendes klinisches Problem, das häufig durch Adenokarzinome verursacht wird. Obwohl sich die verschiedenen Pleuratumoren in ihrer Fähigkeit, einen MPE zu erzeugen, stark unterscheiden, sind die kritischen biologischen Pfade, die die MPE-Bildung bestimmen, schlecht definiert. Ein besseres Verständnis der Tumor-Host-Interaktionen, die zu MPE führen, könnte zu neuen Behandlungsmethoden für diese Erkrankung führen. In dieser Arbeit werden neue Mausmodelle des MPE vorgestellt, die dann eingesetzt werden, um zu entdecken, dass Karzinomzellen, die KRAS-Mutationen beherbergen, MPE produzieren, während Zellen ohne solche Mutationen kein MPE produzieren. Zu diesem Zweck zeigten Zellen des Lewis-Lungenkarzinoms (LLC), des Kolon-Adenokarzinoms (MC38) und des malignen Pleuramesothelioms (AE17), die potente Induktoren des MPE sind, mutierte Kras-Allele, nicht-kanonische Nuklearfaktor (NF)-κB Aktivierung, die durch Inhibitor der NF-κB Kinase α (IKKα) vermittelt wird, Überexpression von proinflammatorischen Chemokinen und die Fähigkeit zur Rekrutierung spezifischer myeloischer Untergruppen von Zellen im Pleuraraum, einschließlich Mastzellen, Makrophagen und Neutrophilen. Im Gegensatz dazu wiesen Hautmelanom- (B16F10) und Pankreas-Adenokarzinom-Zellen (PANO2) der Maus keine Kras-Mutationen auf, es fehlten alternative NF-κB-Signalwege und Chemokin-Expression, und sie waren nicht in der Lage, myeloische Zellen anzuziehen und MPE in syngenen Mäusen zu bilden. Die RNAi-vermittelte Stilllegung von Kras oder IKKα in MPE-kompetenten Zellen hob die MPE-Bildung und die alternative NF-κB-Aktivierung auf, während diese Phänomene in MPE-defekten Zellen nach mutierter Kras-Überexpression rekonstituiert wurden. MPE-enthaltende myeloide Zellen versorgten das pleurale Tumormilieu mit Interleukin-1β (IL-1β), das die IKKα Aktivität und die Chemokin-Sekretion von Tumorzellen pepepetuierte und dadurch die MPE-assoziierte Entzündung aufrechterhielt. Die Behandlung von Mäusen mit Deltarasin, einem neuartigen KRAS-Blocker, Imatinib mesylat, einem Mastzellen- und cKIT-Signal inhibitor, oder mit 17-DMAG (Alvespimycin), einem dualen IKKα/IKKβ-Inhibitor, begrenzte die MPE-Entwicklung. Diese Arbeit etablierte experimentelle Werkzeuge, die zum besseren Verständnis der Pathophysiologie des MPE eingesetzt werden können, identifizierte einen Entzündungszyklus, der durch Tumorzellen und das KRAS-Onkogen initiiert und durch Immunzellen und IL-1β perpetuiert wird, und schuf die Grundlagen für zukünftige zielgerichtete Therapien der Erkrankung.

Table of Contents

1. Introduction

Malignant pleural effusion (MPE) is one of the most challenging cancer-related disorders. MPE is a common clinical problem affecting up to 15% of patients with cancer (Antony et al., 2001). It ranks among the top prevalent metastatic manifestations of tumors of the lungs, breast, pleura, gastrointestinal tract, urogenital tract, and hematopoietic tissues, killing an estimated two million patients worldwide every year and causing 126,825 admissions in U.S. hospitals in 2012 alone (Clive et al., 2014; Taghizadeh et al., 2016).). The appearance of a MPE signals systemic disease, and a short and cumbersome survival (Sugiura et al., 1997). The presence of a MPE at diagnosis is an independent negative prognostic factor in patients with lung cancer and mesothelioma (Wu et al., 2013; Tanrikulu et al., 2010).vCurrent treatment is palliative and benefits only a minority of patients (Burgers et al., 2008). In addition, current therapies are non-etiologic and often ineffective, may cause further morbidity and mortality, and have not yielded significant improvements in survival (Rintoul et al., 2014). Research to unveil the pathogenesis of MPE has been scarce, mainly due to the lack of relevant animal models (Lee et al., 2008).

In addition to its clinical significance, MPE provides a unique setting for the study of tumor-host interactions (Basak et al., 2009). MPE is most commonly caused by adenocarcinomas originating from the lung, breast, or gastrointestinal tract (Antunes et al., 2003). These tumors commonly harbor KRAS proto-oncogene GTPase (KRAS) mutations that result in constitutive downstream signalling. Although *KRAS* mutations exert major cell-autonomous effects (Meylan et al., 2009; Barbie et al., 2009), they also impact paracrine gene expression (Takai et al., 2001; Sparmann et al., 2004). Hence *KRAS* is ideally positioned as the prototype effector mutation of adenocarcinomas responsible for MPE.

To investigate the clinical and mechanistic significance of MPE, we developed mouse models thereof (Stathopoulos et al., 2006, 2007a, 2008a, and 2008b). In this setting, we have shown that nuclear factor kappa B (NF-κB)-dependent signalling by tumor cells is intimately involved in MPE pathogenesis. We subsequently showed that tumor-derived tumor necrosis factor (TNF) promotes MPE via auto/paracrine loop-amplification of NF-κB signalling and performed successful preclinical TNF-neutralization (Stathopoulos et al., 2007a). Coinciding with constitutive NF-κB/TNF signaling in MPE-producing lung adenocarcinomas, we detected *KRAS* mutations. Targeting of KRAS signaling by an aminobiphosphonate resulted in down-regulation of lung adenocarcinoma-triggered MPE by suppression of paracrine effects and macrophage recruitment (Stathopoulos et al., 2008). We next found that MPE formation is not ubiquitous to cancer cells, and critically depends on elaboration of tumor-derived C-C-motif chemokine ligand 2 (CCL2) by mutant *KRAS*-harboring lung adenocarcinoma (Stathopoulos et al., 2008b). These data strengthen a possible association between *KRAS* mutations and MPE, a relationship that had yet to be elucidated.

During preliminary studies, we had observed a specific phenotypic difference of murine tumor cell lines introduced into syngeneic immunocompetent mice: although equally tumorigenic and metastatic when introduced into the dermis or the venous circulation, KRAS-wild-type skin melanoma (B16F10) cells were incapable of forming MPE, in stark contrast to Lewis lung (LLC) and colon (MC38) adenocarcinomas, which harbored KRAS-mutations and were potent inducers of MPE. This difference was not correlated with the ability of these cells to form pleural tumors, as all cell types caused significant intrapleural tumor dissemination. The formation of MPE by LLC and MC38 cells impacted survival, as

mice that received these cell types intrapleurally succumbed earlier to MPE, compared with B16F10 cells.

Importantly, MPE-competent LLC and MC38 tumors beared mutant *Kras* alleles (*ΔKras*^{G12C} and ^{G13R}) responsible for constitutive RAS signaling, in contrast to MPE-defective B16F10 cells that had wild-type *Kras* and displayed low levels of RAS signaling. All cell lines had other significant mutations: AE17 cells had a *Cdkn2a* deletion (Jackaman et al., 2003), while B16F10 cells have mutant *Hras* and *Cdkn2a* deletion (Yang et al., 2007), which were not correlated with MPE competence. Although *ΔKras*-harboring MPE-promoting LLC and MC38 tumors and *wt Kras*-bearing non-MPE-producing B16F10 tumors exhibited similar levels of constitutive and inducible canonical NF-κB activation, LLC and MC38 tumor cells displayed high levels of constitutive nuclear P52 binding without any stimulation, in stark contrast to B16F10 tumor cells, which displayed negligible constitutive and only inducible alternative NF-κB activation.

We made similar observations on seven different human lung cancer cell lines of a correlation between *KRAS* mutation status, RAS activity, and alternative NF-κB signaling. Using microarrays validated at the mRNA and protein levels, we had furthermore found that the presence of *ΔKras* and constitutively active alternative NF-κB signaling in MPE-producing LLC and MC38 cells was associated with a specific proinflammatory gene expression profile. By promoter analysis of differentially regulated genes (http://www.cisreg.ca/oPOSSUM), we determined that the most prominent transcriptional signature of LLC and MC38 cells was that of alternative NF-κB (including *Ccl2, Ptgs2, and Spp1*). In addition, upstream genes involved in regulation of alternative NF-κB signaling were up-regulated in MPE-producing LLC and MC38 cells (including *Aim2, Ifih1, Tbkbp1,* and *Ikbke*).

This proinflammatory phenotype of MPE-promoting LLC and MC38 cells specifically impacted the host response to tumor: after intrapleural delivery of these cells, a robust host NF-κB response was observed and F4/80+ macrophages and CD11b+Gr1+ myeloid suppressor cells were preferentially recruited to the pleural cavity, phenomena not seen when B16F10 cells were injected. This host response to *KRAS* mutant tumor cells impacted MPE formation, as liposomal clodronate-mediated depletion of intrapleural macrophages suppressed MPE formation by LLC and MC38 cells. Finally, forced *Kras*^{G12C} overexpression induced MPE formation and RAS/alternative NF-κB activation in B16F10 tumors, while silencing of *Kras* in MC38 cells using shRNA abrogated MPE formation and RAS/alternative NF-κB activation.

2. Aim

For the purposes of this work, we hypothesized that *KRAS*-dependent alternative NF-κB signalling by tumor cells is causally involved in MPE formation. Mechanistically, *KRAS*-dependent alternative NF-κB activation leads to inflammatory mediator secretion and to the establishment of an *in vivo* inflammatory loop that involves different lineages of myeloid cells that feed and sustain the proinflammatory microenvironment of pleural tumors and culminate in plasma extravasation and the wet phenotype of MPE. To map this *in vivo* inflammatory circuit (Graphical abstract), we set out to achieve the following specific aims:

To define the relationship between KRAS mutations and MPE formation.

Studies were designed to analyze multiple mouse and human cancer cell lines for KRAS and other mutations, RAS pathway activation, and in vivo ability of MPE formation. Murine and human cancer cell lines were genotyped for *KRAS, HRAS, NRAS, EGFR, BRAF, TRP53,* and *STK11* mutations. Tumor cells were assessed for RAF binding reporting for RAS pathway activation. For MPE formation, 1.5 x 10^5 mouse or 10^6 human tumor cells were injected intrapleurally to *C57BL/6* or *NOD/SCID* mice (Stathopoulos et al., 2006; Kraus-Berthier et al., 2000). End-points were MPE volume, pleural tumor number/size, and survival. In addition, human and murine *ΔKRAS* tumor cells were stably transduced with different shRNAs targeting *KRAS* or control shRNAs encoding random sequences. Control- and anti-*KRAS*-shRNA-transduced cells were injected into the pleural cavity of *C57BL/6* or *NOD/SCID* mice for assessment of MPE formation. Finally, human and murine *KRAS* wild-type tumor cells were stably transduced with expression vectors encoding GFP, *wt KRAS, ΔKRAS*^{G12C}, or *ΔKRAS*^{G12D}. *wt KRAS*- and *ΔKRAS*-transduced cells were injected into the pleural cavity of *C57BL/6* or *NOD/SCID* mice for determination of MPE formation.

To identify the critical down-stream signalling pathways responsible for *KRAS*-induced MPE.

For this, mouse and human cancer cells with or without *KRAS* mutations before and after *KRAS* modulation (*KRAS* overexpression or anti-*KRAS* RNAi) were assayed for activation of the PI3K/Akt/mTOR, ERK, and MAPK pathways by ELISA. Growth of parental and mutant cell lines *in vitro* and *in vivo* was determined by substrate reduction (MTT assay) and subcutaneous tumor growth rate, respectively. In addition, the above cell lines with different endogenous or introduced KRAS alleles were assayed for canonical/alternative NF-κB activation by nuclear NF-κB-component binding ELISA. Paracrine gene expression of parental and mutant cell lines *in vitro* was determined by microarray, RT-PCR and ELISA. Canonical/alternative NF-κB effects on MPE formation were determined via stable overexpression of *IκBαDN* (Stathopoulos et al., 2008c) or anti-NF-κB-kinase shRNA in mutant *KRAS*-harboring tumor cells. Canonical/alternative NF-κB mutant cells were tested for MPE formation and gene expression profile and were compared to parental cell lines to identify the NF-κB-dependent transcriptome. Gene expression profiles of multiple MPE-producing and not-producing cells were compared to identify candidate mediators of MPE formation. Subsequently, gene expression profiles of *wt* and *KRAS* mutation-harboring tumor cells, before and after genetic *KRAS* modulation (via RNAi or *KRAS* overexpression) were compared to identify a universal *KRAS* signature on gene expression. Candidate

mediators of MPE formation were cross-examined with the *KRAS* signature to identify *KRAS*-dependent candidate genes likely to impact MPE formation.

To investigate the host inflammatory response to *KRAS*-mutant tumor cells.

Host immune cells were retrieved from MPE generated by *Wt* and *KRAS* mutant tumor cells, as well as by *KRAS*-modulated (via RNAi or overexpression) tumor cells, and were characterized for morphology and surface marker expression (CD45, F4/80, CD11b, Gr1). Key cell subsets recruited to the pleural space specifically in response to *KRAS* mutation-harboring tumor cells were identified. *C57BL/6* NF-κB reporter mice expressing luciferase or a GFP.luc fusion protein (*HIV.LTR.luc*, *HLL*; *NF-κB.GFP.luc*, *NGL*; Stathopoulos et al., 2007b) received intrapleural *wt* and *KRAS* mutation-harboring, as well as *KRAS*-modulated (via RNAi or overexpression) tumor cells. The duration, intensity, and tissue/cell distribution of NF-κB activation was determined by serial bioluminescence imaging and by fluorescent microscopy of tissue preparations from lungs, pleural tissue, bone marrow, spleen and liver. Using cross-examination of *KRAS*-dependent genes identified and the inflammatory response profile characterized above, we identified candidate key mediators of *KRAS* effects on host immunity. Expression of key *KRAS*-associated mediators was targeted in *ΔKRAS*-bearing tumor cells using RNAi and was induced in *wtKRAS* tumor cells, followed by determination of the host NF-κB and immune response. The role of F4/80+ macrophages and CD11b+Gr1+ myeloid suppressor cells in MPE formation was investigated using ablation of pleural macrophages with liposomal clodronate and *in vivo* neutralization of CCL2, the key chemokine recruiting myeloid suppressor cells to tumors, combined with intrapleural delivery of *ΔKRAS*-bearing tumor cells.

To target *KRAS* mutations and down-stream pathways as potential therapy for MPE.

C57BL/6 or *NOD/SCID* mice bearing MPE induced by mouse or human cancer cells were treated with deltarasin (Zimmermann et al., 2013) or saline in prevention (starting from tumor inoculation) and regression (starting from MPE formation) trials designed to block post-translational activation of KRAS. *C57BL/6* or *NOD/SCID* mice bearing MPE induced by mouse or human cancer cells were treated with inhibitors of IKKα, IKKβ (*ie* canonical or alternative NF-κB), or random sequences, in prevention/regression trials as above designed to block KRAS-dependent alternative NF-κB activation.

3. Publication I: Mast cells mediate malignant pleural effusion formation.

3.1. Summary

Inflammation is an enabling hallmark of cancer that may mediate tumor growth and dissemination instead of tumor eradication (Hanahan & Weinberg, 2011). Inflammatory signaling networks in the tumor microenvironment can be initiated and orchestrated by malignant or immune cells; the networks conditionally facilitate tumor progression or regression depending on tumor type, immune effector cell type, and anatomic context (Swamy et al., 2010; Coussens & Pollard, 2011; Floor et al., 2012). The identification of such inflammatory loops is of particular interest in the hunt for anticancer therapies that are anticipated to be more effective and less toxic than conventional chemotherapy (Balkwill & Mantovani, 2012).

In addition to macrophages, neutrophils, and lymphocytes, mast cells (MCs) were recently found to be recruited to pancreatic and other tumors and to facilitate tumor growth (Soucek et al., 2007; Theoharides, 2008). Although they are relatively sparse, MCs are appealing candidates for tumor promotion, since they can release a battery of mediators to orchestrate the tumor milieu (Galli et al., 2005; Theoharides et al., 2007; Chen et al., 2001). However, MCs were found to be tumor-protective or indifferent in other settings (Blair et al., 1997; Sinnamon et al., 2008; Dalton & Noelle, 2012; Pittoni & Colombo, 2012). While the reasons for the divergent MC functions in cancer are not known, new models of MC deficiency lend promise to solve this riddle (Feyerabend et al., 2011; Dudeck et al., 2011).

Here, we quantified MCs in human and murine MPE and evaluated the fate and function of these cells in MPE development. Evaluation of murine MPE-competent lung and colon adenocarcinomas revealed that these tumors actively attract and subsequently degranulate MCs in the pleural space by elaborating CCL2 and osteopontin. MCs were required for effusion development, as MPEs did not form in mice lacking MCs, and pleural infusion of MCs with MPE-incompetent cells promoted MPE formation. Once homed to the pleural space, MCs released tryptase AB1 and IL-1β, which in turn induced pleural vasculature leakiness and triggered NF-κB activation in pleural tumor cells, thereby fostering pleural fluid accumulation and tumor growth. Evaluation of human effusions revealed that MCs are elevated in MPEs compared with benign effusions. Moreover, MC abundance correlated with MPE formation in a human cancer cell–induced effusion model. Treatment of mice with the c-KIT inhibitor imatinib mesylate limited effusion precipitation by mouse and human adenocarcinoma cells. Together, the results of this study indicate that MCs are required for MPE formation and suggest that MC-dependent effusion formation is therapeutically addressable (Figure 1) .

3.2. Contribution

The applicant conceived the main idea behind this study, performed preliminary proof-of-concept experiments using which he obtained funding for the study in the form of an ERC Starting Grant 2010, purchased the equipment required for the study and recruited the team that performed the experiments, designed all experiments, fostered the collaborations reflected in the paper, analyzed the data, compiled graphs and figures, wrote the manuscript, submitted the manuscript for publication, and corresponded with the *J Clin Invest*.

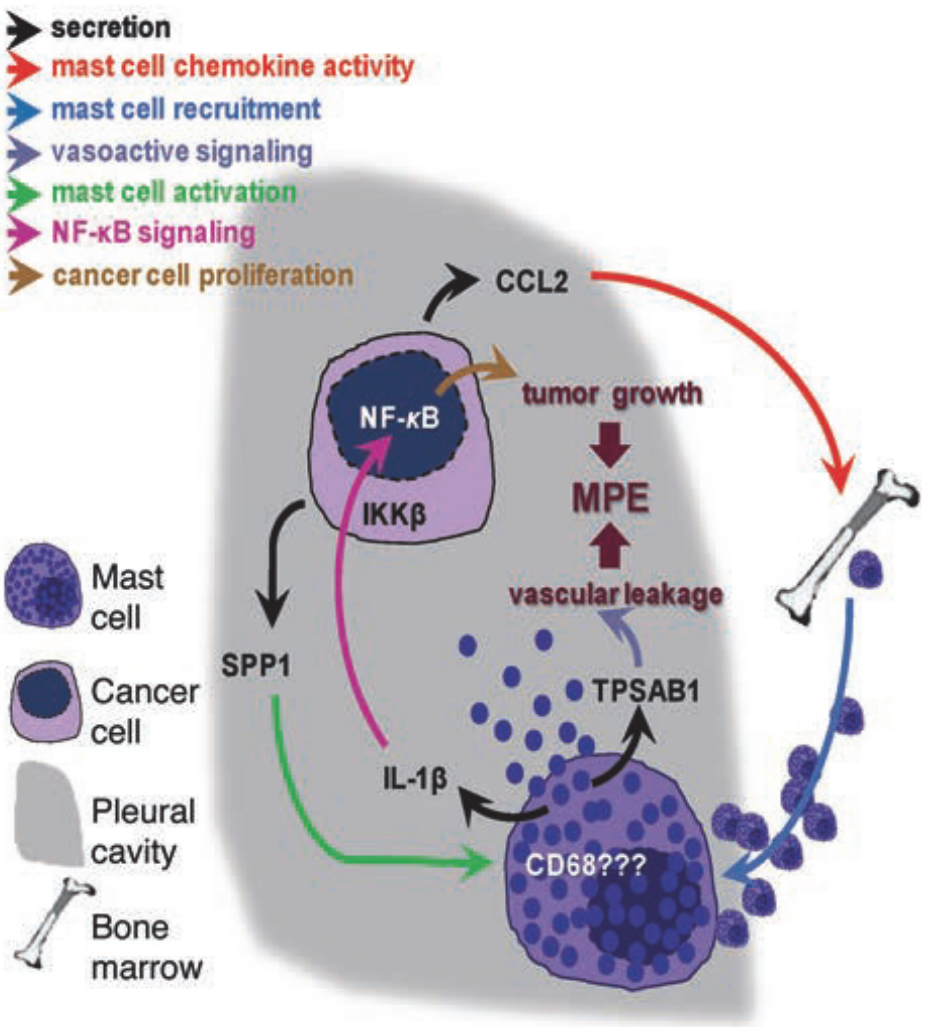

Figure 1. Graphical summary of publication I.

Pleural adenocarcinomas secrete CCL2 and SPP1, which facilitate, respectively, pleural MC accumulation and activation. Upon tumor cell encounter, MCs release TPSAB1 and IL-1β, which increase vascular leakage and tumor NF-κB activation, respectively.

The Journal of Clinical Investigation RESEARCH ARTICLE

Mast cells mediate malignant pleural effusion formation

Anastasios D. Giannou,[1] Antonia Marazioti,[1] Magda Spella,[1] Nikolaos I. Kanellakis,[2] Hara Apostolopoulou,[1] Ioannis Psallidas,[1,3] Zeljko M. Prijovich,[1] Malamati Vreka,[1] Dimitra E. Zazara,[1] Ioannis Lilis,[1] Vassilios Papaleonidopoulos,[1] Chrysoula A. Kairi,[1,4] Alexandra L. Patmanidi,[2] Ioanna Giopanou,[1] Nikolitsa Spiropoulou,[1] Vaggelis Harokopos,[5] Vassilis Aidinis,[6] Dionisios Spyratos,[7] Stamatia Teliousi,[8] Helen Papadaki,[9] Stavros Taraviras,[2] Linda A. Snyder,[10] Oliver Eickelberg,[11] Dimitrios Kardamakis,[12] Yoichiro Iwakura,[13] Thorsten B. Feyerabend,[14] Hans-Reimer Rodewald,[14] Ioannis Kalomenidis,[4] Timothy S. Blackwell,[15] Theodora Agalioti,[1] and Georgios T. Stathopoulos[1,4,11,15]

[1]Laboratory for Molecular Respiratory Carcinogenesis, Department of Physiology, and [2]Stem Cell Biology Laboratory, Department of Physiology, Faculty of Medicine, University of Patras, Rio, Achaia, Greece. [3]Oxford Centre for Respiratory Medicine, Churchill Hospital, Oxford, United Kingdom. [4]First Department of Critical Care and Pulmonary Medicine, University of Athens School of Medicine, General Hospital Evangelismos, Athens, Attica, Greece. [5]Expression Profiling Unit and [6]Division of Immunology, Biomedical Sciences Research Center (BSRC) Alexander Fleming, Vari, Attica, Greece. [7]Department of Pulmonary Medicine, Hospital G. Papanikolaou, Faculty of Medicine, Aristotle University of Thessaloniki, and [8]Department of Cytology, Hospital G. Papanikolaou, Thessaloniki, Greece. [9]Department of Anatomy, Faculty of Medicine, University of Patras, Rio, Achaia, Greece. [10]Oncology Discovery Research, Janssen R&D LLC, Spring House, Pennsylvania, USA. [11]Comprehensive Pneumology Center (CPC), University Hospital, Ludwig-Maximilians University and Helmholtz Zentrum München, Member of the German Center for Lung Research (DZL), Munich, Germany. [12]Department of Radiation Oncology and Stereotactic Radiotherapy, Faculty of Medicine, University of Patras, Rio, Achaia, Greece. [13]Research Institute for Biomedical Sciences, Tokyo University of Science, Tokyo, Japan. [14]Division for Cellular Immunology, Deutsches Krebsforschungszentrum (DKFZ), Heidelberg, Baden-Württemberg, Germany. [15]Department of Medicine, Division of Allergy, Pulmonary and Critical Care Medicine, Vanderbilt University School of Medicine, Nashville, Tennessee, USA.

Mast cells (MCs) have been identified in various tumors; however, the role of these cells in tumorigenesis remains controversial. Here, we quantified MCs in human and murine malignant pleural effusions (MPEs) and evaluated the fate and function of these cells in MPE development. Evaluation of murine MPE-competent lung and colon adenocarcinomas revealed that these tumors actively attract and subsequently degranulate MCs in the pleural space by elaborating CCL2 and osteopontin. MCs were required for effusion development, as MPEs did not form in mice lacking MCs, and pleural infusion of MCs with MPE-incompetent cells promoted MPE formation. Once homed to the pleural space, MCs released tryptase AB1 and IL-1β, which in turn induced pleural vasculature leakiness and triggered NF-κB activation in pleural tumor cells, thereby fostering pleural fluid accumulation and tumor growth. Evaluation of human effusions revealed that MCs are elevated in MPEs compared with benign effusions. Moreover, MC abundance correlated with MPE formation in a human cancer cell–induced effusion model. Treatment of mice with the c-KIT inhibitor imatinib mesylate limited effusion precipitation by mouse and human adenocarcinoma cells. Together, the results of this study indicate that MCs are required for MPE formation and suggest that MC-dependent effusion formation is therapeutically addressable.

Introduction

Inflammation was recently recognized as an enabling hallmark of cancer that may mediate tumor growth and dissemination instead of tumor eradication (1). Inflammatory signaling networks in the tumor microenvironment can be initiated and orchestrated by malignant or immune cells; the networks conditionally facilitate tumor progression or regression depending on tumor type, immune effector cell type, and anatomic context (2–4). The identification of such inflammatory loops is of particular interest in the hunt for anticancer therapies that are anticipated to be more effective and less toxic than conventional chemotherapy (5).

In addition to macrophages, neutrophils, and lymphocytes, mast cells (MCs) were recently found to be recruited to pancreatic and other tumors and to facilitate tumor growth (6, 7). Although they are relatively sparse, MCs are appealing candidates for tumor promotion, since they can release a battery of mediators to orchestrate the tumor milieu (8–11). However, MCs were found to be tumor-protective or indifferent in other settings (12–14). While the reasons for the divergent MC functions in cancer are not known, new models of MC deficiency lend promise to solve this riddle (15, 16).

Malignant pleural effusion (MPE) is extremely common in patients with lung, breast, or other adenocarcinomas (17, 18). No treatment exists, and palliative attempts may cause further morbidity and mortality (19, 20). MPE was recently reclassified as a separate stage of lung cancer, since it was acknowledged to represent a distinct form of metastatic disease with very short survival (18, 21, 22). Simultaneously, we and others used mouse models to hypothesize that MPE is primarily an immune- and vascular-

Authorship note: Timothy S. Blackwell, Theodora Agalioti, and Georgios T. Stathopoulos are co–senior authors.
Conflict of interest: Linda A. Snyder is an employee of Janssen R&D LLC, the manufacturer of anti-CCL2 and anti-CCL12 Abs.
Submitted: November 14, 2014; **Accepted:** March 26, 2015.
Reference information: *J Clin Invest*. 2015;125(6):2317–2334. doi:10.1172/JCI79840.

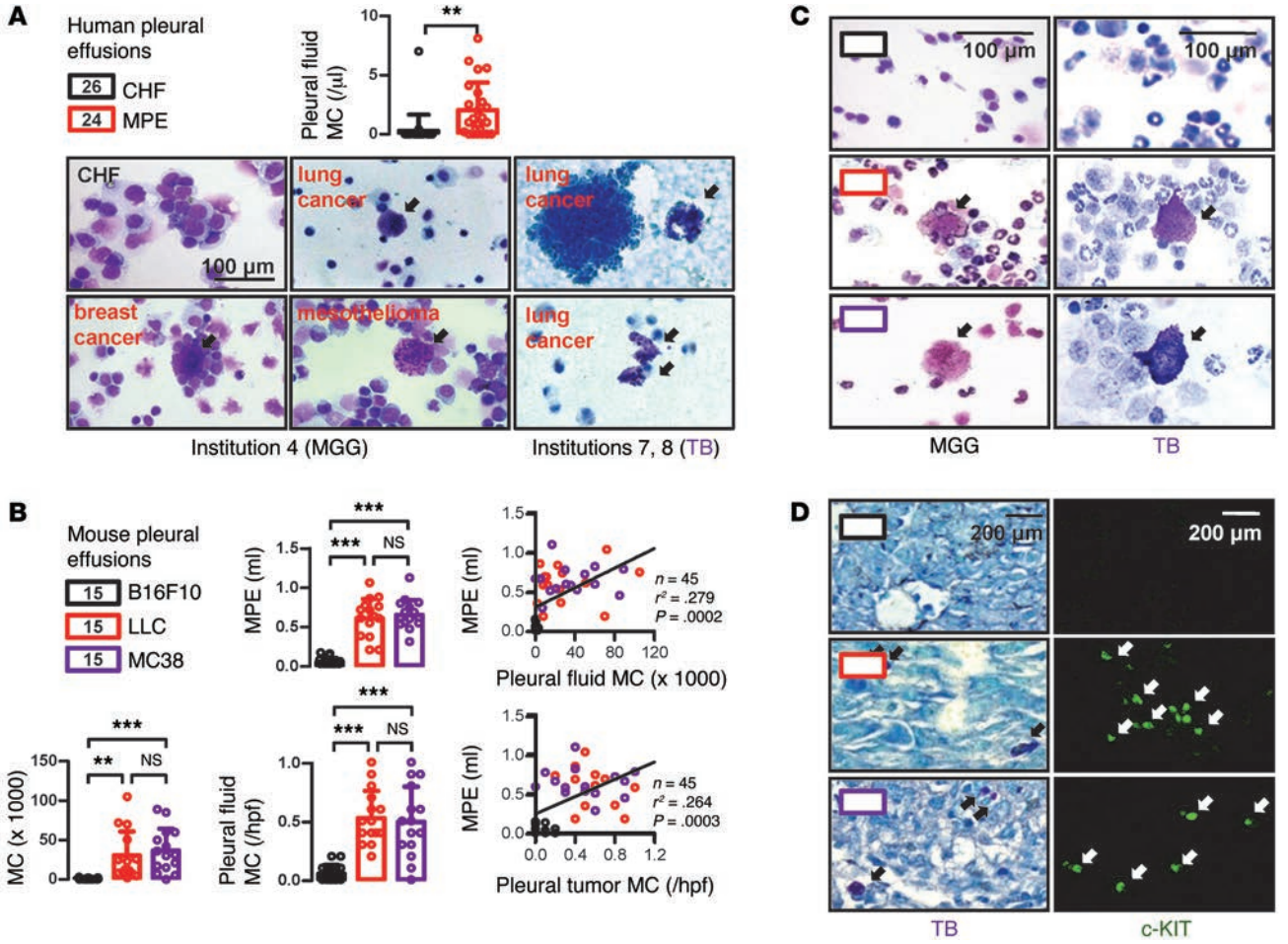

Figure 1. MCs in human and murine MPEs. (**A**) Pleural MCs from patients with MPEs (n = 24) or CHF (n = 26) from 2 Hellenic hospitals. (**B**) MPEs and MCs of C57BL/6 mice 14 days after pleural delivery of 1.5 × 10^5 syngeneic tumor cells (n = 15 mice per tumor cell type). Right: correlation between MPE and tumor-MC abundance and MPE volume, with linear regression line, sample size (n), probability value (P), and squared Pearson correlation coefficient (r^2). Hpf, high-power field. (**C** and **D**) Representative microphotographs of pleural fluid (**C**) and tumor (**D**) MCs from mice from **B**. Data presented as data points, mean ± SD. Numbers in boxes indicate sample size. Arrows indicate MCs. NS, $P > 0.05$; $^{**}P < 0.01$; and $^{***}P < 0.001$, by 2-tailed Student's t test (**A**) or 1-way ANOVA with Bonferroni post hoc tests (**B**).

mediated manifestation of pleural-metastasized cancers (23, 24). However, the immune cells that drive MPE remain unidentified.

Here we describe the discovery of MCs in human and mouse MPEs and the elucidation of their fate and role. We show that MCs are driver cells required for MPEs and uncover the key messengers that instate tumor-MC circuitry during MPE development. Importantly, we provide proof-of-concept data supporting that MC-dependent MPEs are targetable using existing drugs; these data lend promise for translational applications of our findings.

Results

MCs in MPEs. MCs were encountered on May-Gruenwald-Giemsa–stained (MGG-stained) archival specimens of human MPEs from our pleural patient biobank. To rule out a local artifact, MCs were verified on metachromatic toluidine blue–stained (TB-stained) MPE samples from a different hospital. Systematic evaluation of samples and data from our pleural patient biobank revealed substantial MC numbers (millions/cavity) in MPEs that were significantly elevated compared with benign effusions from congestive heart failure (CHF; Figure 1A). Increased MC numbers were also identified in 2 different mouse models of MPEs that develop 14 days after intrapleural delivery of syngeneic Lewis lung carcinoma (LLC; 30,310 ± 30,440 MC/cavity) or MC38 colon (36,590 ± 27,690 MC/cavity adenocarcinoma) cells (25, 26), compared with controls injected with MPE-incompetent B16F10 melanoma cells (999 ± 1,008/cavity) or saline (755 ± 384/cavity; n = 3). In addition, MC abundance was correlated with the volume of experimental effusions (Figure 1B). MPE MCs displayed typical morphology and TB/c-KIT staining, but they were easily overlooked when MGG, Wright, or other conventional staining was employed (Figure 1, C and D, and Figure 2A). MPE MCs were identified as $CD45^+c\text{-}KIT^+Sca1^+Lin^-$ by flow cytometry (27–29), were reduced in c-KIT–defective $c\text{-}Kit^{Wsh}$ mice (30), and were completely absent from MC-eradicated $Cpa3^{Cre/+}$ mice (15) — a mouse model of more complete and selective MC deficiency as compared with $c\text{-}Kit^{Wsh}$ mice — that were challenged with pleural adenocarcinoma cells (Figure 2B). In mice with MPEs, MCs were preferentially located in

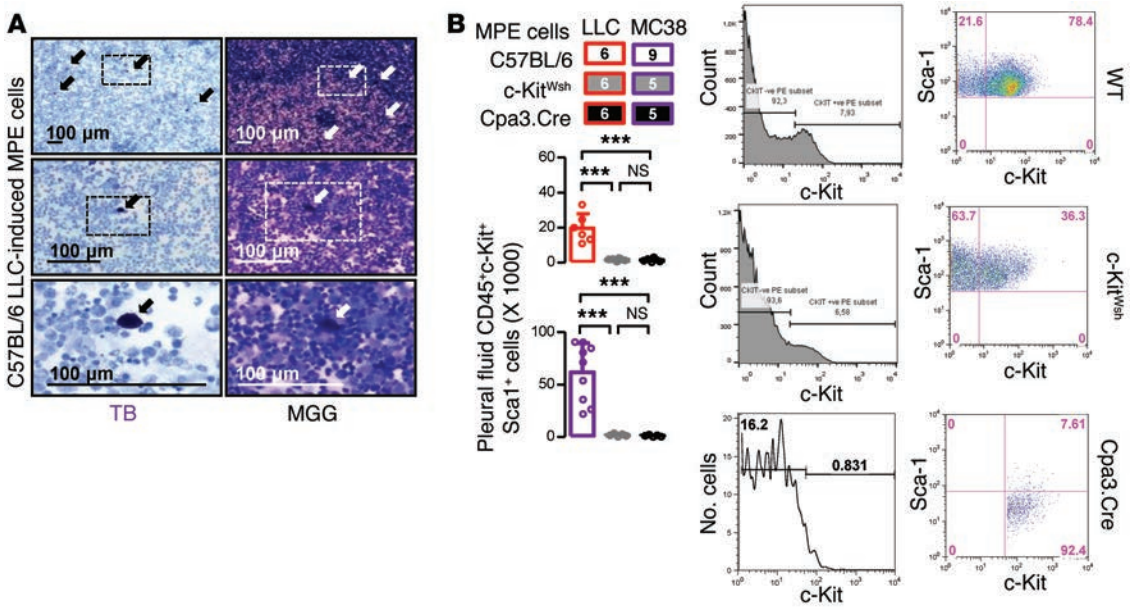

Figure 2. Characterization of MCs from mouse MPEs. (**A**) Representative pleural cell staining from mice from Figure 1B: MCs (arrows) were clearly discernible by TB, but not by routine stains. Each image represents a magnification of the inlay from the image above. (**B**) Flow cytometry gating and data summary of adenocarcinoma-induced MPEs from C57BL/6 (n = 15), *c-Kit*^{Wsh} (n = 11), and *Cpa3*$^{Cre/+}$ (n = 11) mice. Data presented as data points, mean ± SD. Numbers in boxes indicate sample size. Arrows indicate MC. NS, $P > 0.05$; ***$P < 0.001$ by 1-way ANOVA with Bonferroni post hoc tests.

parietal and mediastinal, but not visceral, pleural tumors; most commonly resided in viable, but not necrotic, tumor tissue; and aggregated near or at the tumor front, forming chains or clusters (Figure 3). Hence, pleural MC accumulation is associated with MPE development in humans and mice. Moreover, MPE MCs appear to stream into the malignancy-affected pleural space via the parietal and mediastinal pleural surfaces.

Dynamic MC accumulation in the pleural space. To test MC kinetics during MPE development, we cultured murine BM-derived MCs (BMMCs) using c-KIT ligand (KITL) and interleukin-3 (IL-3), according to previously published protocols (31). BMMCs of C57BL/6 mice stained TB$^+$ (>90%), CD45$^+$c-KIT$^+$Sca1$^+$Lin$^-$ (>80%), and CD25$^+$ (>50%) — and BMMCs of red-fluorescent *mT/mG* mice (32) — formed pseudopodia and moved, confirming the nature of these cells (Figure 4, A–C, and Supplemental Videos 1 and 2; supplemental material available online with this article; doi:10.1172/JCI79840DS1). BMMCs of luminescent CAG-luc-EGFP mice (33) emitted light proportional to cell number, and BMMCs of green fluorescent CAG-EGFP mice (34) were green fluorescent (Figure 4, D and E). When pulsed i.v. into irradiated C57BL/6 recipients adoptively reconstituted with *c-Kit*^{Wsh} BM (35), these tracer BMMCs distributed diffusely. However, when chimeras were challenged exclusively with pleural adenocarcinoma cells, BMMCs accumulated in the thorax concomitant with MPEs (Figure 5, A and B). Similar results were obtained with nonirradiated *c-Kit*^{Wsh} mice pulsed s.c. with tracer BMMCs (Figure 5C). Hence, pleural adenocarcinomas remotely mobilize/recruit MCs via circulating messengers.

CCL2 as an adenocarcinoma-derived mastokine. To identify these messengers, effusion-competent and effusion-incompetent tumor cells were transcriptionally profiled on 2 different occasions (biological n = 2) by microarray analysis. Although 39 genes were overrepresented in MPE-competent adenocarcinoma cells on both occasions, only 2 RNAs possessed cytokine/chemokine activity required for systemic MC recruitment and were selected for further study: *Spp1* and *Ccl2* (encoding osteopontin, or secreted phosphoprotein 1 [SPP1], and CCL2, respectively; Figure 6A and Supplemental Tables 1 and 2). ELISA of tumor cell–conditioned media (CM) validated the microarray, and serum ELISA of pleural tumor–bearing C57BL/6 mice identified a significant difference in serum CCL2, but not SPP1, between adenocarcinoma- and melanoma-bearing mice (Figure 6, B and C). In modified mastotaxis assays (36), tracer BMMCs migrated toward LLC cells expressing random and anti-*Spp1* shRNA (sh), but not toward B16F10 cells or LLC cells expressing sh*Ccl2* (Figure 6D and Figure 7A), implicating CCL2 in MPE-directed mastotaxis. Indeed, forced expression of *Ccl2* plasmid (p) in B16F10 cells restored, and forced expression of sh*Ccl2* in LLC cells inhibited, MPE (25) and MC accumulation. (Figure 7, B and C). Moreover, treatment of mice harboring pleural LLC cells with i.p. CCL2- and/or CCL12-neutralizing Ab (37) blocked MPE (38) and MC accumulation, and direct pleural-delivered recombinant mouse (rm) CCL2 attracted MCs (Figure 7, D–F). Finally, CCL2 (but not SPP1) levels were correlated with MC abundance in human MPEs (Figure 7G). Collectively, these data indicated that CCL2 is a key tumor-secreted MC attractant to the pleural space.

MCs are required for MPEs. We next investigated MC effects on effusion formation. Pleural co-delivery of BMMCs facilitated induction of MPE by B16F10 cells, which are naturally MPE incompetent, without fully instilling the phenotype of adenocarcinoma cells (Figure 8A). Vice versa, both *c-Kit*^{Wsh} and *Cpa3*$^{Cre/+}$

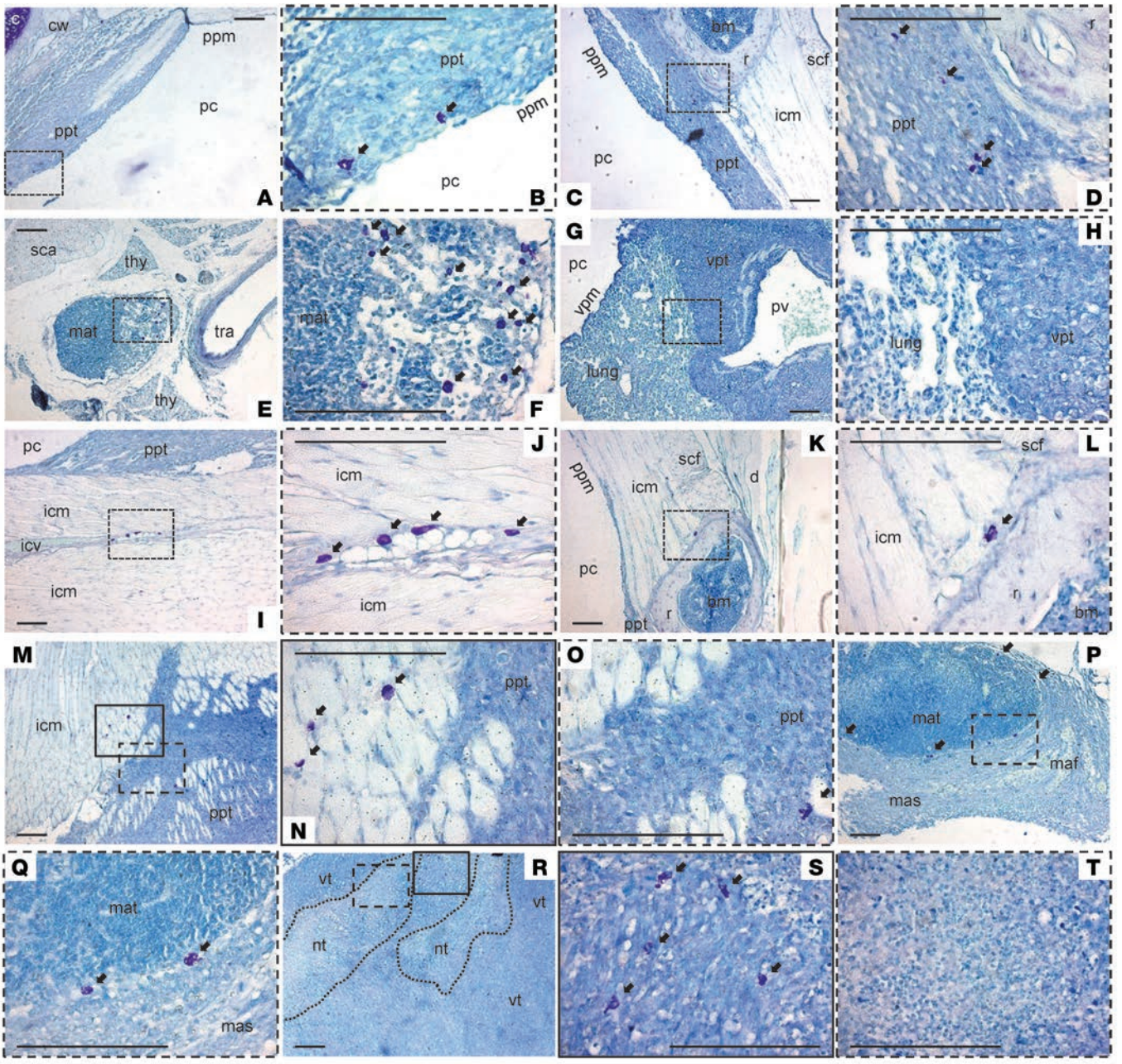

Figure 3. MC topology in experimental MPEs. Whole thoracic sections from mice with pleural tumors and effusions induced by LLC and MC38 adenocarcinomas stained with TB. MCs (arrows) were found in parietal pleural tumors (ppt) and mediastinal tumors (mat), but not in visceral pleural tumors (vpt) (**A**–**H**). MCs appeared to stream in from intercostals vessels, sequentially invading intercostal tissues (fat and muscle) and ppt, forming chains invading into tumors or rings strategically positioned around tumors (**I**–**Q**). MCs were exclusively located in viable (vt), but not necrotic (nt), tumor tissues (**R**–**T**). All scale bars = 300 μm. **B**, **D**, **F**, **H**, **J**, **L**, **N**, and **O**, **Q**, and **S** and **T**: magnified inlays from **A**, **C**, **E**, **G**, **I**, **K**, **M**, **P**, and **R**, respectively. c, rib cartilage; cw, chest wall; ppm, parietal pleural mesothelium; pc, pleural cavity; bm, rib BM; scf, subcutaneous fat; icm, intercostal muscle; thy, thymus; sca, scalene muscle; tra, trachea; vpm, visceral pleural mesothelium; pv, pulmonary vein; icv, intercostal vein; d, dermis; r, rib; maf, mediastinal fat; mas, mediastinum.

mice were protected against MPEs induced by both LLC and MC38 adenocarcinomas (Figure 8, B and C). In addition to MPE accumulation, MC deficiency resulted in retardation of pleural tumor growth, evident macroscopically (Figure 8, B and C), but also by decreased proliferating cell nuclear antigen (PCNA) immunoreactivity (Figure 8D). Since c-KIT is important for non-hematopoietic cells, too, we tested whether MCs are responsible for the phenotype of *c-Kit*^{Wsh} mice. Indeed, donor genotype determined the susceptibility of irradiated C57BL/6 or *c-Kit*^{Wsh} recipients reconstituted with C57BL/6 or *c-Kit*^{Wsh} BM (39) to LLC-triggered MPEs (Figure 8E). Consistent with prior reports, *c-Kit*^{Wsh} mice with pleural tumors were MC-poor (40), whereas *Cpa3*$^{Cre/+}$ mice were MC-eradicated (Figure 8, B and C). Indeed, BMMCs that stained TB$^+$ (>90%), CD45$^+$c-KIT$^-$Sca1$^+$ (>80%), Lin$^+$ (>40%), and CD25$^+$ (>80%) were derivable by IL-3/KITL culture from *c-Kit*^{Wsh} mouse BM (Figure 8F), resembling

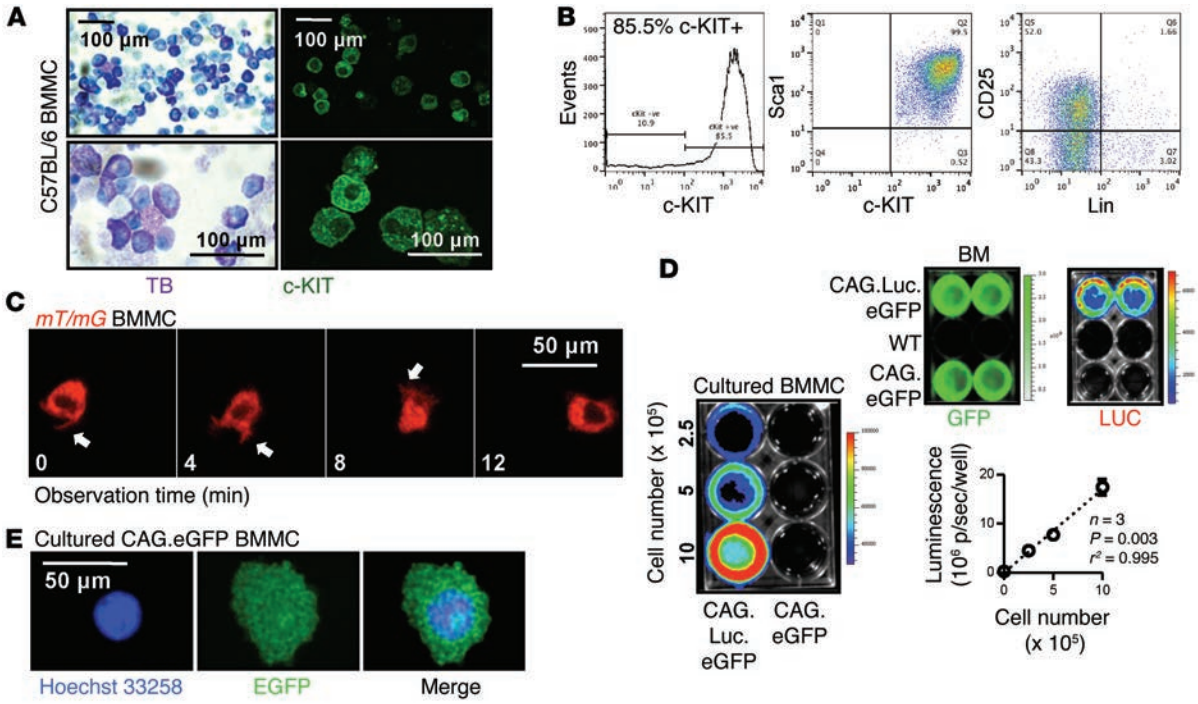

Figure 4. Isolation and characterization of BMMCs. (**A** and **B**) TB and c-KIT staining (**A**) and flow cytometry (**B**) of BMMCs. (**C**) Time-lapse imaging of *mT/mG* BMMCs extending pseudopodia (arrows) and moving at 0.25 mm/hour (see Supplemental Videos 1 and 2). (**D**) Luminescence and fluorescence images of BMMCs from C57BL/6, *CAG-luc-EGFP*, and *CAG-EGFP* mice. Scatterplot: Pearson correlation between luminescence and *CAG-luc-EGFP* BMMC number, with linear regression line, sample size (n = 3), probability value (P), and squared correlation coefficient (r^2). Data presented as mean ± SD. (**E**) *CAG-EGFP* BMMCs stained with nuclear dye.

MC-like innate immune cells described previously (29). We also sought to compare the relative contributions of MCs with those of macrophages during MPE development, since macrophages are the predominant cellular population in MPEs and are also chemoattracted to the pleural space by tumor-derived CCL2 (23, 25). For this, mice expressing *Cre* recombinase under the drive of the *Lyz2* promoter were crossed with mice expressing *Diphtheria* toxin selectively in somatic cells that undergo *Cre*-mediated recombination to generate a macrophage ablation model (*Lyz2-Cre* and *R26-DTA*, respectively; refs. 41, 42). Pleural macrophages of naive C57BL/6 mice were predominantly F4/80$^+$ and CD11b$^+$, but not CD11c$^+$; F4/80$^+$CD11b$^+$ pleural cells were markedly diminished in *Lyz2-Cre R26-DTA* mice compared with single transgenic controls (Figure 9A). Interestingly, *Lyz2-Cre R26-DTA* mice were protected against MPEs induced by both LLC and MC38 adenocarcinomas to a degree comparable to both mouse models of MC deficiency (Figure 9B). Hence, MCs are required for effusion formation, and they are equally important with much more prevalent cell types, such as macrophages. In addition, *c-Kit*^{Wsh} and *Cpa3*$^{Cre/+}$ mice can serve as tumor models of MC depletion and eradication, respectively.

Tumor-secreted osteopontin causes MC degranulation. We next examined the role of tumor-originated osteopontin (encoded by the *SPP1* gene in humans and the *Spp1* gene in mice) — the other candidate detected by tumor cell microarray — in MC-dependent effusions. We had previously identified that SPP1 is a marked mediator of vascular permeability that leads to MPE accumulation (43). In addition to its vasoactive effects, we determined here in multiple ways that tumor-secreted SPP1 promoted MC activation and degranulation. Adenocarcinoma cell-CM caused SPP1-dependent BMMC degranulation, and rmSPP1 directly degranulated BMMCs (Figure 10 and Supplemental Video 3). SPP1 effects were only partial, indicating the presence of additional tumor-elicited players in MC activation. Collectively with our past work, these data established dual functions of tumor-derived SPP1 during effusion development: in addition to inducing vascular leakage, osteopontin degranulates MCs.

Adenocarcinoma-primed MCs secrete tryptase AB1 and IL-1β to foster MPEs. To identify how pleural adenocarcinoma–recruited and pleural adenocarcinoma–primed MCs mediate effusion development, 2 different BMMC cultures were exposed to tumor-CM and were profiled transcriptionally (biological n = 2). Four BMMC transcripts were induced specifically and consistently by adenocarcinoma-CM, including secretory genes *Tpsab1* and *Il1b* and membrane/granule-associated *Cd68* (Figure 11A and Supplemental Tables 3–5). Indeed, adenocarcinoma-CM caused IL-1β release by BMMCs in a SPP1-dependent fashion, and adenocarcinoma-induced MPEs featured substantial IL-1β levels, which were reduced in *c-Kit*^{Wsh} mice (Figure 11, B and C). Staining of *C57BL6* BMMC and MPE cells for IL-1β, c-KIT, CD68, and the granule tag avidin localized IL-1β both in granules and the cytoplasm, and identified that c-KIT$^+$CD68$^+$ MCs are a subset of IL-1β–expressing cells in MPEs (Figure 11, D-F). Importantly, *Il1b*$^{-/-}$ mice (44) were protected from MPEs induced by LLC cells, similar to *c-Kit*^{Wsh} and *Cpa3*$^{Cre/+}$ mice. In multiple MC reconstitution experiments, C57BL/6 — but not

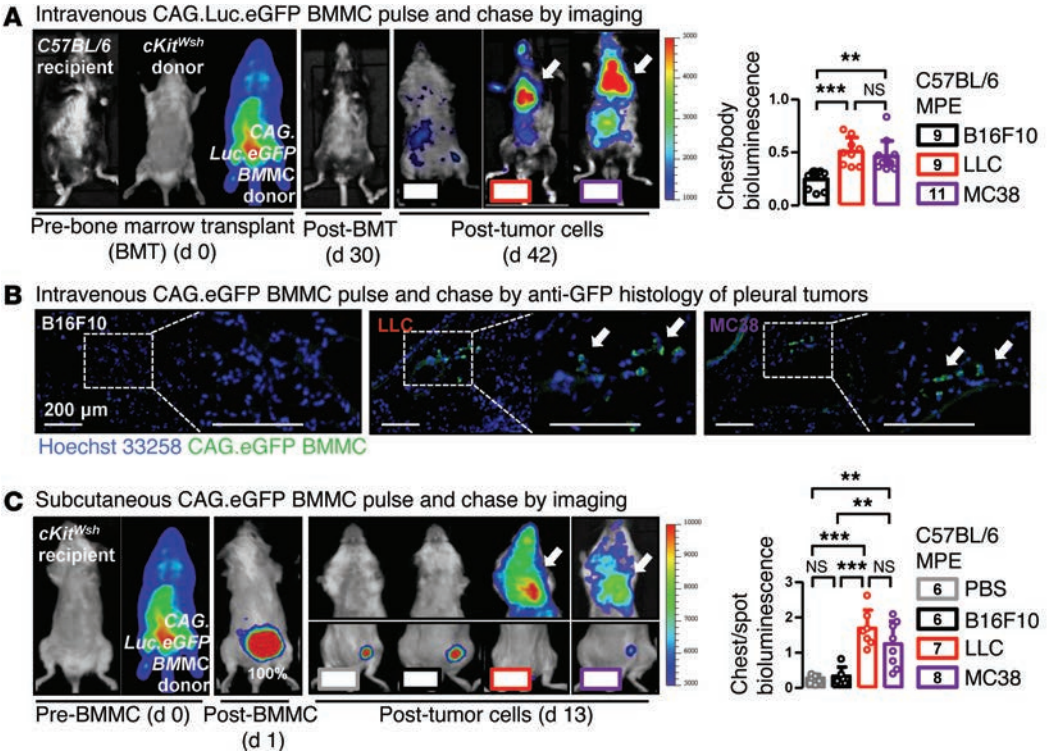

Figure 5. Dynamic MC trafficking to the pleural space. (**A**) Bioluminescence of C57BL/6 chimeras engrafted with *c-Kit*^{Wsh} BM that received 1.5 × 10^5 pleural B16F10 (n = 9), LLC (n = 9), or MC38 (n = 11) tumor cells and same-day i.v. 5 × 10^5 *CAG-luc-EGFP* BMMCs at day 30 after transplant. Note the increased chest signal in mice with adenocarcinoma-induced MPEs (arrows). (**B**) Pleural tumor sections (with magnified inlays) from chimeras as in (**A**) treated with pleural tumor cells followed by i.v. *CAG-EGFP* BMMCs (n = 5/group). Note GFP$^+$ BMMCs in adenocarcinomas 12 days later (arrows). (**C**) Bioluminescence of *c-Kit*^{Wsh} mice that received 8 x 10^5 s.c. *CAG-luc-EGFP* BMMCs followed by next-day pleural injections of PBS (n = 6) or B16F10 (n = 6), LLC (n = 7), or MC38 (n = 8) tumor cells. Note the increased chest signal in mice with adenocarcinomas 13 days later (arrows). Data presented as data points, mean ± SD. Numbers in boxes indicate sample size. NS, $P > 0.05$; $^{**}P < 0.01$; and $^{***}P < 0.001$, by 1-way ANOVA with Bonferroni post hoc tests.

c-Kit^{Wsh} or *Il1b*$^{-/-}$ — BMMCs could restore effusion formation (Figure 11, G and H). Both rmIL-1β and BMMC-CM selectively enhanced LLC and MC38 adenocarcinomas, but not B16F10 melanoma proliferation, in vitro (Figure 11I). rmIL-1β did not induce skin vessel leakage in C57BL/6 mice; on the contrary, rm tryptase AB1 (TPSAB1) did not affect cell proliferation (data not shown), but induced marked vascular hyperpermeability comparable to rmVEGF (Figure 11J). These results indicated that c-KIT–competent MCs facilitate MPE development by secreting TPSAB1 and IL-1β to foster vascular permeability and tumor growth, respectively.

MC-derived IL-1β activates NF-κB in pleural adenocarcinoma cells. NF-κB responds to IL-1α in cancer cells (45) and augments tumor growth and MPEs (46, 47). To test whether MC-derived products activate NF-κB and other important transcription pathways of tumor cells, such as STAT3 and NOTCH, we assessed the expression of 12 target genes of the above pathways by qPCR before and after 4 hours of treatment with BMMC-CM. Interestingly, none of the 12 genes examined was inducible by BMMC-CM in MPE-defective B16F10 cells; however, both NF-κB–target gene *Ccl2* and STAT3-target gene *Myc* were strongly upregulated by BMMC-CM selectively in MPE-competent adenocarcinoma cells (Figure 12A). By imaging a NF-κB reporter (p*NF-κB-Luc*; refs. 47, 48) and by immunoblotting, IL-1β (and IL-1α) and BMMC coculture induced and/or sustained NF-κB in adenocarcinoma, but not in B16F10 cells; this phenomenon was curtailed when *Il1b*$^{-/-}$ BMMCs were used and affected multiple NF-κB–pathway components (Figure 12, B–D, and Figure 13; full, uncut gels can be found in Supplemental Figures). In addition, *Il1r1* mRNA was selectively expressed by adenocarcinoma, but not B16F10 cells (Figure 12E and Supplemental Table 1). In vivo imaging of C57BL/6 and *c-Kit*^{Wsh} mice with pleural LLC cells expressing p*NF-κB-Luc* or a constitutive p*CAG-Luc* reporter verified that MC deficiency diminished tumor-specific NF-κB activation (Figure 14A). We next overexpressed *Ikbkb* (encoding IκB kinase [IKK] β), the main NF-κB–inducing kinase (45), in adenocarcinoma cells (Figure 14B). *Ikbkb*-overexpressing LLC cells were autonomous from IL-1β for NF-κB activation and equally caused MPEs in C57BL/6, *c-Kit*^{Wsh}, and *Cpa3*$^{Cre/+}$ mice (Figure 14, C and D), indicating that MC-elaborated IL-1β promotes MPEs by activating tumor cell IKKβ, thereby possibly establishing a positive feedback loop of enhanced MC recruitment by augmented tumor cell secretion of CCL2.

MC-mediated MPEs are actionable. To investigate whether the proposed pathway is targetable, we used c-KIT inhibitor imatinib mesylate (IM), which is clinically available. IM showed beneficial effects toward limiting LLC-induced effusions, and at the same time hampering pleural MC accumulation and vascular leakiness, when given at physiologically relevant once-daily doses of 1 mg/kg (Figure 15A). We also tested IM in the only

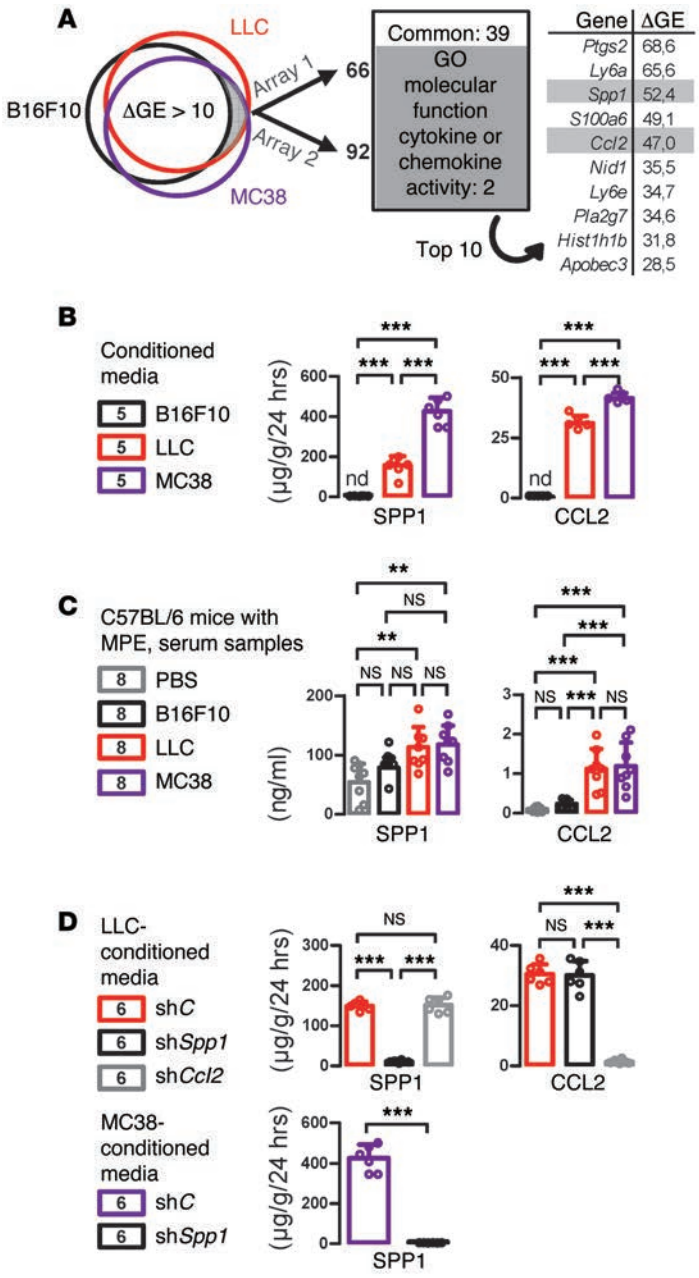

Figure 6. Identification of SPP1 and CCL2 as candidate tumor-derived MC effectors. (**A**) Venn diagram of mouse cancer cell differential gene expression (ΔGE) assessed by 2 microarrays showing 39 transcripts overrepresented in adenocarcinomas (top 10 listed), including *Ccl2* and *Spp1* (biological $n = 3$). (**B**) SPP1 and CCL2 ELISA of cancer cells–CM. (**C**) SPP1 and CCL2 ELISA of C57BL/6 mouse sera at day 14 after pleural PBS or cancer cells. (**D**) SPP1 and CCL2 ELISA of CM from LLC cells stably expressing random (shC), anti-*Spp1* (sh*Spp1*), or anti-*Ccl2* (sh*Ccl2*) shRNA, and MC38 cells stably expressing sh*C* or sh*Spp1*. Data represent 1 representative of 2 experiments and are presented as data points, mean ± SD. Numbers in boxes indicate the sample size. nd, not detected; NS, $P > 0.05$; $^{**}P < 0.01$; and $^{***}P < 0.001$, by 1-way ANOVA with Bonferroni post hoc tests.

available mouse model of MPEs caused by human cancer cells (38); A549 lung adenocarcinoma, but not SKMEL2 melanoma cells, elaborated SPP1/CCL2 and selectively caused MPE and MC accumulation upon pleural inoculation into *NOD/SCID* mice (Figure 15B). In addition, A549-induced MPEs were responsive to IM regression treatment (1 mg/kg daily) initiated on day 15 after establishment of pleural tumors (Figure 15C). Moreover, human MPEs from our biobank contained significantly elevated IL-1β levels compared with matched sera, a phenomenon not observed when CHF or IL-1α levels were examined (Figure 15D). In summary, our present work shows that MCs are required for MPEs, attracted to and activated in the pleural space by CCL2 and SPP1 of tumor cell origin. Once in the pleura, MCs secrete TPSAB1 and IL-1β to foster a hyperpermeable microenvironment and tumor NF-κB activation, respectively (Figure 15E).

Discussion

Here we report a connection between inflammation and cancer: MCs feed the inflammatory pleural environment fostering MPEs. We consistently found MCs in MPEs of patients and mice, and identified a plausible reason for their previous neglect. We also investigated MC trafficking and determined that these BM cells (49, 50) stream into the pleural cavities primarily attracted by tumor-originated CCL2. MCs were required for MPEs, since *c-Kit*^{Wsh} and *Cpa3*$^{Cre/+}$ mice were protected from adenocarcinoma-induced effusions and adoptive transfer of WT BM, as well as MC reconstitution, reinstalled MPEs in protected *c-Kit*^{Wsh} and *Il1b*$^{-/-}$ mice. c-KIT signaling was necessary for mastopoiesis and/or MC maintenance, since *c-Kit*^{Wsh} mice had reduced BMMC yield and decreased MC-like cells (29) in MPEs. Hence, it was shown here that c-KIT–intact MCs are essential for MPE

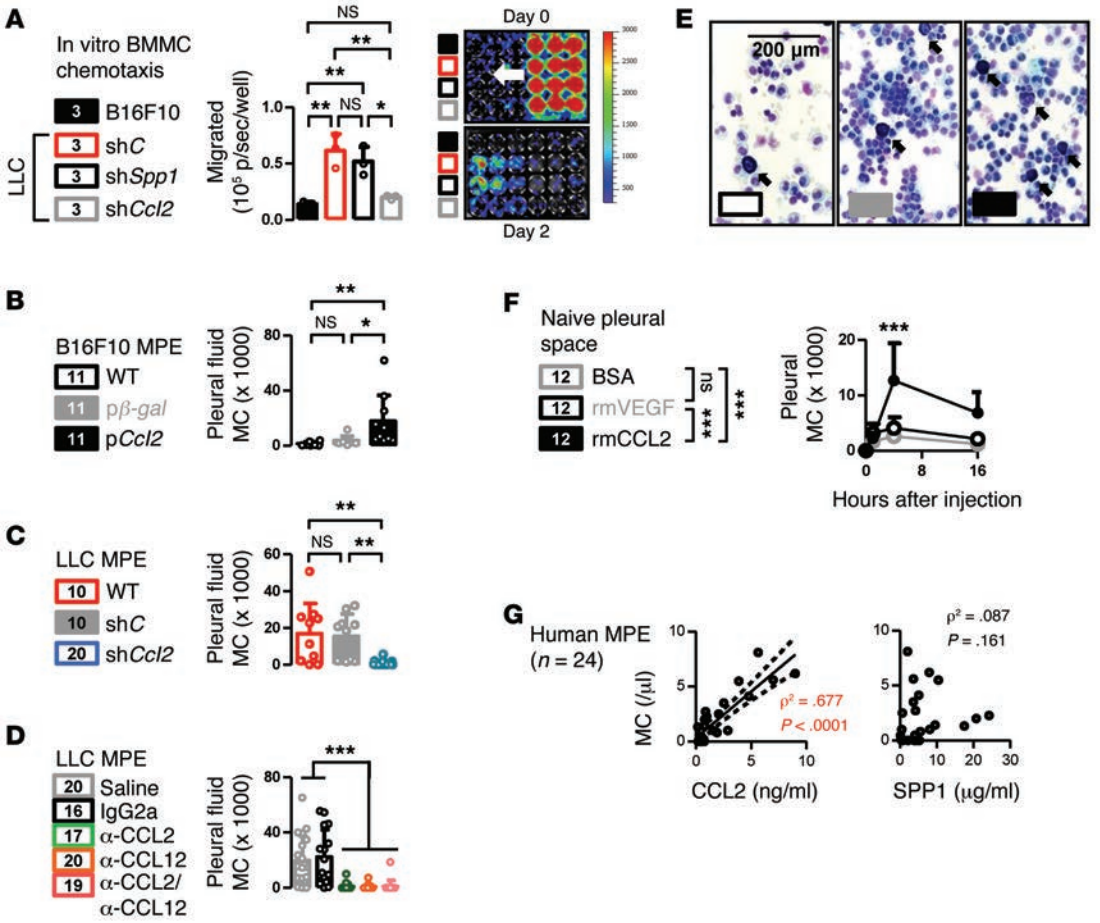

Figure 7. CCL2 is a tumor-derived mastokine. (**A**) Summary and images of 1 representative of 3 bioluminescent mastotaxis assays. Inserts carrying *CAG-luc-EGFP* BMMCs were transferred (arrow) onto wells containing B16F10 or LLC cells expressing sh*C*, sh*Spp1*, or sh*Ccl2* (n = 3/group) and were discarded after 2 days for imaging of transmigrated BMMCs. (**B**) Pleural MCs of C57BL/6 mice at day 14 after pleural *wt, β-gal,* or *Ccl2* plasmid (p*Ccl2*)-expressing B16F10 cells (n = 11/group). (**C**) Pleural MCs of C57BL/6 mice at day 14 after pleural delivery of WT (n = 10), sh*C* (n = 10), or sh*Ccl2*-expressing (n = 20) LLC cells. (**D**) Pleural MC accumulation of C57BL/6 mice at day 14 after pleural LLC cells was inhibited by CCL2 neutralization. Mice were treated with saline (n = 20), IgG (n = 16), or CCL2- (n = 17), CCL12- (n = 20), or both- (n = 19) neutralizing Ab (α) every 3 days after establishment of LLC cells. (**E** and **F**) Pleural MC (arrows) of C57BL/6 mice after pleural delivery of 30 ng BSA, rm VEGF, or rmCCL2 (n = 12/group). (**G**) CCL2 and SPP1 ELISA versus MC abundance of human MPEs from Figure 1A (n = 24) with linear regression line (95% CI), squared Spearman's correlation coefficients (ρ^2), and probability values (P). (**A**–**D**) Data presented as data points, mean ± SD. Numbers in boxes indicate sample size. nd, not detected; NS, $P > 0.05$; *$P < 0.05$; **$P < 0.01$; and ***$P < 0.001$, by 1-way (**A**–**D**) or 2-way (**F**) ANOVA with Bonferroni post hoc tests.

development. Moreover, it was shown that this less prevalent cellular population is as important for effusion formation as predominant immune cells such as macrophages.

Our data support that substantial populations of MCs exist in MPEs of humans and mice, and that they play a functional tumor-promoting role in the pleural space when the latter is taken over by metastatic tumors. This protumor role of pleural MCs appears to be conditional on the pleural space, since MCs were tumor-indifferent or even exerted antitumor functions in other tumor models (6, 12). The marked effusion-promoting effects of pleural-accrued MCs may be explained by the vast abundance of MCs in serosal cavities, a preferential site for their isolation (15). However, it is also conceivable that MCs, potent inflammatory regulators and vasoactors (51, 52), impact effusion formation more heavily than other tumor models, since MPE is mainly caused by inflammation and vasoactive signaling, and since the pleural cavities feature an extensive vascular bed (23, 24). Indeed, MCs secreted multiple inflammatory and vasoactive mediators upon adenocarcinoma encounter: histamine, a known permeability factor (9); TPSAB1 shown here to induce strong vasoactive effects; and IL-1β, a well-known NF-κB stimulus (45). Interestingly, the intrapleural levels of MC-originated TPSAB1 identified here may be responsible for the clinically well-known failure of normal, benign, and malignant pleural fluid to spontaneously coagulate, since TPSAB1 was recently found to cleave fibrinogen (53). Hence, tumor site likely determines MC function in cancer, and the pleural space probably constitutes a preferential theater for deployment of protumor MC effects.

Regardless of the tumor milieu, only certain tumor cells were able to initiate bidirectional signaling with MCs in our hands. First, only tumor cells competent of CCL2 secretion were able to attract substantial numbers of MCs to the pleural cavities. The finding of CCL2 as a cardinal MPE mastokine corrob-

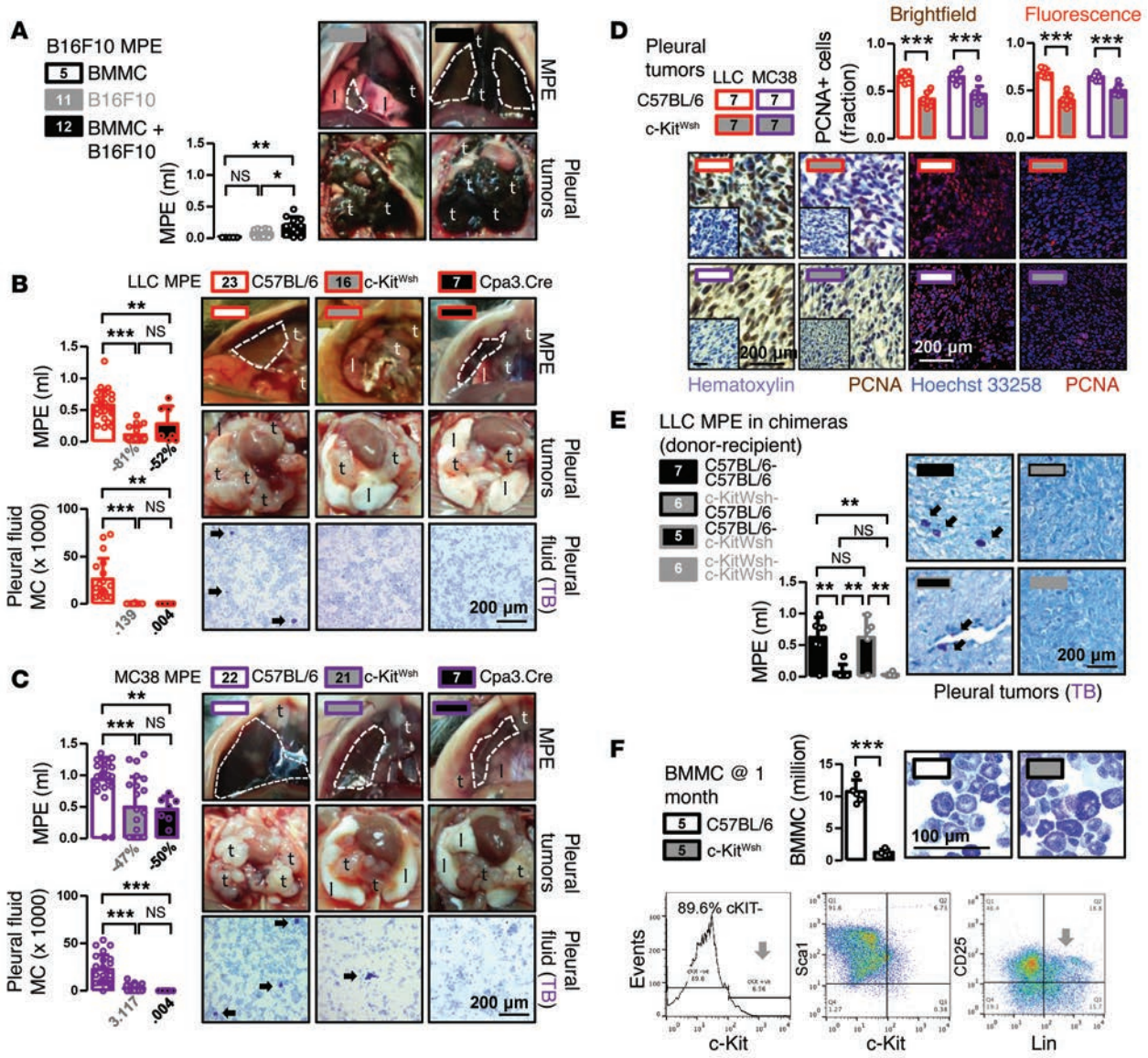

Figure 8. MCs are required for MPEs. (**A**) MPEs and pleural tumors of C57BL/6 mice at day 14 after pleural BMMCs (n = 5), B16F10 cells (n = 11), or both (n = 12). (**B** and **C**) MPEs, pleural tumors, and TB-stained pleural fluid cells including MCs of C57BL/6 (n = 45), *c-Kit*^{Wsh} (n = 37), and *Cpa3*$^{Cre/+}$ (n = 14) mice at day 14 after pleural LLC (**B**) and MC38 (**C**) cells. (**D**) PCNA immunoreactivity of pleural tumors from **B** and **C** (n = 7/group). (**E**) MPEs (graph) and TB-stained pleural tumor MCs (images) of irradiated C57BL/6 and *c-Kit*^{Wsh} recipients of BM transplants from C57BL/6 and *c-Kit*^{Wsh} donors at day 14 after pleural LLC cells (n = 6–7/group). (**F**) BMMC yield of C57BL/6 and *c-Kit*^{Wsh} mice (n = 6 each) at 1 month; data summary, TB-staining, and flow cytometry of *c-Kit*^{Wsh} BMMCs. Arrows indicate shift toward c-KIT$^-$Lin$^+$ phenotype, as compared with Figure 4B. Shown throughout are MPEs (dashed lines), lungs (l), pleural tumors (t), and MCs (arrows). Numbers below columns: percentile MPE inhibition and pleural MCs (thousands) of *c-Kit*^{Wsh} (gray font) and *Cpa3*$^{Cre/+}$ (black font) mice. Data presented as data points, mean ± SD. Numbers in boxes indicate sample size. NS, $P > 0.05$; *$P < 0.05$; **$P < 0.01$; and ***$P < 0.001$, by 2-tailed Student's t-test (**D**) or 1-way ANOVA with Bonferroni post hoc tests (all other graphs).

orates and expands work that identified CCL2 as the culprit for MC accrual to pancreatic tumors (6, 7). However, CCL2-mediated MC recruitment was not enough for full-blown tumor-MC interactions during MPE development; murine adenocarcinoma cells also secreted SPP1 that facilitated MC degranulation. On the contrary, B16F10 cells were unable to activate codelivered BMMCs, thus failing to mount full effusion-inducing properties, since they were found not to express SPP1. Finally, adenocarcinomas were selectively responsive to MC-originated IL-1β and expressed *Il1r1*, while melanoma cells did not. Taken together, our data suggest that MPE-prone adenocarcinomas may initiate circuitry with MCs due to coordinated expression of MC chemoattractants (i.e., CCL2) and effectors (i.e., SPP1), as well as the cognate receptors of MC-originated ligands such as IL-1β. The reason behind the propensity of the adenocarcinoma cells studied here to initiate crosstalk with MCs remains to be determined but can explain, together with the site-specificity discussed above, the differential impact of MCs on different tumors. In addition, these results can serve as a paradigm of how tumor-associated inflammatory cells can conditionally

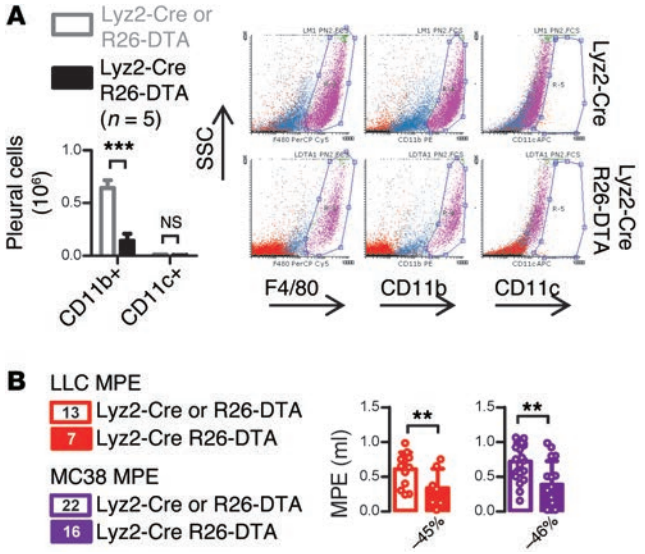

Figure 9. MC effects on MPEs parallel those of macrophages. (**A**) Flow cytometry gating and data summary of pleural cells from *Lyz2-Cre* or *R26-DTA* single transgenic controls, as well as *Lyz2-Cre R26-DTA* macrophage-deficient mice. Data presented as mean ± SD (n = 5/group). (**B**) MPEs of *Lyz2-Cre or R26-DTA* single transgenic controls (n = 35), as well as *Lyz2-Cre R26-DTA* macrophage-deficient mice (n = 23) at day 14 after pleural LLC (n = 20) or MC38 (n = 38) cells. Numbers below columns indicate percentile MPE inhibition of *Lyz2-Cre R26-DTA* mice. Data presented as data points, mean ± SD. Numbers in boxes indicate sample size. NS, $P > 0.05$; $^{**}P < 0.01$; and $^{***}P < 0.001$, by 2-tailed Student's t test.

modulate metastatic disease.

NF-κB integrates inflammatory stimuli from the tumor microenvironment to pivotally influence tumor cell survival and paracrine inflammatory signaling (54). In turn, immune cells stimulate tumor NF-κB, reinforcing a "vicious cycle" between tumor progression and inflammation (5, 55). NF-κB affects MPE progression, stimulated by tumor- and host-originated ligands of an ever-expanding cellular origin (26, 47, 48). Here we show that MC-secreted IL-1β upregulates NF-κB and cellular proliferation of pleural adenocarcinomas. Using in vivo imaging, we show in real time how MCs fuel tumor cell NF-κB and identify that IKKβ relies on MC-derived IL-1β to sustain the transcription factor. These findings are consistent with the recently reported *Nlrp3*-mediated IL-1β release by skin MCs (56), and they also strengthen the link between inflammation and cancer by positioning MCs as "feeder cells" of oncogenic NF-κB, as well as other important tumor cell transcription factors, such as STAT3 (57).

Importantly, the requirement for MCs during MPE development was actionable. Encouraging benefits were obtained from imatinib treatment of mice with syngeneic effusions, and concordant findings were recapitulated in human cancer cell–induced MPEs. These data strengthen the proposed connection and show how MC-targeted therapies can impact nongastrointestinal stromal tumors. The finding of significantly increased MCs and IL-1β in human MPEs compared with both matched serum samples and corresponding samples from patients with CHF suggests that our findings may be applicable to humans with established or impending MPEs, a possibility worth exploring.

In conclusion, we identified the conditional initiation and execution of a circuitry of tumor-initiated, MC-perpetuated inflammatory signaling events that occur during MPE formation. We show how tumor cells co-opt MCs to drive effusion development. In addition to the surprising discovery of MCs as culprits of MPEs, we identify CCL2, SPP1, TPSAB1, IL-1β, and IKKβ as key players in tumor cell–MC interactions in the pleural space. MCs per se, as well as each of the above targets, may present candidates for annihilating the requirement for MCs during MPE formation.

Methods

Further information can be found in Supplemental Methods.

Reagents. CCL2 and CCL12 neutralizing and IgG2a control Abs (37) were a gift from Oncology Discovery Research, Janssen Research & Development LLC. rmCCL2 was from Peprotech; rmIL-1β, rm IL-3, and rmKITL were from Immunotools; rmSPP1 and rmTPSAB1 were from R&D Systems; C48/80 and Evans' blue were from Sigma-Aldrich; ELISA kits were from Peprotech and R&D Systems; IM was from Selleckchem; and Boyden chambers were from Millipore.

Cells. LLC, B16F10, A549, and SKMEL2 (NCI) and MC38 cells (a gift from Barbara Fingleton, Vanderbilt University, Nashville, Tennessee, USA) (38) were cultured and tested as described in the Supplemental Methods. In vivo injections are described elsewhere (25, 26, 38, 47, 48). BM cells were flushed from femurs and tibias and cultured in full DMEM with rmIL-3 ± rmKITL (100 ng/ml each). Nonadherent cells were passaged for 4–6 weeks (31).

Animals. C57BL/6, *c-Kit*^{Wsh}, *NOD/SCID*, *CAG-luc-EGFP*, *CAG-EGFP*, *mT/mG*, *Lyz2-Cre* (39), and *R26-DTA* (40) mice (The Jackson Laboratory); *Cpa3*$^{Cre/+}$ mice (a gift from Hans-Reimer Rodewald, Heidelberg, Germany) (15); and *Il1b*$^{-/-}$ mice (a gift from Yoichiro Iwakura, Tokyo University of Science, Tokyo, Japan) (44) were bred at the Center for Animal Models of Disease of the University of Patras. Experiments were approved a priori by the local Veterinary Administration and were conducted according to 2010/63/EU. Experimental mice and littermate controls were sex-matched, weight-matched (20–25 g), and age-matched (6-12 weeks). For MPE generation, mice received 150,000 murine or 1,000,000 human cancer cells intrapleurally and were sacrificed after 14 or 30 days, respectively (38). IM (1 mg/kg) was given daily i.p. Anti–mouse CCL2 and CCL12 (a murine CCL2 ortholog) and IgG2a control Abs were delivered i.p. at 50 mg/kg every 3 days (37, 38). Harvest and pleural lavage are described elsewhere (25, 26, 38, 47, 48).

Humans. Pleural fluid was obtained during diagnostic thoracenteses in patients with MPEs (due to lung cancer [n = 14], breast cancer [n = 6], and malignant pleural mesothelioma [n = 4]) or CHF treated at General Hospital Evangelismos between 2006 and 2008. Samples from Hospital G. Papanikolaou were diagnostic MPE cyto-

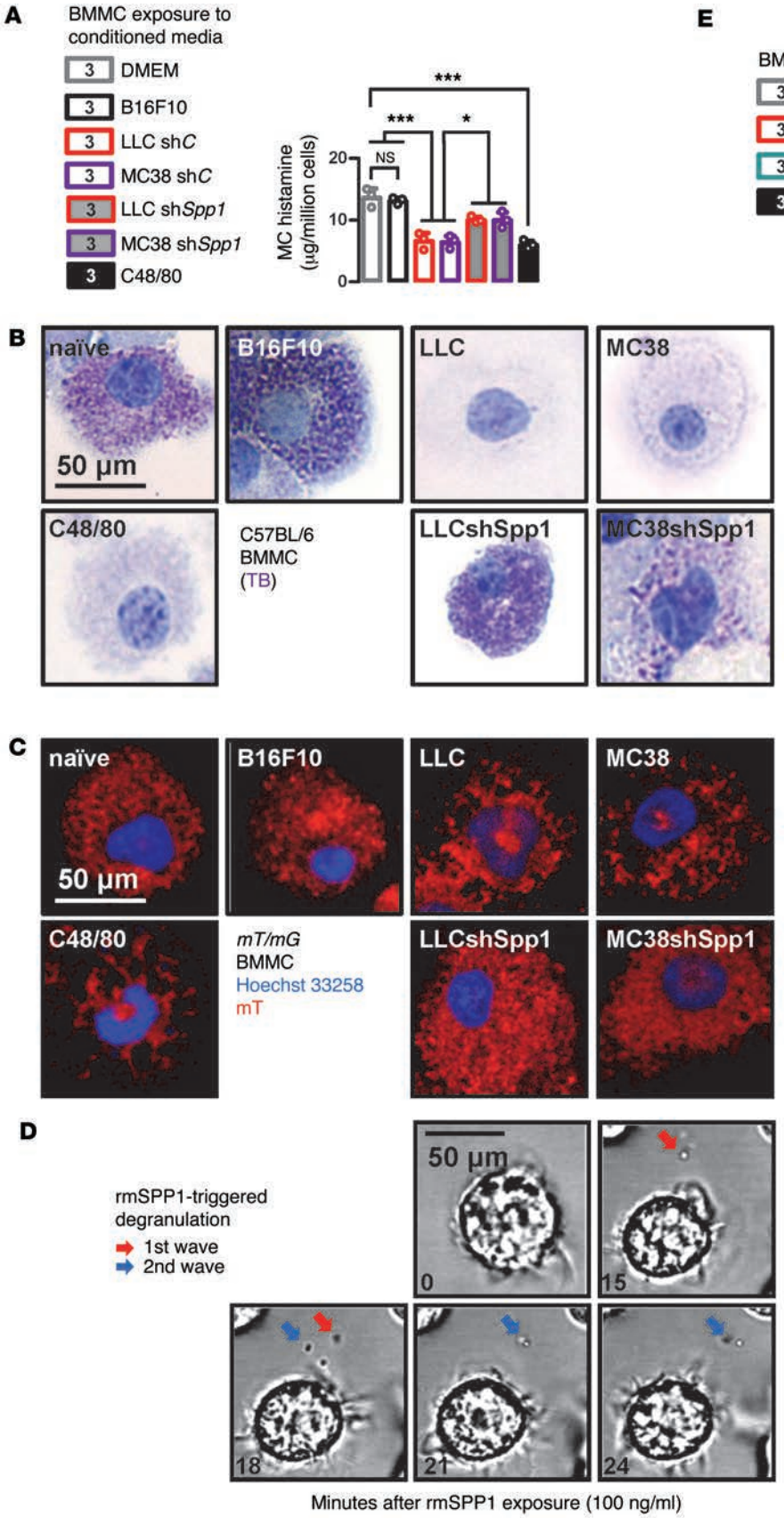

Figure 10. Tumor-secreted osteopontin causes MC degranulation. (**A**) Histamine content of C57BL/6 BMMCs after 2-hour incubation with indicated CM or C48/80 compound (potent MC degranulating compound used as positive control, n = 3/group). Note the partial effect of osteopontin silencing (sh*Spp1*), indicating that additional tumor-elaborated factors degranulate MCs. (**B** and **C**) C57BL/6 (**B**) and *mT/mG* (**C**) BMMC morphology after 2-hour incubation with indicated CM or C48/80 compound indicates that osteopontin is, at least in part, responsible for MC activation. (**D**) Time-lapse phase-contrast images of C57BL/6 BMMCs after direct exposure to rm SPP1 showing 2 consecutive waves of granule ejection (arrows). See also Supplemental Video 3. (**E**) C57BL/6 BMMC histamine content after 4-hour incubation with indicated rm mediators or C48/80 compound (n = 3/group) shows direct MC activation by osteopontin, which is only partial compared with C48/80. Data shown represent 1 representative of 3 experiments and are presented as data points, mean ± SD. Numbers in boxes indicate sample size. nd, not detected; NS, $P > 0.05$; *$P < 0.05$; and ***$P < 0.001$, by 1-way ANOVA with Bonferroni post hoc tests.

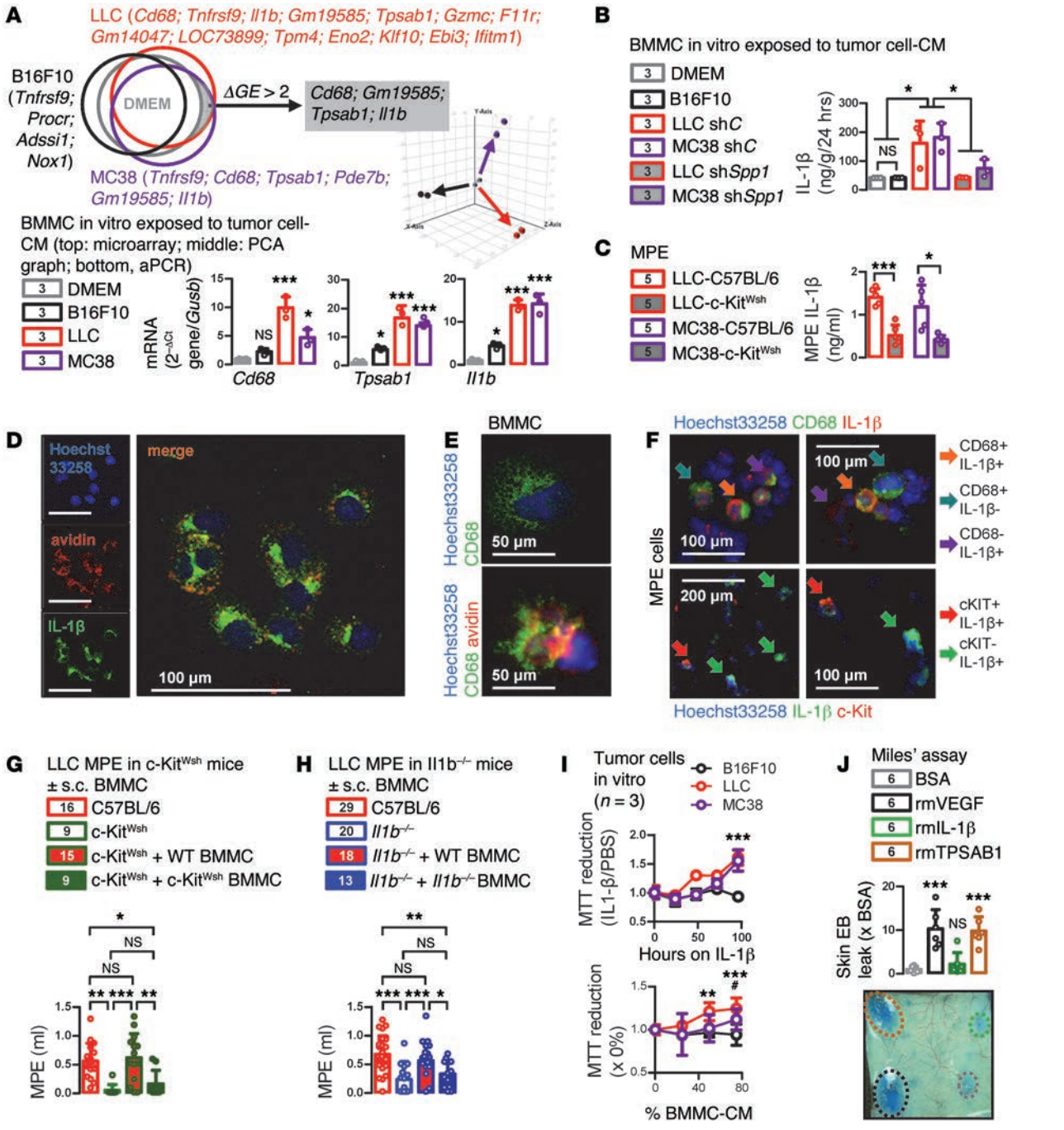

Figure 11. Adenocarcinoma-primed MCs secrete TPSAB1 and IL-1β. (**A**) Microarray (Venn and PCA diagrams, $n = 2$) and qPCR ($n = 3$) of BMMC differential gene expression (ΔGE) after tumor-CM exposure. Comparisons with naive BMMCs. (**B**) C57BL/6 BMMC-CM IL-1β ELISA after 4 hours of sham or tumor-CM exposure ($n = 3$/treatment). (**C**) MPE IL-1β ELISA of mice from Figure 8, B and C ($n = 5$/group). (**D** and **E**) IL-1β (**D**) and CD68 (**E**) immunolocalization in C57BL/6 BMMCs counterstained with Hoechst 33258 (nuclei) and avidin (granules). (**F**) IL-1β colocalization with c-KIT and CD68 in MPE cells. (**G** and **H**) MPEs of C57BL/6 ($n = 45$), *c-Kit*^{Wsh} (**G**, $n = 33$), and *Il1b*$^{-/-}$ (**H**, $n = 51$) mice 14 days after pleural LLC cells with or without s.c. C57BL/6, *c-Kit*^{Wsh}, or *Il1b*$^{-/-}$ BMMCs. (**I**) Proliferation of B16F10, LLC, and MC38 cells ($n = 3$/cell line) at 100 ng/ml IL-1β (top; comparisons of adenocarcinomas with melanoma) and at increasing BMMC-CM concentrations (bottom; comparisons of LLC [stars] and MC38 [number sign] cells with 0% BMMC-CM [control]). (**J**) C57BL/6 skin Evans' blue leak (color-coded areas) induced by BSA or rm cytokines (comparisons with BSA, $n = 6$/group). (**A**, **B**, and **I**) Shown are 1 representative of 3 experiments. Data are presented as data points, mean ± SD. Numbers in boxes indicate sample size. NS, $P > 0.05$; $^*P < 0.05$; $^{**}P < 0.01$; and $^{***}P < 0.001$, by 2-way (**I**) or 1-way (all other graphs) ANOVA with Bonferroni post hoc tests.

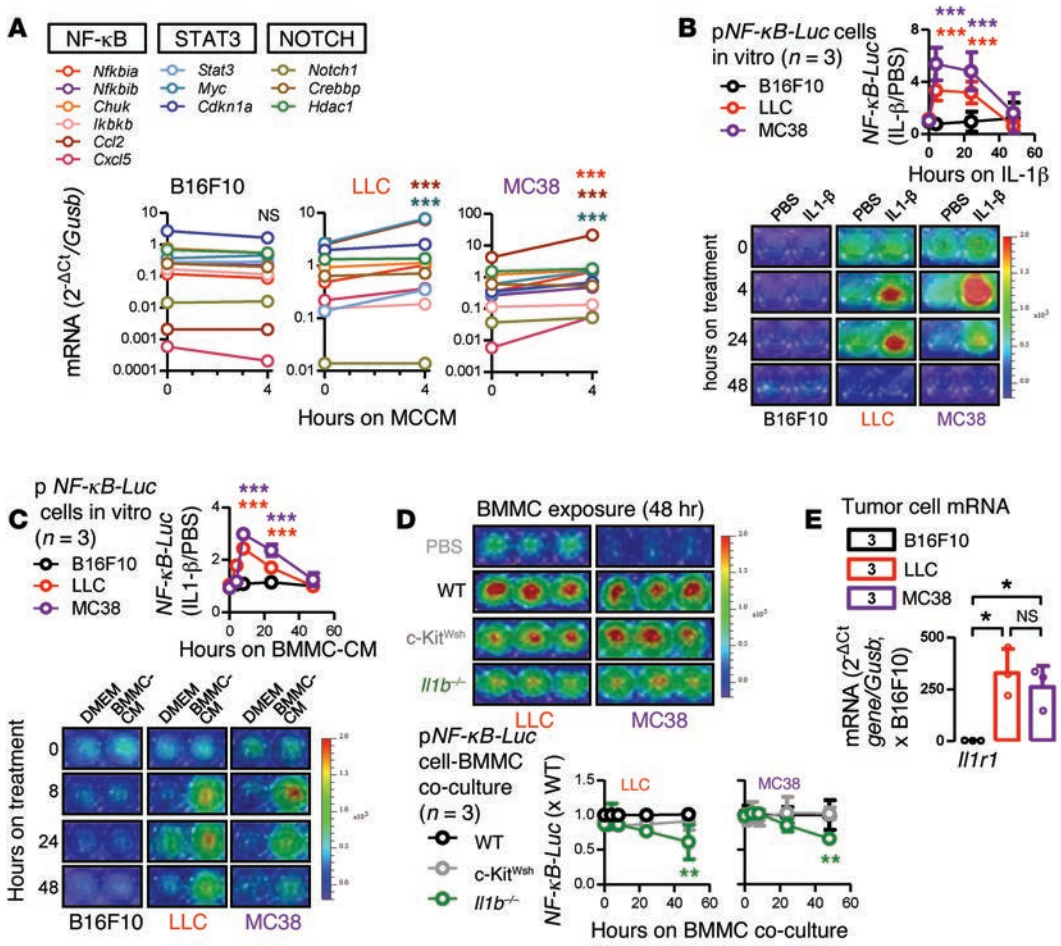

Figure 12. MC-derived IL-1β activates NF-κB in adenocarcinoma cells. (**A**) Tumor cell mRNA expression levels by qPCR of 12 target genes of the NF-κB, STAT3, and NOTCH pathways before and 4 hours after exposure to BMMC-CM. *n* = 3/data point. (**B** and **C**) Cancer cell NF-κB reporter (p*NF-κB-Luc*) activity induced by rmIL-1β (**B**) and BMMC-CM (**C**). *n* = 3/data point. (**D**) Tumor cell p*NF-κB-Luc* activity induced by C57BL/6, *c-Kit*^{Wsh}, or *Il1b*$^{-/-}$ BMMC coculture. *n* = 3/data point. (**E**) *Il1r1* qPCR of tumor cell RNA. *n* = 3/data point. Significance indicators stand for comparison of color-matched data at indicated time-point compared with baseline (**A**), B16F10 cells (**B** and **C**) or with C57BL/6 BMMC (**D**). Shown is 1 representative of 3 experiments. Data presented as mean ± SD (**A**–**D**) or data points, mean ± SD (**E**). Numbers in boxes indicate sample size. NS, $P > 0.05$; *$P < 0.05$; **$P < 0.01$; and ***$P < 0.001$, by 1-way (**E**) or 2-way (all other graphs) ANOVA with Bonferroni post hoc tests.

logic specimens from 20 patients with lung adenocarcinoma aspirated in 2013. Diagnosis and sample handling are described elsewhere (25, 26, 48). All protocols abided by the Helsinki Declaration were approved a priori by the relevant IRB and by all patients via written informed consent.

Cytology and histology. Cell and tissue specimens, prepared as described in the Supplemental Methods, were stained with MGG, TB (0.05%; 5–15 minutes), or the indicated Abs (Supplemental Table 6) and counterstained with hematoxylin, Hoechst 33258 (Sigma-Aldrich; dilution 1:5000), Envision (Dako), and/or avidin (Vector Laboratories). MCs were counted as a percentage of 10,000 cells on cytology or of all cells on histology. Microscopy was done on an AxioObserver D1 (Zeiss) or an SP5 (Leica Microsystems) microscopes.

Flow cytometry. After NH_4Cl red blood cell lysis, cells were suspended in PBS 2% FBS, stained with the indicated Abs (Supplemental Table 6) for 20 minutes, fixed in 1% paraformaldehyde (10 minutes), and analyzed on a FACSCalibur (BD Biosciences). Data were examined using FlowJo.

Constructs. Random (shC), anti-*Ccl2* (sh*Ccl2*), or anti-*Spp1* (sh*Spp1*) shRNAs, as well as *Ccl2* and *β-gal* expression vectors, have been described (25, 41). p*EGFP* and p*EGFP.Ikbkb* (Addgene IDs 58249 and 58251) were cloned from MC38 total RNA using specific primers (Supplemental Table 7). Cells were transfected with 5 μg DNA by X-fect reagent (BD Biosciences — Clontech) and selected by puromycin.

BM cell transfer. For adoptive BM replacement (Figure 5, A and B, and Figure 8E), mice received 10 million BM cells i.v. 12 hours after total-body irradiation (1100 Rad; ref. 35). For MC pulse and chase (Figure 5), irradiated C57BL/6 chimeras engrafted with *c-Kit*^{Wsh} BM (39) received pleural tumor cells at day 30 after transplant, followed by same-day 5×10^5 i.v. *CAG-luc-EGFP* or *CAG-EGFP* BMMCs; nonirradiated *c-Kit*^{Wsh} mice received 8×10^5 s.c. *CAG-luc-EGFP* BMMCs, followed by next-day pleural tumor cells. For intrapleural BMMC delivery (Figure 8A), C57BL/6 mice received 10^5 intrapleural BMMCs, with or without B16F10 cells. For BMMC give-back (Figure 11, G and H), 2.5×10^5 BMMC were administered s.c.

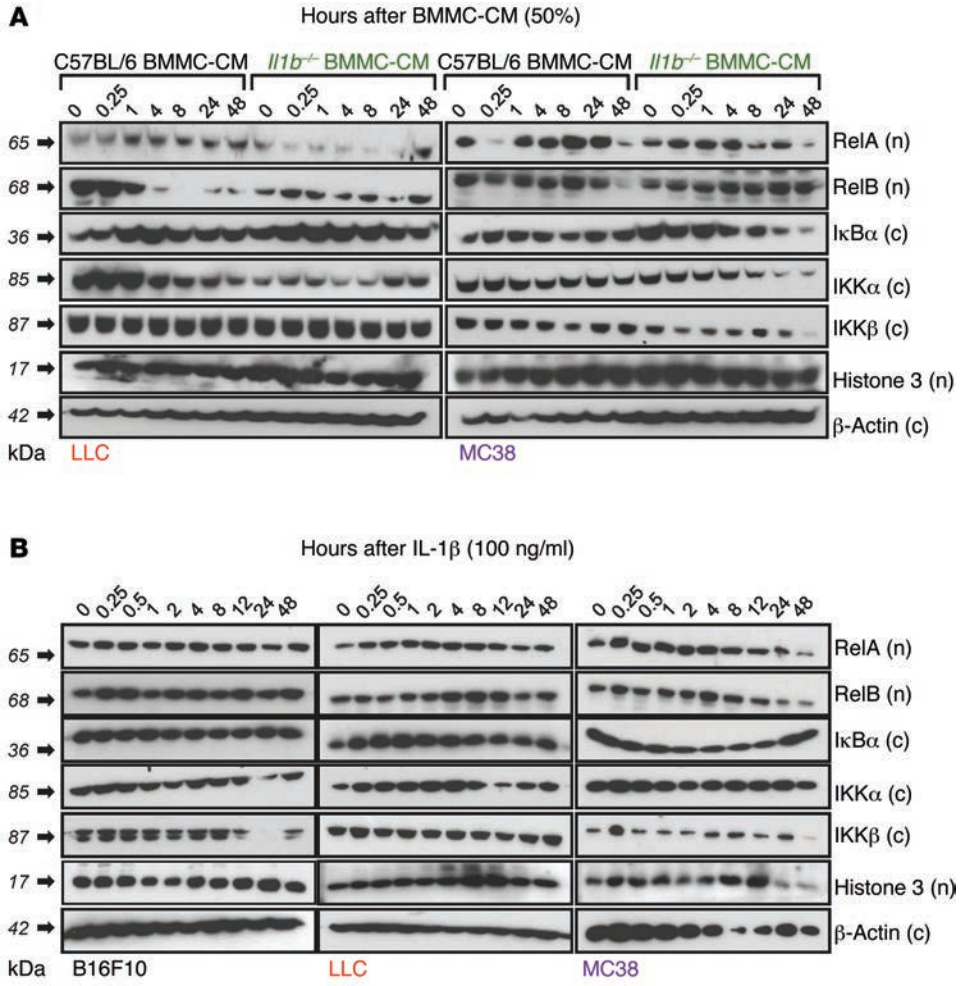

Figure 13. Tumor cell NF-κB subunit profiling after exposure to MC-coditioned media and IL-1β. Immunoblots of cytoplasmic (c) and nuclear (n) tumor cell extracts for NF-κB pathway components after C57BL/6 or *Il1b*$^{-/-}$ BMMC-CM exposure (**A**) or treatment with 100 ng/ml rmIL-1β (**B**).

Bioluminescence imaging. Cells and mice were imaged after the addition of 300 μg/ml D-luciferin to culture media or i.v. delivery of 1 mg D-luciferin on a Xenogen Lumina II. Data were analyzed on Living Image v.4.2 (PerkinElmer) (47, 48).

Vascular permeability assays. Mice with MPEs received 0.8 mg Evans' blue i.v. and were killed after 1 hour for determination of MPE levels of the albumin tracer (48). Intradermal injections of test molecules (1.5 ng/50 μl PBS), cell-free MPEs (50 μl), or cancer cell–conditioned media (50 μl) were followed by Evans' blue injection as above, and euthanasia, skin inversion and imaging after 1 hour (25). Dye leak was determined using Fiji (http://fiji.sc/Fiji).

qPCR and microarray. RNA was isolated using Trizol (Invitrogen) followed by RNAeasy (QIAGEN), RNA was reverse transcribed using Superscript III (Invitrogen), and reverse transcriptase or qPCR was performed using specific primers (Supplemental Table 7). For microarray, 5 μg RNA pooled from triplicate samples was tested for quality, labeled, and hybridized to GeneChip Mouse Gene 1.0 or 2.0 ST arrays (Affymetrix). Data (http://www.ncbi.nlm.nih.gov/geo/; Accession ID: GSE58190) were analyzed as detailed in the Supplemental Methods.

Immunoblotting. Nuclear and cytoplasmic extracts were prepared using NE-PER (Thermo), separated by 10% SDS-PAGE, and electroblotted to PVDF membranes (Millipore). Membranes were probed with specific Ab (Supplemental Table 6), and were visualized by enhanced chemiluminescence.

Cellular assays. Tumor cell proliferation in response to IL-1β or BMMC-CM was determined using MTT reduction (Promega). MC migration was studied in Boyden chambers with 8.0 μm pores (36): cancer cells were cultured in the lower and bioluminescent BMMCs in the upper chambers. After 48 hours, the upper chambers were removed and the bioluminescent signal of transmigrated BMMCs was measured by imaging. MC histamine was measured by the o-phthalaldehyde method (58). All cellular experiments were done at least 3 times, while 1 representative experiment is shown.

Statistics. Sample size was calculated using G*power (http://www.gpower.hhu.de/; ref. 59) assuming $\alpha = 0.05$, $\beta = 0.8$, and $\rho = 0.3$. No data were excluded. Animals were allocated to treatments by alternation, and transgenic animals were enrolled case-control–wise. Data acquisition was blinded on samples previously coded by a nonblinded investigator. All data were examined for normality by Kolmogorov-Smirnof test. Values are given as mean ± SD and median ± interquartile range, as indicated. Sample size (n) refers to biological replicates. Differences in means were examined by

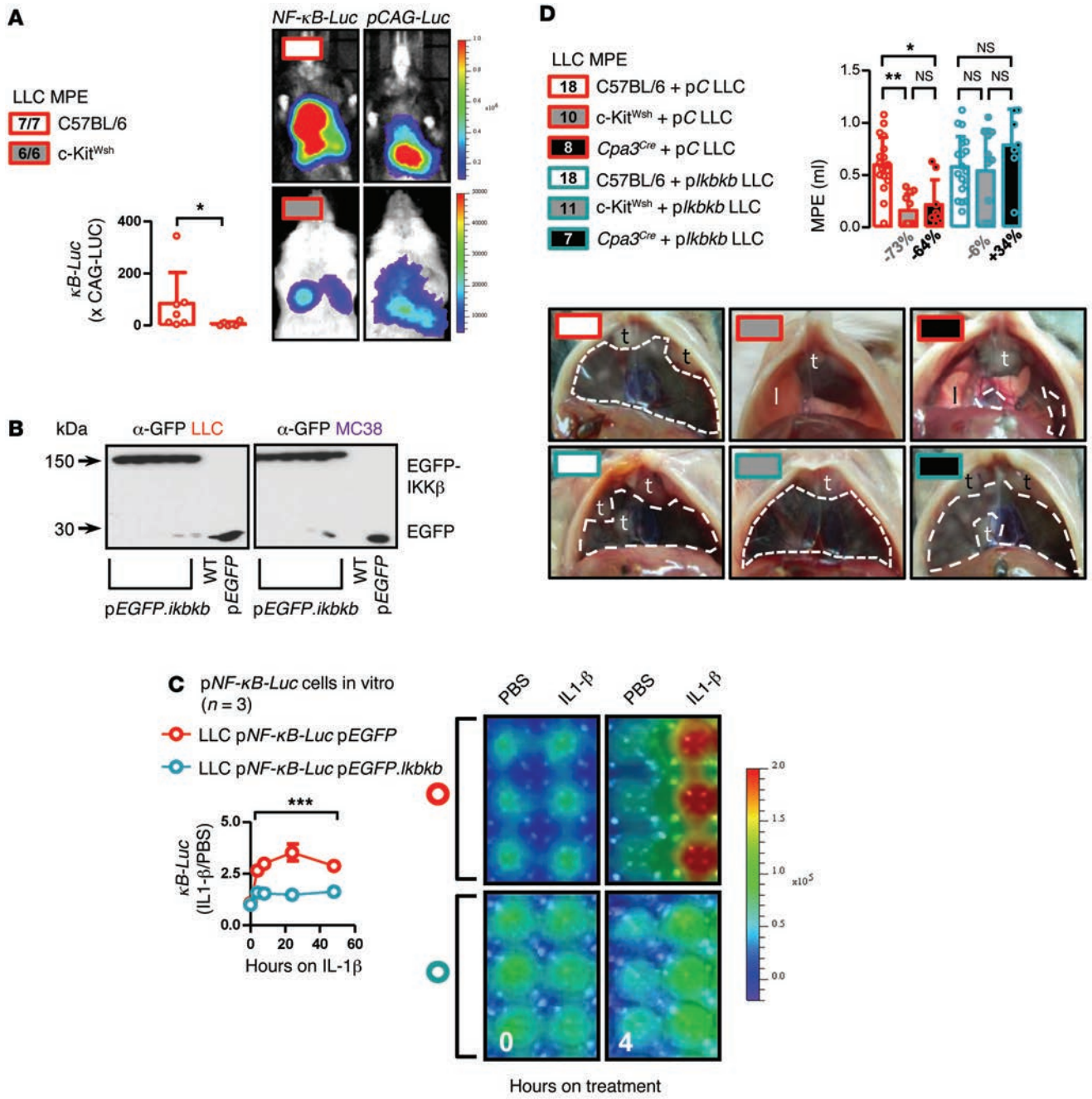

Figure 14. MC-derived IL-1β promotes effusion development via IκB kinase (IKK) β. (**A**) Bioluminescence of C57BL/6 (n = 14) and *c-Kit*^{Wsh} (n = 12) mice 14 days after pleural LLC cells expressing constitutive (p*CAG-Luc*) or NF-κB-dependent (p*NF-κB-Luc*) reporters. (**B**) Validation of adenocarcinoma cells overexpressing p*EGFP* and p*EGFP.Ikbkb*. (**C**) Bioluminescence of p*NF-κB-Luc* LLC cells expressing p*EGFP* or p*EGFP.Ikbkb* in response to 100 ng/ml IL-1β, with comparisons of p*EGFP.Ikbkb* with p*EGFP* cells (n = 3/data-point). Shown is 1 representative of 3 experiments. (**D**) MPEs of C57BL/6 (n = 36), *c-Kit*^{Wsh} (n = 21), and *Cpa3*$^{Cre/+}$ (n = 15) mice 14 days after pleural p*EGFP*- or p*EGFP.Ikbkb*-expressing LLC cells. Shown are MPEs (dashed lines), lungs (l), and pleural tumors (t). Numbers below columns indicate percentile MPE inhibition of *c-Kit*^{Wsh} (gray font) and *Cpa3*$^{Cre/+}$ (black font) mice. Data presented as data points, mean ± SD. Numbers in boxes indicate sample size. NS, $P > 0.05$; *$P < 0.05$; **$P < 0.01$; and ***$P < 0.001$, by Student's t test (**A**), 1-way (**D**), or 2-way (**C**) ANOVA with Bonferroni post hoc tests.

2-tailed Student's t test, or 1-way or 2-way ANOVA with Bonferroni post-tests, as appropriate, and in medians by Mann-Whitney U test or Kruskal-Wallis test with Dunn's post hoc tests. Correlations were done using Pearson's r or Spearman's ρ. P values are 2-tailed, and $P < 0.05$ was considered significant. Analyses and plots were done on Prism v5.0 (GraphPad Software).

Study approval. All animal experiments were approved a priori by the Veterinary Administration of Western Greece according to a full and detailed protocol (approval 276134/14873/2). Human studies were approved a priori by the Ethics Committee of the General Hospital of Athens Evangelismos (Athens, Greece; approval 379-7/12/2006 and extension 323-4/12/2012).

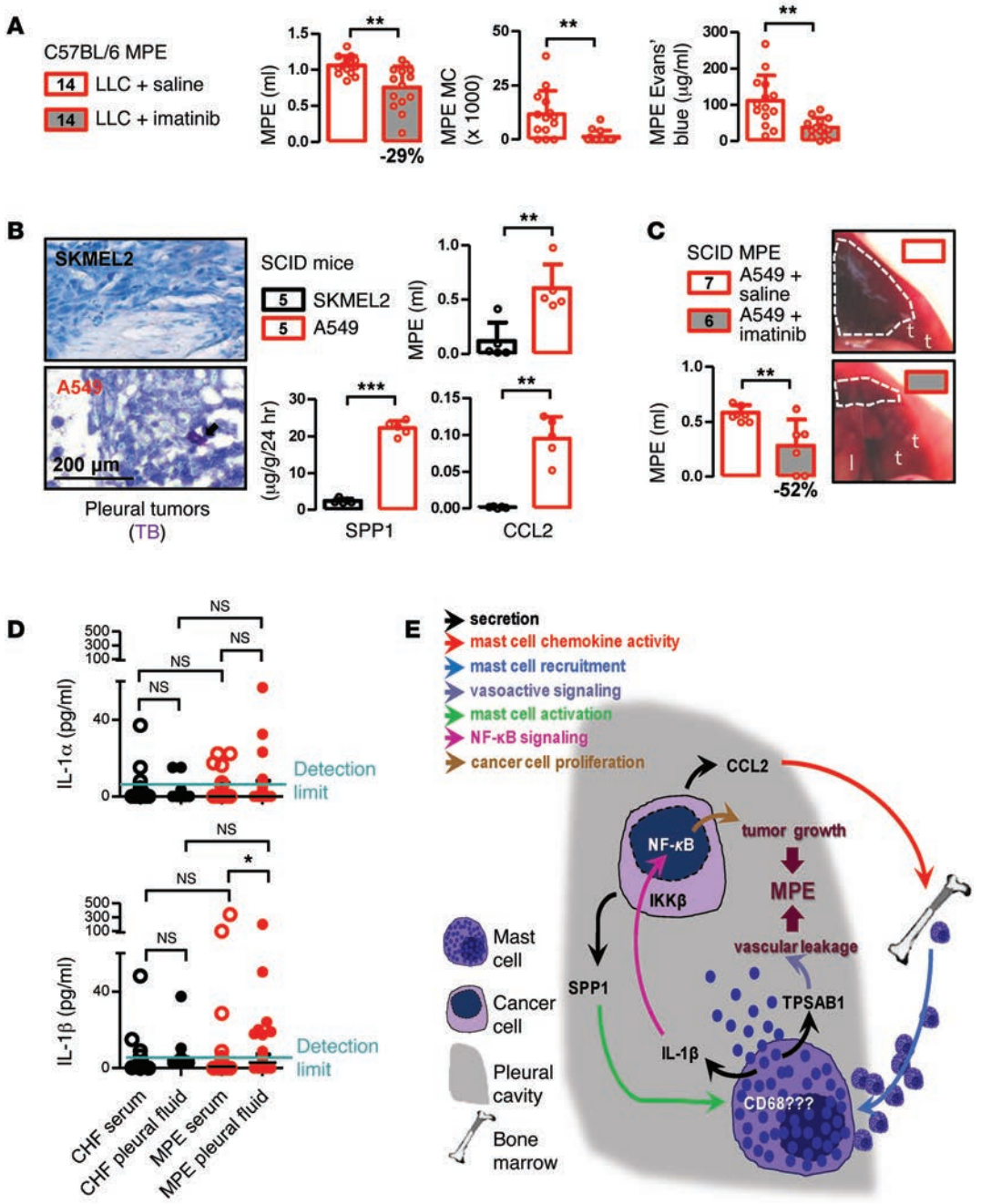

Figure 15. MC-mediated MPEs are actionable in mice and humans. (**A**) MPEs, MPE MCs, and Evans' blue content after i.v. delivery of 0.8 mg of the dye of C57BL/6 mice at day 14 after pleural delivery of 1.5×10^5 LLC cells and daily treatment with intraperitoneal PBS or IM, as indicated (n = 14/group). Percentage indicates IM-mediated MPE inhibition. (**B**) MCs in pleural tumors (arrows) and MPE volume of *NOD/SCID* mice 30 days after pleural human cancer cells, and SPP1/CCL2 ELISA of human tumor cell–CM (n = 5/group). (**C**) A549-induced MPEs of *NOD/SCID* mice at day 30 after establishment of A549 cells, after treatment with PBS (n = 7) or IM (n = 6) starting at day 15 after establishment of A549 cells. Shown are MPEs (dashed lines), lungs (l), and pleural tumors (t). Percentage indicates IM-mediated MPE inhibition. (**D**) Pleural and serum IL-1α/β of patients with CHF (n = 26) and MPEs (n = 24) from Figure 1A. (**E**) Graphical summary of present work: pleural adenocarcinomas secrete CCL2 and SPP1, which facilitate, respectively, pleural MC accumulation and activation. Upon tumor cell encounter, MCs release TPSAB1 and IL-1β, which increase vascular leakage and tumor NF-κB activation, respectively. Data presented as data points and median ± interquartile range (**D**) or mean ± SD (all other graphs). Cytokine measurements in (**B**) were repeated 3 times; shown are data from 1 experiment. Numbers in boxes indicate sample size. NS, $P > 0.05$; $^*P < 0.05$; $^{**}P < 0.01$; and $^{***}P < 0.001$, by Student's t test (**A**–**C**) or Kruskal-Wallis ANOVA with Dunn's post hoc tests (**D**).

Acknowledgments

This work was supported by European Research Council 2010 Starting Independent (260524 to G.T. Stathopoulos) and 2009 Advanced (233074 to H.R. Rodewald) Investigator Grants, by a Hellenic Thoracic Society 2012 Research Award (to A.D. Giannou and G.T. Stathopoulos), by European Respiratory Society 2009 Maurizio Vignola and 2013 Romain Pauwels Research Awards (to G.T. Stathopoulos), by a 2013 European Respiratory Society Long Term Research Fellowship (1824 to I. Psallidas), by a Thorax Foundation (Athens, Greece) 2006 Fellowship (to G.T. Stathopoulos), by US NIH (HL61419) and VA Merit Review Grants (to T.S. Blackwell), and by Ruprecht-Karls-University Heidelberg SFB 938 Project L (to H.R. Rodewald). The authors thank the University of Patras Center for Animal Models of Disease and Advanced Light Microscopy Core for experimental support, Panagiota Stamou and Alexandros Spiridonidis for flow cytometry support, Charis Roussos and Androniki Kollintza for insightful discussions, and Georgia Papaspyrou for editorial assistance.

Address correspondence to: Georgios T. Stathopoulos or Antonia Marazioti, Faculty of Medicine, University of Patras, 1 Asklepiou Street, University Campus, 26504 Rio, Greece. Phone: 30.2610.969154; E-mail: gstathop@upatras.gr (G.T. Stathopoulos); amarazioti@upatras.gr (A. Marazioti).

1. Hanahan D, Weinberg RA. Hallmarks of cancer: the next generation. *Cell*. 2011;144(5):646–674.
2. Swamy M, Jamora C, Havran W, Hayday A. Epithelial decision makers: in search of the 'epimmunome'. *Nat Immunol*. 2010;11(8):656–665.
3. Coussens LM, Pollard JW. Leukocytes in mammary development and cancer. *Cold Spring Harb Perspect Biol*. 2011;3(3):a003285.
4. Floor SL, Dumont JE, Maenhaut C, Raspe E. Hallmarks of cancer: of all cancer cells, all the time? *Trends Mol Med*. 2012;18(9):509–515.
5. Balkwill FR, Mantovani A. Cancer-related inflammation: common themes and therapeutic opportunities. *Semin Cancer Biol*. 2012;22(1):33–40.
6. Soucek L, Lawlor ER, Soto D, Shchors K, Swigart LB, Evan GI. Mast cells are required for angiogenesis and macroscopic expansion of Myc-induced pancreatic islet tumors. *Nat Med*. 2007;13(10):1211–1218.
7. Theoharides TC. Mast cells and pancreatic cancer. *N Engl J Med*. 2008;358(17):1860–1861.
8. Galli SJ, Kalesnikoff J, Grimbaldeston MA, Piliponsky AM, Williams CM, Tsai M. Mast cells as "tunable" effector and immunoregulatory cells: recent advances. *Annu Rev Immunol*. 2005;23:749–786.
9. Theoharides TC, Kempuraj D, Tagen M, Conti P, Kalogeromitros D. Differential release of mast cell mediators and the pathogenesis of inflammation. *Immunol Rev*. 2007;217:65–78.
10. Chen R, et al. Mast cells play a key role in neutrophil recruitment in experimental bullous pemphigoid. *J Clin Invest*. 2001;108(8):1151–1158.
11. Blair RJ, et al. Human mast cells stimulate vascular tube formation. Tryptase is a novel, potent angiogenic factor. *J Clin Invest*. 1997;99(11):2691–2700.
12. Sinnamon MJ, Carter KJ, Sims LP, Lafleur B, Fingleton B, Matrisian LM. A protective role of mast cells in intestinal tumorigenesis. *Carcinogenesis*. 2008;29(4):880–886.
13. Dalton DK, Noelle RJ. The roles of mast cells in anticancer immunity. *Cancer Immunol Immunother*. 2012;61(9):1511–1520.
14. Pittoni P, Colombo MP. The dark side of mast cell-targeted therapy in prostate cancer. *Cancer Res*. 2012;72(4):831–835.
15. Feyerabend TB, et al. Cre-mediated cell ablation contests mast cell contribution in models of antibody- and T cell-mediated autoimmunity. *Immunity*. 2011;35(5):832–844.
16. Dudeck A, et al. Mast cells are key promoters of contact allergy that mediate the adjuvant effects of haptens. *Immunity*. 2011;34(6):973–984.
17. Roberts ME, Neville E, Berrisford RG, Antunes G, Ali NJ. Management of a malignant pleural effusion: British Thoracic Society Pleural Disease Guideline 2010. *Thorax*. 2010; 65(suppl 2):ii32–ii40.
18. Ryu JS, et al. Prognostic impact of minimal pleural effusion in non-small-cell lung cancer. *J Clin Oncol*. 2014;32(9):960–967.
19. Burgers JA, Kunst PW, Koolen MG, Willems LN, Burgers JS, van den Heuvel M. Pleural drainage and pleurodesis: implementation of guidelines in four hospitals. *Eur Respir J*. 2008;32(5):1321–1327.
20. Davies HE, Lee YC. Management of malignant pleural effusions: questions that need answers. *Curr Opin Pulm Med*. 2013;19(4):374–379.
21. Postmus PE, et al. The IASLC Lung Cancer Staging Project: proposals for revision of the M descriptors in the forthcoming (seventh) edition of the TNM classification of lung cancer. *J Thorac Oncol*. 2007;2(8):686–693.
22. Wu SG, et al. Survival of lung adenocarcinoma patients with malignant pleural effusion. *Eur Respir J*. 2013;41(6):1409–1418.
23. Stathopoulos GT, Kalomenidis I. Malignant pleural effusion: tumor-host interactions unleashed. *Am J Respir Crit Care Med*. 2012;186(6):487–492.
24. Marazioti A, Blackwell TS, Stathopoulos GT. The lymphatic system in malignant pleural effusion. Drain or immune switch? *Am J Respir Crit Care Med*. 2014;189(6):626–627.
25. Stathopoulos GT, et al. A central role for tumor-derived monocyte chemoattractant protein-1 in malignant pleural effusion. *J Natl Cancer Inst*. 2008;100(20):1464–1476.
26. Stathopoulos GT, et al. Host derived interleukin-5 promotes adenocarcinoma-induced malignantpleural effusion. *Am J Respir Crit Care Med*. 2010;182(10):1273–1281.
27. Murdoch C, Muthana M, Coffelt SB, Lewis CE. The role of myeloid cells in the promotion of tumour angiogenesis. *Nat Rev Cancer*. 2008;8(8):618–631.
28. Ema H, et al. Adult mouse hematopoietic stem cells: purification and single-cell assays. *Nat Protoc*. 2006;1(6):2979–2987.
29. Brickshawana A, Shapiro VS, Kita H, Pease LR. Lineage(–)Sca1+c-Kit(–)CD25+ cells are IL-33-responsive type 2 innate cells in the mouse bone marrow. *J Immunol*. 2011;187(11):5795–5804.
30. Tono T, et al. c-kit Gene was not transcribed in cultured mast cells of mast cell-deficient Wsh/Wsh mice that have a normal number of erythrocytes and a normal c-kit coding region. *Blood*. 1992;80(6):1448–1453.
31. Okayama Y, Kawakami T. Development, migration, and survival of mast cells. *Immunol Res*. 2006;34(2):97–115.
32. Muzumdar MD, Tasic B, Miyamichi K, Li L, Luo L. A global double-fluorescent Cre reporter mouse. *Genesis*. 2007;45(9):593–605.
33. Cao YA, et al. Shifting foci of hematopoiesis during reconstitution from single stem cells. *Proc Natl Acad Sci U S A*. 2004;101(1):221–226.
34. Okabe M, Ikawa M, Kominami K, Nakanishi T, Nishimune Y. 'Green mice' as a source of ubiquitous green cells. *FEBS Lett*. 1997;407(3):313–319.
35. Chen J, et al. Adoptive transfer of syngeneic bone marrow-derived cells in mice with obesity-induced diabetes: selenoorganic antioxidant ebselen restores stem cell competence. *Am J Pathol*. 2009;174(2):701–711.
36. Kitaura J, et al. IgE– and IgE+Ag-mediated mast cell migration in an autocrine/paracrine fashion. *Blood*. 2005;105(8):3222–3229.
37. Tsui P, et al. Generation, characterization and biological activity of CCL2 (MCP-1/JE) and CCL12 (MCP-5) specific antibodies. *Hum Antibodies*. 2007;16(3-4):117–125.
38. Marazioti A, et al. Beneficial impact of CCL2 and CCL12 neutralization on experimental malignant pleural effusion. *PLoS One*. 2013;8(8):e71207.
39. Wolters PJ, et al. Tissue-selective mast cell reconstitution and differential lung gene expression in mast cell-deficient Kit(W-sh)/Kit(W-sh) sash mice. *Clin Exp Allergy*. 2005;35(1):82–88.
40. Yamazaki M, et al. C-kit gene is expressed by skin mast cells in embryos but not in puppies of Wsh/Wsh mice: age-dependent abolishment of c-kit gene expression. *Blood*. 1994;83(12):3509–3516.
41. Clausen BE, Burkhardt C, Reith W, Renkawitz R, Förster I. Conditional gene targeting in macrophages and granulocytes using LysMcre mice. *Transgenic Res*. 1999;8(4):265–277.
42. Voehringer D, Liang HE, Locksley RM. Homeostasis and effector function of lymphopenia-induced "memory-like" T cells in constitutively T cell-depleted mice. *J Immunol*. 2008;180(7):4742–4753.
43. Psallidas I, et al. Secreted phosphoprotein-1 directly provokes vascular leakage to fos-

ter malignant pleural effusion. *Oncogene*. 2013;32(4):528–535.
44. Horai R, et al. Production of mice deficient in genes for interleukin (IL)-1α, IL-1β, IL-1α/β, and IL-1 receptor antagonist shows that IL-1β is crucial in turpentine-induced fever development and glucocorticoid secretion. *J Exp Med*. 1998;187(9):1463–1475.
45. Ling J, et al. KrasG12D-induced IKK2/β/NF-κB activation by IL-1α and p62 feedforward loops is required for development of pancreatic ductal adenocarcinoma. *Cancer Cell*. 2012;21(1):105–120.
46. Greten FR, et al. IKKβ links inflammation and tumorigenesis in a mouse model of colitis-associated cancer. *Cell*. 2004;118(3):285–296.
47. Stathopoulos GT, et al. Nuclear factor-κB affects tumor progression in a mouse model of malignant pleural effusion. *Am J Respir Cell Mol Biol*. 2006;34(2):142–150.
48. Stathopoulos GT, et al. Tumor necrosis factor-α promotes malignant pleural effusion. *Cancer Res*. 2007;67(20):9825–9834.
49. Chen CC, Grimbaldeston MA, Tsai M, Weissman IL, Galli SJ. Identification of mast cell progenitors in adult mice. *Proc Natl Acad Sci U S A*. 2005;102(32):11408–11413.
50. Maaninka K, Lappalainen J, Kovanen PT. Human mast cells arise from a common circulating progenitor. *J Allergy Clin Immunol*. 2013;132(2):463–469.
51. Zhang Y, Ramos BF, Jakschik BA. Augmentation of reverse arthus reaction by mast cells in mice. *J Clin Invest*. 1991;88(3):841–846.
52. Tilley SL, Wagoner VA, Salvatore CA, Jacobson MA, Koller BH. Adenosine and inosine increase cutaneous vasopermeability by activating A(3) receptors on mast cells. *J Clin Invest*. 2000;105(3):361–367.
53. Prieto-García A, et al. Mast cell restricted mouse and human tryptase·heparin complexes hinder thrombin-induced coagulation of plasma and the generation of fibrin by proteolytically destroying fibrinogen. *J Biol Chem*. 2012;287(11):7834–7844.
54. DiDonato JA, Mercurio F, Karin M. NF-κB and the link between inflammation and cancer. *Immunol Rev*. 2012;246(1):379–400.
55. Dong G, Chen Z, Kato T, Van Waes C. The host environment promotes the constitutive activation of nuclear factor-κB and proinflammatory cytokine expression during metastatic tumor progression of murine squamous cell carcinoma. *Cancer Res*. 1999;59(14):3495–3504.
56. Nakamura Y, Franchi L, Kambe N, Meng G, Strober W, Núñez G. Critical role for mast cells in interleukin-1β-driven skin inflammation associated with an activating mutation in the nlrp3 protein. *Immunity*. 2012;37(1):85–95.
57. Yeh HH, Lai WW, Chen HH, Liu HS, Su WC. Autocrine IL-6-induced Stat3 activation contributes to the pathogenesis of lung adenocarcinoma and malignant pleural effusion. *Oncogene*. 2006;25(31):4300–4309.
58. Fujiwara M, Ishida Y, Nimura N, Toyama A, Kinoshita T. Postcolumn fluorometric detection system for liquid chromatographic analysis of amino and imino acids using o-phthalaldehyde/N-acetyl-L-cysteine reagent. *Anal Biochem*. 1987;166(1):72–78.
59. Faul F, Erdfelder E, Lang AG, Buchner A. G*Power 3: A flexible statistical power analysis program for the social, behavioral, and biomedical sciences. *Behavior Research Methods*. 2007;39(2):175–191.

Supplemental Information

A requirement for mast cells in malignant pleural effusion

Anastasios D. Giannou, Antonia Marazioti, Magda Spella, Hara Apostolopoulou, Nikolaos I. Kanellakis, Ioannis Psallidas, Zeljko M. Prijovich, Malamati Vreka, Dimitra E. Zazara, Ioannis Lilis, Vassilios Papaleonidopoulos, Chrysoula A. Kairi, Alexandra L. Patmanidi, Ioanna Giopanou, Nikolitsa Spiropoulou, Vaggelis Harokopos, Vassilis Aidinis, Dionisios Spyratos, Stamatia Teliousi, Helen Papadaki, Stavros Taraviras, Linda A. Snyder, Oliver Eickelberg, Dimitrios Kardamakis, Yoichiro Iwakura, Thorsten B. Feyerabend, Hans-Reimer Rodewald, Ioannis Kalomenidis, Timothy S. Blackwell, Theodora Agalioti, and Georgios T. Stathopoulos.

SUPPLEMENTAL TABLES

Table S1, related to Figure 2A. Transcripts overrepresented in Lewis lung carcinoma and MC38 colon adenocarcinoma cells compared with B16F10 melanoma cells. Mean adenocarcinoma/melanoma differential gene expression (*Δ*GE) from two independent microarray analyses of cancer cell global gene expression using mouse gene ST 1.0 and 2.0 (mGST1, mGST2). Gene symbols in red font were further examined in this study.

Gene symbol	Gene name	*Δ*GE mGST1	*Δ*GE mGST2	*Δ*GE mean
Ptgs2	prostaglandin-endoperoxide synthase 2	33.47	103.66	68.57
Ly6a	lymphocyte antigen 6 complex, locus A	36.90	94.30	65.60
Spp1	secreted phosphoprotein 1	59.60	45.21	52.41
S100a6	S100 calcium binding protein A6 (calcyclin)	51.29	46.96	49.12
Ccl2	chemokine (C-C motif) ligand 2	26.57	67.39	46.98
Nid1	nidogen 1	13.06	58.03	35.54
Ly6e	lymphocyte antigen 6 complex, locus E	58.51	10.84	34.68
Pla2g7	phospholipase A2, group VII	31.15	38.05	34.60
Hist1h1b	histone cluster 1, H1b	15.49	48.03	31.76
Apobec3	apolipoprotein B mRNA editing enzyme, catalytic polypeptide 3	12.73	44.27	28.50
Pxdn	peroxidasin homolog (Drosophila)	28.80	27.28	28.04
Prrx1	paired related homeobox 1	21.03	33.06	27.05
Il1r1	interleukin 1 receptor, type I	15.31	37.87	26.59
Stambpl1	STAM binding protein like 1	13.83	36.92	25.37
Gatm	glycine amidinotransferase	33.03	17.37	25.20
Emp2	epithelial membrane protein 2	14.39	35.95	25.17
F2r	coagulation factor II (thrombin) receptor	16.63	31.87	24.25
Apcdd1	adenomatosis polyposis coli down-regulated 1	27.54	19.60	23.57
S100a4	S100 calcium binding protein A4	23.03	17.71	20.37
Bgn	biglycan	15.76	23.72	19.74
Gpr149	G protein-coupled receptor 149	13.98	24.02	19.00
Dkk2	dickkopf homolog 2 (Xenopus laevis)	15.47	22.21	18.84
Ptgs1	prostaglandin-endoperoxide synthase 1	23.60	12.62	18.11
Vcam1	vascular cell adhesion molecule 1	13.17	22.29	17.73
Htra1	HtrA serine peptidase 1	15.10	19.14	17.12
Vcan	versican	17.54	16.38	16.96
Ptges	prostaglandin E synthase	22.57	11.30	16.94
Ptprn	protein tyrosine phosphatase, receptor type, N	15.34	17.36	16.35
Slc14a1	solute carrier family 14 (urea transporter), member 1	15.75	16.84	16.30
Hspb8	heat shock protein 8	13.59	18.37	15.98
Dhrs9	dehydrogenase/reductase (SDR fam.) memb. 9	14.08	17.60	15.84
Flnc	filamin C, gamma	12.76	18.19	15.48
Flrt2	fibronectin leucine rich transmembrane protein 2	12.92	17.57	15.25
Ltbp1	latent TGF beta binding protein 1	13.04	16.78	14.91
Thbs2	thrombospondin 2	17.49	10.14	13.82
Itga3	integrin alpha 3	11.91	14.58	13.25
Axl	AXL receptor tyrosine kinase	13.74	11.02	12.38
Il18rap	interleukin 18 receptor accessory protein	11.32	11.23	11.28
Kcnn	potassium intermediate/small conductance calcium-activated channel, subf. N, member 4	10.60	11.04	10.82

Table S2, related to Figure 2A. Transcripts overrepresented in B16F10 melanoma cells compared with Lewis lung carcinoma and MC38 colon adenocarcinoma cells. Mean melanoma/adenocarcinoma differential gene expression (*Δ*GE) from two independent microarray analyses of cancer cell global gene expression using mouse gene ST 1.0 and 2.0 (mGST1, mGST2).

Gene symbol	Gene name	*Δ*GE mGST1	*Δ*GE mGST2	*Δ*GE mean
Tyrp1	tyrosinase-related protein 1	211.95	139.32	175.64
Dct	dopachrome tautomerase	199.29	131.38	165.33
Pmel	silver	96.20	128.08	112.14
Slc45a2	solute carrier family 45, member 2	87.47	50.22	68.84
Syt4	synaptotagmin IV	63.58	74.06	68.82
Mlana	melan-A	61.03	59.64	60.34
Plagl1	pleiomorphic adenoma gene-like 1	67.68	24.95	46.31
Glrb	glycine receptor, beta subunit	37.91	47.74	42.83
Vgll3	vestigial like 3 (Drosophila)	47.77	18.13	32.95
Bace2	beta-site APP-cleaving enzyme 2	26.74	38.56	32.65
Rab38	RAB38, member of RAS oncogene family	38.95	24.84	31.90
Gjc3	gap junction protein, gamma 3	10.27	47.33	28.80
Rasgrp3	RAS, guanyl releasing protein 3	20.02	36.00	28.00
Tyr	tyrosinase	11.24	40.94	26.09
Cdh19	cadherin 19, type 2	19.26	31.69	25.48
Ankfn1	ankyrin-repeat and fibronectin type III domain1	22.89	25.59	24.24
Gpm6a	glycoprotein m6a	25.34	22.18	23.76
Mc1r	melanocortin 1 receptor	19.61	27.20	23.40
Nrcam	neuron-glia-CAM-related cell adhesion molecule	16.74	27.25	22.00
Dmxl2	Dmx-like 2	15.19	28.54	21.87
Fndc3c1	fibronectin type III domain containing 3C1	18.97	24.11	21.54
Tspan10	tetraspanin 10	13.11	29.05	21.08
Itga4	integrin alpha 4	27.07	12.76	19.91
Sytl2	synaptotagmin-like 2	14.59	21.37	17.98
Prkcq	protein kinase C, theta	23.21	12.60	17.91
Pde11a	phosphodiesterase 11A	18.16	17.40	17.78
Lama4	laminin, alpha 4	21.39	14.07	17.73
Tspan6	tetraspanin 6	10.81	24.13	17.47
Slc35f1	solute carrier family 35, member F1	21.65	12.41	17.03
Robo1	roundabout homolog 1 (Drosophila)	10.17	21.77	15.97
Rab27a	RAB27A, member RAS oncogene family	11.22	19.91	15.56
Tspan12	tetraspanin 12	15.54	13.68	14.61
Mcoln3	mucolipin 3	11.06	17.64	14.35
Mlph	melanophilin	10.55	17.92	14.24
Sirpa	signal-regulatory protein alpha	15.21	13.16	14.19
4932411E22Rik	RIKEN cDNA 4932411E22 gene	10.45	17.31	13.88
Cntfr	ciliary neurotrophic factor receptor	11.17	16.30	13.73
Cyp2j6	cytochrome P450, fam. 2, subf. j, polypept. 6	10.58	16.31	13.44
Myo7a	myosin VIIA	11.47	15.32	13.39
Ckb	creatine kinase, brain	10.06	16.41	13.24
Pax3	paired box gene 3	12.38	13.53	12.95
Pkia	protein kinase inhibitor, alpha	12.14	13.11	12.63
Snca	synuclein, alpha	10.28	14.94	12.61
Chchd10	coiled-coil-helix-coiled-coil-helix domain 10	11.81	12.79	12.30
Gpr143	G protein-coupled receptor 143	13.21	11.27	12.24
Nr4a3	nuclear receptor subfamily 4, gr. A, member 3	13.22	10.47	11.84
Dock3	dedicator of cyto-kinesis 3	12.19	10.77	11.48
C530028O21Rik	RIKEN cDNA C530028O21 gene	10.69	12.23	11.46
Plp1	proteolipid protein (myelin) 1	11.00	10.32	10.66
Erbb3	v-erb-b2 erythroblastic leukemia viral oncogene 3	10.63	10.22	10.43

Table S3, related to Figure 5A. Transcripts significantly induced or suppressed in bone marrow-derived mast cells by Lewis lung adenocarcinoma-conditioned media. Differential gene expression (*Δ*GE) between Lewis lung carcinoma (LLC)-conditioned media-treated BMMC and non-conditioned media (DMEM)-treated BMMC (n = 2) assessed by microarray (mouse Gene ST2.0, Affymetrix, Sta.Clara, CA). A positive *Δ*GE indicates induction and a negative *Δ*GE suppression by adenocarcinoma-conditioned media. Selected cut-offs were $P < .05$ and ΔGE > 2.

Gene symbol	Gene name	P[a]	xΔGE[b]
Cd68	CD68 antigen	0.034	+5.70
Tnfrsf9	tumor necrosis factor receptor superfamily, member 9	0.010	+4.28
Il1b	interleukin 1 beta	0.027	+4.00
Gm19585	predicted gene, 19585	0.019	+3.58
Tpsab1	tryptase alpha/beta 1	0.040	+3.48
Gzmc	granzyme C	0.022	+3.18
F11r	F11 receptor	0.045	+2.83
Gm14047	predicted gene 14047	0.003	+2.48
LOC73899|LOC100503558	uncharacterized LOC73899|LOC100503558	0.009	+2.38
Tpm4	tropomyosin 4	0.036	+2.37
Eno2	enolase 2, gamma neuronal	0.040	+2.24
Klf10	Kruppel-like factor 10	0.019	+2.13
Ebi3	Epstein-Barr virus induced gene 3	0.033	+2.11
Ifitm1	interferon induced transmembrane protein 1	0.019	+2.01
Fdps	farnesyl diphosphate synthetase	0.016	-2.23
Sc4mol	sterol-C4-methyl oxidase-like	0.016	-2.25
Insig1	insulin induced gene 1	0.028	-3.13

[a]*P*, Paired Student's t-test probability value; [b] *Δ*GE, difference in gene expression between BMMC treated with LLC-conditioned media and BMMC treated with non-conditioned media. Gene symbols in ***bold*** type were induced in an adenocarcinoma-restricted fashion. *Tnfrsf9* was induced by all tumor-conditioned media.

Table S4, related to Figure 5A. Transcripts significantly induced or suppressed in bone marrow-derived mast cells by MC38 colon adenocarcinoma-conditioned media. Differential (>2-fold) gene expression (*Δ*GE) between MC38 colon adenocarcinoma-conditioned media-treated BMMC and non-conditioned media (DMEM)-treated BMMC (n = 2) assessed by microarray (mouse Gene ST2.0, Affymetrix, Sta.Clara, CA). A positive *Δ*GE indicates induction and a negative *Δ*GE suppression by adenocarcinoma-conditioned media.

Gene symbol	Gene name	P[a]	xΔGE[b]
Tnfrsf9	tumor necrosis factor receptor superfamily, member 9	0.033	+4.19
Cd68	CD68 antigen	0.020	+3.86
Tpsab1	tryptase alpha/beta 1	0.045	+3.47
Pde7b	phosphodiesterase 7B	0.046	+2.44
Gm19585	predicted gene, 19585	0.012	+2.27
Il1b	interleukin 1 beta	0.047	+2.20
Mrgprb13	MAS-related GPR, member B13	0.001	-2.06

[a]*P*, Paired Student's t-test probability value; [b] *Δ*GE, difference in gene expression between BMMC treated with MC38-conditioned media and BMMC treated with non-conditioned media. Gene symbols in ***bold*** type were induced in an adenocarcinoma-restricted fashion. *Tnfrsf9* was induced by all tumor-conditioned media.

Table S5, related to Figure 5A. Transcripts significantly induced or suppressed in bone marrow-derived mast cells by B16F10 melanoma-conditioned media. Differential (>2-fold) gene expression (*Δ*GE) between B16F10 melanoma-conditioned media-treated BMMC and non-conditioned media (DMEM)-treated BMMC (n = 2) assessed by microarray (mouse Gene ST2.0, Affymetrix, Sta.Clara, CA). A positive *Δ*GE indicates induction and a negative *Δ*GE suppression by adenocarcinoma-conditioned media.

Gene symbol	Gene name	P[a]	xΔGE[b]
Tnfrsf9	tumor necrosis factor receptor superfamily, member 9	0.019	+4.19
Procr	protein C receptor, endothelial	0.036	+2.41
Adssl1	adenylosuccinate synthetase like 1	0.045	+2.13
Nox1	NADPH oxidase 1	0.0004	+2.09

[a]*P*, Paired Student's t-test probability value; [b] *Δ*GE, difference in gene expression between BMMC treated with B16F10-conditioned media and BMMC treated with non-conditioned media. Gene symbols in ***bold*** type were induced in an adenocarcinoma-restricted fashion. *Tnfrsf9* was induced by all tumor-conditioned media.

Table S6, related to Methods. Antibodies used for these studies

Method[a]	Target	Provider[b]	Catalog #	Dilution	Conjugate[c]
IF, FC	cKIT	eBioscience	12-1171-83	1:200, 0.1 µg/10^6 cells	PE
IF	CD68	AbD Serotec	MCA1957 A488T	1:100	FITC
IF	IL-1β	Abcam	ab9722	1:100	-
HIS, IF	PCNA	Abcam	ab2426	1:2000, 1:200	-
IF	GFP	Santa Cruz	sc-8334	1:200	-
FC	Sca1	Biolegend	108106	0.1 µg/10^6 cells	FITC
FC	Lin (CD3ε)	eBioscience	13-0031-82	0.1 µg/10^6 cells	biotin followed by streptavidin-APC or streptavidin-PerCP
FC	Lin (B220)	eBioscience	13-0452-82	0.1 µg/10^6 cells	
FC	Lin (CD11b)	eBioscience	13-0112-82	0.1 µg/10^6 cells	
FC	Lin (TER-119)	Biolegend	116204	0.1 µg/10^6 cells	
FC	Lin (CD19)	eBioscience	13-0191-85	0.1 µg/10^6 cells	
FC	Lin (Gr1)	eBioscience	13-5931-82	0.1 µg/10^6 cells	
FC	Lin (CD8a)	eBioscience	13-0081-85	0.1 µg/10^6 cells	
FC	CD25	eBioscience	12-0251	0.1 µg/10^6 cells	PerCP
FC	CD45	Biolegend	103116	0.1 µg/10^6 cells	APC-Cy7
FC	F4/80	Biolegend	123128	0.1 µg/10^6 cells	PerCP
FC	CD11b	eBioscience	12-0112-82	0.1 µg/10^6 cells	PE
FC	CD11c	eBioscience	17-0114-82	0.1 µg/10^6 cells	APC
WIB	GFP	Santa Cruz	sc-9996	1:500	-
WIB	RelA	Santa Cruz	sc-372-G	1:500	-
WIB	IκBα	Santa Cruz	sc-371	1:500	-
WIB	β-actin	Santa Cruz	sc-47778	1:500	-
WIB	RelB	Cell Signaling	4954	1:1000	-
WIB	IKKα	Cell Signaling	2682	1:1000	-
WIB	IKKβ	Cell Signaling	2684	1:1000	-
WIB	histone 3	Cell Signaling	9175	1:1000	-
WIB	Rabbit anti-goat IgG	Santa Cruz	sc-2922	1:5000	HRP
WIB	Goat anti-rabbit IgG	Southern Biotech	4030-05	1:8000	HRP
WIB	Goat anti-mouse IgG		1030-05	1:8000	HRP
IF	donkey anti-rabbit & anti-mouse IgG	Invitrogen	A21206 A21202	1:1000	Alexa 488
IF	donkey anti-rabbit & anti-mouse IgG	Invitrogen	A10042 A10037	1:1000	Alexa 568

[a]Application: HIS, histology; IF, immunofluorescence; FC, flow cytometry; WIB, Western immunoblotting.
[b]Providers*:* eBioscience, San Diego, CA; AbD Serotec, Kidlington, UK; Abcam, Cambridge, UK; Santa Cruz Biotechnology, San Diego, CA; Cell Signaling, Danvers, MA; Southern Biotech, Birmingham, AL; Invitrogen, Carlsbad, CA.
[c]Conjugates*:* FITC, fluorescein isothiocyanate; PE, phycoerythrin; PerCP, peridinin-chlorophyll protein; APC, allophycocyanin; HRP, horse radish peroxidase.

Table S7, related to Methods. PCR primers used for these studies

Method[a]	Primer	Sequence	Amplicon length
qPCR	*GusbF*	TTACTTTAAGACGCTGATCACC	165 bp
qPCR	*GusbR*	ACCTCCAAATGCCCATAGTC	
qPCR	*Cd68F*	GACCTACATCAGAGCCCGAG	90 bp
qPCR	*Cd68R*	GAATGTCCACTGTGCTGCCT	
qPCR	*Tpsab1F*	TGCTGAAACTCACAAACCCT	139 bp
qPCR	*Tpsab1R*	GGCAGGTTTACACCATTGTC	
qPCR	*Il1bF*	TTTGACAGTGATGAGAATGACC	162 bp
qPCR	*Il1bR*	AATGAGTGATACTGCCTGCC	
qPCR	*Il1r1F*	TGGAAGTCTTGTGTGCCCTT	150 bp
qPCR	*Il1r1R*	GCCACATTCCTCACCAACAG	
qPCR	*NfkbiaF*	AGCAAATGGTGAAGGAGCTG	112 bp
qPCR	*NfkbiaR*	AAGTGCAGGAACGAGTCTCC	
qPCR	*NfkbibF*	CTGAACCTGAGGACGAGGAC	115 bp
qPCR	*NfkbibR*	GTTGTCGGTTTTGGCTCCTG	
qPCR	*ChukF*	AACCAGCCTCTCAGTGTGTT	106 bp
qPCR	*ChukR*	CTGGATGCAAATGGTCCTTCA	
qPCR	*IkbkbF*	CAGTGCCTGTGACAGCTTAC	115 bp
qPCR	*IkbkbR*	TTGCTCCTTCACAGTGTCCT	
qPCR	*Ccl2F*	CTACAAGAGGATCACCAGCAG	145 bp
qPCR	*Ccl2R*	TTCTGATCTCATTTGGTTCCGA	
qPCR	*Cxcl5F*	AGGAGGTCTGTCTGGATCCA	117 bp
qPCR	*Cxcl5R*	CACTGGCCGTTCTTTCCAC	
qPCR	*Stat3F*	AATGGAAATTGCCCGGATCG	134 bp
qPCR	*Stat3R*	TCTGCTGCTTCTCTGTCACT	
qPCR	*MycF*	CTCGAGCTGTTTGAAGGCTG	138 bp
qPCR	*MycR*	CGCAGATGAAATAGGGCTGT	
qPCR	*Cdkn1aF*	TCTGAGCGGCCTGAAGATTC	133 bp
qPCR	*Cdkn1aR*	GGGCACTTCAGGGTTTTCTC	
qPCR	*Notch1F*	TGAAGAACGGAGCCAACAAG	147 bp
qPCR	*Notch1R*	GCAATCGGTCCATGTGATCC	
qPCR	*CrebbpF*	CAGTGAATCGCATGCAGGTTT	147 bp
qPCR	*CrebbpR*	GAACTGAGGCCATGCTGTTC	
qPCR	*Hdac1F*	ACGACGAATCCTATGAAGCCA	148 bp
qPCR	*Hdac1R*	GCGTGTCCTTTGATGGTCAG	
CL	*IkbkbF*	ATGAGCTGGTCACCGTCCCTCCCAACCC	2274 bp
CL	*IkbkbR*	TCAGTCACAGGCCTGCTCCAGGC	

[a]Application: RT, reverse transcriptase-polymerase chain reaction; qPCR, quantitative (real-time) PCR; CL, cloning;

SUPPLEMENTAL MOVIES

Supplemental Movie S1. Spontaneously moving bone marrow-derived mast cell from red fluorescent mouse (high power). BMMC were obtained from *mT/mG* mouse after 4 weeks of culture with interleukin-3 and KIT ligand, were placed in DMEM drops onto uncovered glass slides, and were observed using time-lapse fluorescence microscopy on a SP5 confocal microscope at magnification x 600 (Leica, Heidelberg, Germany).

Supplemental Movie S2. Spontaneously moving bone marrow-derived mast cells from red fluorescent mouse (low power). BMMC were obtained from *mT/mG* mouse after 4 weeks of culture with interleukin-3 and KIT ligand, were placed in DMEM drops onto uncovered glass slides, and were observed using time-lapse fluorescence microscopy on a SP5 confocal microscope at magnification x 400 (Leica, Heidelberg, Germany).

Supplemental Movie S3. Bone marrow-derived mast cell (BMMC) degranulation induced by recombinant mouse (rm) osteopontin (SPP1). BMMC were obtained from wild-type mice after 4 weeks of culture with interleukin-3 and KIT ligand, were placed in 50 μL DMEM drops onto uncovered glass slides, and were observed using time-lapse phase-contrast microscopy on a SP5 confocal microscope at magnification x 600 (Leica, Heidelberg, Germany). rmSPP1 was added (50 μl, 30 ng/ml) after 10 sec video time.

SUPPLEMENTAL METHODS

Reagents

Anti-mouse CCL2 and CCL12 neutralizing antibodies, as well as IgG2a control antibody were kindly provided by Oncology Discovery Research, Janssen R&D LLC (Spring House, PA) (37); rmCCL2 was from Peprotech (London, UK); rmIL-1β, rm IL-3, and rmKITL were from Immunotools (Friesoythe, Germany); rmSPP1 and rmTPSAB1 were from R&D Systems (Minneapolis, MN); C48/80 and Evans' blue were from Sigma-Aldrich (St. Louis, MO); and imatinib mesylate was from Selleckchem (Houston, TX).

Cells

LLC, B16F10, A549, and SKMEL2 cells (NCI Tumor Repository, Frederick, MD) and MC38 cells (gift from Dr. Barbara Fingleton, Vanderbilt University, Nashville, TN) (38) were cultured at 37^0C in 5% CO_2-95% air using DMEM supplemented with 10% FBS, 2 mM L-glutamine, 1 mM pyruvate, 100 U/ml penicillin, and 100 mg/ml streptomycin. Cell lines were tested biannually for identity (by the short tandem repeat method) and for *Mycoplasma Spp.* (by PCR). For *in vivo* injections, cells were harvested using trypsin, incubated with Trypan blue, counted as described elsewhere, and injected through a left intercostal space, as described elsewhere (25, 26, 38, 47, 48). Only 95% viable cells were used *in vivo*.

Animals

C57BL/6 (#000664), *cKit^{Wsh}* (#005051), *NOD/SCID* (#001303), *CAG.Luc.eGFP* (#008450), *CAG.eGFP* (#003291), *mT/mG* (#007676), *Lyz2.Cre* (Ref. 39; #004781), and *Dta* (Ref. 40; # 009669) mice from Jackson Laboratories (Bar Harbor, MN), as well as *Cpa3.Cre* (gift from Dr. Hans-Reimer Rodewald, Heidelberg, Germany) (15) and *Il1b-/-* mice (gift from Dr. Yoichiro Iwakura, Tokyo University of Science, Tokyo, Japan) (44), were bred at the Center for Animal Models of Disease of the University of Patras. Experiments were approved *a priori* by the local Veterinary Administration and were conducted according to Directive 2010/63/EU (http://eur-lex.europa.eu/LexUriServ/LexUriServ.do?uri=OJ:L:2010:276:0033:0079:EN:PDF). Experimental mice and littermate controls were sex-, weight (20-25 g)-, and age (6-12 week)-matched; both male and female mice were used.

Cancer models and drug treatments

For MPE generation, mice received 150,000 murine or 1,000,000 human cancer cells intrapleurally and were sacrificed after 14 or 30 days, respectively. For pleural lavage, 1 mL normal saline was injected intrapleurally and was withdrawn starting after 30 seconds waiting time. Both techniques are described elsewhere (25, 26, 38, 47, 48). Imatinib mesylate (1 mg/kg in 100 μL PBS) or PBS (100 μL) were given daily intraperitoneally. Anti-mouse CCL2, CCL12 (a murine CCL2 ortholog), and IgG2a control antibodies were delivered intraperitoneally at 50 mg/kg every three days (37, 38).

Human samples

Pleural fluid was obtained during diagnostic thoracenteses in patients with MPE due to lung cancer (n = 14), breast cancer (n = 6), and malignant pleural mesothelioma (n = 4), as well as patients with CHF treated at Institution #6 between January 2006 and December 2008. Detailed clinical, cytologic, biochemical, and biologic data were available for these patients, including a semi-quantitative radiologic score of their effusion size and aspirate measurements, within the framework of a large clinical protocol. Samples from Institutions #9 and #10 were diagnostic MPE cytologic specimens from 20 patients with lung adenocarcinoma aspirated between June and August 2013. Diagnosis and sample handling were done as described elsewhere (25, 26, 38, 47, 48). All protocols abided by the Helsinki Declaration, were approved *a priori* by the local hospital ethics committees and by all patients via written informed consent.

Cytology & histology

Pleural fluid cytocentrifugal specimens (5 x 10^4 cells each) and cells cultured on glass slides were fixed with 4% paraformaldehyde or with Mota's fixative (8% lead acetate, 4% glacial acetic acid, and 50% ethanol in distilled water) for 5 minutes and were stained with May-Gruenwald-Giemsa or toluidine blue (0.05% for 5-15 minutes). Alternatively, cells were labeled with the indicated antibodies (Supplemental Table S6) and counterstained with hematoxylin or Hoechst 33258 (Sigma-Aldrich, St. Louis, MO; dilution 1:5000) with or without MC granule-labeling avidin (Vector Labs, Burlingame, CA). Distinct cell types were enumerated as a percentage of 500 cells on the slide. For MC counting, 10,000 cells per slide were counted. For histology, lungs with pleural tumors or whole thoraces fixed in 4% paraformaldehyde overnight and desalted in EDTA for two weeks (only whole thoraces) were embedded in paraffin or in OCT (Sakura, Tokyo, Japan) and were stored at -80oC. 5-μm paraffin or 10-μm-cryosections were mounted on glass slides. Sections were stained with toluidine blue or labeled using the indicated antibodies (Supplemental Table S6) and counterstained with Hoechst 33258 or with the Envision color development system (Dako, Carpinteria, CA). Immunoreactivity was quantified as described previously (25, 26, 38, 47, 48). Bright-field and fluorescent microscopy were carried out using either an AxioObserver D1 (Zeiss, Jena, Germany) inverted microscope or an SP5 (Leica, Heidelberg, Germany) confocal microscope.

BMMC

Bone marrow cells were flushed from *C57BL/6*, *cKit^{Wsh}*, *CAG.Luc.eGFP*, *CAG.eGFP*, *mT/mG* and *Il1b-/-* femurs and tibias using full DMEM, and were simply cultured in full culture media (the same used for cancer cell line cultures), supplemented with rmIL-3 with or without rmKITL (100 ng/mL each). Non-adherent cells were passaged twice-weekly for four to six weeks, as described elsewhere (31).

Flow cytometry

After NH_4Cl red blood cell lysis, pleural cells or BMMC were suspended in PBS 2% FBS, stained with the indicated antibodies (Supplemental Table S6) for 20 minutes, fixed in 1 % paraformaldehyde for 10 minutes, analyzed on a FACSCalibur cytometer (BD Biosciences, Alameda, CA), and data were examined using FlowJo software (FlowJo, Ashland, OR).

Constructs & Transfections

For RNA interference, random (sh*C*), anti-*Ccl2* (sh*Ccl2*), or anti-*Spp1* (sh*Spp1*) shRNA 64-mers were cloned into the *pSuper.retro.puro* backbone (Oligoengine, Seattle, WA). shRNA sequences were AGCTTTTCCAAAAA-target-TCTCTTGAA-target reverse complement-GGG and target sequences were sh*C*: CTGTCTATCGAAGAATGGG; sh*Ccl2*: TGTGAAGTTGACCCGTAAA; and sh*Spp1* GCTTATGGACTGAGGTCAA (25, 41). The *Ccl2* and *β-gal* expression vectors have been described elsewhere (25). All new plasmids were deposited with Addgene (http://www.addgene.org/). A newly engineered pMIGR1-based (Addgene ID 27490) bicistronic retroviral expression vector was generated by replacing the eGFP sequences with the puromycin resistance gene (Addgene ID 58250). *Ikbkb* cDNA was cloned via RT-PCR from MC38 total RNA using specific primers (Supplemental Table S7) and was subcloned into peGFP-C1. *Egfp* and *Egfp.Ikbkb* cDNAs were subcloned into the new retroviral expression vector (Addgene ID's 58249 and 58251, respectively). Cells were transfected with 5 μg DNA by the standard calcium phosphate procedure and either studied transiently or stable clones were generated by puromycin selection.

Adoptive bone marrow transplants and bone marrow-derived mast cell transfer

For adoptive bone marrow replacement (Figures 5, A and B and 8E), mice received ten million intravenous bone marrow cells 12 hours after total-body irradiation (1100 Rad), as described elsewhere (35). One mouse in each experiment was not engrafted (sentinel) and was observed till moribund between days 5 and 15 post-irradiation. For adoptive BMMC transfer for purposes of MC pulse and chase studies (Figure 5), irradiated *C57BL/6* chimeras engrafted with *cKit^{Wsh}* bone marrow (39) received pleural tumor cells at day 30 post-transplant, followed by same-day 5 x 10^5 iv *CAG.Luc.eGFP* or *CAG.eGFP* BMMC, and *cKit^{Wsh}* mice without prior irradiation received 8 x 10^5 sc *CAG.Luc.eGFP* BMMC followed by next-day pleural tumor cells. For intrapleural BMMC delivery (Figure 8A), naïve *C57BL/6* mice received 10^5 intrapleural BMMC, with or without B16F10 cells. For functional BMMC give-back studies (Figure 11, G and H), *C57BL/6*, *cKit^{Wsh}*, and *Il1b-/-* mice received 2.5 x 10^5 sc BMMC.

Bioluminescence imaging

Cells and mice were serially imaged on a Xenogen Lumina II and data were analyzed using Living Image v.4.2 (Perkin-Elmer, Waltham, MA), after addition of 300 μg/mL D-luciferin to culture media or delivery of 1 mg intravenous D-luciferin (47, 48).

ELISA

CCL2, SPP1, IL-1β and IL-1α levels of cell culture supernatants, of cell-free MPE, and sera were determined using dedicated murine and human ELISA kits according to the manufacturer's instructions (Peprotech, London, UK and R&D, Minneapolis, MN).

Vascular Permeability Assays

Mice with MPE received i.v. 0.8 mg Evans' blue and were killed after one hour for determination of MPE levels of the albumin-binding dye (48). Intradermal injections of test molecules (1.5 ng/50 μL PBS), cell-free MPE (50 μL), or cancer cell-conditioned media (50 μL) performed at different spots of the shaved dorsal mouse skin were followed by immediate Evans' blue injections as above, euthanasia, skin inversion and imaging after one hour. The surface area of dye leak was determined using Fiji academic freeware (http://fiji.sc/Fiji), as described elsewhere (25).

Real-time qPCR, and microarray

RNA was isolated using Trizol (Invitrogen, Carlsbad, CA) followed by RNAeasy (Qiagen, Hilden, Germany), was reverse transcribed using Superscript III (Invitrogen), and qPCR was performed using SYBR Green Master Mix in a StepOnePlus cycler (Applied Biosystems, Carlsbad, CA). Reverse transcriptase-PCR primers are given in Supplemental Table S7. For microarray, cells cultured in triplicate independent wells for each cell line-condition were subjected to RNA extraction as above. Five μg pooled RNA was tested for RNA quality on an ABI2000 bioanalyzer (Agilent Technologies, Sta. Clara, CA), labeled, and hybridized to GeneChip Mouse Gene 1.0 or 2.0 ST arrays (Affymetrix, Sta. Clara, CA). For analysis, the Affymetrix Expression Console (parameters: annotation confidence, full; summarization method: iter-PLIER include DABG; background: PM-GCBG; normalization method: none) was used, followed by normalization of all arrays together using a Lowess multiarray algorithm. Intensity-dependent estimation of noise was used for statistical analysis of differential expression. Microarray data are available at the GEO database (http://www.ncbi.nlm.nih.gov/geo/; Accession ID: GSE58190).

Immunoblotting

Cells were lysed in radioimmunoprecipitation assay buffer [25mM Tris-HCl (pH 7.6), 150mM NaCl, 1% NP-40, 1% sodium deoxycholate, 0.1% SDS]. Nuclear and cytoplasmic extracts were prepared using the dedicated NE-PER kit (Thermo Scientific, Walthal, MA) and analyzed by 10% sodium dodecyl sulphate polyacrylamide gel electrophoresis followed by electroblotting to PVDF membranes (Millipore, Billerica, MA). Membranes were incubated with primary antibodies at the indicated concentrations followed by HRP-conjugated appropriate secondary antibodies (Supplemental Table S6), and were visualized by enhanced chemiluminescence (Millipore).

Cellular assays

Tumor cell proliferation in response to IL-1β or BMMC-CM was determined using MTT reduction (Promega, Madison, WI). Mast cell migration was studied in

Boyden chambers with 8.0 μm pore size (Millipore) using a method modified from Kitaura et al (36). Equal numbers of cancer cells were cultured in the lower and of bioluminescent BMMC in the upper chambers. After 48 hr the upper chambers were removed and the bioluminescent signal of transmigrated BMMC was measured using bioluminescent imaging. MC histamine content was measured by a microplate-adapted o-phthalaldehyde method (58). For this, BMMC exposed to various stimuli for varying time-intervals were lysed in ultrapure water by osmotic shock and six freeze-thaw cycles. O-phthalaldehyde was added and fluorescence was determined on a Victor 3 plate reader (Perkin Elmer, Waltham, MA) using specific parameters (excitation: 360 nm; emission: 450 nm). Glycine, which contains one -NH_2 group, was used for standard curve generation and histamine quantification. All cellular experiments were done at least thrice, while one representative experiment is shown.

Statistics

Sample size was calculated using power analysis on G*power academic freeware (59), assuming $\alpha = 0.05$, $\beta = 0.8$, and $\rho = 0.3$ (http://www.gpower.hhu.de/). No data were excluded from analysis. Animals were allocated to different treatments by alternation and transgenic animals were enrolled case-control-wise. Data were collected by at least two blinded investigators from samples coded by a non-blinded investigator. All data were examined for normality of distribution by Kolmogorov-Smirnof test. Normally and not normally distributed values are given as mean ± SD and median ± interquartile range, respectively. Sample size (n) always refers to biological and not technical replicates. Differences in means between two or multiple groups were examined, respectively, by two-tailed Student's t-test or one-way ANOVA with Bonferoni post-tests, and in medians between two or multiple groups by Mann-Whitney U-test or Kruskal-Wallis test with Dunn's post-tests, as appropriate. Two-way ANOVA with Bonferoni post-tests was employed for comparison of the effects of two parameters on outcome. Correlations were done using Pearson's R or Spearman's ρ, as appropriate. All P values are two-tailed and were considered significant when <.05. All statistical analyses were done and plots were created using Prism v5.0 (GraphPad, La Jolla, CA).

Study approval

All animal experiments were approved a priori by the Veterinary Administration of Western Greece according to a full and detailed protocol (approval # 276134/14873/2). Human studies were approved a priori by the Ethics Committee of the General Hospital of Athens Evangelismos (Athens, Greece; approval #379-7/12/2006 and extension #323-4/12/2012).

Immunoblots shown in Figure 13A. Dashed lines indicate blot areas shown in the main Figure.

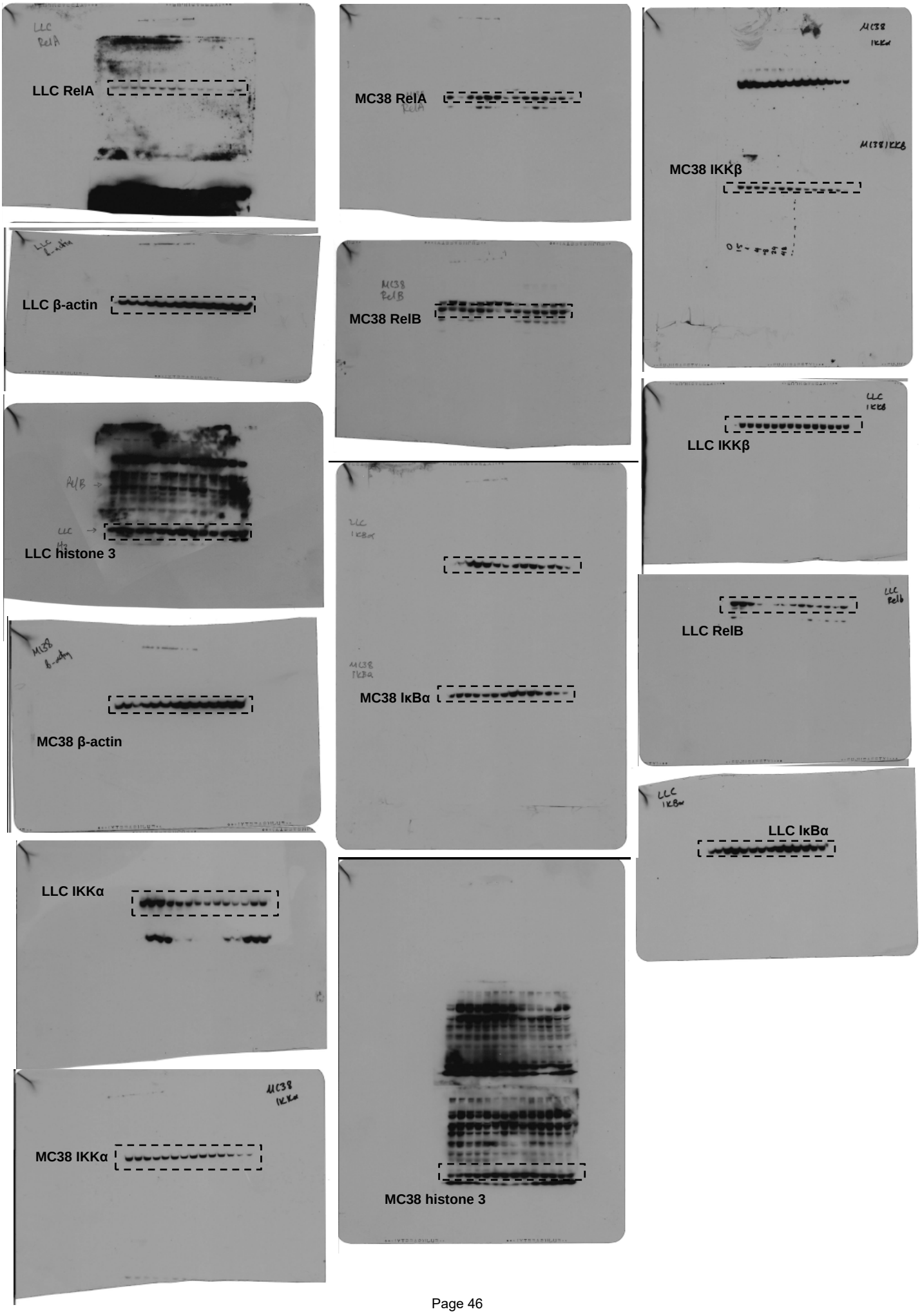

Immunoblots shown in Figure 13B. Dashed lines indicate blot areas shown in the main Figure.

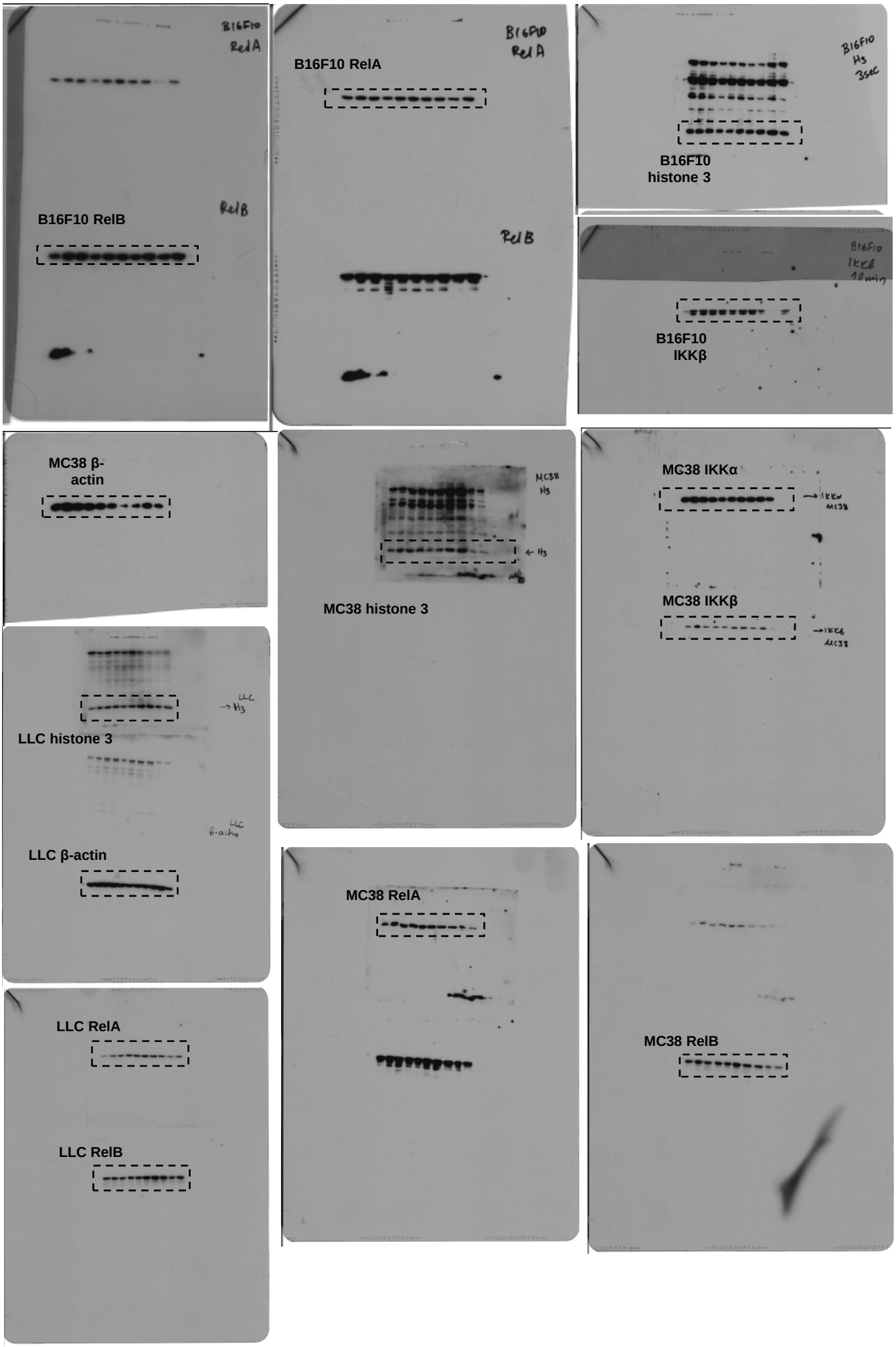

Immunoblots shown in Figure 13B continued. Dashed lines indicate blot areas shown in the main Figure.

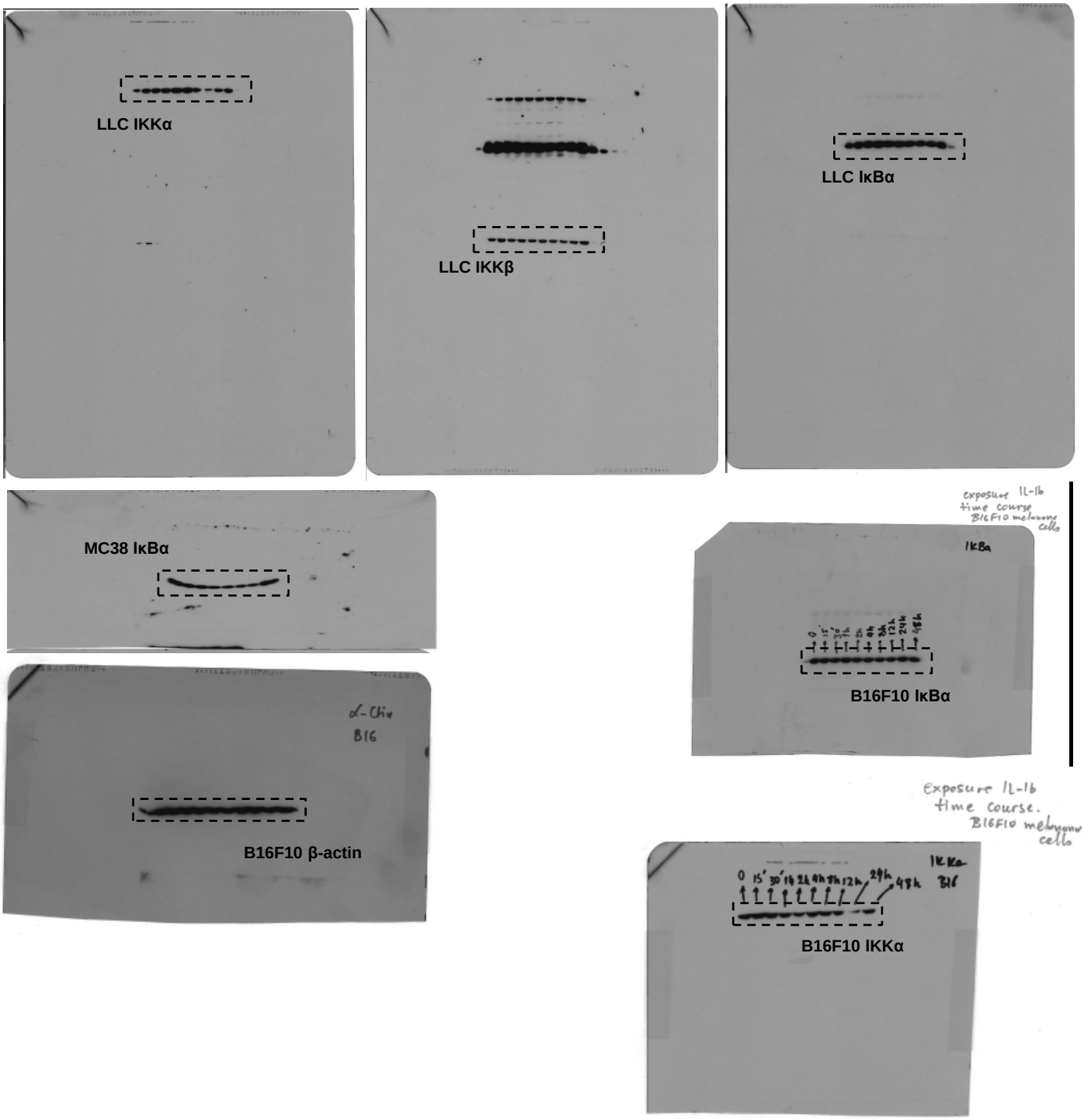

Immunoblots shown in Figure 14B. Dashed lines indicate blot areas shown in the main Figure.

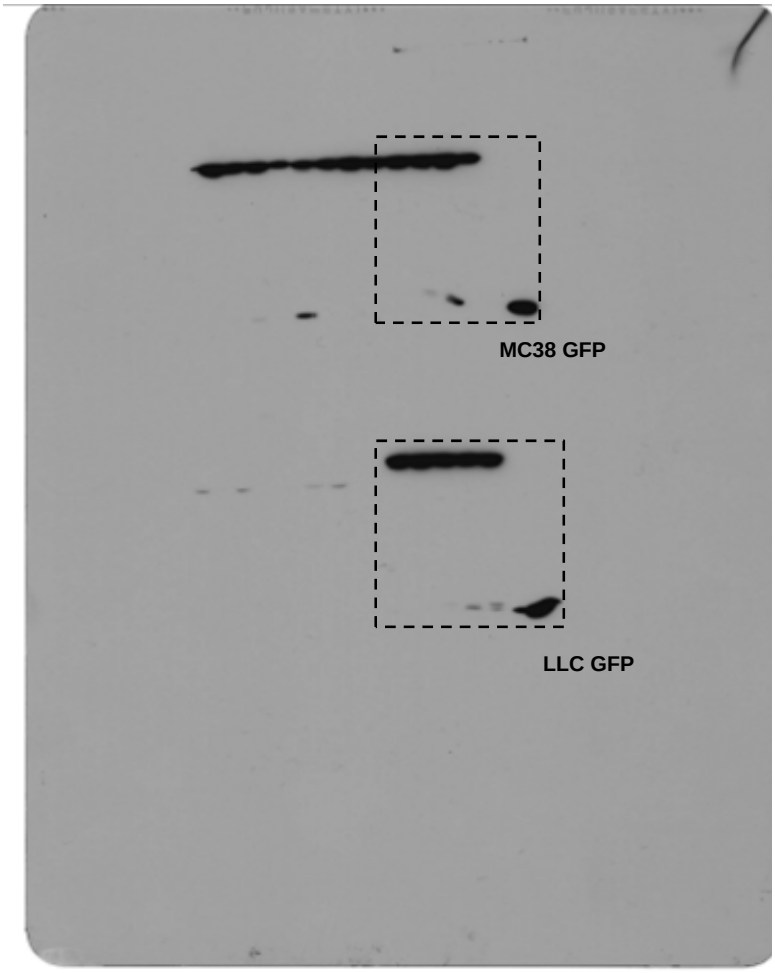

4. Publication II: Mutant KRAS promotes malignant pleural effusion formation.

4.1. Summary

The reason why some patients with pleural tumors develop MPE while others do not remains unknown (Ryu et al., 2014). This dichotomous phenotype of 'wet' pleural carcinomatosis associated with a MPE versus 'dry' pleural carcinomatosis without a MPE is critical, since patients with even minimal effusions face a worse prognosis and limited treatment options (Ryu et al., 2014; Wu et al., 2013). Our previous work on experimental mouse models of MPE revealed that pleural tumour-secreted C–C motif chemokine ligand 2 (CCL2) mediates MPE formation by stimulating angiogenesis and vascular leakage and by driving myeloid cells, including monocytes and mast cells, from the bone marrow to the pleural metastatic milieu (Stathopoulos et al., 2008; Marazioti et al., 2013; Giannou et al., 2015). However, the molecular culprits responsible for tumor cell CCL2 secretion and subsequent MPE precipitation remain unknown.

EGFR, *KRAS*, *PIK3CA*, *BRAF*, *MET*, *EML4/ALK*, *RET* and other mutations have been identified in pleural tumour biopsies and pleural fluid aspirates from MPE patients (Kimura et al., 2006; Wu et al., 2008; Han et al., 2011; Smits et al., 2012; Li et al., 2013; Kang et al., 2015; Tsai et al., 2012; Tsai et al., 2015). *EGFR* mutations were recently implicated in MPE development and patients with *KRAS*-mutant lung adenocarcinomas were found to have more frequent pleural metastases compared with wild-type ones (Roscilli et al., 2016; Tsai et al., 2015; Raparia et al., 2015; Renaud et al., 2016). However, no study has addressed the role of *KRAS* mutations in MPE development.

We hypothesized that the ability of a tumour cell to induce a MPE once it homes to the pleural space is linked with an underlying molecular signature. To test this and to model the biologic events that follow pleural metastasis, we determined the mutation status of multiple murine and human cancer cell lines and simultaneously tested their ability to induce MPE by directly injecting them into the pleural space of appropriate recipient mice. Here we show that mutant KRAS is important for MPE induction in mice. Pleural disseminated, mutant KRAS bearing tumor cells upregulate and systemically release chemokine ligand 2 (CCL2) into the bloodstream to mobilize myeloid cells from the host bone marrow to the pleural space via the spleen. These cells promote MPE formation, as indicated by splenectomy and splenocyte restoration experiments. In addition, KRAS mutations are frequently detected in human MPE and cell lines isolated thereof, but are often lost during automated analyses, as indicated by manual versus automated examination of Sanger sequencing traces. Finally, the novel KRAS inhibitor deltarasin and a monoclonal antibody directed against CCL2 are equally effective against an experimental mouse model of MPE, a result that holds promise for future efficient therapies against the human condition (Figure 2).

4.2. Contribution

The applicant conceived the main idea behind this study, performed preliminary proof-of-concept experiments using which he obtained funding for the study in the form of an ERC Starting Grant 2010, purchased the equipment required for the study and recruited the team that performed the experiments, designed all experiments, fostered the collaborations

reflected in the paper, analyzed the data, compiled graphs and figures, wrote the manuscript, submitted the manuscript for publication, and corresponded with *Nat Commun*.

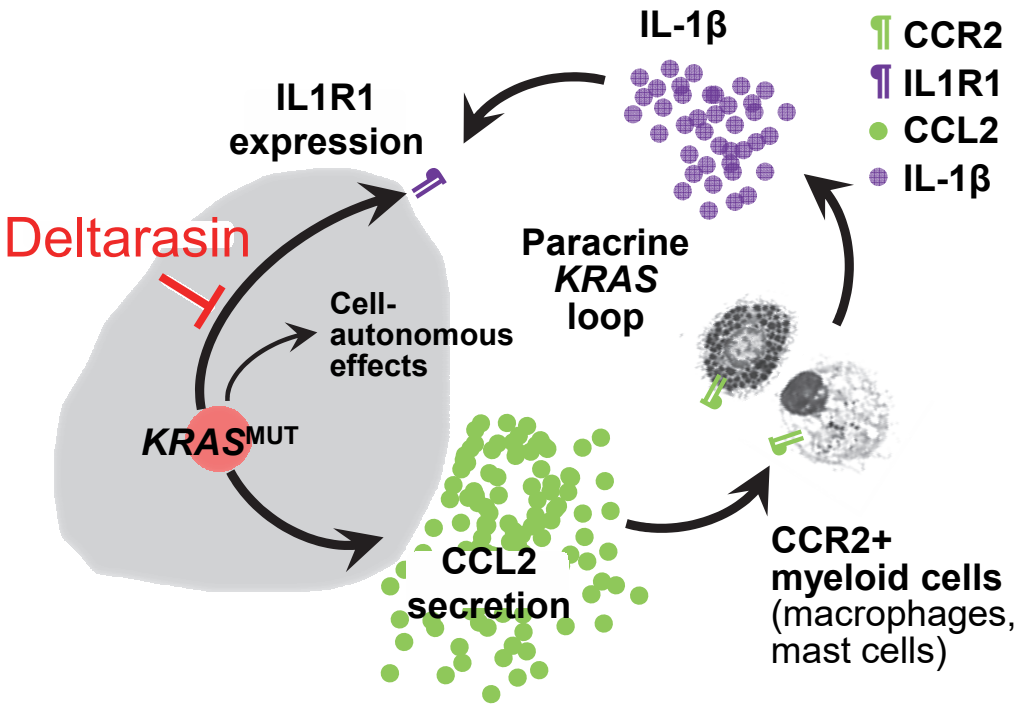

Figure 2. Graphical summary of publication II.

Graphical abstract of the proposed mechanism of in vivo restricted KRAS dependence via CCL2.

nature COMMUNICATIONS

4.3. Publication II

ARTICLE

Received 20 May 2016 | Accepted 8 Mar 2017 | Published 16 May 2017

DOI: 10.1038/ncomms15205 OPEN

Mutant *KRAS* promotes malignant pleural effusion formation

Theodora Agalioti[1,*], Anastasios D. Giannou[1,*], Anthi C. Krontira[1,*], Nikolaos I. Kanellakis[1,2], Danai Kati[1], Malamati Vreka[1,3], Mario Pepe[3], Magda Spella[1], Ioannis Lilis[1], Dimitra E. Zazara[1], Eirini Nikolouli[1], Nikolitsa Spiropoulou[1], Andreas Papadakis[1], Konstantina Papadia[4], Apostolos Voulgaridis[5], Vaggelis Harokopos[6], Panagiota Stamou[7], Silke Meiners[3], Oliver Eickelberg[3], Linda A. Snyder[8], Sophia G. Antimisiaris[4], Dimitrios Kardamakis[9], Ioannis Psallidas[1,2,**], Antonia Marazioti[1,**] & Georgios T. Stathopoulos[1,3,**]

Malignant pleural effusion (MPE) is the lethal consequence of various human cancers metastatic to the pleural cavity. However, the mechanisms responsible for the development of MPE are still obscure. Here we show that mutant *KRAS* is important for MPE induction in mice. Pleural disseminated, mutant *KRAS* bearing tumour cells upregulate and systemically release chemokine ligand 2 (CCL2) into the bloodstream to mobilize myeloid cells from the host bone marrow to the pleural space via the spleen. These cells promote MPE formation, as indicated by splenectomy and splenocyte restoration experiments. In addition, *KRAS* mutations are frequently detected in human MPE and cell lines isolated thereof, but are often lost during automated analyses, as indicated by manual versus automated examination of Sanger sequencing traces. Finally, the novel *KRAS* inhibitor deltarasin and a monoclonal antibody directed against CCL2 are equally effective against an experimental mouse model of MPE, a result that holds promise for future efficient therapies against the human condition.

[1] Laboratory for Molecular Respiratory Carcinogenesis, Department of Physiology, Faculty of Medicine, University of Patras, 26504 Rio, Greece. [2] Oxford Centre for Respiratory Medicine, Oxford University Hospitals NHS Trust, Churchill Hospital Old Road, Oxford OX3 7LE, UK. [3] Comprehensive Pneumology Center (CPC) and Institute for Lung Biology and Disease (iLBD), University Hospital, Ludwig-Maximilians University and Helmholtz Zentrum München, Member of the German Center for Lung Research (DZL), 81377 Munich, Germany. [4] Laboratory for Pharmaceutical Technology, Department of Pharmacy, School of Health Sciences, University of Patras, and Foundation for Research and Technology Hellas, Institute of Chemical Engineering, FORTH/ICE-HT, 26504 Rio, Greece. [5] Department of Pulmonary Medicine, Rio University Hospital, Faculty of Medicine, University of Patras, 26504 Rio, Greece. [6] Genomics Facility, Biomedical Sciences Research Center 'Alexander Fleming', Vari, Attica 16672, Greece. [7] Department of Hematology, Faculty of Medicine, University of Patras, Rio, Achaia 26504, Greece. [8] Oncology Discovery Research, Janssen R&D LLC, Spring House, Pennsylvania, 19477 USA. [9] Department of Radiation Oncology and Stereotactic Radiotherapy, Faculty of Medicine, University of Patras, 26504 Rio, Greece. * These authors contributed equally to this work. ** These authors jointly supervised this work. Correspondence and requests for materials should be addressed to G.T.S. (email: gstathop@upatras.gr).

The pleural cavities of two million cancer patients per year are affected by malignant pleural effusion (MPE), caused by primary malignant pleural mesothelioma or by metastatic cancers originating from the lung, breast, gastrointestinal tract or elsewhere[1]. MPE manifests with vascular leakiness that leads to fluid accumulation in the pleural space and is etiologically associated with fulminant inflammation and neovascularization, rather than mere tumour-induced lymphatic obstruction[2]. However, the reason why some patients with pleural tumours develop MPE while others do not remains unknown[3]. This dichotomous phenotype of 'wet' pleural carcinomatosis associated with a MPE versus 'dry' pleural carcinomatosis without a MPE is critical, since patients with even minimal effusions face a worse prognosis and limited treatment options[3,4]. Our previous work on experimental mouse models of MPE revealed that pleural tumour-secreted C–C motif chemokine ligand 2 (CCL2) mediates MPE formation by stimulating angiogenesis and vascular leakage and by driving myeloid cells, including monocytes and mast cells, from the bone marrow to the pleural metastatic milieu[5–7]. However, the molecular culprits responsible for tumour cell CCL2 secretion and subsequent MPE precipitation remain unknown.

EGFR, *KRAS*, *PIK3CA*, *BRAF*, *MET*, *EML4/ALK*, *RET* and other mutations have been identified in pleural tumour biopsies and pleural fluid aspirates from MPE patients[8–16]. *EGFR* mutations were recently implicated in MPE development and patients with *KRAS*-mutant lung adenocarcinomas were found to have more frequent pleural metastases compared with wild-type ones[17–19]. However, no study has addressed the role of *KRAS* mutations in MPE development.

We hypothesized that the ability of a tumour cell to induce a MPE once it homes to the pleural space is linked with an underlying molecular signature. To test this and to model the biologic events that follow pleural metastasis, we determined the mutation status of multiple murine and human cancer cell lines and simultaneously tested their ability to induce MPE by directly injecting them into the pleural space of appropriate recipient mice. Our results indicate that pleural homed cancer cells harboring activating *KRAS* mutations are competent of MPE induction. Moreover, we provide evidence that this genotype-phenotype link is primarily mediated via mutant *KRAS*-dependent CCL2 signalling that results in the recruitment of CD11b + Gr1 + myeloid cells to the pleural space, a phenomenon requiring intact splenic function. Importantly, we show that *KRAS* mutations are detectable in human MPE by careful analyses of Sanger sequencing traces and that mutant *KRAS*-mediated MPE is actionable.

Results

A link between *KRAS* mutations and MPE. To identify a possible MPE-associated genotype, we cross-examined five murine *C57BL/6*-derived and five human cancer cell lines for genotype and MPE competence. For this, we directly injected 1.5×10^5 mouse or 10^6 human tumour cells or 3×10^6 HEK293T benign human embryonic kidney cells into the pleural cavities of *C57BL/6* (mouse cells) or *NOD/SCID* (human cells) mice. In parallel, we Sanqer-sequenced the *Kras*, *Egfr*, *Pik3ca* and *Braf* transcripts of mouse cells after reverse-transcribing them to cDNAs and amplifying them with specific primers (Supplementary Table 1), and obtained mutation data for *KRAS*, *EGFR*, *PIK3CA* and *BRAF* genes of human cells from COSMIC[20]. *KRAS* mutations of human cells were also verified in-house. Among mouse cells, three *Kras*-mutant (Lewis lung carcinoma, LLC; MC38 colon adenocarcinoma; and AE17 malignant pleural mesothelioma, bearing heterozygous $Kras^{G12C}$, $Kras^{G13R}$, and $Kras^{G12C}$ mutations, respectively) and two *Kras* wild-type (B16F10 skin melanoma and PANO2 pancreatic adenocarcinoma) cell lines were identified, which were all free of additional mutations in *Egfr*, *Pik3ca* or *Braf* genes (Fig. 1a; Table 1). Among human cells, A549 lung adenocarcinoma cells and their derivatives, long-term passaged (LTP) A549 cells that have suffered Y chromosome loss, featured a heterozygous $KRAS^{G12S}$ mutation, while SKMEL2 skin melanoma, HT-29 colon adenocarcinoma, and HEK293T human embryonic kidney cells were *KRAS* wild-type (Table 1). These human cell lines also had wild-type *EGFR*, *PIK3CA* and *BRAF* genes, with the exception of HT-29 cells that harbor *BRAF* and *PIK3CA* mutations[20]. *KRAS*-mutant cell lines exhibited enhanced *KRAS* mRNA expression and RAS activity compared to *KRAS* wild-type cells (Supplementary Fig. 1a–d). Interestingly, upon pleural injection to appropriate hosts, all cell lines produced extensive pleural carcinomatosis, but exclusively *KRAS*-mutant cells gave rise to MPE (Fig. 1b–d; Table 1). To definitely test this in an isogenic cellular system, we derived lung adenocarcinoma cell lines from *C57BL/6* and *FVB* mice. For this, *C57BL/6* mice received ten and *FVB* mice four weekly intraperitoneal injections of the lung carcinogen urethane ($1\,g\,kg^{-1}$), as described elsewhere[21,22], and were killed after 10 months, followed by long-term lung tumour culture *in vitro*[23]. The resulting cell lines (*C57BL/6* and FVB-derived urethane-induced lung adenocarcinoma, CULA and FULA cells, respectively) were tumourigenic when implanted subcutaneously in syngeneic mice. Importantly, three different FULA cell lines had three different *Kras* mutations (including Q61H, Q61R and G12V mutations), while CULA cells were *Kras* wild-type (Fig. 1a; Table 1). In accordance with the results from existing cell lines, all *Kras*-mutant FULA cell lines were MPE-competent, while *Kras*-wild-type CULA cells were not (Fig. 1b–d; Table 1). In summary, out of the 12 different cell lines tested, six out of six *KRAS*-mutant cell lines were MPE-competent and none out of six MPE-incompetent, while none out of six *KRAS*-wild-type cell lines was MPE-competent, and six out of six MPE-incompetent ($P = 0.0022$; χ^2-test), indicating a statistically significant association between mutant *KRAS* and MPE.

Myeloid cells in mutant *KRAS*-dependent MPE. *Kras*-mutant tumour cell-triggered MPE was clinically important as mice with MPE succumbed significantly ($P < 0.0001$; log-rank test) earlier compared with mice with dry pleural carcinomatosis from *Kras*-wild-type cells (Supplementary Fig. 1e). In addition to early lethality, mutant *Kras*-dependent MPE development was associated with a massive influx of myeloid cells into the pleural space. This was investigated using irradiated *C57BL/6* chimeras reconstituted with luminescent bone marrow from ubiquitously luminescent *CAG.Luc.eGFP* donor mice fully backcrossed to the *C57BL/6* strain[6,7,24]. Fourteen days after pleural tumour cell injection, only chimeras injected with *Kras*-mutant tumour cells showed an increased thoracic bioluminescent signal (Supplementary Fig. 1f). This *KRAS*-dependent inflammatory response associated with MPE formation was predominated by both polymorphonuclear and mononuclear myeloid cells that expressed both CD11b and Gr1, and either Ly6c or Ly6g (Fig. 1e,f; Supplementary Figs 1g and 2a). MPE development triggered by *KRAS*-mutant cancer cells was associated with an influx of increased numbers of all kinds of myeloid cells into the pleural space, but not with the presence of newly-appearing morphologically or molecularly distinct cell types, since differential pleural cell counts and flow cytometry results were similar percentage-wise in mice with or without a MPE (Supplementary Fig. 2a). In addition to triggering a myeloid inflammatory response, *KRAS*-mutant pleural tumours and MPEs

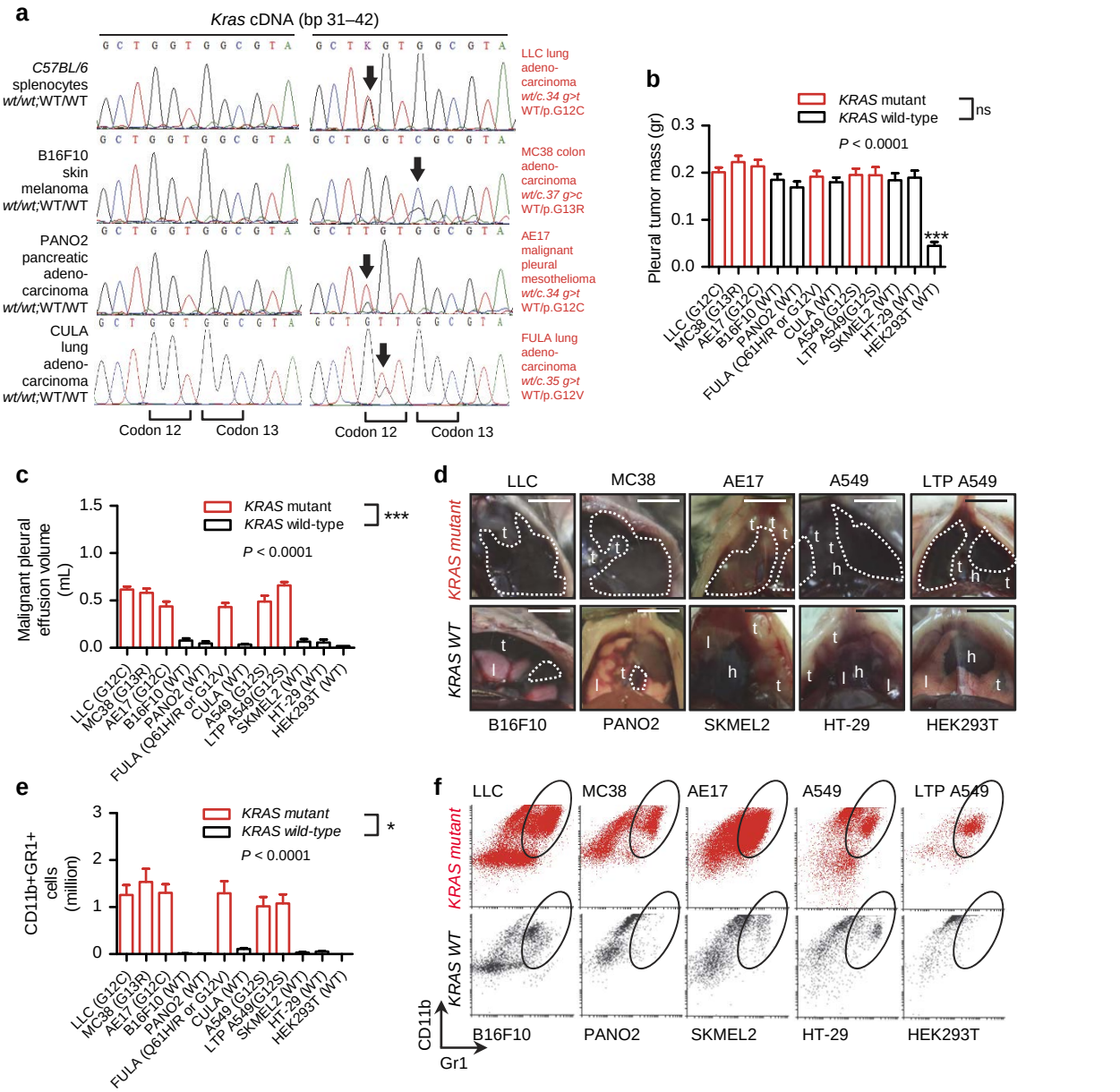

Figure 1 | Selective induction of malignant pleural effusions by *KRAS*-mutant tumour cells. Mutation status of and malignant pleural disease induction by twelve murine and human tumour cell lines after pleural delivery to appropriate recipient mice. (**a**) *Kras* cDNA Sanger sequencing traces of *C57BL/6* mouse splenocytes (control) and of five *C57BL/6* mouse tumour cell lines. Black arrows indicate heterozygous missense mutations in *Kras* codons 12 and 13. (**b**) Data summary of pleural tumor mass ($n = 53$, 26, 19, 30, 19, 27, 20, 16, 14, 14, 14, and 15, respectively, for LLC, MC38, AE17, B16F10, PANO2, FULA, CULA, A549, LTP A549, SKMEL2, HT-29, and HEK293T cells). (**c**) Data summary of malignant pleural effusion (MPE) volume ($n = 53$, 26, 19, 30, 19, 27, 20, 16, 14, 14, 14, and 15, respectively, for LLC, MC38, AE17, B16F10, PANO2, FULA, CULA, A549, LTP A549, SKMEL2, HT-29, and HEK293T cells). (**d**) Representative images of MPEs (dashed lines), pleural tumours (t), lungs (l), and hearts (h) imaged through the diaphragm. Scale bars, 1 cm. (**e**) Data summary of pleural CD11b + Gr1 + cells ($n = 5$–16 animals/group were analysed). (**f**) Representative dotplots and gating strategy for the quantification of pleural CD11b + Gr1 + cells. Data are presented as mean ± s.e.m. *P*, probability values for overall comparisons by one-way ANOVA. * and ***: $P < 0.05$ and $P < 0.001$ for the comparison between HEK293T cells and any other cell line (**b**) or for the comparison between any *Kras*-mutant and any *Kras*-wild-type cell line (**c**,**e**) by Bonferroni post-tests. *WT*, wild-type; LLC, *C57BL/6* Lewis lung carcinoma; MC38, *C57BL/6* colon adenocarcinoma; AE17, *C57BL/6* malignant pleural mesothelioma; B16F10, *C57BL/6* malignant skin melanoma; PANO2, *C57BL/6* pancreatic adenocarcinoma; FULA, *FVB* urethane-induced lung adenocarcinoma; CULA, *C57BL/6* urethane-induced lung adenocarcinoma; A549, human lung adenocarcinoma; LTP A549, long-term passaged A549 cells having lost the Y chromosome; SKMEL2, human malignant skin melanoma; HT-29, human colon adenocarcinoma; HEK293T, human embryonic kidney cells.

showed enhanced angiogenic and vasoactive potential in several *in vivo* assay systems compared with *KRAS*-wild-type tumours (Supplementary Fig. 2b–d). However, we did not detect an increased proliferative or clonogenic capacity specifically characterizing *KRAS*-mutant cells and tumours compared with *KRAS*-wild-type ones (Supplementary Fig. 2e–i). This was in accord with the equal total mass of pleural tumors per mouse observed across pleural-injected *KRAS*-mutant and wild-type tumour cells (Fig. 1b). Collectively, these results suggested that mutant *KRAS*-driven MPE is associated with induction of an inflammatory, angiogenic, and vasoactive response in the pleural space, but not necessarily with enhanced pleural tumour growth.

Table 1 | Incidence of murine malignant pleural effusions and mutation status of twelve tumour cell lines.

n = 265	MPE			*KRAS*	*EGFR*	*BRAF*	*PIK3CA*	*P value*
	No	Yes	%					
LLC	1	52	98	G12C	WT	WT	WT	0.0537
MC38	1	25	96	G13R	WT	WT	WT	0.2954
AE17	3	16	84	G12C	WT	WT	WT	1.0000
B16F10	24	6	20	WT	WT	WT	WT	0.000012
PANO2	18	1	5	WT	WT	WT	WT	0.00000064
FULA	3	24	89	G12V/Q61R/H	WT	WT	WT	0.6796
CULA	18	2	10	WT	WT	WT	WT	0.000003
A549	2	14	88	G12S	WT	WT	WT	1.0000
LTP A549	0	14	100	G12S	WT	WT	WT	0.2443
SKMEL2	13	1	7	WT	WT	WT	WT	0.000012
HT-29	13	1	7	WT	WT	V600E/T119S	P449T	0.000012
HEK293T	15	0	0	WT	WT	WT	WT	0.00000044

AE17, *C57BL/6* malignant pleural mesothelioma; A549, human lung adenocarcinoma; B16F10, *C57BL/6* malignant skin melanoma; CULA, *C57BL/6* urethane-induced lung adenocarcinoma; FULA, *FVB* urethane-induced lung adenocarcinoma; HT-29, human colon adenocarcinoma; HEK293T, human embryonic kidney cells; LLC, *C57BL/6* Lewis lung carcinoma; LTP A549, long-term passaged A549 cells having lost the Y chromosome; MC38, *C57BL/6* colon adenocarcinoma; PANO2, *C57BL/6* pancreatic adenocarcinoma; SKMEL2, human malignant skin melanoma; WT, wild-type. Shown is number of mice (*n*) that developed dry pleural carcinomatosis (no MPE; $<100\,\mu l$ pleural fluid) and number (*n*) and percentage (%) of mice that developed MPE ($\geq 100\,\mu l$ pleural fluid). $P<0.0001$ for overall comparison by χ^2-test. *P*, probability values for comparison with AE17 cells, the *KRAS*-mutant cell line with the lowest MPE incidence by Fischer's exact tests.

Mutant *KRAS* promotes MPE. To corroborate the link between *KRAS* mutations and MPE, we undertook both shRNA-mediated *KRAS* silencing in cell lines harboring mutant *KRAS*, as well as mutant *KRAS* overexpression in cell lines harboring wild-type *KRAS*. Stable transduction of six different *Kras*-mutant mouse tumour cells with lentiviral-delivered *Kras*-specific shRNA (sh*Kras*) resulted in diminished expression of both murine *Kras* isoforms (2A and 2B) and decreased RAS signalling compared with random (control, sh*C*) shRNA, whereas overexpression of mutant $Kras^{G12C}$ isoforms in murine and human cell lines carrying wild-type *KRAS* via retroviral transduction enhanced the respective KRAS protein levels and increased RAS signalling (Supplementary Fig. 3). Manipulation of *KRAS* signalling did not result in obvious enhancements of tumour cell proliferation or survival *in vitro*; on the contrary, overexpression of $Kras^{G12C}$2A in PANO2 cells and of $Kras^{G12C}$2B in B16F10 cells slowed their growth rate (Supplementary Fig. 4). However, upon direct inoculation of all parental and daughter *KRAS*-modulated cell lines into the pleural space of appropriate (*C57BL/6*, *FVB* or *NOD/SCID*) host mice, all mice developed similar extent of pleural carcinomatosis, but expression of mutant *KRAS* was a cardinal determinant of MPE in all cell lines examined (Fig. 2a,b; Table 2; Supplementary Fig. 5). More specifically, *Kras* silencing universally abrogated MPE formation by LLC, MC38, AE17 and three different FULA cell lines, that is, in cells harbouring either *KRAS* G12C (LLC & AE17 cells), G13R (MC38 cells), G12V, Q61H or Q61R (FULA cells) mutations, whereas oncogenic $Kras^{G12C}$ expression conferred MPE competence to B16F10, PANO2, SKMEL2, and HEK293T cells. Remarkably: (i) expression of $Kras^{G12C}$ isoform 2A conferred enhanced MPE competence to PANO2 cells compared with $Kras^{G12C}$ isoform 2B, although the later was more abundantly expressed by *KRAS*-mutant cancer cells; and (ii) mutant *KRAS* expression converted even benign HEK293T cells to MPE competence (Fig. 2a,b; Table 2; Supplementary Fig. 5). Using pleural injection of parental and *KRAS*-modulated MC38 and PANO2 cells into *C57BL/6* chimeras reconstituted with *CAG.Luc.eGFP* bone marrow, we identified that mutant *KRAS* is not only responsible for MPE development, but also for the associated pleural influx of CD11b + Gr1 + cells (Fig. 2c; Supplementary Fig. 5c,d). Taken together, these results indicated that mutant *KRAS* is dispensable for pleural tumour growth, but important for MPE development and for the associated systemic recruitment of CD11b + Gr1 + myeloid cells, and suggested that *KRAS* must be responsible for the secretion of a solute mediator of MPE by tumour cells.

***KRAS*-mutant tumour cells signal via CCL2 to host cells.** To identify the MPE mediator(s) downstream of mutant *KRAS* and to tease out the transcriptional signature of mutant *KRAS* on tumour cells, we performed comparative microarray-based transcriptome profiling of *Kras*-mutant and wild-type mouse tumour cells versus benign airway cells. Unsupervised clustering according to global gene expression revealed that *Kras*-mutant cell lines clustered closely together (Supplementary Fig. 6a). Individual gene analysis identified 25 transcripts overrepresented more than 10-fold in *KRAS*-mutant, but not in *KRAS*-wild-type, cell lines compared with benign cells (Fig. 3a; Table 3). Microarray results were verified by qPCR and ELISA (Fig. 3b; Supplementary Figs 6b,c). Furthermore: (i) manipulation of mutant *KRAS* expression resulted in parallel changes in *Ccl2* expression; (ii) cell culture media conditioned by *KRAS*-mutant tumour cells featured markedly elevated CCL2 levels compared with media conditioned by *KRAS*-wild-type tumour cells; and (iii) mice bearing in their pleural space *KRAS*-mutant tumour cells featured markedly elevated serum CCL2 levels compared with mice harbouring *KRAS*-wild-type tumour cells (Supplementary Fig. 6d–g). To corroborate CCL2 as the downstream effector of mutant *KRAS* that mediates MPE *in vivo*, we directly delivered LLC ($Kras^{G12C}$), MC38 ($Kras^{G13R}$), and PANO2 cells overexpressing $Kras^{G12C}$ isoform 2A into the pleural space of *Ccr2*-gene-deficient mice (*Ccr2* − / −; the gene encoding the cognate receptor of CCL2)[25] and *C57BL/6* controls. In accord with our hypothesis, *Ccr2* − / − mice were protected against MPE induced by all three *Kras*-mutant tumour cell lines and displayed reduced CCR2 expression by pleural fluid cells and decreased accumulation of CD11b + Gr1 + cells in the pleural space (Fig. 3c; Supplementary Fig. 6h,i). Collectively, these data suggest that mutant *KRAS* drives MPE development via systemic CCL2 signalling to CCR2 + host cells.

Mutant *KRAS* recruits splenic CD11b + Gr1 + cells to MPE. We next sought to identify the systemic recruitment patterns of myeloid cells during MPE development. For this, *C57BL/6* chimeras reconstituted with *CAG.Luc.eGFP* bone marrow were inoculated with *Kras*-mutant pleural tumour cells and were serially imaged for bioluminescence. Although immediately after pleural tumour cell delivery the myeloid-emitted bioluminescent signal was primarily identified over the hematopoietic bones, it sequentially translocated to the upper left abdomen (days 10–12 post-tumour cell injection) before appearing in the thorax at days

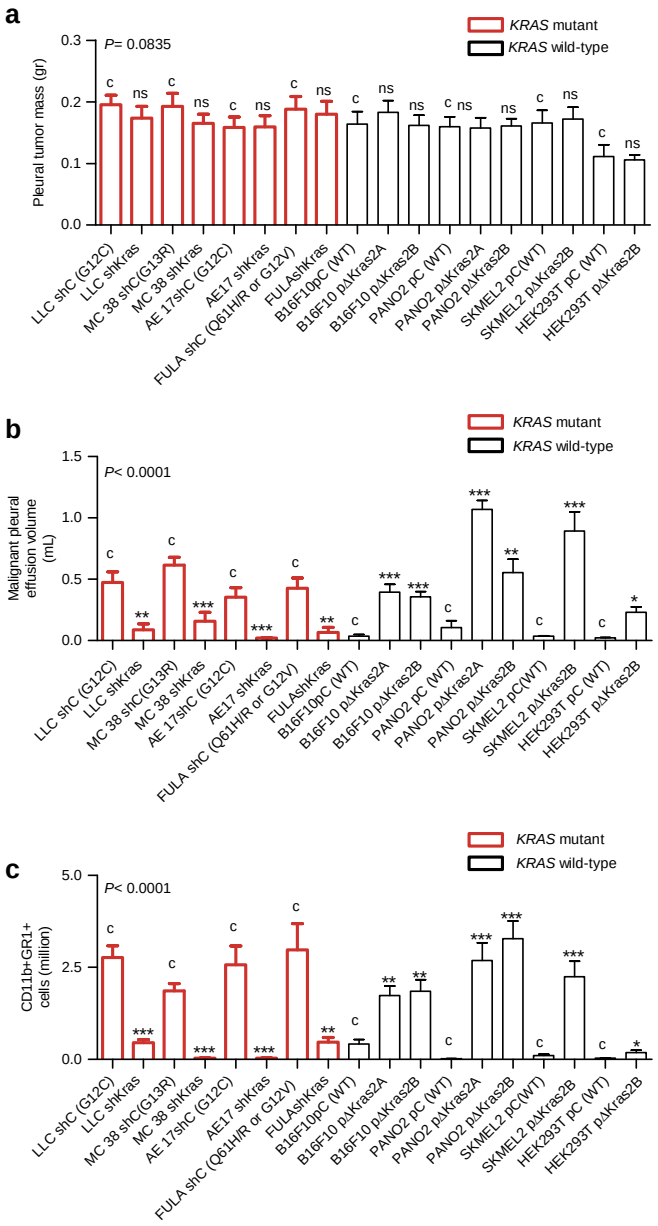

Figure 2 | Mutant *KRAS* promotes malignant pleural effusion development. Impact of shRNA-mediated *Kras* silencing on MPE competence of cell lines harboring mutant *Kras*, and of mutant $Kras^{G12C}$ overexpression in cell lines harboring wild-type *KRAS*. (**a**) Data summary of pleural tumor mass ($n=14, 12, 11, 14, 11, 11, 9, 9, 11, 10, 13, 16, 12, 16, 9, 10, 9$, and 9, respectively, for LLC sh*C*, LLC sh*Kras*, MC38 sh*C*, MC38 sh*Kras*, AE17 sh*C*, AE17 sh*Kras*, FULA sh*C*, FULA sh*Kras*, B16F10 p*C*, B16F10 p*ΔKras*2A, B16F10 p*ΔKras*2B, PANO2 p*C*, PANO2 p*ΔKras*2A, PANO2 p*ΔKras*2B, SKMEL2 p*C*, SKMEL2 p*ΔKras*2B, HEK293T p*C*, and HEK293T p*ΔKras*2B cells). (**b**) Data summary of MPE volume ($n=14, 12, 11, 14, 11, 11, 9, 9, 11, 10, 13, 16, 12, 16, 9, 10, 9$, and 9, respectively, for LLC sh*C*, LLC sh*Kras*, MC38 sh*C*, MC38 sh*Kras*, AE17 sh*C*, AE17 sh*Kras*, FULA sh*C*, FULA sh*Kras*, B16F10 p*C*, B16F10 p*ΔKras*2A, B16F10 p*ΔKras*2B, PANO2 p*C*, PANO2 p*ΔKras*2A, PANO2 p*ΔKras*2B, SKMEL2 p*C*, SKMEL2 p*ΔKras*2B, HEK293T p*C*, and HEK293T p*ΔKras*2B cells). (**c**) Data summary of pleural CD11b + Gr1 + cells ($n=7$–11/group were analysed). Data are presented as mean ± s.e.m. *P*, probability values for overall comparisons by one-way ANOVA. ns, *, **, and ***: $P>0.05$, $P<0.05$, $P<0.01$, and $P<0.001$ for the comparison between the indicated cell line and the respective control (**c**) by Student's t-test or one-way ANOVA with Bonferroni post-tests, as appropriate. *WT*, wild-type; sh*C*, random shRNA; sh*Kras*, anti-*Kras*-specific shRNA; p*C*, control (empty) overexpression vector; p*ΔKras*2A and p*ΔKras*2B, overexpression vectors encoding mutant mouse $Kras^{G12C}$ isoforms A and B, respectively; *WT*, wild-type; LLC, *C57BL/6* Lewis lung carcinoma; MC38, *C57BL/6* colon adenocarcinoma; AE17, *C57BL/6* malignant pleural mesothelioma; B16F10, *C57BL/6* malignant skin melanoma; PANO2, *C57BL/6* pancreatic adenocarcinoma; FULA, *FVB* urethane-induced lung adenocarcinoma; SKMEL2, human malignant skin melanoma; HEK293T, human embryonic kidney cells.

12–14 post tumour cell injection (Supplementary Fig. 7a). Splenectomy abolished this abdominal myeloid-borne signal that was recapitulated from explanted spleens (Fig. 3d). In addition, CCR2 + CD68 + myeloid cells were identified in the splenic marginal zones and the pleural cavities of mice with MPE induced by *KRAS*-mutant cells, but not of naive mice (Supplementary Fig. 7b). These results suggested that CD11b + Gr1 + myeloid cells are mobilized by mutant *KRAS*-driven CCL2-mediated signalling from the bone marrow to MPE via the spleen. On the basis of this evidence and the existing literature[26–28], we hypothesized that the splenic passage of CD11b + Gr1 + cells is essential for MPE formation. To test

Table 2 | Incidence of malignant pleural effusions caused by parental and *KRAS* -modulated tumour cell lines.

n = 206	MPE			*P value*
	no	yes	%	
LLC shC (G12C)	3	11	79	c
LLC sh*Kras*	10	2	17	0.0048
MC38 shC (G13R)	0	11	100	C
MC38 sh*Kras*	10	4	29	0.0005
AE17 shC (G12C)	1	10	91	c
AE17 sh*Kras*	11	0	0	<0.0001
FULA shC (G12V, Q61R/H)	1	8	89	c
FULA sh*Kras*	8	1	11	0.0034
B16F10 pC (WT)	10	1	9	c
B16F10 p*ΔKras*2A	0	10	100	<0.0001
B16F10 p*ΔKras*2B	1	12	92	<0.0001
PANO2 pC (WT)	14	2	13	c
PANO2 p*ΔKras*2A	0	12	100	<0.0001
PANO2 p*ΔKras*2B	4	12	75	0.0010
SKMEL2 pC (WT)	9	0	0	c
SKMEL2 p*ΔKras*2B	2	8	80	0.0007
HEK293T pC (WT)	9	0	0	c
HEK293T p*ΔKras*2B	2	7	78	0.0023

AE17, *C57BL/6* malignant pleural mesothelioma; B16F10, *C57BL/6* malignant skin melanoma; FULA, *FVB* urethane-induced lung adenocarcinoma; HEK293T, human embryonic kidney cells; LLC, *C57BL/6* Lewis lung carcinoma; MC38, *C57BL/6* colon adenocarcinoma; PANO2, *C57BL/6* pancreatic adenocarcinoma; SKMEL2, human malignant skin melanoma; WT, wild-type.
Shown is number of mice (*n*) that developed dry pleural carcinomatosis (no MPE; <100 μl pleural fluid) and number (*n*) and percentage (%) of mice that developed MPE (≥100 μl pleural fluid).
$P<0.0001$ for overall comparison by χ^2 test. *P*, probability values for comparison with parental control cells (c) by Fischer's exact tests.

this, we delivered MC38 cells ($Kras^{G13R}$) or PANO2 cells expressing mutant $Kras^{G12C}$ isoform 2A or 2B to the pleural cavities of splenectomized and sham-operated *C57BL/6* mice after allowing two weeks for recovery. Indeed, splenectomy markedly protected *C57BL/6* mice from MPE, prolonged their survival, and prevented pleural accumulation of CD11b + Gr1 + myeloid cells (Fig. 3e; Supplementary Fig. 7c,d). Similarly, splenectomy protected *NOD/SCID* mice from A549-induced MPE ($KRAS^{G12S}$; Supplementary Fig. 7e), further suggesting that myeloid and not lymphoid splenic cells promote MPE in these lymphoid-deficient mice. Splenectomy-conferred protection was long-lived, as even mice collected 30 days post-tumour cell injection did not have MPE (Supplementary Fig. 7c). To address whether splenic CD11b + Gr1 + cells are required for MPE development, tumour-naive and tumour-bearing *CAG.Luc.eGFP* mice were used as splenocyte donors to splenectomized pleural MC38 ($Kras^{G13R}$)-bearing *C57BL/6* mice. These *CAG.Luc.eGFP* donors received pleural injections of saline (naive splenocyte), control shRNA-expressing MC38 cells (MC38 sh*C*-educated splenocyte) or *Kras* specific-shRNA expressing MC38 cells (MC38 sh*Kras*-educated splenocyte) and 13 days later, their spleens were collected and processed to single-cell suspensions. In parallel, splenectomized or sham-operated *C57BL/6* hosts received pleural MC38 cell injections. At post-injection day 9, splenectomized animals received five million intravenous splenocytes obtained from naive, sh*C* or sh*Kras* MC38-bearing donors whereas, at post-injection day 13, these mice were analysed for MPE incidence, volume, survival, and for Luc + CD11b + Gr1 + recruited pleural cells (derived from transplanted splenocytes). Interestingly, only splenocytes from donors inoculated with MC38 cells bearing intact mutant *KRAS* signalling were able to translocate to the pleura and promote MPE formation in splenectomized mice harbouring pleural MC38 cells (Supplementary Fig. 7f–h). Taken together, these results indicated that *KRAS*-mutant pleural tumours induce the sequential recruitment of CD11b + Gr1 + cells from the bone marrow to the spleen and into the pleural cavity. Furthermore, that during MPE formation, bone marrow-borne, splenic CD11b + Gr1 + cells are conditioned by solute mediators secreted by *KRAS*-mutant pleural tumours (possibly CCL2) and functionally contribute to MPE development.

***KRAS* mutations in human MPE**. We next Sanger-sequenced the *KRAS* transcripts of 12 human MPEs caused by metastatic lung adenocarcinomas according to established protocols[16]. Interestingly, *KRAS* mutations were present in numerous MPEs, but were not always readily detectable by automated Sanger sequencing trace analysis using BioEdit software[29], since mutant base traces were often hidden underneath wild-type traces superimposed by the other *KRAS* allele, or by tumour-infiltrating stromal cells (Fig. 4a,b; Table 4). We also analysed recently published data of the site of recurrence of 481 resected non-small cell lung cancers according to *KRAS* and *EGFR* mutation status, and found that *KRAS* mutations overall were highly significantly ($P<0.0001$; Fischer's exact test) associated with pleural recurrence (Table 4). We went on to derive cell lines from eight patients with lung adenocarcinoma-induced MPE that were initially tested *KRAS* wild-type. Interestingly, *KRAS* mutations were frequently identified in MPE cell lines initially tested
wild-type (Fig. 4c–e; Table 4). These results suggested that: (i) *KRAS* mutations are present in a substantial proportion of patients with lung adenocarcinoma-caused MPE in Europe; (ii) *KRAS* mutation frequency may be underestimated in MPE samples analysed automatically; and (iii) our observations in mice may also hold true in humans.

Targeting KRAS is effective against MPE development. To determine the potential efficacy of KRAS inhibition against MPE, the novel KRAS inhibitor deltarasin[30] was administered daily intraperitoneally at 15 mg kg^{-1}, side-by-side with a saline control treatment, to mice with established pleural tumours. For this, treatments commenced at day 4–14 post-mouse tumour cell injections and at day 14 post-human tumour cell injections to allow initial tumour implantation in the pleural space[6,7]. At day 13 after pleural injection of MC38 cells ($Kras^{G13R}$), deltarasin-treated *C57BL/6* mice developed fewer and smaller MPEs,

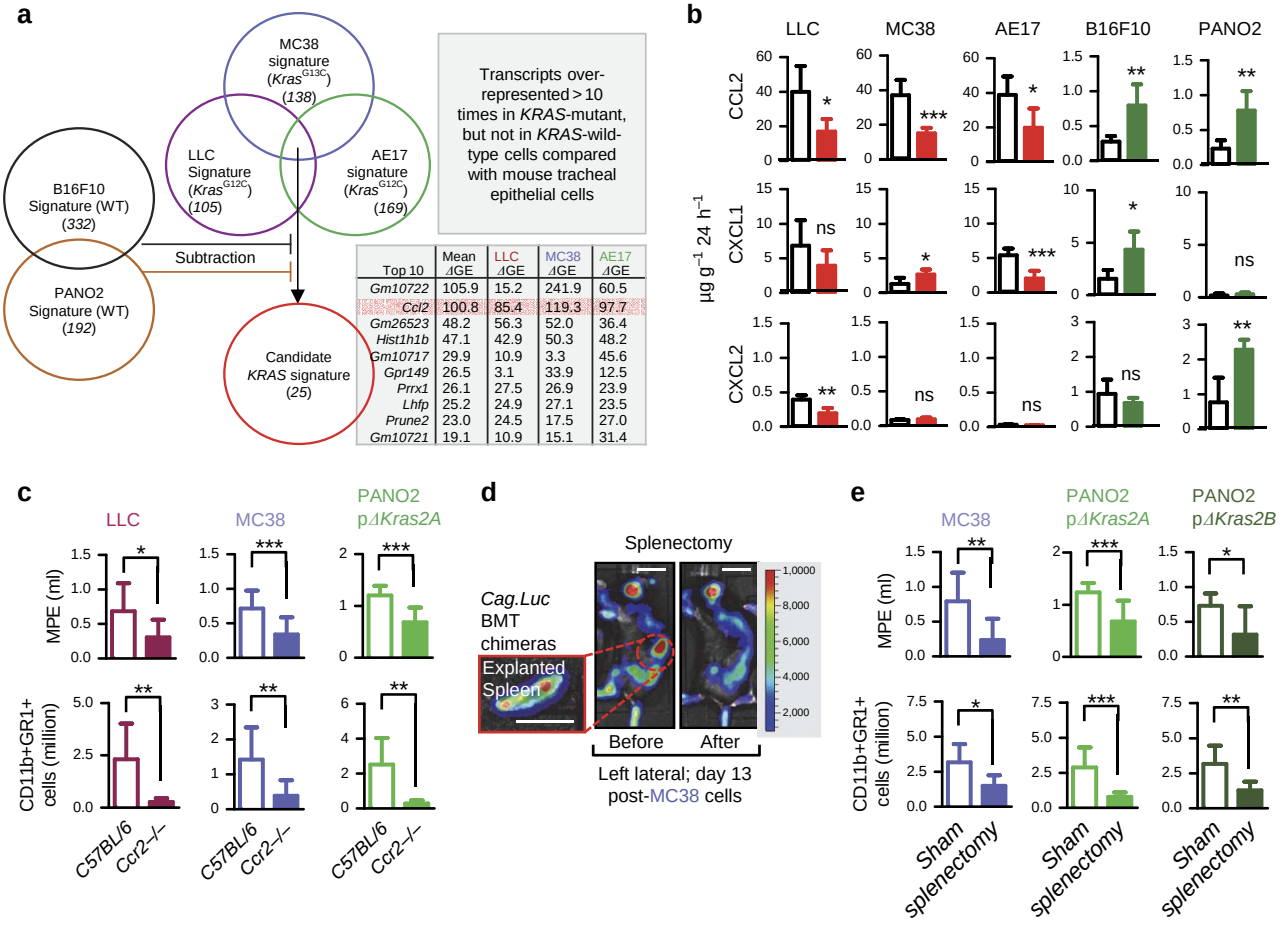

Figure 3 | Mutant *KRAS* signals via CCL2 to recruit splenic myeloid cells to malignant pleural effusions. (**a**) Comparative transcriptome analysis of mouse tumour cell lines with defined *Kras* mutation status versus benign airway epithelial cells by microarray. Diagram depicting the analytic strategy employed to identify the transcriptional signature of mutant *Kras* comprised of 25 genes (top ten shown in table), among which *Ccl2* ranked second. (**b**) Chemokine protein secretion by parental (white bars: cells stably expressing random shRNA or control overexpression vector) and *Kras*-modulated (red bars: cells stably expressing anti-*Kras*-specific shRNA; green bars: cells stably expressing vector encoding mutant mouse $Kras^{G12C}$ isoform B) murine cell lines by ELISA showing transcriptional regulation of CCL2, but not of CXCL1 and CXCL2, by mutant *Kras* ($n=5$–7/group). (**c**) Data summaries of malignant pleural effusion (MPE) volume (top; LLC: $n=9$/group; MC38: $n=14$–15/group; PANO2 p*Δ*Kras2A: $n=8$–18/group) and pleural CD11b + Gr1 + cells (bottom; LLC: $n=9$/group; MC38: $n=14$–15/group; PANO2 p*Δ*Kras2A: $n=5$/group) of *Ccr2* − / − and *C57BL/6* control mice after intrapleural injection of three different tumour cell lines. p*Δ*Kras2A, vector encoding mouse $Kras^{G12C}$ isoform A. (**d**) Representative bioluminescent images of chimeric *C57BL/6* mouse transplanted with bioluminescent bone marrow from *CAG.Luc.eGFP* donor before and after splenectomy performed at day 13 after intrapleural MC38 cells. Scale bars, 1 cm. (**e**) Data summaries of MPE volume (top; $n=9$/group) and pleural CD11b + Gr1 + cells (bottom; $n=9$/group) of *C57BL/6* mice pretreated with sham surgery or splenectomy followed by intrapleural injection of MC38 cells, or PANO2 cells expressing p*Δ*Kras2A or p*Δ*Kras2B two weeks later. Data are presented as mean ± s.d. ns, *, **, and ***: $P>0.05$, $P<0.05$, $P<0.01$, and $P<0.001$ for comparison with parental lines (**b**), between the two mouse strains (**c**), or between different surgeries (**e**) by Student's t-test.

retarded pleural tumour dissemination and decreased pleural CD11b + Gr1 + accumulation compared with controls (Fig. 5a; Table 5). Furthermore, *in vitro* treatment of MC38 cells with deltarasin resulted in almost complete elimination of CCL2 secretion (Fig. 5b). To test the impact of KRAS blockade in a more human-relevant setting, *NOD/SCID* mice received deltarasin and control treatments starting at two weeks after pleural delivery of one million A549 cells ($KRAS^{G12S}$). At day 30 after tumour cell injection, deltarasin-treated mice had markedly decreased MPE volume and incidence compared with controls (Fig. 5c; Table 5). We also explored direct intrapleural targeted deltarasin delivery against experimental MPE, since chronic *KRAS* inhibition may result in marked toxicity. For this, *C57BL/6* mice received pleural MC38 cells, followed by a single intrapleural injection of liposomal-encapsulated deltarasin (15 mg kg^{-1}; one single dose equal to the daily intraperitoneal drug dose administration) or empty liposomes[31,32] on day seven post-tumour cells. Interestingly, single-dose intrapleural liposomal deltarasin exhibited equal efficacy with repetitive intaperitoneal drug treatment, halting both MPE accumulation and CD11b + Gr1 + cell influx (Fig. 5d; Table 5). We finally cross-examined the effects of deltarasin and of a well-characterized neutralizing anti-CCL2 antibody[6,7,33,34]. For this, *C57BL/6* mice received intrapleural PANO2 cells stably expressing $Kras^{G12C}$ isoforms 2A or 2B. After 4 or 14 days, respectively, mice started receiving daily intraperitoneal deltarasin (15 mg kg^{-1}) or anti-CCL2 antibody (50 mg kg^{-1}) every 3 days. Control mice received daily saline injections and IgG2a control antibody (50 mg kg^{-1}) every 3 days. Interestingly, both treatments were equally effective in reducing MPE incidence and volume, as well as CD11b + Gr1 + cell accumulation (Fig. 5e; Table 5). These results indicated that deltarasin is effective in halting MPE

Table 3 | Candidate mutant *Kras* transcriptome signature.

Gene symbol	Gene name	ΔGE LLC*	ΔGE MC38*	ΔGE AE17*
Asns	Asparagine synthetase	+12.7	+11.6	+11.2
Bcat1	Branched chain aminotransferase 1, cytosolic	+11.2	+17.6	+12.2
Casp3	Caspase 3	+12.7	+16.0	+17.4
Ccl2	Chemokine (C-C motif) ligand 2	+85.4	+119.3	+97.7
Ccl7	Chemokine (C-C motif) ligand 7	+11.3	+14.4	+17.8
Cep170	Centrosomal protein 170	+15.3	+11.6	+13.5
Dab2	Disabled 2, mitogen-responsive phosphoprotein	+12.7	+18.2	+10.4
Dusp9	Dual specificity phosphatase 9	+13.1	+15.5	+17.0
Gm10717	Predicted gene 10717	+10.9	+33.3	+45.6
Gm10721	Predicted gene 10721	+10.9	+15.1	+31.4
Gm10722	Predicted gene 10722	+15.2	+241.9	+60.5
Gm26523	Predicted gene, 26523	+56.3	+52.0	+36.4
Gpr149	G protein-coupled receptor 149	+33.1	+33.9	+12.5
Hist1h1b	Histone cluster 1, H1b	+42.9	+50.3	+48.2
Hjurp	Holliday junction recognition protein	+10.3	+14.4	+11.3
Lhfp	Lipoma HMGIC fusion partner	+24.9	+27.2	+23.5
Mpp1	Membrane protein, palmitoylated	+10.6	+16.3	+21.3
Nid1	Nidogen 1	+13.6	+16.0	+15.0
Nid1	Nidogen 1	+10.3	+15.2	+11.3
Prrx1	Paired related homeobox 1	+27.5	+26.9	+23.9
Prune2	Prune homolog 2 (*Drosophila*)	+24.5	+17.5	+27.0
Psat1	Phosphoserine aminotransferase 1	+12.3	+13.3	+11.1
S100a4	S100 calcium binding protein A4	+13.4	+12.5	+10.1
Slc30a4	Solute carrier family 30 (Zinc transporter), member 4	+20.6	+11.7	+16.2
Snora17	Small nucleolar RNA, H/ACA box 17	+18.3	+11.5	+26.6

The 25 transcripts identified from comparative analyses of global gene expression between five murine cancer cell lines (LLC, MC38, AE17, B16F10, and PANO2 cells) and benign airway epithelial cells by alphabetic order.
*ΔGE, fold-difference in gene expression between *Kras*-mutant tumour cells and benign airway epithelial cells. *Ccl2* was the most consistently over-represented transcript across all three cell lines examined. LLC, *C57BL/6* Lewis lung carcinoma; MC38, *C57BL/6* colon adenocarcinoma; AE17, *C57BL/6* malignant pleural mesothelioma.

induction by *KRAS*-mutant tumour cells and suggested that mutant *KRAS*-driven MPE in humans may also be actionable.

Discussion

The dichotomous phenotype of primary and metastatic pleural tumours, some of which are associated with an MPE whereas others are not, is of paramount clinical importance, and prompted us to hypothesize that a causative molecular signature underlines MPE formation[2–4]. We show that cancer cells bearing different *KRAS* mutations cause MPE upon pleural dissemination and that mutant *KRAS* is important for experimental MPE development. Furthermore, that mutant *KRAS*-driven MPE is attributed to a CCL2-dependent signalling cascade that is necessary for the sequential translocation of CD11b + Gr1 + cells from the bone marrow to the spleen and the tumour-involved pleural cavity, where, in turn, these cells promote MPE formation. Proof-of-principle clinical data indicate that *KRAS* mutations are present in a substantial proportion of MPE patients in Europe and that they might be underestimated by automated sequencing analyses. Finally, we show that pharmacologic interception of this newly identified *KRAS*-driven, CCL2-mediated pathway to MPE can prevent MPE development.

The newly identified genotype-disease connection between mutant *KRAS* and MPE was corroborated using 12 different isogenic cellular systems of parental and daughter *KRAS*-modulated cell lines. In each and single one of these systems, mutant *KRAS* was required and sufficient for MPE. Particularly impressive was the switch of PANO2 cells upon $Kras^{G12C}$2A expression from complete MPE incompetence during a month's observation to acute and lethal MPE induction within 7 days. The same is true for benign HEK293T that were rendered MPE-proficient by isolated expression of $Kras^{G12C}$2B *per se*. But is the proposed mutant *KRAS*-MPE link clinically relevant? *KRAS* mutations are not frequently found in human MPE as opposed to *EGFR* and *EML4/ALK* mutations[8–16]. First, we believe that *KRAS* mutations are not looked for because they are considered not actionable and mutually exclusive to *EGFR* mutations, notions that are currently being revisited[8–16,35,36]. We show the clinical data that indicate that *KRAS* mutations are frequent in European patients with MPE from lung adenocarcinoma and that they might be underappreciated. A recent study also showed how *KRAS* mutations can be missed in MPE samples, but persist in cultured cell lines derived from the same patients[16], a finding recapitulated in patients from our centre. To this end, most MPE sequencing studies were performed in Asian populations with high *EGFR* and *EML/ALK* and low *KRAS* mutation frequencies[8–16,35,36]. A recent study of European patients with resected lung tumours clearly showed that *KRAS* mutations are linked with pleural spread[19]. Third, pleural tumours are diffuse-multifocal and probably multiclonal[36] and it is conceivable that mutant *KRAS* MPE-initiating cells escape detection in focal pleural tumour tissue biopsies and low-volume pleural fluid aspirates.

We do not claim that *KRAS* mutations are the only ones that cause MPE in humans and postulate mutant *KRAS* effects to be class effects shared by all driver mutations aligned along the KRAS pathway, including *EGFR*, *KRAS*, *PIK3CA*, *BRAF*, *MET*, *EML4/ALK*, *RET* and others. To this end, mutant *EGFR* was recently shown to cause MPE when expressed in H1299 human lung adenocarcinoma cells[17]. However, possible pathogenic roles for other lung cancer drivers in MPE remain to be shown. Together with the advent of MPE sequencing techniques[8–16], such developments could lead to targeted therapies for MPE in the near future. Moreover, MPE is a clinically heterogeneous set of diseases from a number of primary sites. *KRAS* mutations are more relevant to patients with lung, pancreatic, and colon cancers and leukaemias. In other tumors (that is, breast cancer) other

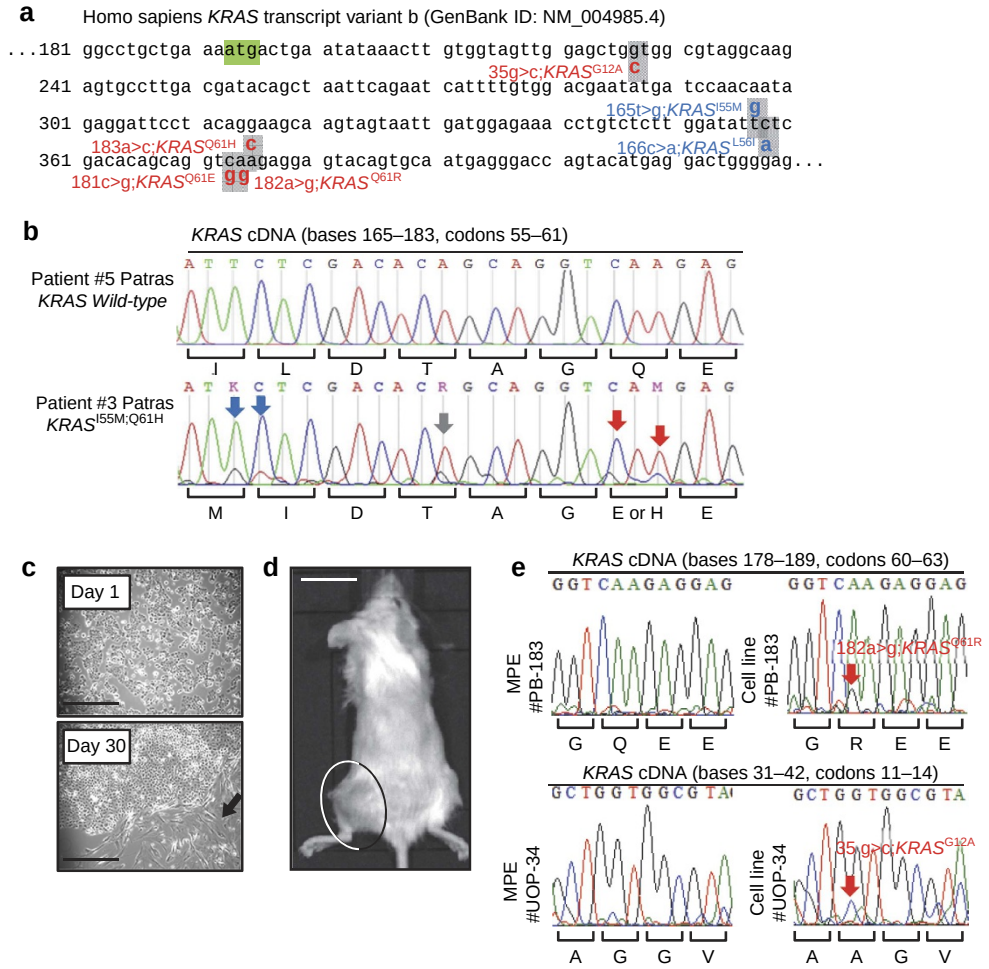

Figure 4 | *KRAS* mutations in human malignant pleural effusions. (**a**–**c**) Sanger sequencing results of human malignant pleural effusions (MPE) caused by metastatic lung adenocarcinomas from Institution 1. (**a**) Partial sequence of *Homo Sapiens KRAS* isoform b transcript showing start codon (green box) and missense mutations identified (grey boxes and callouts). Red and blue fonts indicate, respectively, known pathogenic mutations and mutations of unknown significance based on COSMIC[20]. (**b**) Partial Sanger-sequencing traces from two patients showing corresponding sequences of patient with wild-type *KRAS* alleles and of another with four different *KRAS* mutations. Arrows indicate missense mutations of pathogenic (red) and unknown (blue) significance based on COSMIC[20], as well as nonsense mutations (grey). Note that mutant *KRAS* traces hide under wild-type traces superimposed by wild-type *KRAS* alleles and/or by RNA from tumour or MPE-infiltrating benign somatic cells. Importantly, some mutations were not detected by the analysis software (see letters above mutant trace). Note also multiple mutations in the same patient suggesting a possible multiclonal origin of this MPE. (**c**–**e**) Patient-derived MPE cell line isolation from eight patients from Institution 1 that were initially tested *KRAS* wild-type. (**c**) Arrow shows focal clonal expansion of cultured MPE cells that gave rise to cell line PB-183. Scale bars, 50 μm. (**d**) PB-183-induced tumour in *NOD/SCID* mouse four weeks after subcutaneous injection of a million cells ($n=5$). Scale bar, 1 cm. (**e**) Partial Sanger-sequencing traces of *KRAS* cDNA from the initial MPE cells and from two MPE-derived cell lines indicate *KRAS* mutations (red arrows and fonts) that were not identified in the initial samples. Note that even in MPE cell lines mutant *KRAS* traces hide under wild-types traces superimposed by wild-type alleles. Again, the mutation was not detected by the software (see letters above mutant trace).

mutations may be functionally involved in MPE formation (that is, HER2), a postulation that awaits experimental confirmation. To this end, future human studies aimed at identifying genotype–phenotype linkages in various tumours need to be tailored appropriately and need not rely on cross-sectional frequency observation design. Prospectively genotyped, case-matched, and longitudinally observed patient cohorts are more likely to give answers to questions such as the *KRAS*-MPE link proposed here.

In addition to the novel cancer genome-phenotype association, we further show here that mutant *KRAS*-driven MPE is mediated via CCL2-dependent paracrine signalling to CD11b + Gr1 + myeloid cells. The well-studied cell-autonomous effects of mutant *KRAS* conferring addictive proliferation advantages to the tumour cell[35,37] may be complemented by this paracrine axis and may temporally precede its clinical manifestation, since mutant *KRAS* likely promotes pleural metastasis prior to MPE development[18,19]. As opposed to neutrophil chemoattractants such as CXCL1, CXCL2 (ref. 25), tumour-elaborated CCL2 is a potent monocyte/macrophage mobiliser promoting angiogenesis and metastasis[34,38] and was identified here as the transcriptional target of mutant *KRAS* in tumour cells. This finding complements previous observations implicating CCL2 in mutant *KRAS*-driven inflammation in the lung epithelium[39] and in MPE formation[5,6]. Interestingly, mutant *HRAS* also induces IL-8 signalling[40] and the results imply that different RAS proteins may control distinct chemokine repertoires in order to mobilize defined myeloid cell subsets to tumour sites.

Our present and previous findings[5–7] indicate that pleural tumour-originated CCL2 mobilizes two distinct cell populations from the bone marrow: mast cells and CD11b + Gr1 + cells[41,42], both known to respond to CCL2 (refs 7,25), to facilitate breast

Table 4 | *KRAS* mutations in human malignant pleural effusions.

Present study

MPEs sequenced (*n*)	missense *KRAS* mutations discovered (*n*)	mutant patients (*n*)	Known pathogenic mutations	Novel mutations of unknown causality
12	8	5	G12A, Q61H/E/R	I55M, L56I

n (%)	Bulk MPE RNA	MPE cell lines
KRAS WT	8	3
KRAS MUT	0	5

Renaud, S., *et al.*[19]

n(%)	*WT*	*EGFR MUT*	*KRAS MUT*	*P*
Bone	57(12)	0(0)	61(13)	1.0000
Liver	39(8)	8(2)	9(2)	< 0.0001
Brain	26(5)	16(3)	9(2)	< 0.0001
Pleura	37(8)	2(0)	89(19)	0.0039
Lung	89(19)	1(0)	22(5)	< 0.0001
Adrenal	10(2)	0(0)	6(1)	< 0.0001
	1.0000	< 0.0001	< 0.0001	

n (%)	*KRAS WT*	*KRAS MUT*
Pleura	39(8)	89(19)
Other	246(51)	107(22)

MPE, malignant pleural effusions; MUT, mutant; WT, wild type.
Present study: top—incidence and type of *KRAS* mutations detected in 12 human MPE caused by metastatic lung adenocarcinomas from Institution 1. Bottom—summary of *KRAS* mutations of MPE cell lines isolated from eight patients from Institution 1 that were initially tested *KRAS* wild-type versus corresponding MPE samples. $P = 0.0256$ by Fischer's exact test.
Renaud *et al.*[19]: site of recurrence of 481 patients with resected non-small-cell lung cancer according to mutation status[19] shows increased pleural dissemination rates in patients with *KRAS*-mutations. Top—metastatic site by genotype. $P < 0.0001$ by χ^2-test. *P* values for comparison with bone metastases or WT tumours by Fischer's exact tests. Bottom: pleural versus any other metastatic site by *KRAS* genotype. $P < 0.0001$ by Fischer's exact test.
n(%), of patients.

cancer metastasis to the lungs[34], and to sustain tumour growth by promoting angiogenesis[28]. CD11b + Gr1 + cells were previously identified in MPE[42] along with mast cells that were shown to promote MPE by fostering tumour growth and vascular permeability[7]. Here we show that the spleen is an important intermediate organ for MPE development, similar to other tumour models, with its marginal zone functioning as a reservoir for bone-marrow-derived CD11b + Gr1 + cell progenitors that are subsequently rapidly deployed to tumour sites[43,44]. Our experiments, in line with the work of others[26–28,43,44] incriminate the spleen as a pro-tumour organ and suggest that the splenic environment is essential for CD11b + Gr1 + cell recruitment to MPE. As splenectomy provided marked protection to mice against incipient MPE, splenectomy at the time of pleurodesis or catheter placement may yield considerable benefit to patients with MPE, a notion worth exploring.

Finally, we present evidence that mutant *KRAS*-mediated MPE is actionable by the novel inhibitor of KRAS membrane transport deltarasin, lending hope for clinical targeting of the oncogene in the future[30,35]. Importantly, a CCL2 neutralizing antibody[6,7,33,34] was as effective as deltarasin, strengthening the *KRAS*-CCL2 connection and indicating that intercepting downstream of mutant oncogene targets may be an alternative to their direct targeting. In addition to the clinical significance of *KRAS* and other driver mutations of lung and other cancers in MPE that needs to be established, open questions that remain include whether the hypoxic pleural environment impacts MPE development and whether it triggers phenotypic changes in pleural metastasized tumour cells, including the *KRAS*/CCL2 axis reported here.

In summary, we show that *KRAS* mutations are causally linked with MPE in mice. We also show that this link rests on a defined innate immune response and that it might be at play in humans with the condition. We believe that this work opens up avenues of potential progress towards aetiologic MPE therapy, by providing preclinical proof-of-concept data on immediate and feasible targeted interventions, such as splenectomy and KRAS and CCL2 blockade, which could provide meaningful benefits to patients with MPE in the future.

Methods

Study approval. Human MPE samples from twenty patients with lung adenocarcinoma-associated MPE from Institution 1 were obtained and biobanked according to a prospectively placed, standardized and Institutional Ethics Committee-approved protocol (approval number 22699/21.11.2013) that abides by the Declaration of Helsinki. Written informed consent was obtained from each patient. Mouse experiments were carefully designed and were prospectively approved by the Veterinary Administration of the Prefecture of Western Greece (protocol approval numbers 3741/16.11.2010, 60291/3035/19.03.2012, and 118018/578/30.04.2014), and were conducted according to Directive 2010/63/EU (http://eur-lex.europa.eu/LexUriServ/LexUriServ.do?uri=OJ:L:2010:276:0033:0079:EN:PDF).

Reagents. Evans' blue and 3-(4,5-dimethylthiazol-2-yl)-2,5-diphenyltetrazolium bromide (MTT) assay powder were from Sigma-Aldrich (St Louis, MO); D-luciferin was from Gold Biotechnology (St Louis, MO); Mouse Gene ST2.0 microarrays and relevant reagents were from Affymetrix (Santa Clara, CA); murine CCL2, CXCL1, and CXCL2 and human CCL2 ELISA kits were from Peprotech EC (London, UK);

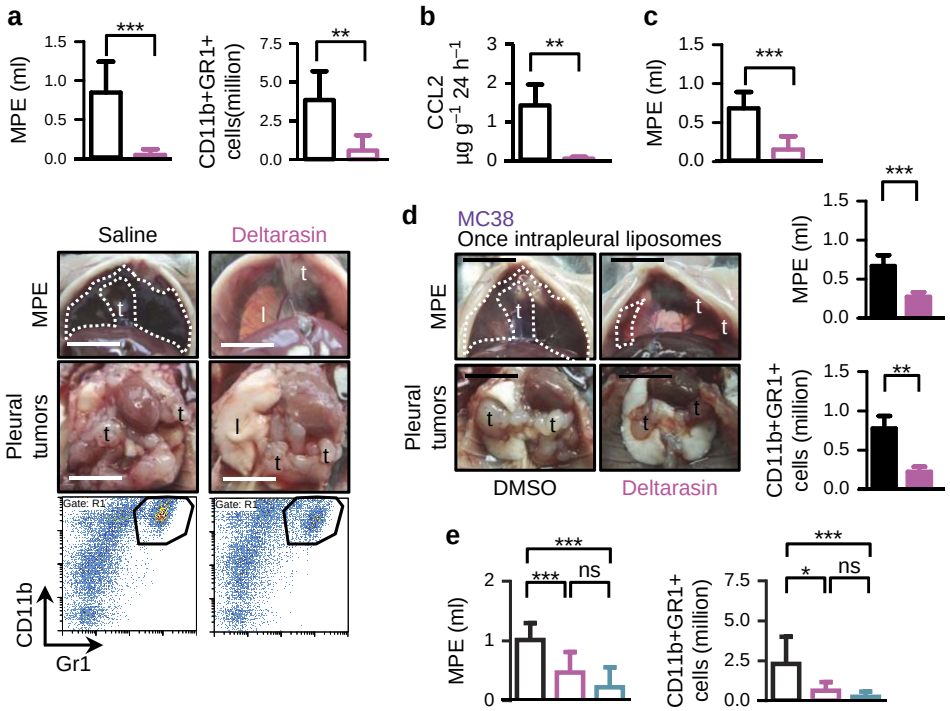

Figure 5 | Mutant *KRAS*-mediated malignant pleural effusions are actionable. (**a**) *C57BL/6* mice received pleural MC38 cells ($\Delta Kras^{G13R}$), were allowed seven days for pleural tumour development, and were randomized to daily intraperitoneal saline (100 µl) or deltarasin (15 mg kg^{-1}) treatments. Shown are data summaries of malignant pleural effusion (MPE) volume and CD11b + r1 + cells (both $n = 8$/group), representative images of pleural effusions (dashed lines) and tumours (t), and representative dotplots of CD11b + Gr1 + cells (polygon gates) at day 13 post-MC38 cells. Scale bars, 1 cm. (**b**) MC38 cells were treated *in vitro* with saline or deltarasin (15 µgml^{-1}). Shown is CCL2 secreted at 24 h ($n = 5$/group). (**c**) *NOD/SCID* mice received pleural LTP A549 cells ($\Delta KRAS^{G12S}$), were allowed 14 days for pleural tumour development, and were randomized to daily intraperitoneal saline (100 µl) or deltarasin (15 mg kg^{-1}) treatments. Shown is data summary of MPE volume at day 30 post-tumour cells. (**d**) *C57BL/6* mice received pleural MC38 cells followed by a single intrapleural injection of liposomes containing 1% DMSO or 15 mg kg^{-1} deltarasin in 1% DMSO at day 7 post-tumour cells. Shown are representative images of pleural effusions (dashed lines) and tumours (t), and data summaries of MPE volume ($n = 15$–16/group) and CD11b + Gr1 + cells ($n = 9$/group) at day 13 post-MC38 cells. Scale bars, 1 cm. (**e**) *C57BL/6* mice received pleural PANO2 cells stably expressing mutant *Kras* vectors (p$\Delta Kras2A$ or p$\Delta Kras2B$), were allowed 4 or 14 days, respectively, for pleural tumour development and were then randomized to intraperitoneal treatment with daily saline plus IgG2a antibody every three days (50 mg kg^{-1} in 100 µl saline), daily deltarasin (15 mg kg^{-1} in 100 µl saline), or anti-CCL2 antibody every three days (50 mg kg^{-1} in 100 µl saline). Shown are data summaries of MPE volume (n 27, 10, and 20 mice/group, respectively) and CD11b + Gr1 + cells ($n = 24$, 8, and 14/group, respectively) at day 14 post-tumour cells. Data are presented as mean ± s.d. ns, *, **, and ***: $P > 0.05$, $P < 0.05$, $P < 0.01$, and $P < 0.001$ for the indicated comparisons by Student's t-test (a-d) or one-way ANOVA with Bonferroni post-tests (**e**).

Table 5 | Incidence of malignant pleural effusions in *KRAS*-targeted mice.

	Treatments	No MPE	MPE	*P value*
Experiment from Fig. 5a MC38-induced MPE daily intraperitoneal treatments installed at day 7 post-MC38 cells	Saline (100 µl)	1	7	—
	Deltarasin (15 mg kg^{-1} in 100 µl saline)	7	1	0.0101
Experiment from Fig. 5c LTP A549-induced MPE daily intraperitoneal treatments installed at day 14 post-MC38 cells	Saline (100 µl)	0	10	—
	Deltarasin (15 mg kg^{-1} in 100 µl saline)	5	4	0.0108
Experiment from Fig. 5d MC38-induced MPE once intrapleural treatment at day 7 post-MC38 cells 100 µl injectate volume	Liposomes (saline 1% DMSO)	2	14	
	Liposomes (15 mg kg^{-1} deltarasin in saline 1% DMSO	8	7	0.0151
Experiment from Fig. 5e PANO2 p$\Delta Kras2A/2B$-induced MPE intraperitoneal treatments installed at day 4 or 14 days post-tumour cells, respectively	Daily saline (100 µl) + IgG2a every three days (50 mg kg^{-1} in 100 µl saline)	0	27	—
	Daily deltarasin (15 mg kg^{-1} in 100 µl saline)	3	7	0.0157
	α-CCL2 every 3 days (50 mg kg^{-1} in 100 µl saline)	14	6	<0.0001

CCL, C–C motif chemokine ligand; DMSO, dimethyl sulfoxide; LTP A549, long-term passaged A549 cells having lost the Y chromosome; MC38, *C57BL/6* colon adenocarcinoma; MPE, malignant pleural effusion; PANO2, *C57BL/6* pancreatic adenocarcinoma; Δ, mutant.
MPE incidence of *C57BL/6* mice that received *KRAS*-mutant pleural tumour cells followed by deltarasin or anti (α)-CCL2 treatments. Shown are numbers of mice (n) and probability (P) values for comparison with controls by Fischer's exact test. $P < 0.0001$ for overall comparison of experiment from Fig. 5e by χ^2-tests.

primer sets and antibodies are listed in Supplementary Tables 1 and 2, respectively; RAS activation assay was from Merck Millipore (Darmstadt, Germany); deltarasin was from MedChem Express (Princeton, NJ) and from Cayman Europe (Tallinn, Estonia); anti-mouse CCL2 neutralizing antibody, as well as IgG2a control antibody were from Oncology Discovery Research, Janssen R&D LLC (Radnor, PA)[33,34]; 1, 2-Distearoyl-sn-glycero-3-phosphocholine, phosphatidylglycerol and cholesterol were from Avanti Polar Lipids, Inc. (Alabaster, AL).

Mice. *C57BL/6* (#000664), *NOD/SCID* (#001303), *CAG.Luc.eGFP* (#008450), and *Ccr2*$^{-/-}$ (#004999) mice from Jackson Laboratories (Bar Harbor, ME) were bred in the University of Patras Center for Animal Models of Disease. All experiments entailing murine cell lines were done using mice on the *C57BL/6* background or *CAG.Luc.eGFP* mice backcrossed >F12 to the *C57BL/6* background. All experiments entailing human cell lines were done using mice on the *NOD/ShiLtJ* background. Nine hundred and seventy-five sex-, weight (20–25 g)- and age (6–12 week)-matched male and female (50% of mice from each sex were enrolled in each experimental arm) experimental mice were used for these studies. The exact animal numbers per experiment are given in Tables 1, 2 and 5 and in the Legends to Figures.

Cells. *C57BL/6* mouse B16F10 skin melanoma and PANO2 pancreatic and Lewis lung carcinomas (LLC), as well as human SKMEL2 skin melanoma, A549 lung and HT-29 colon adenocarcinomas were from the National Cancer Institute Tumour Repository (Frederick, MD); human HEK293T embryonic kidney cells were from the American Type Culture Collection (Manassas, VA); *C57BL/6* mouse MC38 colon adenocarcinoma cells were a gift from Dr Barbara Fingleton (Vanderbilt University, Nashville, TN, USA)[6,7,45], *C57BL/6* mouse AE17 malignant pleural mesothelioma cells from Dr Y.C. Gary Lee (University of Western Australia, Perth, Australia)[46], and human LTP A549 cells that have suffered chromosome Y loss from Dr Haralabos P. Kalofonos (University of Patras, Greece). Primary lung adenocarcinoma cells from *C57BL/6* and *FVB* mice (CULA and FULA cells, respectively) were generated as described elsewhere[23]. Briefly, *C57BL/6* and *FVB* mice received ten and four consecutive weekly intraperitoneal injections of urethane (1 g kg^{-1}) and were killed ten months later. Lung tumours were isolated under sterile conditions, strained to single cell suspensions, and cultured for >100 passages over two years. Primary airway cells were derived by culturing stripped murine tracheal epithelium. Cell lines were authenticated annually using the short tandem repeat method, microarray, and Sanger sequencing and were tested for *Mycoplasma Spp.* biannually by PCR using designated primers (Supplementary Table 1). All cell lines were cultured at 37 °C in 5% CO_2-95% air using full culture medium (DMEM supplemented with 10% FBS, 2 mM L-glutamine, 1 mM pyruvate, 100 U ml^{-1} penicillin, and 100 mg ml^{-1} streptomycin). For *in vivo* injections, cells were collected with trypsin, incubated with Trypan blue, counted by microscopy in a haemocytometer, their concentration was adjusted in PBS, and cell were injected through a left intercostal space or in the skin, as described elsewhere[5–7]. Only 95% viable cells were used for *in vivo* injections.

Sequencing plasmids and microarrays. Total cellular RNA was isolated using Trizol (Invitrogen, Thermo Fisher Scientific, Waltham, MA) followed by RNAeasy column purification and genomic DNA removal (Qiagen, Hilden, Germany). One μg purified total RNA was reverse transcribed using an Oligo(dT)$_{18}$ primer and Superscript III (Invitrogen, Thermo Fisher Scientific, Waltham, MA) according to the manufacturer's instructions. For sequencing reactions, *Kras*, *Egfr*, Braf and *Pik3ca* cDNAs (or parts of these cDNAs) were amplified in PCR reactions using the corresponding primers (Supplementary Table 1) and Phusion Hot Start Flex polymerase (New England Biolabs, Ipswich, MA). cDNA fragments were purified with NucleoSpin gel and PCR clean-up columns (Macherey-Nagel, Düren, Germany) and were directly Sanger-sequenced with their corresponding forward and reverse primers by VBC Biotech (Vienna, Austria). For RNA interference, the following proprietary lentiviral shRNA pools of three were obtained from Santa Cruz Biotechnology (Palo Alto, CA): random control shRNA (sh*C*, sc-108080-V), GFP control (sc-108084-V), and anti-*Kras*.shRNA (sh*Kras*, sc-33876-V). Anti-*Kras* lentiviral shRNA target sequences were: 5′-CTACAGGAAACAAGTAGTA-3′, 5′-GAACAGTAGACACGAAACA-3′ and 5′-CCATTCAGTTTCCATGTTA-3′. For this study, the following new plasmids were constructed in-house and were deposited with Addgene (https://www.addgene.org/Georgios_Stathopoulos/), accompanied by their full sequence files: (i) a pMIGR1-based puromycin resistance bicistronic retroviral expression vector (Addgene ID 64335) was constructed by replacing the eGFP sequences of pMIGR1 vector downstream of IRES with puromycin resistance sequences; (ii) a pMIGR1-based hygromycin resistance bicistronic retroviral expression vector (Addgene ID 64374) was constructed by replacing the eGFP sequences of pMIGR1 vector downstream of IRES with hygromycin resistance sequences. Both puromycin and hygromycin resistance genes were subcloned by restriction enzymes from available construct; (iii) the derivatives of these vectors, namely eGFP.retro.puro (Addgene ID 64336), eGFP.retro.hygro (Addgene ID 64375), eGFP.KRAS^{wt}-2B retro.puro (Addgene ID 64371), eGFP.KRAS^{G12C}-2B.retro.puro (Addgene ID 64372), eGFP.KRAS^{G12C}-2B.retro.hygro (Addgene ID 64376), eGFP.KRAS^{G12C}-2A.retro.puro (Addgene ID 64373). Murine *Kras*^{G12C} isoform 2A and 2B cDNAs were amplified using a first stand synthesis reverse transcription reaction from 1 μg total LLC RNA using specific primers (Supplementary Table 1) and Phusion Hot Start Flex polymerase (New England Biolabs, Ipswich, MA). Similarly, wild type *Kras*2B cDNA was amplified using a first stand synthesis reverse transcription reaction from 1 μg total PANO2 cellular RNA.The corresponding cDNAs were cloned into a peGFP.C1 vector (Clontech, Mountain View, CA) between BglII and EcoRI restriction sites, in-frame with eGFP and were verified by sequencing. The eGFP, as well as the wild type eGFP.KRAS2B and mutant eGFP.KRAS^{G12C}2A and 2B-encoding sequences were restricted out from the corresponding peGFP.C1-based constructs described above using enzymes AgeI and SmaI, were gel purified, and were subcloned into the (AgeI/HpaI-restricted) retroviral bicistronic expression vectors upstream of IRES-puromycin (ID 64336) and/or IRES-hygromycin (ID 64375) resistance genes, respectively. Retroviral particles were obtained by transfecting a 3 mm well of confluent HEK293T cells with the desired bicistronic retroviral vectors (expressing either eGFP or wild type or mutant eGFP.KRAS) along with VSV-G envelope expressing plasmid pMD2.G (Addgene ID12259) and pCMV-Gag-Pol expressing the retroviral structure proteins (Cell Biolabs Inc, San Diego, CA) at 1.5:1:1 mass stoichiometry via the $CaCl_2$/BES method. After two days, the cultured medium (2 ml for each retroviral type) was collected and passed through a 45 μM filter to remove cellular debris. This supernatant material was supplemented with 8 ml medium and was subsequently overlaid on a 100 mm plate containing 70% confluent mouse cancer cells. After 48 h, the medium was removed and the cells were incubated with selection medium (full cell culture medium supplemented with either 2–10 μg ml^{-1} puromycin or 50–100 μg ml^{-1} hygromycin). Stable clones were selected and subcultured. All other cell lines were transfected with standard DNA amounts using X-Fect (Clontech, Mountain View, CA).

Mouse experiments. Experimental pleural carcinomatosis was induced by pleural delivery of 1.5×10^5 murine cancer cells, 10^6 human cancer cells or 3×10^6 HEK293T cells. MPE models and splenectomy have been described elsewhere[5–7]. For bioluminescence imaging, mice were serially imaged on a Xenogen Lumina II and data were analysed using Living Image v.4.2 (Perkin-Elmer, Waltham, MA), after delivery of 1 mg intravenous D-luciferin (Gold Biotechnology, St Louis, MO) by retro-orbital injection. For splenocyte give-back, spleens were removed under sterile conditions from *CAG.Luc.eGFP* donors ($n = 3$ per group), 13 days after intrapleural injection with saline or tumour cells. Single-cell suspensions were prepared by passing spleens through 70 μm nylon cell strainers (BD Biosciences, Bedford, MA), followed by delivery of 100 μl saline containing 5×10^6 splenocytes to splenectomized hosts.

Mouse models. For induction of malignant pleural carcinomatosis with or without a MPE, mice were anaesthetized using isoflurane inhalation and received intrapleural injections of 100 μl PBS containing 150,000 murine, 1,000,000 human cancer cells or 3,000,000 HEK293T cells. Mice were killed when moribund for survival and pleural fluid and tumour analyses. Mice with pleural fluid volume ≥100 μl (equals the initial injection volume) were judged to have a MPE ('wet' pleural metastasis, that is, active pleural fluid exudation) and were subjected to pleural fluid aspiration, whereas animals with pleural fluid volume <100 μl were judged not to have a MPE ('dry' pleural carcinomatosis) and were subjected to pleural lavage. For this, 1 ml normal saline was injected intrapleurally and was withdrawn after 30 s. Following pleural fluid or lavage retrieval, the chest was opened and pleural tumours were stripped and weighed. For subcutaneous tumour formation, mice received 1,000,000 subcutaneous cancer cells and were followed longitudinally. Three vertical tumour dimensions ($\delta 1$, $\delta 2$ and $\delta 3$) were monitored serially and tumour volume was calculated using the formula $\pi \times \delta 1 \times \delta 2 \times \delta 3/6$. Both models have been described elsewhere[5–7].

Cytology histology and microscopy. Before further processing, MPE fluids were subjected to red blood cell lysis in ten-fold excess red blood cells lysis buffer (155 mM NH_4Cl, 12 mM $NaHCO_3$, 0,1 mM EDTA). Total pleural cell counts were determined microscopically on a haemocytometer and cytocentrifugal specimens (5×10^4 cells each) of total pleural fluid cells (or of CD45 + CD11b + Gr1 + sorted cells) were fixed with methanol for 2 min. Cells were stained with May–Grünwald working solution (May–Grünwald stain in 1 mM Na_2HPO_4, 2.5 mM KH_2PO_4, pH = 6.4) for 6 min, then with Giemsa working solution (Giemsa stain in 2 mM Na_2HPO_4, 5 mM KH_2PO_4, pH = 6.4) for 40 min, then washed with H_2O, and dried. Slides were mounted with Entellan (Merck Millipore, Darmstadt, Germany) and coverslipped and were microscopically analysed. For flow cytometry and fluorescence-activated cell sorting (FACS) staining, 10^6 nucleated pleural fluid cells suspended in 50 μl FACS buffer (PBS supplemented with 2% FBS and 0,1% NaN_3) were stained with the indicated antibodies according to manufacturer's instructions (Supplementary Table 2) for 20 min in the dark, were washed with FACS buffer from excess antibody, and were resuspended in 1 ml FACS buffer for further analysis. Spleens fixed in 10% formaldehyde overnight were embedded in paraffin and stored at room temperature. Five-micrometre paraffin sections were mounted on glass slides. Pleural tumours fixed in 10% paraffin or in 4% paraformaldehyde overnight were embedded in paraffin or in optimal cutting temperature (OCT; Sakura, Tokyo, Japan) and were stored at room temperature or −80 °C,

respectively, till further analyses. Five-micrometre-thick paraffin or 10-μm-thick cryosections were mounted on glass slides. Sections were labelled using the indicated antibodies (Supplementary Table 2) and were counterstained with Hoechst 33258 or with Envision colour development system (Dako, Carpinteria, CA). Immunoreactivity was quantified as described previously[5–7]. Bright-field and fluorescent microscopy were carried out using either an AxioObserver D1 inverted microscope (Zeiss, Jena, Germany) or an SP5 confocal microscope (Leica, Heidelberg, Germany).

Flow cytometry and cell sorting. A CyFlow ML instrument with FloMax Software (Partec, Münster, Germany) was used for cell cytometry, sorting, and data analysis. CD45 + CD11b + Gr1 + cells were identified, enumerated by true volumetric counting, and their total numbers were calculated as fraction of total MPE cell counts, or were sorted and collected in FACS buffer at 5×10^4 cells per ml.

Cellular assays. *In vitro* cancer cell proliferation was determined using the 3-(4,5-dimethylthiazol-2-yl)-2,5-diphenyltetrazolium bromide (MTT) assay. For this, 2×10^4 cells per well were plated onto 96-well plates. Daily thereafter, 15 μl of 5 mM MTT working solution in PBS was added to wells to be measured that day. The plate was incubated for 4 h at 37 °C in a 5% CO_2 humidified incubator followed by addition of 100 μl acidified isopropanol per well for sediment solubilization and absorbance measurement at 492 nm on a MR-96 A photometer (Mindray, Shenzhen, China). For soft agar colony formation assay, 7.5×10^3 cells were plated in 60 mm culture vessels in semi-solid 0.7% agarose in full culture medium and were incubated for 30 days at 37 °C in a 5% CO_2 humidified incubator. 2 ml fresh culture medium was added to each vessel biweekly. After incubation, 500 μl MTT working solution was added to each vessel and plates were dried, inverted, photographed and colonies were counted.

Vascular permeability assays. Mice with MPE received 0.8 mg intravenous Evans' blue and were killed after 1 h for determination of MPE levels of the albumin-binding dye[5–7]. Intradermal injections of 50 μl cell-free pleural lavage or MPE were performed at different spots of the shaved dorsal mouse skin followed immediately by Evans' blue injections as above, and euthanasia, skin inversion and imaging after one hour. The surface area of dye leak was determined using Fiji academic freeware (http://fiji.sc/Fiji), as described elsewhere[5–7].

Chick chorioallantoic membrane assay. Fertilized White Leghorn chicken eggs, as soon as embryogenesis started, were placed for incubation under constant humidity at 37 °C. On day 4, a square window was opened in the shell and then sealed with adhesive tape. On day 9, a 1 cm^2 rubber O-ring was placed on the surface of the CAM and 50 μl PBS or cell-free MPE or pleural lavage supernatants were added inside the ring's restricted area. After 48 h, CAM tissues were fixed in Carson's solution (saline-buffered formalin) and angiogenesis was evaluated using Fiji.

Real-time quantitative PCR and microarray hybridization and analysis. qPCR was performed using first strand synthesis reactions along with the indicated primers and KAPA SYBR FAST qPCR Kit (Kapa Biosystems, Wilmington, MA) in a StepOne cycler (Applied Biosystems, Carlsbad, CA). The CT values from triplicate qPCR reactions were extracted from the StepOne cycler (Applied Biosystems, Carlsbad, CA) onto Excel spreadsheets and were analysed with the relative quantification method $2^{-\Delta\Delta CT}$. The expression level of a given mRNA per sample/condition was determined relatively to reference gene mRNA levels. For microarray, triplicate cultures of 10^6 cells (for each cell line/condition) were subjected to RNA extraction as above. Five μg of pooled total RNA were tested for RNA quality on an ABI2000 bioanalyser (Agilent Technologies, Sta. Clara, CA), labelled, and hybridized to GeneChip Mouse Gene 1.0 or 2.0 ST arrays according to manufacturer's instructions (Affymetrix, Sta. Clara, CA). For microarray analysis, the Affymetrix Expression Console was used (parameters: annotation confidence, full; summarization method: iter-PLIER include DABG; background: PM-GCBG; normalization method: none), followed by normalization of all arrays together using a Lowess multi-array algorithm. Intensity-dependent estimation of noise was used for statistical analysis of differential expression. Unsupervised hierarchical clustering of microarray data and Venn diagrams were performed using the MatLab 2014 program. Microarray data are publicly available at the GEO database (http://www.ncbi.nlm.nih.gov/geo/; Accession ID: GSE58190 and GSE85021).

RAS activation assay and immunoblotting. Total protein extracts were prepared by lysing 10^7 cultured cells in Mg^2 + Lysis/Wash buffer (25 mM HEPES pH = 7.5, 150 mM NaCl, 1% NP-40, 10 mM $MgCl_2$, 1 mM EDTA, 2% glycerol). RAS activation assay was performed with RAS Activation Assay Kit (Merck Millipore, Darmstadt, Germany) by incubating total cell lysates with Raf-1 Ras-Binding Domain (RBD)-coated agarose beads according to the manufacturer's instructions. Total protein extracts and Raf-1 RBD agarose bead samples were analysed using 6–20% SDS–PAGE followed by standard blotting to PVDF membranes (Merck Millipore, Darmstadt, Germany). Membranes were incubated with primary antibodies, followed by incubation with the appropriate HRP-conjugated secondary antibodies at the manufacturers' indicated dilutions (Supplementary Table 2), and were visualized by chemiluminescence film exposure, using the enhanced chemiluminescence substrate (Merck Millipore, Darmstadt, Germany). Full uncropped immunoblots are shown in Supplementary Figures 8–10.

Enzyme-linked immunosorbent assays (ELISA). CCL2, CXCL1 and CXCL2 levels of cell culture supernatants, as well as CCL2 levels of cell-free MPE and corresponding sera were determined using dedicated murine and human ELISA kits according to the manufacturer's instructions (Peprotech, London, UK and R&D, Minneapolis, MN).

Bone marrow transplantation. For adoptive bone marrow replacement, *C57BL/6* hosts received ten million intravenous bone marrow cells flushed from the femurs and tibias of *CAG.Luc.eGFP* donors, 12 h after total-body irradiation (1,100 rad), as described elsewhere[6,7]. One mouse in each experiment was not engrafted (sentinel) and was observed till moribund between days 5 and 15 post-irradiation. The mice were left to recover at least for one month before subjecting them to experimentally induced MPE.

Liposome preparation and physicochemical characterization. Deltarasin-encapsulating liposomes were prepared by the DRV technique as described elsewhere[31,32] by freeze drying 30 mg of empty DSPC/PG/Chol (9:1:5 (mol:mol:mol)) unilamelar sonicated vesicles with 1 ml of deltarasin solution (5 mg ml^{-1}) in PBS, or plain PBS (for empty liposomes), followed by controlled re-hydration. The liposome size was decreased by extrusion though Lipo-so-fast extruder, polycarbonate membranes (Avestin Europe) with 400 nm diameter pore. Liposomes lipid concentration, size distribution and surface charge (zeta-sizer, Malvern) were estimated as reported elsewhere[31,32], as well as drug encapsulation efficiency after measuring the non-liposomal drug absorption at 284 nm.

***In vivo* drug treatments.** Treatments were initiated 4–14 days post-mouse and 14 days post-human pleural tumour cell injections. Deltarasin (15 mg kg^{-1} in 100 μl PBS), or 100 μl PBS were given daily intraperitoneally. Anti-mouse CCL2 or IgG2a control antibodies were delivered intraperitoneally at 50 mg kg^{-1} in 100 μl PBS every three days[6,7]. Deltarasin-encapsulating liposomes were prepared as described above and elsewhere[31,32] and were delivered intrapleurally seven days post-intrapleural MC38 cells.

Human MPE. MPE cell concentrates from patients with lung adenocarcinoma-associated MPE from Institution 1 ($n = 20$) were obtained and biobanked according to standard protocols, were handled similar to mouse MPE samples, and were subjected to RNA extraction, cDNA synthesis, PCR with human *KRAS*-specific primers (Supplementary Table 1), and direct Sanger sequencing. Some MPE cells were cultured for one month, tumor cell clones were picked and pooled, were inoculated into the flank of *NOD/SCID* mice to test their tumorigenicity, and were sequenced as above.

Statistics. Sample size was calculated using G*power (http://www.gpower.hhu.de/;[47]) assuming errors $\alpha = 0.05$ and $\beta = 0.05$, and effect size $d = 1.5$. Experiments were done in a fractionated fashion until statistical significance ($P < 0.05$ with $\alpha < 0.05$) was reached or ruled out ($P > 0.05$ with $\beta < 0.05$). No data were excluded from analyses and controls and intervention animals were enrolled as necessary per interim power analyses. Greater numbers of animals were added to follow-up experiments in groups where outliers increased the dispersion of the data, generating uneven experimental groups. Animals were allocated to treatments by alternation, and transgenic animals were enrolled case-control-wise. Data acquisition was blinded on samples previously coded by a non-blinded investigator. All data were examined for normality by Kolmogorov–Smirnov test and were found to be normally distributed. Values are given as frequencies, mean ± s.e.m., or mean ± s.d., as indicated. Sample size (n) refers to biological replicates, except from cell line qPCR data, where n refers to technical replicates. Differences in frequencies were examined by χ^2 or Fischer's exact tests, as appropriate. Differences in means were examined by two-tailed Student's t-test, or one-way or two-way ANOVA with Bonferroni post-tests, as appropriate. Survival proportions were examined by Kaplan–Meier analysis using the log-rank test for overall and pairwise comparisons. P values are two-tailed, and $P < 0.05$ was considered significant. Analyses and plots were done on Prism v5.0 (GraphPad Software, La Jolla, CA).

Data availability. The microarray data have been deposited at the Gene Expression Omnibus database (http://www.ncbi.nlm.nih.gov/geo/) under the accession codes GSE58190 and GSE85021). The vectors have been deposited at the Addgene plasmid depository (http://www.addgene.org/Georgios_Stathopoulos/) and plasmid ID's are given in the text. Primary mouse lung adenocarcinoma cells were deposited at the Laboratory for Molecular Respiratory Carcinogenesis (LMRC) core cell line facility (http://www.lmrc.upatras.gr/) and are available upon request (lmrc@upatras.gr). The authors declare that all the other data supporting the

findings of this study are available within the article and its Supplementary Information files and from the corresponding author upon reasonable request.

References

1. Davies, H. E. *et al.* Effect of an indwelling pleural catheter versus chest tube and talc pleurodesis for relieving dyspnea in patients with malignant pleural effusion: the TIME2 randomized controlled trial. *JAMA* **307,** 2383–2389 (2012).
2. Stathopoulos, G. T. & Kalomenidis, I. Malignant pleural effusion: tumor-host interactions unleashed. *Am. J. Respir. Crit. Care Med.* **186,** 487–492 (2012).
3. Ryu, J. S. *et al.* Prognostic impact of minimal pleural effusion in non-small-cell lung cancer. *J. Clin. Oncol.* **32,** 960–967 (2014).
4. Wu, S. G. *et al.* Survival of lung adenocarcinoma patients with malignant pleural effusion. *Eur. Respir. J.* **41,** 1409–1418 (2013).
5. Stathopoulos, G. T. *et al.* A central role for tumor-derived monocyte chemoattractant protein-1 in malignant pleural effusion. *J. Natl. Cancer Inst.* **100,** 1464–1476 (2008).
6. Marazioti, A. *et al.* Beneficial Impact of CCL2 and CCL12 Neutralization on experimental malignant pleural effusion. *PLoS ONE* **8,** e71207 (2013).
7. Giannou, A. D. *et al.* Mast cells mediate malignant pleural effusion formation. *J. Clin. Invest.* **125,** 2317–2334 (2015).
8. Kimura, H. *et al.* EGFR mutation status in tumour-derived DNA from pleural effusion fluid is a practical basis for predicting the response to gefitinib. *Br. J. Cancer* **95,** 1390–1395 (2006).
9. Wu, S. G. *et al.* Frequent epidermal growth factor receptor mutations in malignant pleural effusion of lung adenocarcinoma. *Eur. Respir. J.* **32,** 924–930 (2008).
10. Han, H. S. *et al.* EGFR mutation status in primary lung adenocarcinomas and corresponding metastatic lesions: discordance in pleural metastases. *Clin. Lung Cancer* **12,** 380–386 (2011).
11. Smits, A. J. *et al.* EGFR and KRAS mutations in lung carcinomas in the Dutch population: increased EGFR mutation frequency in malignant pleural effusion of lung adenocarcinoma. *Cell Oncol.* **35,** 189–196 (2012).
12. Li, Y. *et al.* Clinical significance of EML4-ALK fusion gene and association with EGFR and KRAS gene mutations in 208 Chinese patients with non-small cell lung cancer. *PLoS ONE* **8,** e52093 (2013).
13. Kang, J. Y. *et al.* Comparison of PNA clamping and direct sequencing for detecting KRAS mutations in matched tumour tissue, cell block, pleural effusion and serum from patients with malignant pleural effusion. *Respirology* **20,** 138–146 (2015).
14. Tsai, T. H. *et al.* RNA is favourable for analysing EGFR mutations in malignant pleural effusion of lung cancer. *Eur. Respir. J.* **39,** 677–684 (2012).
15. Tsai, T. H. *et al.* Clinical and prognostic implications of RET rearrangements in metastatic lung adenocarcinoma patients with malignant pleural effusion. *Lung Cancer.* **88,** 208–214 (2015).
16. Roscilli, G. *et al.* Human lung adenocarcinoma cell cultures derived from malignant pleural effusions as model system to predict patients chemosensitivity. *J. Transl. Med.* **14,** 61 (2016).
17. Tsai, M. F. *et al.* EGFR-L858R mutant enhances lung adenocarcinoma cell invasive ability and promotes malignant pleural effusion formation through activation of the CXCL12-CXCR4 pathway. *Sci. Rep.* **5,** 13574 (2015).
18. Raparia, K., Villa, C., Raj, R. & Cagle, P. T. Peripheral lung adenocarcinomas with KRAS mutations are more likely to invade visceral pleura. *Arch. Pathol. Lab. Med.* **139,** 189–193 (2015).
19. Renaud, S. *et al.* Specific KRAS amino acid substitutions and EGFR mutations predict site-specific recurrence and metastasis following non-small-cell lung cancer surgery. *Br. J. Cancer* **115,** 346–353 (2016).
20. Ikediobi, O. N. *et al.* Mutation analysis of 24 known cancer genes in the NCI-60 cell line set. *Mol. Cancer Ther.* **5,** 2006–2012 (2006).
21. Stathopoulos, G. T. *et al.* Epithelial NF-kappaB activation promotes urethane-induced lung carcinogenesis. *Proc. Natl Acad. Sci. USA* **104,** 18514–18519 (2007).
22. Doris, K. *et al.* Allergic inflammation does not impact chemical-induced carcinogenesis in the lungs of mice. *Respir. Res.* **11,** 118 (2010).
23. Giopanou, I. *et al.* Tumor-derived osteopontin isoforms cooperate with TRP53 and CCL2 to promote lung metastasis. *Oncoimmunology* **6,** e1256528 (2016).
24. Cao, Y. A. *et al.* Shifting foci of hematopoiesis during reconstitution from single stem cells. *Proc. Natl Acad. Sci. USA* **101,** 221–226 (2004).
25. Zlotnik, A. & Yoshie, O. The chemokine superfamily revisited. *Immunity* **36,** 705–716 (2012).
26. Sawanobori, Y. *et al.* Chemokine-mediated rapid turnover of myeloid-derived suppressor cells in tumor-bearing mice. *Blood* **111,** 5457–5466 (2008).
27. Swirski, F. K. *et al.* Identification of splenic reservoir monocytes and their deployment to inflammatory sites. *Science* **325,** 612–616 (2009).
28. Yang, L. *et al.* Expansion of myeloid immune suppressor Gr + CD11b + cells in tumor-bearing host directly promotes tumor angiogenesis. *Cancer Cell* **6,** 409–421 (2004).
29. Hall, T. A. BioEdit: a user-friendly biological sequence alignment editor and analysis program for Windows 95/98/NT. *Nucleic Acids Symp. Ser.* **41,** 95–98 (1999).
30. Zimmermann, G. *et al.* Small molecule inhibition of the KRAS-PDEδ interaction impairs oncogenic KRAS signaling. *Nature* **497,** 638–642 (2013).
31. Markoutsa, E. *et al.* Mono and dually decorated nanoliposomes for brain targeting, *in vitro* and *in vivo* studies. *Pharm. Res.* **31,** 1275–1289 (2014).
32. Matloob, A. H., Mourtas, S., Klepetsanis, P. & Antimisiaris, S. G. Increasing the stability of curcumin in serum with liposomes or hybrid drug-in-cyclodextrin-in-liposome systems: a comparative study. *Int. J. Pharm.* **476,** 108–115 (2014).
33. Tsui, P. *et al.* Generation, characterization and biological activity of CCL2 (MCP-1/JE) and CCL12 (MCP-5) specific antibodies. *Hum. Antibodies* **16,** 117–125 (2007).
34. Qian, B. Z. *et al.* CCL2 recruits inflammatory monocytes to facilitate breast-tumour metastasis. *Nature* **475,** 222–225 (2011).
35. Stephen, A. G., Esposito, D., Bagni, R. K. & McCormick, F. Dragging Ras Back in the Ring. *Cancer Cell* **25,** 272–281 (2014).
36. Basak, S. K. *et al.* The malignant pleural effusion as a model to investigate intratumoral heterogeneity in lung cancer. *PLoS ONE* **4,** e5884 (2009).
37. Weinstein, I. B. & Joe, A. Oncogene addiction. *Cancer Res.* **68,** 3077–3080 (2008).
38. Borsig, L., Wolf, M. J., Roblek, M., Lorentzen, A. & Heikenwalder, M. Inflammatory chemokines and metastasis–tracing the accessory. *Oncogene* **33,** 3217–3224 (2014).
39. Ji, H. *et al.* K-ras activation generates an inflammatory response in lung tumors. *Oncogene* **25,** 2105–2112 (2006).
40. Sparmann, A. & Bar-Sagi, D. Ras-induced interleukin-8 expression plays a critical role in tumor growth and angiogenesis. *Cancer Cell* **6,** 447–458 (2004).
41. Theocharides, T. C. & Kalogeromitros, D. The critical role of mast cells in allergy and inflammation. *Ann. N. Y. Acad. Sci.* **1088,** 78–99 (2006).
42. Murray, P. J. & Wynn, T. A. Protective and pathogenic functions of macrophage subsets. *Nat. Rev. Immunol.* **11,** 723–737 (2011).
43. Ugel, S. *et al.* Immune tolerance to tumor antigens occurs in a specialized environment of the spleen. *Cell Rep.* **2,** 628–639 (2012).
44. Cortez-Retamozo, V. *et al.* Origins of tumor associated neutrophils and macrophages. *Proc. Natl Acad. Sci. USA* **109,** 2491–2496 (2012).
45. Stathopoulos, G. T. *et al.* Host-derived Interleukin-5 Promotes Adenocarcinoma-induced Malignant Pleural Effusion. *Am. J. Respir. Crit. Care Med.* **182,** 1273–1281 (2010).
46. Jackaman, C. *et al.* IL-2 intratumoral immunotherapy enhances CD8 + T cells that mediate destruction of tumor cells and tumor-associated vasculature: a novel mechanism for IL-2. *J. Immunol.* **171,** 5051–5063 (2003).
47. Faul, F., Erdfelder, E., Lang, A. G. & Buchner, A. G*Power 3: a flexible statistical power analysis program for the social, behavioral, and biomedical sciences. *Behav. Res. Methods.* **39,** 175–191 (2007).

Acknowledgements

This work was supported by European Research Council 2010 Starting Independent Investigator and 2015 Proof of Concept Grants (#260524 and #679345, respectively; to G.T.S.). We thank the University of Patras Centre for Animal Models of Disease and Advanced Light Microscopy Core for experimental support. The authors also thank Drs Barbara Fingleton (Vanderbilt University, Nashville, TN, U.S.A.), Y.C. Gary Lee (University of Western Australia, Perth, Australia), and Haralabos P. Kalofonos (University of Patras, Greece) for the kind provision of cell lines critical to this work.

Author contributions

T.A., A.D.G. and A.C.K. conceived, designed and carried out most experiments, analysed the data, provided critical intellectual input and wrote the paper draft; N.I.K., D.K., M.V. and M.P. analysed the microarray data, performed PCR, qPCR and Sanger sequencing and analysed the relevant data; M.S., I.L. the D.E.Z. performed immunohistochemistry and microscopy; performed CCR2 and CD68 immunolocalization; E.N. carried out *KRAS* silencing; M.V. and N.S. carried out *in vivo* experiments; A.P. and D.K. performed mutant *KRAS* overexpression; K.P. and S.G.A. prepared liposomes; A.V., A.C.K., A.M., N.I.K., I.P., L.K., M.V. and G.T.S. established clinical protocols and obtained and processed clinical samples; V.H. performed microarrays; P.S. carried out flow cytometry; S.M., O.E., L.A.S. and I.P. provided intellectual input and analytical tools related to KRAS/CCL2 signalling; D.K. performed total body irradiation; A.M. and G.T.S. conceived the idea, supervised the study, designed and carried out experiments, analysed data, wrote the paper and guarantee the study's integrity. All authors concur with the submitted manuscript.

Additional information

Supplementary Information accompanies this paper at http://www.nature.com/naturecommunications

Competing interests: L.A.S. is an employee of the company that produces the anti-CCL2 antibodies. The remaining authors declare no competing financial interests.

Reprints and permission information is available online at http://npg.nature.com/reprintsandpermissions/

How to cite this article: Agalioti, T. *et al.* Mutant *KRAS* promotes malignant pleural effusion formation. *Nat. Commun.* **8,** 15205 doi: 10.1038/ncomms15205 (2017).

Publisher's note: Springer Nature remains neutral with regard to jurisdictional claims in published maps and institutional affiliations.

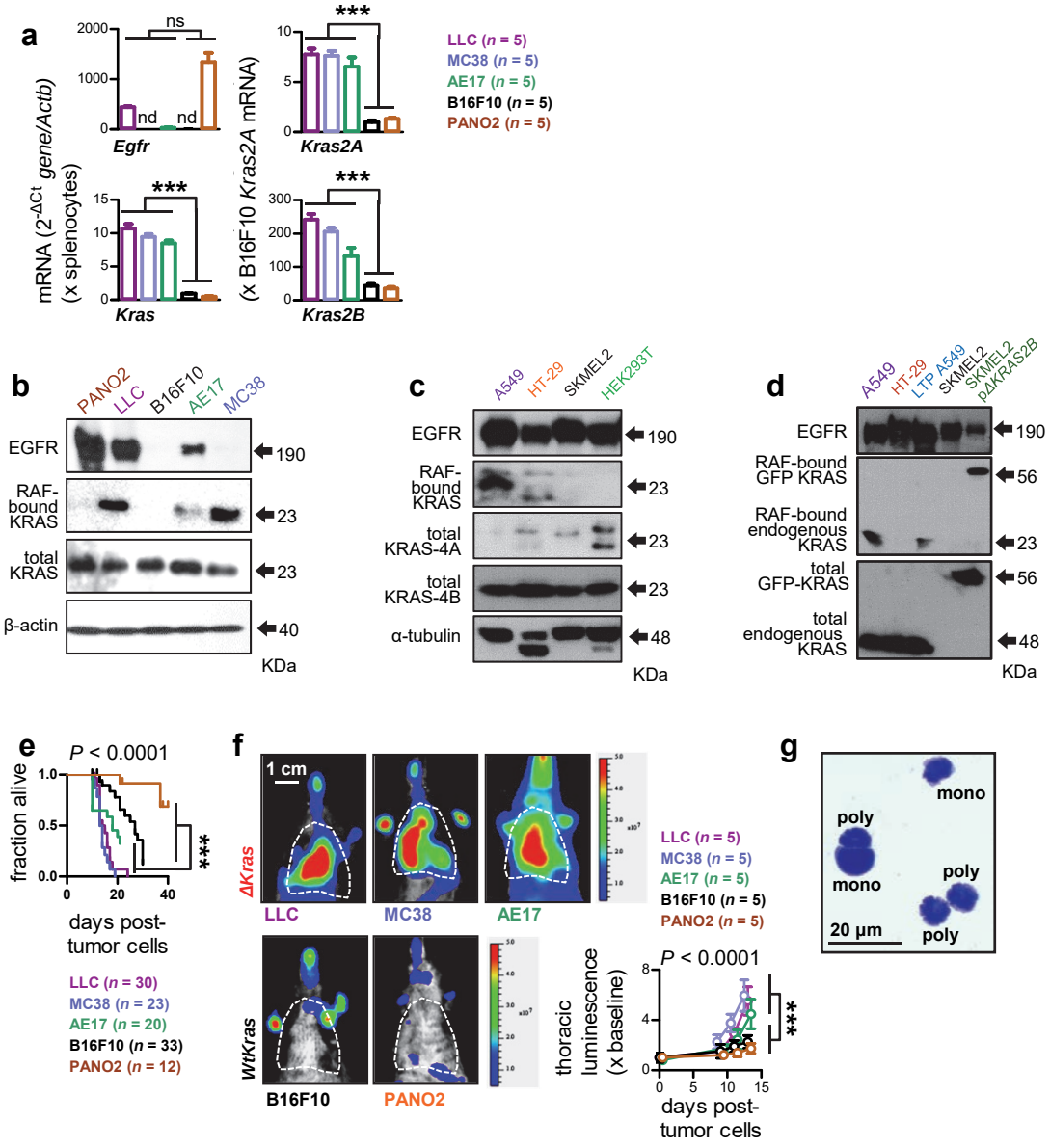
a
mRNA (2-ΔCt gene/Actb) (x splenocytes)
Egfr
Kras
(x B16F10 Kras2A mRNA)
Kras2A
Kras2B
ns
nd
***
LLC (n = 5)
MC38 (n = 5)
AE17 (n = 5)
B16F10 (n = 5)
PANO2 (n = 5)
b
PANO2
LLC
B16F10
AE17
MC38
EGFR
RAF-bound KRAS
total KRAS
β-actin
KDa
c
A549
HT-29
SKMEL2
HEK293T
EGFR
RAF-bound KRAS
total KRAS-4A
total KRAS-4B
α-tubulin
KDa
d
A549
HT-29
LTP A549
SKMEL2
SKMEL2 pΔKRAS2B
EGFR
RAF-bound GFP KRAS
RAF-bound endogenous KRAS
total GFP-KRAS
total endogenous KRAS
KDa
e
P < 0.0001
fraction alive
days post-tumor cells
LLC (n = 30)
MC38 (n = 23)
AE17 (n = 20)
B16F10 (n = 33)
PANO2 (n = 12)
f
1 cm
ΔKras
WtKras
LLC
MC38
AE17
B16F10
PANO2
thoracic luminescence (x baseline)
P < 0.0001
days post-tumor cells
g
mono
poly
20 μm

Supplementary Figure 1 | *KRAS* expression patterns of mouse and human tumour cells and lethality and myeloid inflammatory response in malignant pleural effusions (MPE) induced by *Kras*-mutant murine tumour cells. a, Total *Kras*, *Kras* isoform A and B, and *Egfr* mRNA expression of five mouse tumour cell lines relative to *Actb* by qPCR (n = 4/group). Data are presented as mean ± SD. ns and ***: $P > 0.05$ and $P < 0.001$ for the comparison between any *Kras*-mutant and any *Kras*-wild-type cell line by one-way ANOVA with Bonferroni post-tests. **b-d,** EGFR, active KRAS, KRAS isoform, and total KRAS protein expression of mouse and human tumour cells relative to β-actin by immunobloting. **e,** Kaplan-Meier plot of the survival of *C57BL/6* mice after intrapleural injection of 1.5×10^5 mouse tumour cells. P: overall probability value; ***: $P < 0.001$ for the comparison between any *Kras*-mutant and any *Kras*-wild-type cell line by log-rank test. **f,** Representative bioluminescent images taken 14 days after pleural tumour cells and data summary of longitudinal chest light emission measurements from total body-irradiated *C57BL/6* chimeras transplanted with luminescent bone marrow from *CAG.Luc.eGFP* donors (n = 3/group/time-point). Data are presented as mean ± SD. P: overall probability value; ***: $P < 0.001$ for the comparison between any *Kras*-mutant and any *Kras*-wild-type cell line by two-way ANOVA with Bonferroni post-tests. **g,** Representative image of May-Gruenwald-Giemsa-stained CD11b+Gr1+ cells sorted by fluorescence-assisted cell sorting from a LLC-induced MPE, showing mixed polymorphonuclear (poly) and mononuclear (mono) morphology. *Wt*, wild-type; *Δ*, mutant; LLC, *C57BL/6* Lewis lung carcinoma; MC38, *C57BL/6* colon adenocarcinoma; AE17, *C57BL/6* malignant pleural mesothelioma; B16F10, *C57BL/6* malignant skin melanoma; PANO2, *C57BL/6* pancreatic adenocarcinoma; FULA, *FVB* urethane-induced lung adenocarcinoma; CULA, *C57BL/6* urethane-induced lung adenocarcinoma; A549, human lung adenocarcinoma; LTP A549, long-term passaged A549 cells having lost the Y chromosome; SKMEL2, human malignant skin melanoma; HT-29, human colon adenocarcinoma; HEK293T, human embryonic kidney cells.

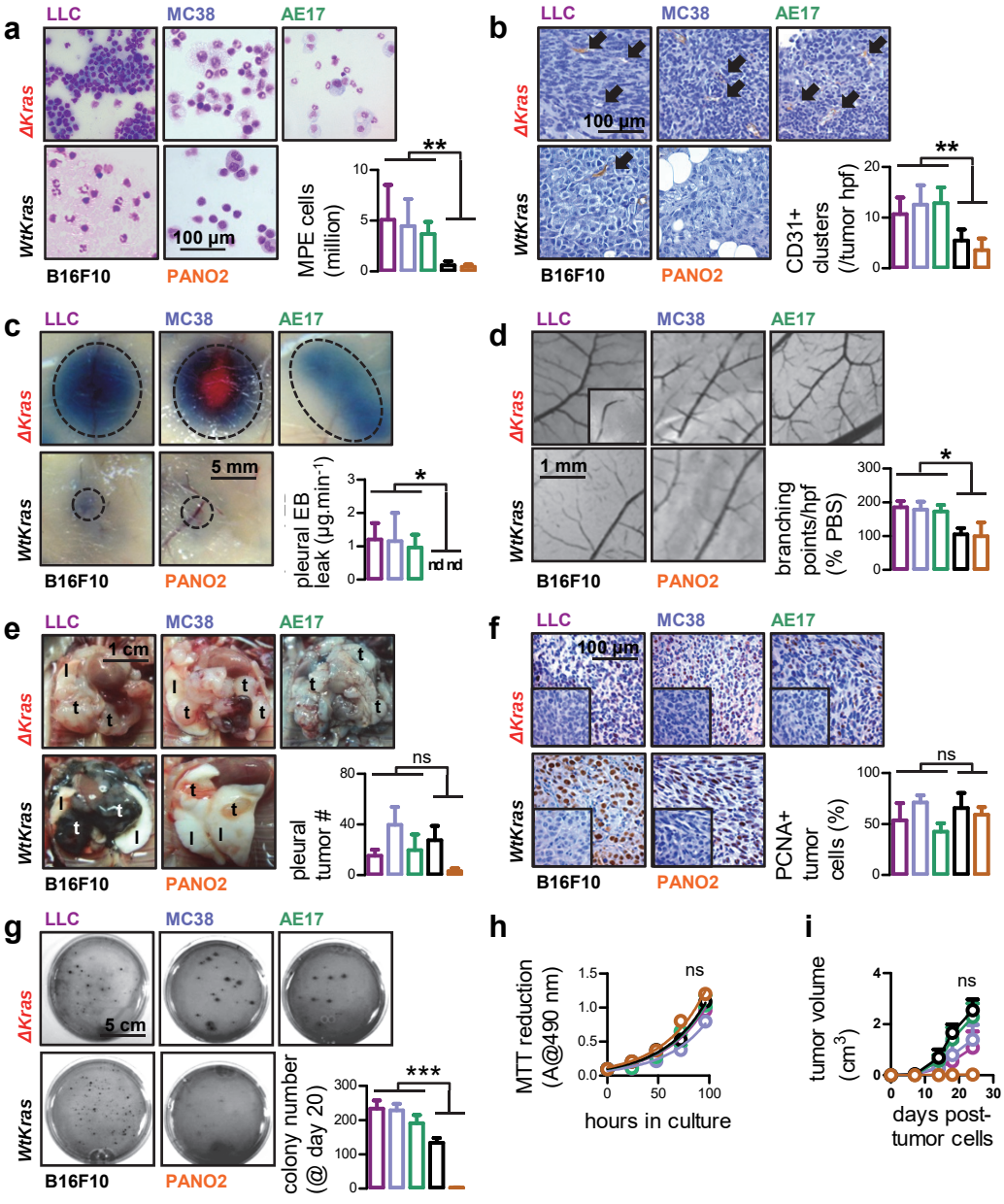
a
LLC
MC38
AE17
ΔKras
WtKras
100 μm
B16F10
PANO2
MPE cells (million)
**
b
100 μm
CD31+ clusters (/tumor hpf)
c
5 mm
pleural EB leak (μg.min-1)
*
nd nd
d
1 mm
branching points/hpf (% PBS)
e
1 cm
l
t
pleural tumor #
ns
f
PCNA+ tumor cells (%)
g
5 cm
colony number (@ day 20)
***
h
MTT reduction (A@490 nm)
hours in culture
i
tumor volume (cm3)
days post-tumor cells

Supplementary Figure 2 | Features of malignant pleural disease of *C57BL/6* mice induced by five syngeneic tumour cell lines: association of inflammation, angiogenesis, and vascular hyperpermeability with the presence of *Kras* mutations. a, b, e, f, 1.5 x 10^5 LLC, MC38, AE17, B16F10, or PANO2 tumour cells were delivered by direct pleural injection and the recipient *C57BL/6* mice (n = 10-15/group) were sacrificed after two weeks. Cell line colour codes are as in Extended Data Fig. 1a. **a,** Representative pleural fluid cytocentrifugal specimens (images) and total pleural fluid cell numbers (graph; *n* = 8-15/group). **b,** Representative microphotographs of pleural tumour tissue CD31 immunoreactivity (images) and pleural tumour microvessel (black arrows) density (graph; *n* = 10-15/group). **e,** Representative lung explants with lungs (l) and pleural tumours (t) (images) and pleural tumour foci abundance (graph; *n* = 10-15/group). **f,** Representative microphotographs of pleural tumour tissue proliferating cell nuclear antigen (PCNA) immunoreactivity (images) and pleural tumour cell proliferation index (graph; *n* = 5-10/group). **c,** Images: 50 µL cell-free MPE or pleural lavage supernatants obtained from experiment shown in (a, b, e, f) were injected intradermally into the shaved rear skin of *C57BL/6* mice (*n* = 5/group) followed by delivery of 0.8 mg intravenous albumin tracer Evans' blue. Mice were sacrificed and skins were inverted and imaged after 30 min for quantification of skin extravasation areas (dashed lines). Graph: 1.5 x 10^5 LLC, MC38, AE17, B16F10, or PANO2 tumour cells were delivered by direct pleural injection and the *C57BL/6* recipient mice (*n* = 5-12/group) received 0.8 mg intravenous albumin tracer Evans' blue two weeks later, and were sacrificed one hour thereafter. Shown are levels of bloodstream-to-pleural space extravasated albumin-bound Evans' blue. **d,** Phosphate-buffered saline (PBS) or 50 µL cell-free MPE or pleural lavage supernatants obtained from experiment shown in (a, b, e, f) were placed on fenestrated chick chorioallantoic membranes (*n* = 5/group) and membranes were imaged after five days. Shown are representative membrane vascular networks (images; insert is PBS control) and the increase in the number of branching points relative to PBS control (graph). **g,** 7,5 x 10^3 tumour cells were placed on soft agar-containing 60 mm Petri dishes (*n* = 5/group) and imaged after a month. Shown are representative colonies (images) and colony numbers (graph). **h,** 3 x 10^3 tumour cells were placed in DMEM-containing 96-well culture dishes (*n* = 5/group) and MTT reduction was monitored longitudinally. **I,** A million tumour cells were injected subcutaneously into the rear flank of *C57BL/6* mice (*n* = 5/group) and tumour dimensions were monitored longitudinally. Data are presented as mean ± SD. ns, *, ** and ***: $P > 0.05$, $P < 0.05$, $P < 0.01$, and $P < 0.001$ for the comparison between any *Kras*-mutant and any *Kras*-wild-type cell line by one (a-g)- or two (h and i)-way ANOVA with Bonferroni post-tests. LLC, *C57BL/6* Lewis lung carcinoma; MC38, *C57BL/6* colon adenocarcinoma; AE17, *C57BL/6* malignant pleural mesothelioma; B16F10, *C57BL/6* malignant skin melanoma; PANO2, *C57BL/6* pancreatic adenocarcinoma.

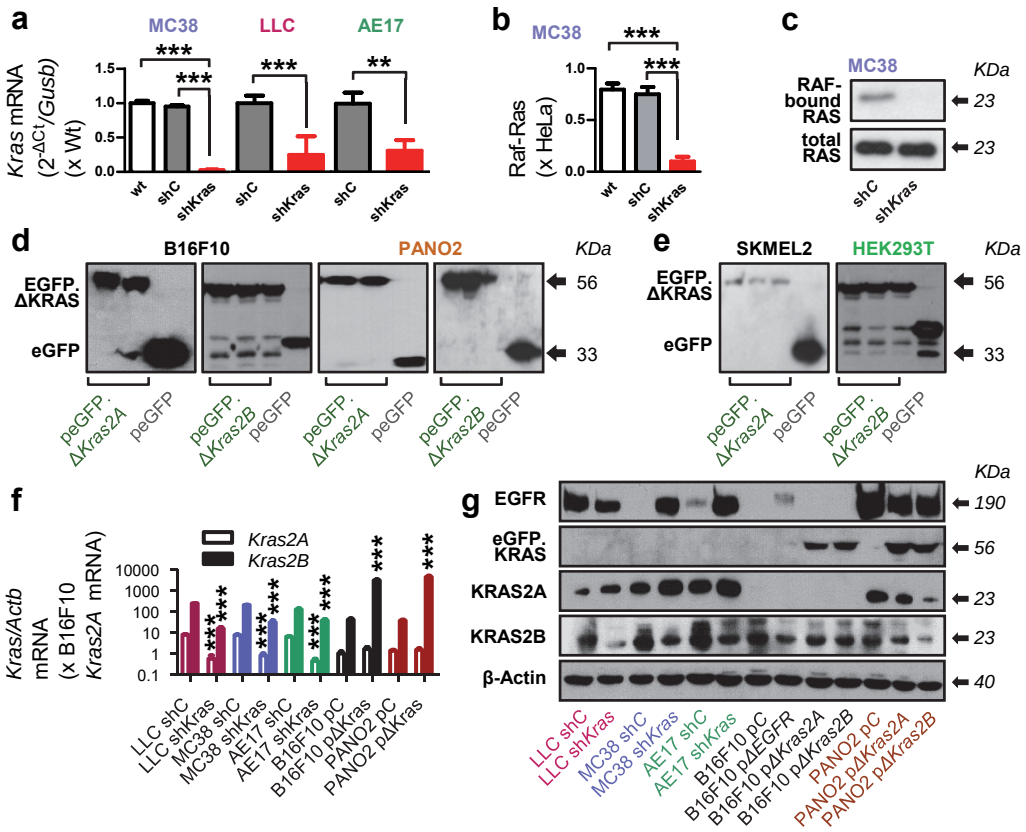
a
MC38
LLC
AE17
Kras mRNA
(2-ΔCt/Gusb)
(x Wt)
wt
shC
shKras
b
MC38
Raf-Ras
(x HeLa)
c
MC38
KDa
RAF-bound RAS
total RAS
23
d
B16F10
PANO2
EGFP.ΔKRAS
eGFP
56
33
peGFP.ΔKras2A
peGFP
peGFP.ΔKras2B
e
SKMEL2
HEK293T
f
Kras2A
Kras2B
Kras/Actb mRNA
(x B16F10 Kras2A mRNA)
LLC shC
LLC shKras
MC38 shC
MC38 shKras
AE17 shC
AE17 shKras
B16F10 pC
B16F10 pΔKras
PANO2 pC
PANO2 pΔKras
g
EGFR
eGFP.KRAS
KRAS2A
KRAS2B
β-Actin
190
40
B16F10 pΔEGFR
B16F10 pΔKras2A
B16F10 pΔKras2B
PANO2 pC
PANO2 pΔKras2A
PANO2 pΔKras2B

Supplementary Figure 3 | Manipulation of mutant *KRAS* isoform expression. *Kras*-mutant mouse tumour cell lines were stably transfected with anti-mouse random (sh*C*) or *Kras* (sh*Kras*) shRNA pools. *KRAS*-wild-type mouse and human cell lines were stably transfected with in-house cloned eukaryotic expression vectors encoding enhanced green fluorescent protein (*peGFP*), eGFP in-frame with mouse mutant *Kras*^{G12C} transcript variant A cloned from LLC total RNA (p*eGFP.ΔKras2A*), or eGFP in-frame with mouse mutant *Kras*^{G12C} transcript variant B cloned from LLC total RNA (p*eGFP.ΔKras or* p*eGFP.ΔKras2B*). **a,** Total *Kras* mRNA expression by qPCR relative to *Gusb* control (*n* = 5-6/group). **b,** Cytoplasmic RAS-activity as determined by binding of Raf-1-RBD coated agarose beads ELISA, relative to HeLa cytoplasmic extracts (*n* = 5/group). **c,** Cytoplasmic RAS-activity as determined by binding of Raf-1RBD coated agarose beads immunoblot relative to total cytoplasmic RAS. **d, e,** Anti-eGFP immunoblots. **f,** *Kras* isoform mRNA expression by qPCR relative to β-actin (*Actb)* control (*n* = 5/group). **g,** Anti-EGFR, eGFP, and KRAS isoform immunoblots relative to β-actin loading control. Data are presented as mean ± SD. ** and ***: $P < 0.01$ and $P < 0.001$ for the indicated comparisons (a and b) and for comparison with the respective parental cell line by Student's t-test (a), and one (a and b)- or two (f)-way ANOVA with Bonferroni post-tests. LLC, *C57BL/6* Lewis lung carcinoma; MC38, *C57BL/6* colon adenocarcinoma; AE17, *C57BL/6* malignant pleural mesothelioma; B16F10, *C57BL/6* malignant skin melanoma; PANO2, *C57BL/6* pancreatic adenocarcinoma; FULA, *FVB* urethane-induced lung adenocarcinoma; CULA, *C57BL/6* urethane-induced lung adenocarcinoma; A549, human lung adenocarcinoma; LTP A549, long-term passaged A549 cells having lost the Y chromosome; SKMEL2, human malignant skin melanoma; HT-29, human colon adenocarcinoma; HEK293T, human embryonic kidney cells.

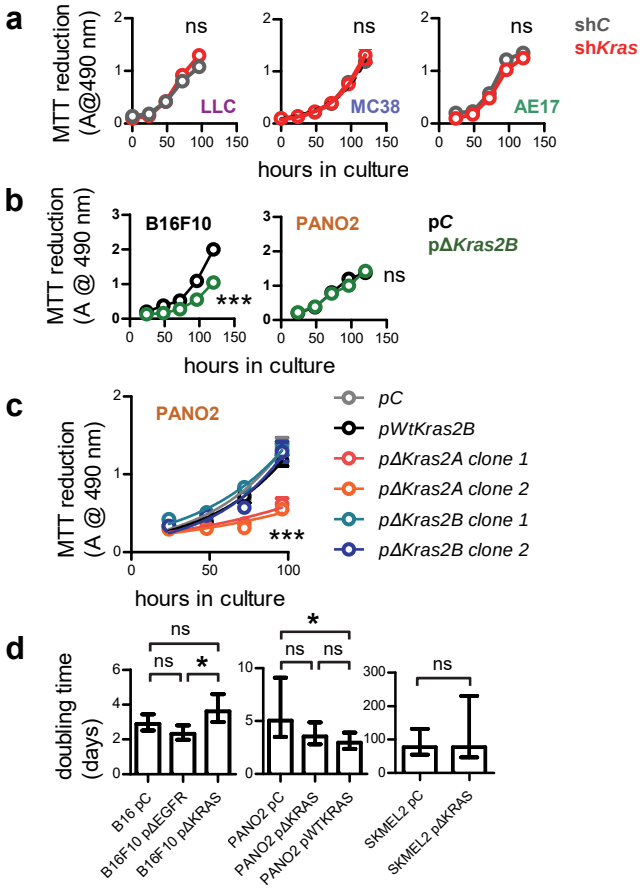
a
MTT reduction (A@490 nm)
ns
LLC
MC38
AE17
shC
shKras
hours in culture
b
MTT reduction (A @ 490 nm)
B16F10
PANO2
***
ns
pC
pΔKras2B
hours in culture
c
PANO2
***
hours in culture
pC
pWtKras2B
pΔKras2A clone 1
pΔKras2A clone 2
pΔKras2B clone 1
pΔKras2B clone 2
d
doubling time (days)
ns
*
B16 pC
B16F10 pΔEGFR
B16F10 pΔKRAS
PANO2 pC
PANO2 pΔKRAS
PANO2 pWTKRAS
SKMEL2 pC
SKMEL2 pΔKRAS

Supplementary Figure 4 | Effect of manipulation of mutant *KRAS* isoform expression on tumour cell proliferation. *Kras*-mutant mouse tumour cell lines were stably transfected with anti-mouse random (sh*C*) or *Kras* (sh*Kras*) shRNA pools. KRAS-wild-type mouse and human cell lines were stably transfected with in-house cloned eukaryotic expression vectors encoding enhanced green fluorescent protein (*peGFP*), eGFP in-frame with mouse mutant $Kras^{G12C}$ transcript variant A cloned from LLC total RNA (p*eGFP.ΔKras2A*), or eGFP in-frame with mouse mutant $Kras^{G12C}$ transcript variant B cloned from LLC total RNA (p*eGFP.ΔKras or* p*eGFP.ΔKras2B*). 3 x 10^3 control or *KRAS*-manipulated tumour cells were placed in DMEM-containing 96-well culture dishes (n = 5/group) and MTT reduction was monitored longitudinally. **a-c,** Raw MTT absorbance data presented as mean ± SD. ns and ***: $P > 0.05$ and $P < 0.001$ for comparison with the respective control vector-transfected cell line by two-way ANOVA with Bonferroni post-tests. **d,** Doubling time data calculated by least-squares fit non-linear regression presented as mean ± 95% confidence interval. ns and *: $P > 0.05$ and $P < 0.05$ for the indicated comparisons by one-way ANOVA with Bonferroni post-tests. LLC, *C57BL/6* Lewis lung carcinoma; MC38, *C57BL/6* colon adenocarcinoma; AE17, *C57BL/6* malignant pleural mesothelioma; B16F10, *C57BL/6* malignant skin melanoma; PANO2, *C57BL/6* pancreatic adenocarcinoma; SKMEL2, human malignant skin melanoma.

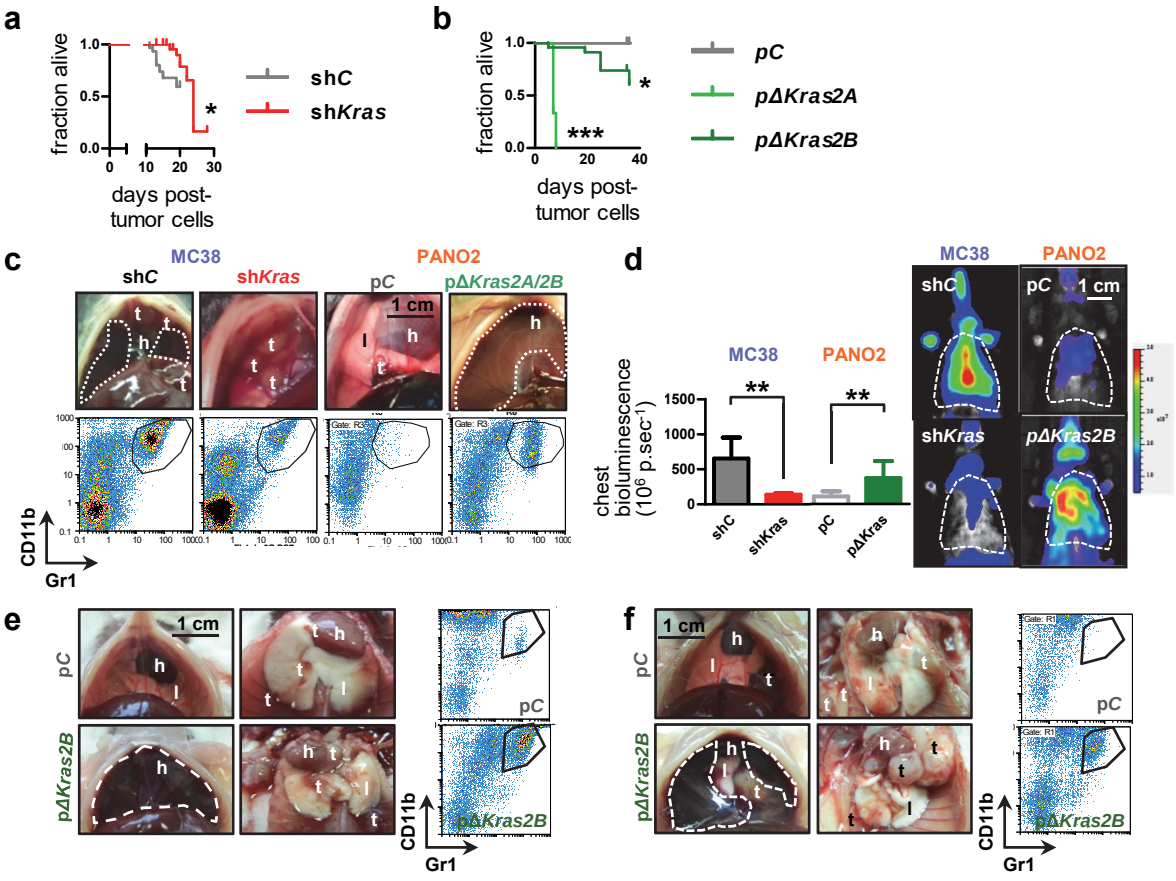
a
fraction alive
1.0
0.5
0.0
0
10
20
30
*
days post-tumor cells
shC
shKras
b
fraction alive
1.0
0.5
0.0
0
20
40
*
***
days post-tumor cells
pC
pΔKras2A
pΔKras2B
c
MC38
PANO2
shC
shKras
pC
pΔKras2A/2B
1 cm
CD11b
Gr1
d
MC38
PANO2
chest bioluminescence (10^6 p.sec^-1)
1500
1000
500
0
**
**
shC
shKras
pC
pΔKras
shC
pC
1 cm
shKras
pΔKras2B
e
1 cm
pC
pΔKras2B
CD11b
Gr1
f
1 cm
pC
pΔKras2B
CD11b
Gr1

Supplementary Figure 5 | Mutant *KRAS* in malignant pleural effusion development. a, Kaplan-Meier plots of survival of *C57BL/6* mice that received 1.5 x 10^5 intrapleural LLC, MC38, or AE17 cells (all *Kras* mutant) stably expressing random (sh*C*; *n* = 40; grey line) or anti-*Kras* (sh*Kras*; *n* = 35; red line) shRNA. **b,** Kaplan-Meier plots of survival of *C57BL/6* mice that received 1.5 x 10^5 intrapleural PANO2 cells (*Kras* wild-type) stably expressing empty (p*C*; *n* = 8; grey line) or mutant *Kras* isoform 2A (p*ΔKras2A*; *n* = 12; light green line) or 2B (p*ΔKras2B*; *n* = 23; dark green line) expression vectors. **a, b,** * and ***: *P* < 0.05 and P < 0.001 for comparison with parental lines by log-rank test. **c,** Representative images (top) of effusions (dashed lines), pleural tumours (t), hearts (h), and lungs (l), and representative dotplots (bottom) of CD11b+Gr1+ cells (polygon gates) from selected experiments described in Fig. 2. **d,** Representative bioluminescent images and data summary of chest light emission (*n* = 5-7/group) of total body-irradiated *C57BL/6* chimeras transplanted with luminescent bone marrow from *CAG.Luc.eGFP* donors at day 14 after pleural injections of the indicated tumour cells. Data are presented as mean ± SD. **: *P* < 0.01 for the indicated comparisons by by Student's t-test. **e, f,** Representative images of malignant pleural disease induced by SKMEL2 (e) and HEK293T (f) cells bearing wild-type (*Wt*) *KRAS* stably expressing empty (p*C*) or mutant *Kras* isoform 2B (p*ΔKras2B*) expression vectors. Shown are representative images of effusions (dashed lines), pleural tumours (t), hearts (h), and lungs (l) and representative dotplots and gating strategy for quantification of CD11b+Gr1+ cells. *Δ*, mutant. LLC, *C57BL/6* Lewis lung carcinoma; MC38, *C57BL/6* colon adenocarcinoma; AE17, *C57BL/6* malignant pleural mesothelioma; B16F10, *C57BL/6* malignant skin melanoma; PANO2, *C57BL/6* pancreatic adenocarcinoma.

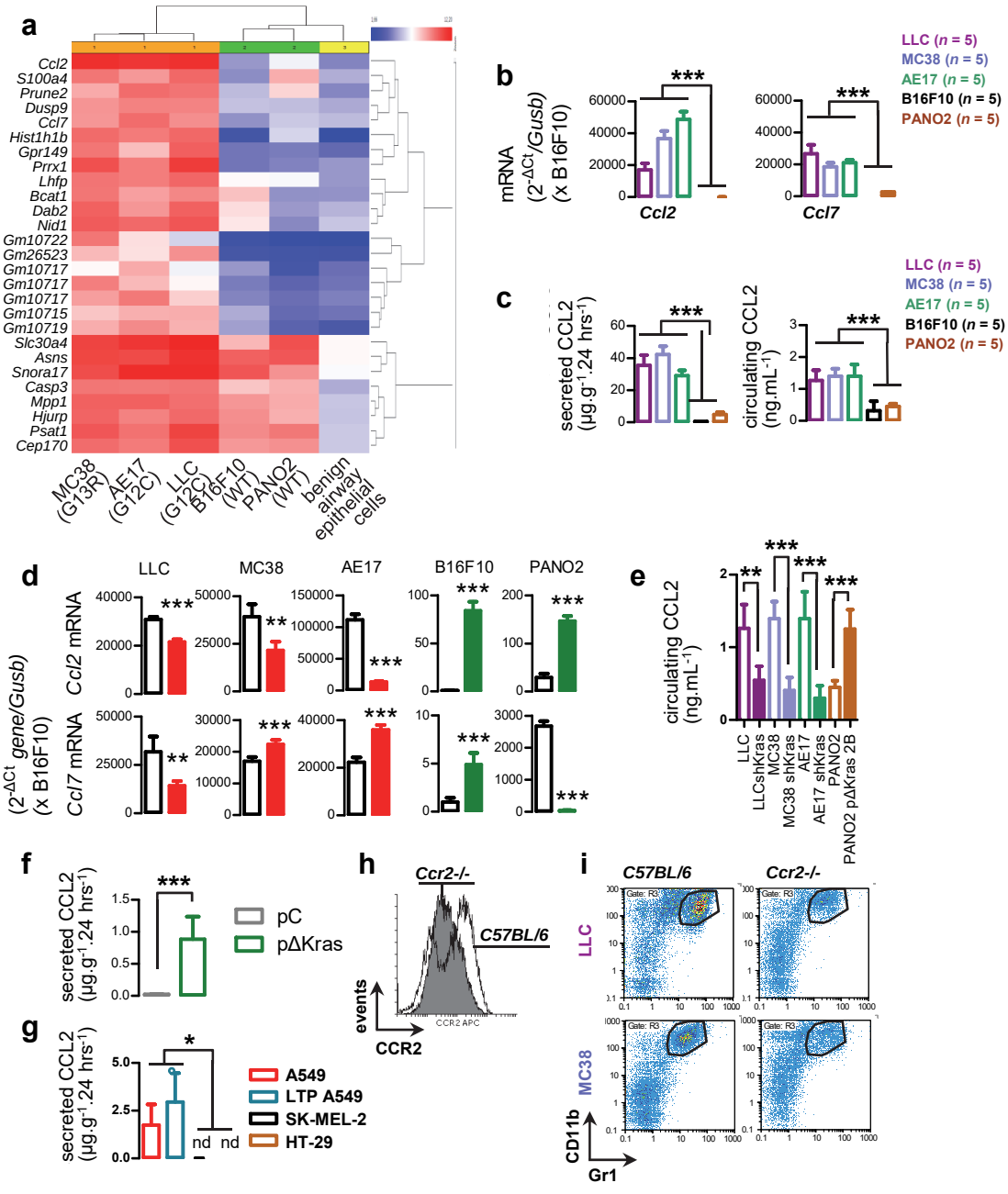
a
Ccl2
S100a4
Prune2
Dusp9
Ccl7
Hist1h1b
Gpr149
Prrx1
Lhfp
Bcat1
Dab2
Nid1
Gm10722
Gm26523
Gm10717
Gm10717
Gm10717
Gm10715
Gm10719
Slc30a4
Asns
Snora17
Casp3
Mpp1
Hjurp
Psat1
Cep170
MC38 (G13R)
AE17 (G12C)
LLC (G12C)
B16F10 (WT)
PANO2 (WT)
benign airway epithelial cells
b
mRNA (2-ΔCt/Gusb) (x B16F10)
Ccl2
Ccl7
LLC (n = 5)
MC38 (n = 5)
AE17 (n = 5)
B16F10 (n = 5)
PANO2 (n = 5)
c
secreted CCL2 (µg.g-1.24 hrs-1)
circulating CCL2 (ng.mL-1)
d
LLC
MC38
AE17
B16F10
PANO2
Ccl2 mRNA
Ccl7 mRNA
(2-ΔCt gene/Gusb) (x B16F10)
e
circulating CCL2 (ng.mL-1)
LLC
LLCshKras
MC38
MC38 shKras
AE17
AE17 shKras
PANO2
PANO2 pΔKras 2B
f
secreted CCL2 (µg.g-1.24 hrs-1)
pC
pΔKras
g
secreted CCL2 (µg.g-1.24 hrs-1)
nd
nd
A549
LTP A549
SK-MEL-2
HT-29
h
Ccr2-/-
C57BL/6
events
CCR2
CCR2 APC
i
C57BL/6
Ccr2-/-
LLC
MC38
CD11b
Gr1

Supplementary Figure 6 | Mutant *KRAS* signals via CCL2/CCR2 to recruit CD11b+Gr1+ myeloid cells to the pleural space. a, Comparative analysis of global gene expression of five *C57BL/6* mouse-derived tumour cell lines with defined *Kras* mutation status by Affymetrix mouse gene ST2.0. Shown is unsupervised clustering of cell lines by differentially expressed genes (*Δ*GE) comprising the mutant Kras signature of 25 genes described in Fig. 3a and Table 3. **b,** *Ccl2* and *Ccl7* mRNA expression by five *C57BL/6* mouse-derived tumour cell lines. **c,** Enhanced CCL2 elaboration of *Kras*-mutant murine cell lines in vitro by ELISA (*n* = 6/group; left) and increased serum CCL2 levels of mice with MPEs induced by *Kras*-mutant murine cell lines *in vivo* by ELISA (*n* = 6/group; right). (b, c) Colour codes are as in Extended Data Fig. 1. **d,** *Ccl2* and *Ccl7* mRNA expression by parental (white bars: cells stably expressing random shRNA or control overexpression vector) and *Kras*-modulated (red bars: cells stably expressing anti-*Kras*-specific shRNA; green bars: cells stably expressing vector encoding mutant mouse $Kras^{G12C}$ isoform B) murine cell lines from Fig. 2 relative to *Gusb* by qPCR showing transcriptional control of *Ccl2* by mutant *Kras* (*n* = 5/group). **e,** Serum CCL2 levels of mice bearing pleural tumours with or without MPE induced by parental and *Kras*-modulated murine cell lines from Fig. 2 by ELISA (*n* = 6/group). **f,** CCL2 secretion of HEK293T cells stably expressing empty (p*C*) or mutant *Kras* isoform 2B (p*ΔKras*2B) expression vectors, assessed by ELISA (*n* = 6/group). **g,** Enhanced CCL2-elaboration of *KRAS*-mutant human cell lines by ELISA (*n* = 6/group). **h,** *Ccr2-/-* and *C57BL/6* control mice received intrapleural injections of three different tumour cell lines, as described in Fig. 3c. Shown are representative histograms of pleural cell CCR2 expression by flow cytometry (*n* = 7/group), **i,** Representative dotplots of CD11b+Gr1+ cells (polygon gates) from experiment in (h).Data are presented as mean ± SD. *, **, and ***: $P < 0.05$, $P < 0.01$, and $P < 0.001$ for comparison with parental lines (d-f) or between any KRAS wild-type and any KRAS-mutant cell line (b, c, g) by Student's t-test (d-f) or one-way ANOVA with Bonferroni post-tests (b, c, g). CCL, C-C-motif chemokine ligand; CCR, C-C-motif chemokine receptor; *Wt*, wild-type; *Δ*, mutant. LLC, *C57BL/6* Lewis lung carcinoma; MC38, *C57BL/6* colon adenocarcinoma; AE17, *C57BL/6* malignant pleural mesothelioma; B16F10, *C57BL/6* malignant skin melanoma; PANO2, *C57BL/6* pancreatic adenocarcinoma; A549, human lung adenocarcinoma; LTP A549, long-term passaged A549 cells having lost the Y chromosome; SKMEL2, human malignant skin melanoma; HT-29, human colon adenocarcinoma.

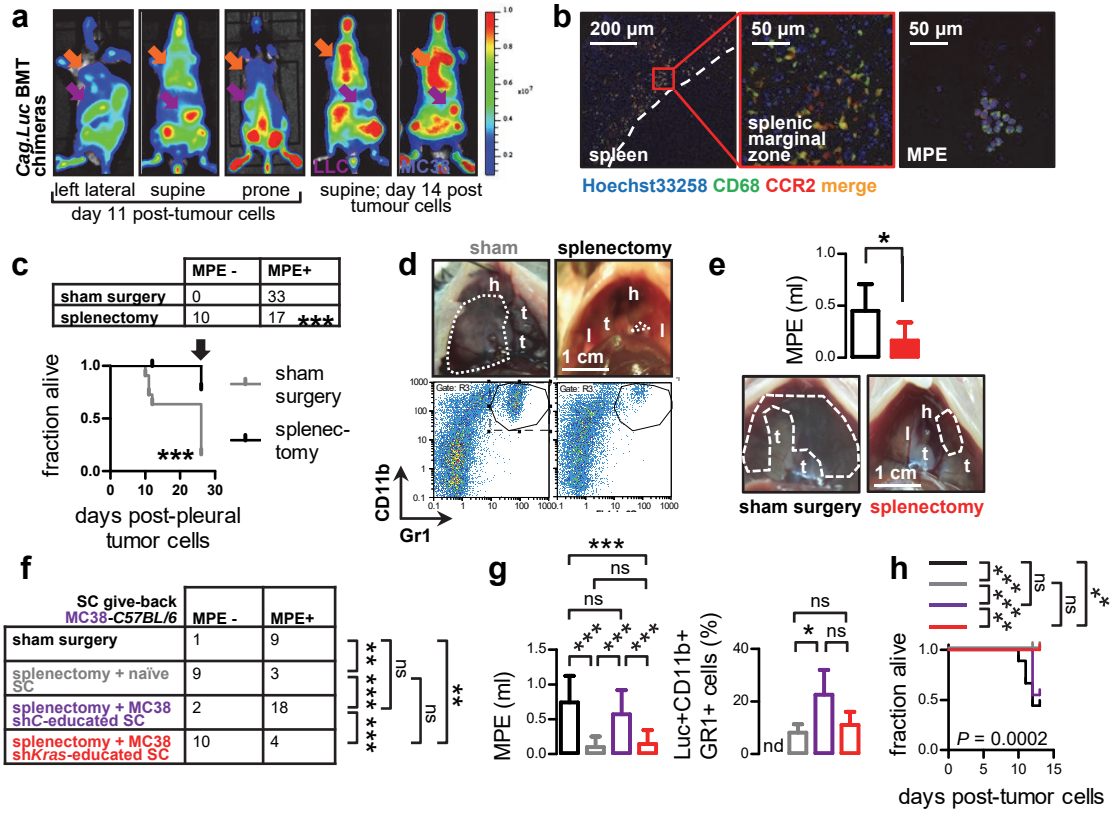
a
Cag.Luc BMT chimeras
LLC
MC38
left lateral
supine
prone
day 11 post-tumour cells
supine; day 14 post tumour cells
b
200 µm
50 µm
50 µm
spleen
splenic marginal zone
MPE
Hoechst33258 CD68 CCR2 merge
c
MPE -
MPE+
sham surgery
0
33
splenectomy
10
17 ***
fraction alive
sham surgery
splenec-tomy
days post-pleural tumor cells
d
sham
splenectomy
h
t
l
1 cm
CD11b
Gr1
e
MPE (ml)
sham surgery
splenectomy
f
SC give-back MC38-C57BL/6
MPE -
MPE+
sham surgery
1
9
splenectomy + naïve SC
9
3
splenectomy + MC38 shC-educated SC
2
18
splenectomy + MC38 shKras-educated SC
10
4
g
MPE (ml)
Luc+CD11b+ GR1+ cells (%)
nd
h
fraction alive
P = 0.0002
days post-tumor cells

Supplementary Figure 7 | CD11b+Gr1+ myeloid cells traffic to the pleural space via the spleen to promote malignant pleural effusion development. a, Representative whole-body bioluminescent images of mice from experiment described in Supplementary Fig. 1f showing sequential increases of the bone marrow cell-emitted signal in the left subphrenic (magenda arrows) and the thoracic (orange arrows) areas. **b,** Immunofluorescent detection of CCR2 and CD68 in spleens and MPE cells of experimental mice from Fig. 1 localized myeloid cells to the marginal zone (magnified area). **c, d,** *C57BL/6* mice received sham surgery or splenectomy followed by pleural injections of MC38 or PANO2 cells expressing p*ΔKras2A* or p*ΔKras2B*. Shown are MPE incidence table (*n*) and Kaplan-Meier survival plot (c) and representative images of effusions (dashed lines), pleural tumours (t), hearts (h), and lungs (l), and representative dotplots of CD11b+Gr1+ cells (polygon gates) (d). ***: $P < 0.001$ for comparison with sham surgery by Fischer's exact test (table) or by log-rank test (survival plot). Note that even splenectomized mice harvested at late time-points (black arrow in c) did not have MPE, indicating a prolonged protective effect of the intervention. **e,** *NOD/SCID* mice received sham surgery or splenectomy followed by pleural A549 lung adenocarcinoma cells with endogenous mutant *KRAS*^{G12S}. Shown are data summary of effusion volume (n = 6-9/group) and representative images of effusions (dashed lines), pleural tumours (t), hearts (h), and lungs (l). Data are presented as mean ± SD. *: $P < 0.05$ for the indicated comparison by Student's t-test. **f-h,** *C57BL/6* mice received sham surgery or splenectomy followed by pleural MC38 cells after 14 days. At post-injection day 9, splenectomized animals were reconstituted with three million intravenous splenocytes (SC) from *CAG.Luc.eGFP* donors pre-treated 13 days earlier with pleural saline (naïve SC), control shRNA-expressing MC38 cells (MC38 sh*C*-educated SC), or anti-*Kras* shRNA-expressing MC38 cells (MC38 sh*Kras*-educated SC). Shown are MPE incidence table (f), data summaries of effusion volume (*n* as in incidence table under f) and Luc+CD11b+Gr1+ bone marrow-borne splenocytes (n = 5/group) (g), and Kaplan-Meier survival plot (h). Data are presented as mean ± SD. ns, **, and ***: $P > 0.05$, $P < 0.01$, and $P < 0.001$ for the comparisons indicated by χ^2 and Fischer's exact tests (f), by log-rank test (h), or by one-way ANOVA with Bonferroni post-tests (g). SC, splenocyte; Luc, luciferase. *Wt*, wild-type; *Δ*, mutant; MC38, *C57BL/6* colon adenocarcinoma; PANO2, *C57BL/6* pancreatic adenocarcinoma.

Uncropped blots of Supplementary Figure 1B; dashed lines indicate portion shown in composite Figure

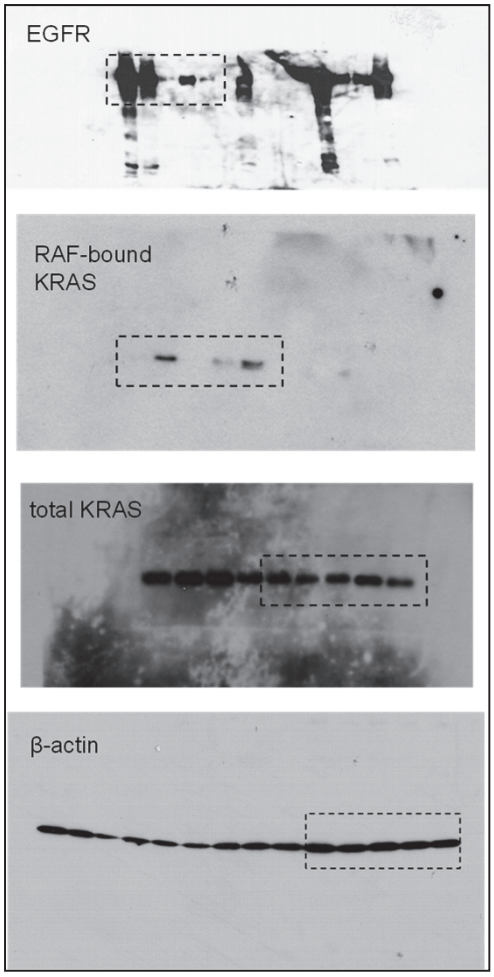

Uncropped blots of Supplementary Figure 1C; dashed lines indicate portion shown in composite Figure

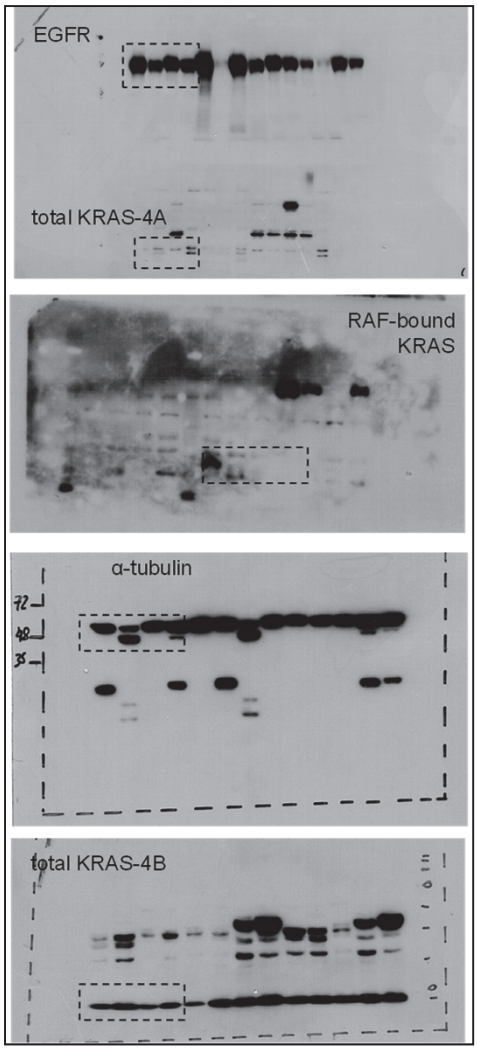

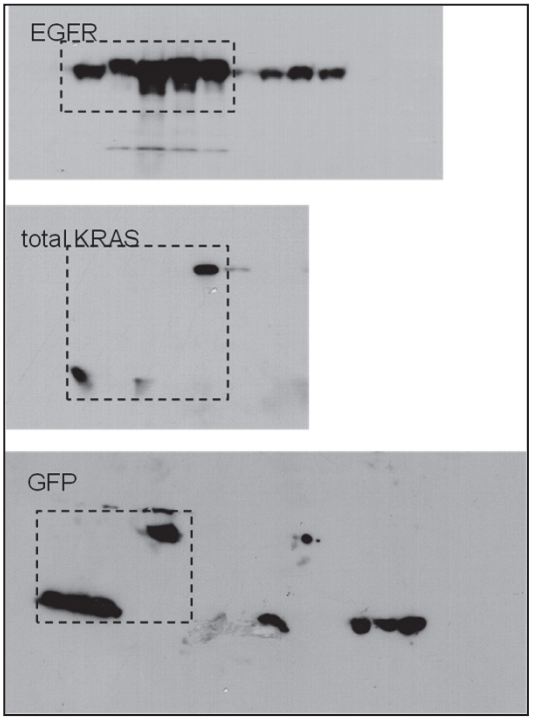

Uncropped blots of Supplementary Figure 1D; dashed lines indicate portion shown in composite Figure

Supplementary Figure 8 | Full blots shown in Supplementary Figure 1.

Uncropped blots of Supplementary Figure 3C; dashed lines indicate portion shown in composite Figure

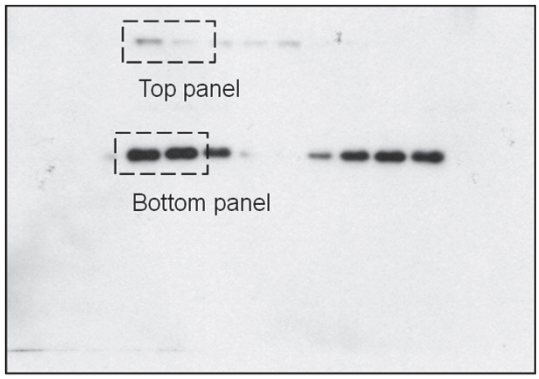

Uncropped blots of Supplementary Figure 3D; dashed lines indicate portion shown in composite Figure

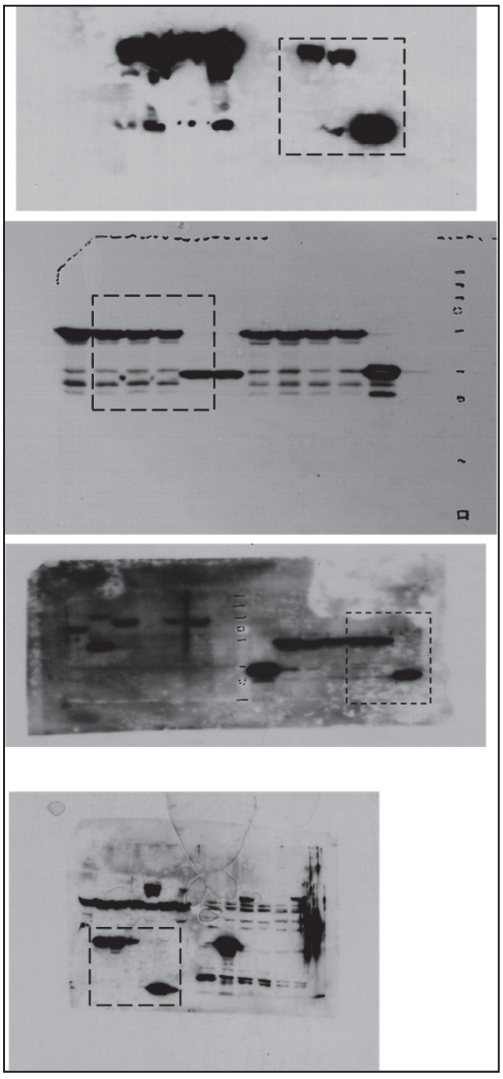

Uncropped blots of Supplementary Figure 3E; dashed lines indicate portion shown in composite Figure

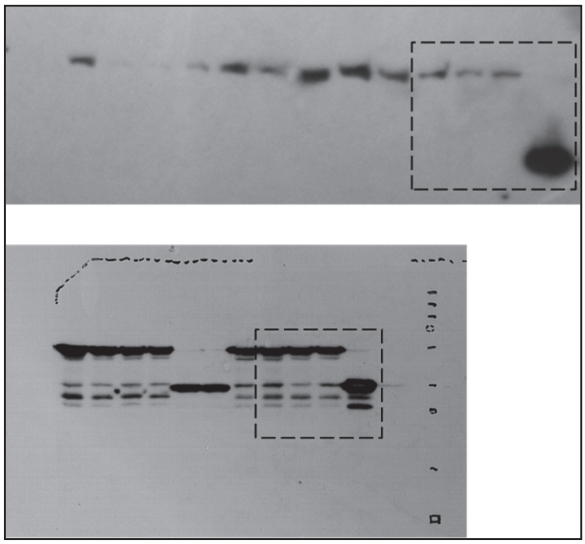

Supplementary Figure 9 | Full blots shown in Supplementary Figures 3c-e.

Uncropped blots of Supplementary Figure 3G; dashed lines indicate portion shown in composite Figure

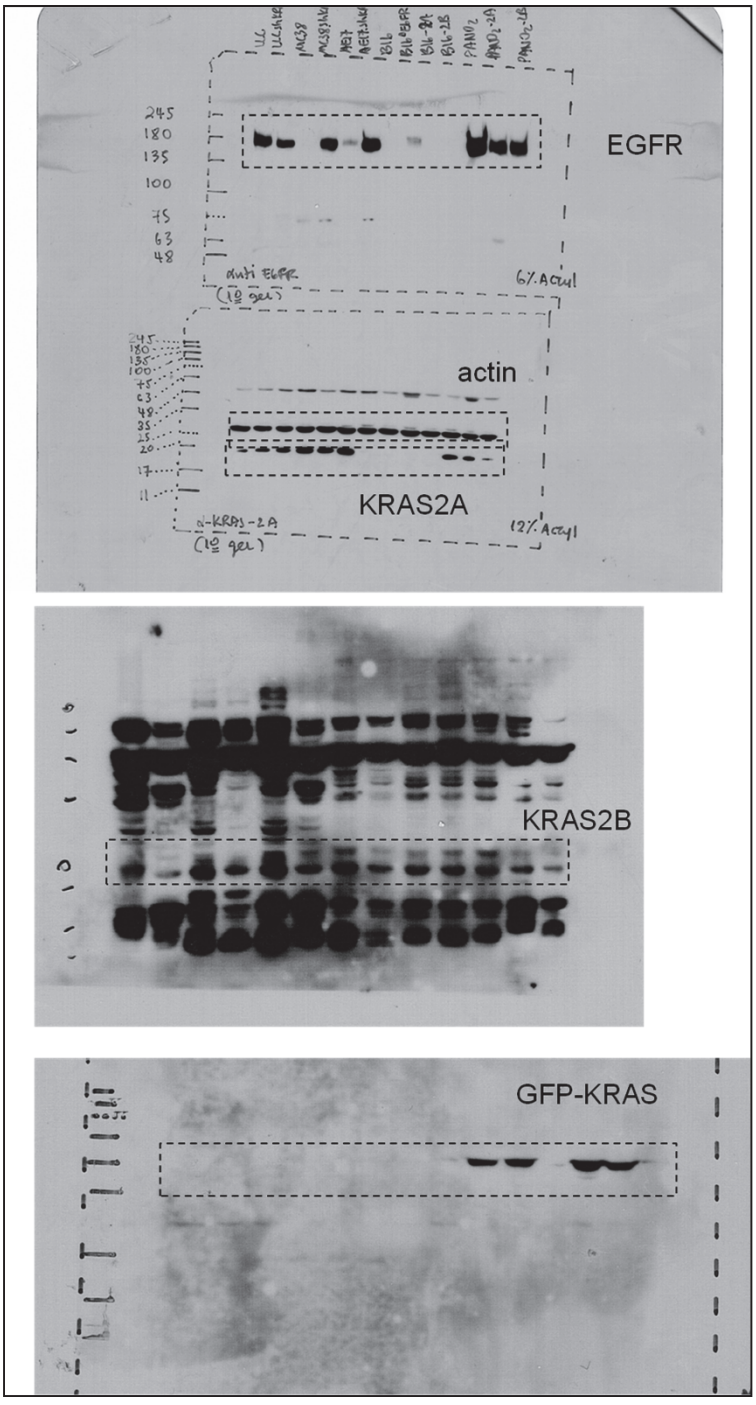

Supplementary Figure 10 | Full blots shown in Supplementary Figure 3g.

Supplementary Table 1 | Oligonucleotide primers used in this study.

Method[a]	Primer	Sequence	Amplicon (bp)
Seq	mKrasF	CCATTTCGGACCCGGAG	905
Seq	mKrasR	CTTTAGTCTCTTCCACAGGCA	
Seq	mEgfrF1	GCCTGATAACTGGACTGACCT	F1/R1 1673
Seq	mEgfrR1	AGAATCAACTCTCGGAACTTTGG	F2R2 2261
Seq	mEgfrF2	CTCCTCTTCTTCCCGCACTG	F2/R 2073
Seq	mEgfrR2	AGAATCTGAGACCTCTGGCTG	1S1/R1 1174
Seq	mEgfrR	GCATAGGTGGCAGACATTATTGG	1S2/R1 672
Seq	mEgfr1S1	ACAACTGCATCCAGTGTGCC	1S1/R2 1759
Seq	mEgfr1S2	GGCCATCAAGGAGTTAAGAG	1S1/R 1571
Seq	mEgfr2S1	AGAGAATCCCTTTGGAGAACC	2S2/R2 1256
Seq	mEgfr2S2	CCACCACTCATGCTGTACAACC	2S2/R 1068
Seq	mEgfr2S3	GTCGTTGGCCTGAACATCAC	2S3/R2 731
Seq	mPik3caF1	ATTCTGACTCCATAAGGCGG	2S3/R 543
Seq	mPik3caR1	GAACCAATCAAACTCCAACTC	1493
Seq	mPik3caF2	GCTGAACCCTATTGGTGTTACTG	
Seq	mPik3caR2	GCTCAAGTCCTAATGTTGTTCCT	1958
Seq	mBrafF1	CGCTGTCTTCGGAAATACCA	
Seq	mBrafR1	AATTCTTTCCATCATGCCTGACC	1551
Seq	mBrafF2	GGCGGGTTCCAGAGGTG	
Seq	mBrafR2	CACTCCACCGAGATTTCACTG	2066
Seq	hKRASF	TCCCAGGTGCGGGAGAGAG	
Seq	hKRASR	GCTAACAGTCTGCATGGAGCAGG	722
PCR	*MycoF*	GGGAGCAAACAGGATTAGATACCCT	
PCR	*MycoR*	TGCACCATCTGTCACTCTGTTAACCTC	270
qPCR	mEfgrtv1F	ATCAAAGTTCTGGGTTCGGG	
qPCR	mEfgrtv1R	CATCACATAGGCTTCGTCAAGG	156
qPCR	mEfgrtv2F	AACTGTACCTATGGATGTGCTG	
qPCR	mEfgrtv2R	GGATTTGGAAGAAACTGGAAGG	154
qPCR	mKrasF	CGCCTTGACGATACAGCTAAT	
qPCR	mKrasR	TGACCTGCTGTGTCGAGAAT	132
qPCR	mKras2AF	AGATGTGCCTATGGTCCTGG	
qPCR	mKras2AR	GCATCCTCCACTCTCTGTCT	144
qPCR	mKras2BF	ACTCTGAAGATGTGCCTATGGT	
qPCR	mKras2BR	TCGTCAACACCCTGTCTTGT	148
qPCR	mCcl2F	CTACAAGAGGATCACCAGCAG	
qPCR	mCcl2R	TTCTGATCTCATTTGGTTCCGA	145
qPCR	mCcl7F	CATCCACATGCTGCTATGTCA	
qPCR	mCcl7R	CTTCCATGCCCTTCTTTGTCT	126
qPCR	mGusbF	TTACTTTAAGACGCTGATCACC	
qPCR	mGusbR	ACCTCCAAATGCCCATAGTC	165
qPCR	mGapdhF	TGTGTCCGTCGTGGATCTGA	
qPCR	mGapdhR	TTGCTGTTGAAGTCGCAGGAG	150
CL	mKrasF	GGAGATCTATGACTGAGTATAAACTTGTGGTGG	
CL	mKras2AR	GGGAATTCTTACATTATAACGCATTTTTTAATT	526
CL	mKras2BR	GGGAATTCTCACATAACTGTACACCTTGTCCTT	583

[a]Application: Seq, sequencing; RT, reverse transcriptase-polymerase chain reaction; PCR, DNA polymerase chain reaction; qPCR, quantitative (real-time) PCR; CL, cloning.

Supplementary Table 2 | Antibodies used in this study.

Method[a]	Target	Provider[b]	Catalog #	Dilution/Dose	Conjugate[c]
WIB	KRAS2A	Santa Cruz	sc-522	1:200	-
WIB	KRAS2B	Santa Cruz	sc-521	1:200	-
WIB	β-Actin	Santa Cruz	sc-47778	1:200	-
WIB	eGFP	Santa Cruz	sc-9996	1:200	-
WIB	α-Tubulin	Sigma	T5168	1:4000	-
WIB	EGFR	Abcam	ab52894	1:10000	-
WIB	Goat anti-mouse IgG	Southern Biotech	1030-05	1:8000	HRP
WIB	Goat anti-rabbit IgG	Southern Biotech	4030-05	1:8000	HRP
HIS	CD31	Abcam	ab124432	1:1000	-
HIS	PCNA	Santa Cruz	sc-56	1:50	-
FC	CD45	eBioscience	11-0451	0.1 μg/10^6 cells	FITC
FC	CD11b	eBioscience	12-0112	0.1 μg/10^6 cells	PE
FC	Gr1	BD	552093	0.1 μg/10^6 cells	PerCP-Cy5.5
FC	Gr1	eBioscience	25-5931-82	0.1 μg/10^6 cells	PE-Cy7
FC	Luciferase	Abcam	ab16466	0.5 μg/10^6 cells	
FC, IF	CCR2	R&D	FAB5538A	1 μL/10^6 cells, 1:500	APC
IF	CD68	Serotec	MCA1957	1:500	-
IVN	CCL2	Janssen R&D	C1142	50 mg/Kg intraperitoneally every three days	-

[a]Application: WIB, Western immunoblotting; HIS, histology; FC, flow cytometry; IF, immunofluorescence; IVN, *in vivo* neutralization.

[b]Providers*:* Santa Cruz Biotechnology, San Diego, CA; Sigma Aldrich, Taufkirchen, Germany; Abcam, Cambridge, UK; Southern Biotech, Birmingham, AL; eBioscience, San Diego, CA; AbD Serotec, Kidlington, UK; R&D Systems, Minneapolis, MN; Oncology Discovery Research, Janssen R&D LLC, Spring House, PA.

[c]Conjugates*:* FITC, fluorescein isothiocyanate; PE, phycoerythrin; PerCP, peridinin-chlorophyll protein; Cy, cyanine; APC, allophycocyanin; HRP, horse radish peroxidase.

5. Publication III: Myeloid-derived interleukin-1β drives oncogenic KRAS-NF-κB addiction in malignant pleural effusion.

5.1. Summary

To meet the pressing need for mechanistic insights into the pathobiology of MPE, we previously developed immunocompetent mouse models of the condition that unveiled inflammatory tumor-to-host signaling networks causing active plasma extravasation into the pleural space (Stathopoulos et al., 2012). Nuclear factor (NF)-κB activity in tumor cells was pivotal for MPE formation in preclinical models, driving pro-inflammatory gene expression and promoting pleural tumor cell survival (Stathopoulos et al., 2006 & 2007a; Psallidas et al., 2010). However, the mechanism of oncogenic NF-κB activation of MPE-competent pleural tumor cells remained unknown. In parallel, we recently pinned mutant KRAS as a molecular determinant of the propensity of pleural-metastasized tumor cells for MPE formation: mutant KRAS delivered its pro-MPE effects by directly promoting C-C chemokine motif ligand 2 (CCL2) secretion by pleural tumor cells, resulting in pleural accumulation of MPE-fostering myeloid cells (Agalioti et al., 2017). However, a unifying mechanism linking KRAS mutations with oncogenic NF-κB activation and MPE competence of pleural tumor cells was missing.

KRAS mutations have been previously linked to elevated or aberrant NF-κB activity via cell-autonomous and paracrine mechanisms. KRAS-mutant tumors, including lung and pancreatic adenocarcinomas, require active NF-κB signaling and NF-κB inhibition blocks KRAS-induced tumor growth (Agalioti et al., 2017; Meylan et al., 2009; Stathopoulos et al., 2007b; Ling et al., 2012; Xue et al., 2011). In turn, NF-κB activation of KRAS-mutant tumor cells has been associated with enhanced RAS signaling, drug resistance, and stemness (Karabela et al., 2012; Daniluk et al., 2012). Despite significant research efforts, the NF-κB-activating kinases (IκB kinases, IKK) and pathways (canonical, involving IκBα, IKKβ, and RelA/P50, versus non-canonical, comprising IκBβ, IKKα, and RelB/P52) that mediate this oncogenic addiction between mutant KRAS and NF-κB signaling are still elusive and diverse, and different studies indicate that IKKα, IKKβ, IKKγ, IKKε, and/or TANK-binding kinase 1 (TBK1) are key for this (Meylan et al., 2009; Stathopoulos et al., 2007b; Ling et al., 2012; Xue et al., 2011; Seguin et al., 2014; Nottingham et al., 2014; Xia et al., 2012; Maier et al., 2013; Bassères et al., 2014; Barbie et al., 2009; Rajurkar et al., 2017).

Here we used immunocompetent mouse models of MPE to show that mutant KRAS determines the responsiveness of pleural tumor cells to host-delivered interleukin (IL)-1β signals by directly regulating IL-1 receptor 1 (IL1R1) expression. The non-canonical IKKα-RelB pathway of KRAS-mutant tumor cells is further shown to mediate MPE development and this is fueled by host-provided interleukin IL-1β. Indeed, IKKα is required for the MPE-competence of KRAS-mutant tumor cells by activating non-canonical NF-κB signaling. IL-1β fuels addiction of mutant KRAS to IKKα resulting in increased CXCL1 secretion that fosters MPE-associated inflammation. Importantly, IL-1β-mediated NF-κB induction in KRAS-mutant tumor cells, as well as their resulting MPE-competence, can only be blocked by co-inhibition of both KRAS and IKKα, a strategy that overcomes drug resistance to individual treatments. Hence we show that mutant KRAS facilitates IKKα-mediated responsiveness of tumor cells to host IL-1β, thereby establishing a host-to-tumor signaling

circuit that culminates in inflammatory MPE development and drug resistance. These studies were largely facilitated by a new contruct developed in the applicants own and mother laboratory, which made screening of a large number of compounds for inducible NF-κB activity possible *in vitro* and *in vivo* (Figure 3).

5.2. Contribution

The applicant conceived the main idea behind this study, performed preliminary proof-of-concept experiments using which he obtained funding for the study in the form of an ERC Starting Grant 2010, purchased the equipment required for the study and recruited the team that performed the experiments, designed all experiments, fostered the collaborations reflected in the paper, analyzed the data, compiled graphs and figures, wrote the manuscript, submitted the manuscript for publication, and corresponded with *Nat Commun*.

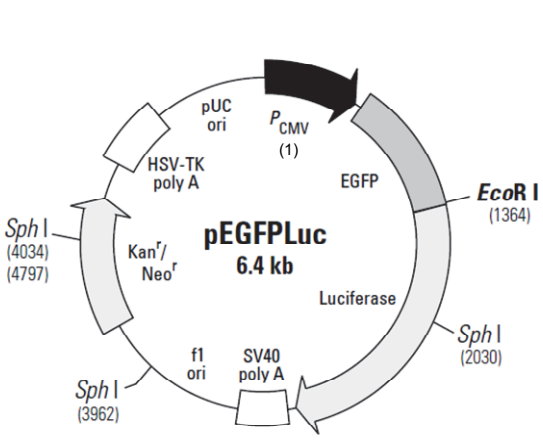


```
1   TAGTTATTAATAGTAATCAATTACGGGGTC
31  ATTAGTTCATAGCCCATATATGGAGTTCCG
61  CGTTACATAACTTACGGTAAATGGCCCGCC
91  TGGCTGACCGCCCAACGACCCCCGCCCATT
121 GACGTCAATAATGACGTATGTTCCCATAGT
151 AACGCCAATAGGGACTTTCCATTGACGTCA
181 ATGGGTGGAGTATTTACGGTAAACTGCCCA
211 CTTGGCAGTACATCAAGTGTATCATATGCC
241 AAGTACGCCCCCTATTGACGTCAATGACGG
271 TAAATGGCCCGCCTGGCATTATGCCCAGTA
301 CATGACCTTATGGGACTTTCCTACTTGGCA
331 GTACATCTACGTATTAGTCATCGCTATTAC
361 CATGGTGATGCGGTTTTGGCAGTACATCAA
391 TGGGCGTGGATAGCGGTTTGACTCACGGGG
421 ATTTCCAAGTCTCCACCCCATTGACGTCAA
451 TGGGAGTTTGTTTTGGCACCAAAATCAACG
481 GGACTTTCCAAAATGTCGTAACAACTCCGC
511 CCCATTGACGCAAATGGGCGGTAGGCGTGT
541 ACGGTGGGAGGTCTATATAAGCAGAGCTGG
571 TTTAGTGAACCGTCAGATCCGCTAGCGCTA
601 CCGGTCGCCACCATGGTGAGCAAGGGCGAG
```

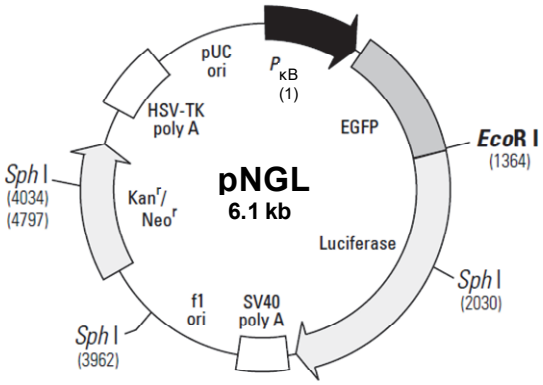


```
1   TAGTTATTAATAACGACGGCCAGTGCCAAG
31  CTTGGGACTTTCCACGTGGGACTTTCCATC
61  CGCGGAAGGGACTTTCCATATGGGACTTTC
91  CATCCGCGGAAGGGACTTTCCATATGGGAC
121 TTTCCATCCGCGGAAGGGACTTTCCACGTG
151 GGACTTTCCTCTAGAGGATCCGGCCCCGCC
181 CAGCGTCTTGTCATTGGCGAATTCGAACAC
211 GCAGATGCAGTCGGGGCGGCGCGGTCCGAG
241 GTCCACTTCGCATATTAAGGTGACGCGTGT
271 GGCCTCGAACACCGAGCGACCCTGCAGCGA
301 CCCGCTTAACAGCGTCAACAGCGTGCCGCA
331 GATCTCGAGGAGCTTGGCGAGATTTTACCG
361 GTCGCCACCATGGTGAGCAAGGGCGAG
```

Figure 3. Making of the NF-κB reporter plasmid used in this study.

Map and partial sequence of origin (1) of originating plasmid before cloning (top) and of final NF-κB reporter plasmid (NF-κB.GFP.Luc; pNGL). CMV promoter is shown in blue and κB binding sites of NF-κB reporter plasmid are shown in red.

nature COMMUNICATIONS

5.3. Publication III

ARTICLE

DOI: 10.1038/s41467-018-03051-z OPEN

Myeloid-derived interleukin-1β drives oncogenic *KRAS*-NF-κB addiction in malignant pleural effusion

Antonia Marazioti[1], Ioannis Lilis[1], Malamati Vreka[1,2], Hara Apostolopoulou[1], Argyro Kalogeropoulou[3], Ioanna Giopanou[1], Georgia A. Giotopoulou[1], Anthi C. Krontira[1], Marianthi Iliopoulou[1], Nikolaos I. Kanellakis[1], Theodora Agalioti[1], Anastasios D. Giannou[1], Celestial Jones-Paris[4], Yoichiro Iwakura[5], Dimitrios Kardamakis[6], Timothy S. Blackwell[4], Stavros Taraviras[3], Magda Spella[1] & Georgios T. Stathopoulos[1,2]

Malignant pleural effusion (MPE) is a frequent metastatic manifestation of human cancers. While we previously identified *KRAS* mutations as molecular culprits of MPE formation, the underlying mechanism remained unknown. Here, we determine that non-canonical IKKα-RelB pathway activation of *KRAS*-mutant tumor cells mediates MPE development and this is fueled by host-provided interleukin IL-1β. Indeed, IKKα is required for the MPE-competence of *KRAS*-mutant tumor cells by activating non-canonical NF-κB signaling. IL-1β fuels addiction of mutant *KRAS* to IKKα resulting in increased CXCL1 secretion that fosters MPE-associated inflammation. Importantly, IL-1β-mediated NF-κB induction in *KRAS*-mutant tumor cells, as well as their resulting MPE-competence, can only be blocked by co-inhibition of both *KRAS* and IKKα, a strategy that overcomes drug resistance to individual treatments. Hence we show that mutant *KRAS* facilitates IKKα-mediated responsiveness of tumor cells to host IL-1β, thereby establishing a host-to-tumor signaling circuit that culminates in inflammatory MPE development and drug resistance.

[1] Department of Physiology, Laboratory for Molecular Respiratory Carcinogenesis, Faculty of Medicine, University of Patras, 26504 Rio, Achaia, Greece. [2] Comprehensive Pneumology Center (CPC) and Institute for Lung Biology and Disease (iLBD), University Hospital, Ludwig-Maximilians University and Helmholtz Zentrum München, Member of the German Center for Lung Research (DZL), 81377 Munich, Bavaria, Germany. [3] Stem Cell Biology Laboratory, Department of Physiology, Faculty of Medicine, University of Patras, 26504 Rio, Achaia, Greece. [4] Division of Allergy, Pulmonary and Critical Care, Department of Internal Medicine, Vanderbilt University School of Medicine, T-1218 MCN, Nashville, TN 37232-2650, USA. [5] Research Institute for Biomedical Sciences, Tokyo University of Science, Tokyo, Chiba 278-0022, Japan. [6] Department of Radiation Oncology and Stereotactic Radiotherapy, Faculty of Medicine, University of Patras, 26504 Rio, Achaia, Greece. Magda Spella and Georgios T. Stathopoulos are co-senior authors. Correspondence and requests for materials should be addressed to A.M. (email: amarazioti@upatras.gr) or to G.T.S. (email: gstathop@upatras.gr)

Malignant pleural effusion (MPE) is one of the most challenging cancer-related disorders. It ranks among the top prevalent metastatic manifestations of tumors of the lungs, breast, pleura, gastrointestinal tract, urogenital tract, and hematopoietic tissues, killing an estimated two million patients worldwide every year and causing 126,825 admissions in U.S. hospitals in 2012 alone[1,2]. The presence of a MPE at diagnosis is an independent negative prognostic factor in patients with lung cancer and mesothelioma[3,4]. In addition, current therapies are non-etiologic and often ineffective, may cause further morbidity and mortality, and have not yielded significant improvements in survival[5,6].

To meet the pressing need for mechanistic insights into the pathobiology of MPE, we developed immunocompetent mouse models of the condition that unveiled inflammatory tumor-to-host signaling networks causing active plasma extravasation into the pleural space[7]. Nuclear factor (NF)-κB activity in tumor cells was pivotal for MPE formation in preclinical models, driving pro-inflammatory gene expression and promoting pleural tumor cell survival[8–10]. However, the mechanism of oncogenic NF-κB activation of MPE-competent pleural tumor cells remained unknown. In parallel, we recently pinned mutant *KRAS* as a molecular determinant of the propensity of pleural-metastasized tumor cells for MPE formation: mutant *KRAS* delivered its pro-MPE effects by directly promoting C-C chemokine motif ligand 2 (CCL2) secretion by pleural tumor cells, resulting in pleural accumulation of MPE-fostering myeloid cells[11]. However, a unifying mechanism linking *KRAS* mutations with oncogenic NF-κB activation and MPE competence of pleural tumor cells was missing.

KRAS mutations have been previously linked to elevated or aberrant NF-κB activity via cell-autonomous and paracrine mechanisms. *KRAS*-mutant tumors, including lung and pancreatic adenocarcinomas, require active NF-κB signaling[12–14] and NF-κB inhibition blocks *KRAS*-induced tumor growth[14–16]. In turn, NF-κB activation of *KRAS*-mutant tumor cells has been associated with enhanced RAS signaling, drug resistance, and stemness[17,18]. Despite significant research efforts, the NF-κB-activating kinases (IκB kinases, IKK) and pathways (canonical, involving IκBα, IKKβ, and *Rel*A/P50, versus non-canonical, comprising IκBβ, IKKα, and *Rel*B/P52) that mediate this oncogenic addiction between mutant *KRAS* and NF-κB signaling are still elusive and diverse, and different studies indicate that IKKα, IKKβ, IKKγ, IKKε, and/or TANK-binding kinase 1 (TBK1) are key for this[17–24].

Here we use immunocompetent mouse models of MPE to show that mutant *KRAS* determines the responsiveness of pleural tumor cells to host-delivered interleukin (IL)-1β signals by directly regulating IL-1 receptor 1 (IL1R1) expression. IKKα is further shown to critically mediate IL-1β signaling in *KRAS*-mutant tumor cells, culminating in marked MPE-promoting effects delivered by C-X-C chemokine motif ligand 1 (CXCL1), and in oncogenic addiction with mutant *KRAS* evident as drug resistance. Importantly, simultaneous inhibition of IKKα and *KRAS* is effective in annihilating mutant *KRAS*-IKKα addiction in MPE.

Results

Non-canonical NF-κB signaling of *KRAS*-mutant cancer cells. We first evaluated resting-state NF-κB activity of five mouse cancer cell lines with defined *KRAS* mutations and MPE capabilities in syngeneic *C57BL/6* mice[11]: Lewis lung carcinoma (LLC; MPE-competent; $Kras^{G12C}$), MC38 colon adenocarcinoma (MPE-competent; $Kras^{G13R}$), AE17 malignant pleural mesothelioma (MPE-competent; $Kras^{G12C}$), B16F10 skin melanoma, and PANO2 pancreatic adenocarcinoma (both MPE-incompetent and $Kras^{WT}$) cells. Parallel transient transfection of these cell lines with reporter plasmids encoding *Photinus Pyralis* LUC under control of either a constitutive (p*CAG.LUC*) or a NF-κB-dependent (*pNF-κB.GFP.LUC*; p*NGL*) promoter[8–11,25] (Fig. 1a) revealed that unstimulated NF-κB activity did not segregate by *KRAS* mutation status (Fig. 1b). However, when PANO2 cells, a cell line with relatively low NF-κB activity, were transiently transfected with $pKras^{G12C}$, their NF-κB expression levels were elevated (Fig. 1c). Moreover, *KRAS* mutant (MUT) cells displayed elevated DNA-binding activity of non-canonical NF-κB subunits P52 and *Rel*B by functional NF-κB enzyme-linked immunosorbent assay (ELISA) and enhanced nuclear immunofluorescent localization of *Rel*B compared with $KRAS^{WT}$ cells (Fig. 1d, e). Immunoblotting of cytoplasmic and nuclear extracts revealed that $KRAS^{MUT}$ cells had increased levels of cytoplasmic *Rel*A and IκBα and of nuclear *Rel*B, IκBβ, and IKKα compared with $Kras^{WT}$ cells (Fig. 1f). These results suggest that $KRAS^{MUT}$ cancer cells exhibit non-canonical endogenous NF-κB activity.

Resistance of *KRAS*-mutant cancer cells to IKKβ inhibition. We next examined the effects of small molecule inhibitors of the proteasome (bortezomib[26]), of IKKβ (IMD-0354[27]), or of heat shock protein 90 (HSP90) (17-dimethylaminoethylamino-17-demethoxygeldanamycin (17-DMAG)[28]) that display significant inhibitory activity against IKKβ and/or IKKα (of note, a specific IKKα inhibitor does not exist) on NF-κB reporter activity and cellular proliferation of our murine cancer cell lines (Fig. 1g, h; Supplementary Table 1). Bortezomib, an indirect inhibitor of IKKβ via cytoplasmic accumulation of non-degraded IκBα[16,26], attenuated endogenous NF-κB activity of $Kras^{WT}$ cells but paradoxically activated NF-κB in $KRAS^{MUT}$ cells, at the same time more effectively killing $KRAS^{WT}$ than $KRAS^{MUT}$ cells in vitro. Similarly, IKKβ-selective IMD-0354[27] blocked NF-κB activity and cellular proliferation of unstimulated $KRAS^{WT}$ cells but not of $KRAS^{MUT}$ cells. Interestingly, the HSP90 and dual IKKα/IKKβ inhibitor 17-DMAG[29] was equally effective in limiting NF-κB activity and cellular proliferation of all cell lines irrespective of *KRAS* mutation status. These results suggest the existence of endogenous resistance of *KRAS*-mutant cells to IKKβ inhibition, which can be overcome by combined HSP90/IKKα/IKKβ inhibition.

IL-1-inducible NF-κB activation of *KRAS*-mutant cancer cells. We next studied NF-κB activation patterns of our murine cancer cells in response to exogenous stimuli. For this, cells were stably transfected with p*NGL*, were pretreated with saline or bortezomib (1 μM ~5–10-fold the 50% NF-κB inhibitory concentration obtained from $Kras^{WT}$ cells; Supplementary Table 1), were exposed to 60 different candidate NF-κB-pathway ligands at 1 nM concentration[30], and were longitudinally monitored for NF-κB-dependent LUC activity by bioluminescence imaging of live cells in vitro (Fig. 2a, b; Supplementary Table 2). Incubation with lipopolysaccharide (LPS) and tumor necrosis factor (TNF) resulted in markedly increased NF-κB activity in all cells irrespective of *KRAS* status, while lymphotoxin β activated NF-κB in all but PANO2 cells, effects that peaked by 4–8 h of incubation and subsided by 16–24 h. Uniquely, IL-1α and IL-β induced NF-κB exclusively in $KRAS^{MUT}$ cells. In addition, bortezomib exaggerated endogenous and inducible NF-κB activation of $KRAS^{MUT}$ cells, in contrast to $KRAS^{WT}$ cells that displayed efficient NF-κB blockade by bortezomib. In line with the above, *Il1r1* (encoding IL1R1, cognate to IL-1α/β) expression, but not *Tnfrsf1a/Tnfrsf1b* (encoding TNF receptors) or *Il1a/Il1b* expression (that was undetectable in all cell lines), was exclusively restricted to

KRAS^{MUT} MPE-proficient tumor cells (Fig. 2c, d). We subsequently tested whether inducible NF-κB activation occurs in tumor cells entering the pleural space in vivo, simulating incipient pleural carcinomatosis[4,7]. For this, naive *C57BL/6* mice were pulsed with a million intrapleural p*NGL*-expressing tumor cells and were serially imaged for NF-κB-dependent bioluminescence. Amazingly, *KRAS*^{MUT} MPE-competent cells responded to the pleural environment with markedly escalated NF-κB activity within 4 h after injection, while *KRAS*^{WT} MPE-incompetent cells showed diminishing NF-κB signals (Fig. 3a). Interestingly, this

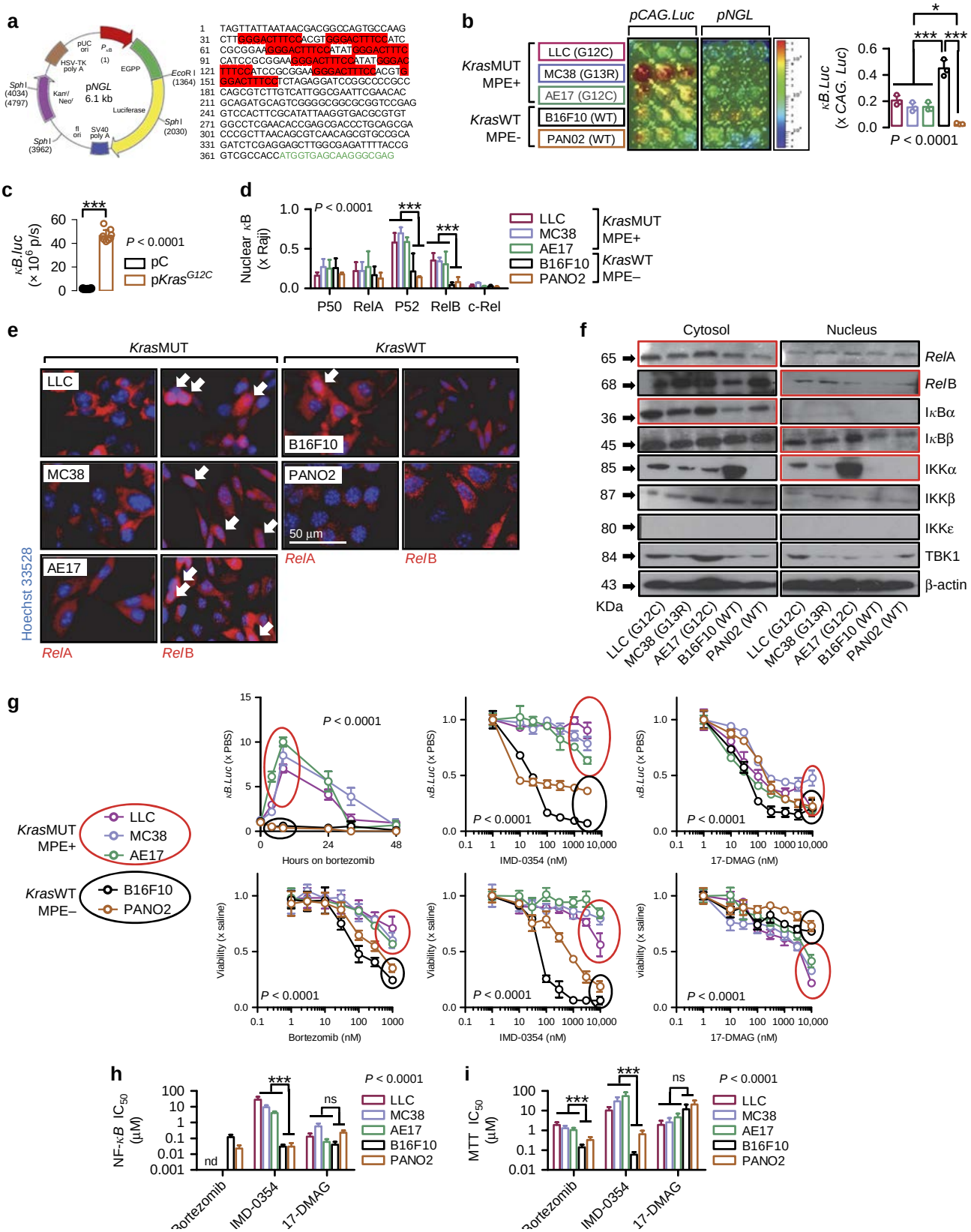

in vivo NF-κB response of *KRAS*^{MUT} cells was abolished in IL-1β-deficient (*Il1b*−/−[31]), but not in TNF-deficient (*Tnf*−/−[32]), mice (Fig. 3b), indicating that *KRAS*^{MUT} tumor cells selectively respond to IL-1β of the pleural environment by activating NF-κB.

Mutant *KRAS* promotes non-canonical NF-κB signaling. To define the role of mutant *KRAS* in the aberrant NF-κB activation patterns of *KRAS*^{MUT} tumor cells, including non-canonical endogenous NF-κB activity, resistance to IKKβ inhibition, and IL-1β-inducibility, we undertook short hairpin RNA (shRNA)-mediated *KRAS* silencing (sh*Kras*) and plasmid-mediated overexpression of a mutant dominant-negative form of IκBα (p*IκBα*DN; inhibits canonical NF-κB signaling) in *KRAS*^{MUT} cell lines, as well as plasmid-mediated overexpression of mutant *KRAS* (p*Kras*^{G12C}) in *KRAS*^{WT} cell lines[11,33]. Stable p*IκBα*DN expression in MC38 cells (*Kras*^{G13R}) resulted in decreased *Rel*A and sustained *Rel*B nuclear-binding activity, while sh*Kras* did not affect *Rel*A but abolished *Rel*B nuclear-binding activity (Fig. 4a). sh*Kras* also eliminated nuclear *Rel*B localization in these cells without affecting *Rel*A (Fig. 4b) and abolished nuclear IKKα immunoreactivity of LLC (*Kras*^{G12C}) and MC38 cells (Fig. 4c). sh*Kras* expression reversed the endogenous resistance of MC38 cells to bortezomib and IMD-0354, rendering them as sensitive as *KRAS*^{WT} cells (Fig. 4d, e). In addition, sh*Kras* annihilated IL-1β-induced NF-κB transcriptional activity of p*NGL*-expressing LLC, MC38, and AE17 (*Kras*^{G12C}) cells (Fig. 4f), and p*Kras*^{G12C} transmitted this phenotype to *Kras*^{WT} PANO2 cells (Fig. 4g). Importantly, sh*Kras* abrogated the in vivo NF-κB response of pleural-inoculated MC38 cells, which was reinstated in PANO2 cells by stable p*Kras*^{G12C} expression (Fig. 4h, i). In parallel, *KRAS* silencing in *KRAS*^{MUT} cells significantly decreased, whereas p*Kras*^{G12C} overexpression in *KRAS*^{WT} cells significantly increased *Il1r1* expression, as well as resting-state and IL-1β-inducible nuclear immunoreactivity for *Rel*B, IκBβ, and IKKα (Fig. 4j–l). Collectively, these data indicate that mutant *KRAS* induces non-canonical NF-κB signaling of cancer cells in unstimulated and IL-1β-stimulated conditions.

IKKα in mutant *KRAS*-dependent MPE. To define the NF-κB-activating kinase responsible for aberrant NF-κB signaling of *KRAS*^{MUT} cancer cells, we stably expressed shRNAs specifically targeting IKKα, IKKβ, IKKε, and TBK1 transcripts (*Chuk*, *Ikbkb*, *Ikbke*, and *Tbk1*, respectively) in our p*NGL*-expressing cell lines and validated them (Fig. 5a). In addition, we cloned these murine transcripts into an eukaryotic expression vector and generated stable transfectants of our cell lines. Interestingly, resting-state NF-κB transcriptional activity across *KRAS*^{MUT} cells was markedly suppressed by sh*Chuk* but not by sh*Ikbkb* or sh*Tbk1*, while sh*Ikbke* yielded minor NF-κB inhibition in MC38 and AE17 cells. On the contrary, endogenous NF-κB-mediated transcription of B16F10 cells was exclusively silenced by sh*Ikbkb* and, to a lesser extent, sh*Ikbke*, and of PANO2 cells by no shRNA (Fig. 5b). In a reverse approach, overexpression of any kinase resulted in enhanced NF-κB activity in all *KRAS*^{MUT} cells, of IKKβ only in B16F10 cells, and of no kinase in PANO2 cells (Fig. 5c). In addition to intrinsic, IKKα also mediated IL-1β-inducible NF-κB activity of *KRAS*^{MUT} tumor cells, since sh*Chuk* but not sh*Ikbkb* abolished IL-1β-induced NF-κB activity across *KRAS*^{MUT} cell lines (Fig. 5d). In line with the above, sh*Chuk* abolished the immunoreactivity of MC38 cell nuclear extracts for *Rel*B, IκBβ, and IKKα, both at resting and IL-1β-stimulated states (Fig. 5e). Taken together, these data suggest that *KRAS*-mutant cancer cells respond to pleural IL-1β via IKKα-mediated non-canonical NF-κB activation. Based on these results and our previous identification of the importance of *KRAS* mutations and NF-κB signaling in MPE development[8–11], we hypothesized that IKKα is required for sustained NF-κB activation and MPE induction by pleural-homed *KRAS*^{MUT} cancer cells. To test this, we injected IKK-silenced p*NGL*-expressing LLC cells (*Kras*^{G12C}; MPE-competent) into the pleural space of *C57BL/6* mice. Indeed, recipients of IKKα-silenced LLC cells displayed significant reductions in MPE incidence and volume, pleural inflammatory cell influx, and pleural tumor NF-κB activity and prolonged survival. IKKε silencing delivered more modest and equivocal beneficial effects, while IKKβ and TBK1 silencing had no impact (Fig. 6a–c; Supplementary Table 3). These experiments were repeated with IKKα- and IKKβ-silenced MC38 cells (*Kras*^{G13R}; MPE-competent) stably expressing p*NGL*, confirming that IKKα is cardinal for oncogenic NF-κB activation and MPE precipitation by pleural-metastatic *KRAS*^{MUT} tumor cells (Fig. 6d–f; Supplementary Table 3). However, standalone overexpression of IKKα or IKKβ did not confer MPE competence to *KRAS*^{WT} PANO2 cells, as opposed to p*Kras*^{G12C} (Fig. 6g–i; Supplementary Table 3), in accord with our previous observations[11]. Collectively, these results suggest that mutant *KRAS*-potentiated IL-1β signaling results in *KRAS*^{MUT} addiction to IKKα activity, which is required but not sufficient for oncogenic NF-κB activation and MPE formation.

Myeloid IL-1β fosters mutant *KRAS*-IKKα addiction in MPE. To study the importance of host-delivered IL-1β in the proposed *KRAS*^{MUT}-IKKα addiction culminating in MPE, we delivered p*NGL*-expressing *KRAS*^{MUT} LLC and MC38 cells into the pleural space of *Il1b*−/−, *Tnf*−/−, and *WT C57BL/6* mice. Interestingly, *Il1b*−/− but not *Tnf*−/− mice displayed decreased MPE incidence, volume, inflammatory cell influx, and oncogenic NF-κB

Fig. 1 *Kras*-mutant tumor cells exhibit non-canonical endogenous NF-κB activity. Five different *C57BL/6* mouse tumor cell lines with (*Kras*^{MUT}: LLC, MC38, AE17) or without (*Kras*^{WT}: B16F10, PANO2) *Kras* mutations were assessed for activation and inhibition of resting NF-κB activity in vitro. **a** Map of NF-κB reporter plasmid (NF-κB.GFP.Luc; p*NGL*). Partial p*NGL* sequence at origin (1) showing κB-binding motifs (red) and GFP sequence (green). **b** Representative image and data summary ($n = 3$) of area under curve of cumulative bioluminescence emitted by cells transiently transfected with reporter plasmids p*CAG.LUC* or p*NGL*. **c** Data summary ($n = 8$) of bioluminescence emitted by PANO2 cells stably expressing p*NGL* reporter plasmid at 48 h after transient transfection with p*C* or p*Kras*^{G12C}. **d** Data summary ($n = 5$) of DNA NF-κB motif binding activity of nuclear extracts by NF-κB ELISA relative to nuclear extracts of Raji leukemia cells. **e** Immunofluorescent detection of *Rel*A and *Rel*B in cells grown on glass slides ($n = 3$) showing increased nuclear localization of *Rel*B in *Kras*^{MUT} cells and of *Rel*A in *Kras*^{WT} cells (arrows). **f** Immunoblots of cytoplasmic and nuclear extracts for NF-κB pathway members and β-actin (representative of $n = 3$ independent experiments). Data presented as mean ± s.d. *P*, overall probability by one-way (**b**) and two-way (**d**) ANOVA or Student's *t*-test (**c**). $^{*}P < 0.05$ and $^{***}P < 0.001$ for the indicated comparisons by Bonferroni post-tests. **g** Data summary ($n = 3$) of p*NGL* reporter activity after 4-h treatment and of cell proliferation by MTT assay after 72-h treatment in response to bortezomib, IMD-0354, or 17-DMAG. Data presented as mean ± s.d. from $n = 3$ replicates/data point. *P*, probability of no difference between cell lines by extra sum-of-squares *F* test. **h**, **i** Data summary of 50% inhibitory concentrations (IC_{50}) of NF-κB activity (by p*NGL* reporter activity) and cell proliferation (by MTT; **g**). Data presented as mean ± s.d. from $n = 3$ independent experiments. *P*, probability of no difference by two-way ANOVA. ns and triple asterisks (***): $P > 0.05$ and $P < 0.001$, respectively, for the indicated comparisons by Bonferroni post-tests. nd not determined

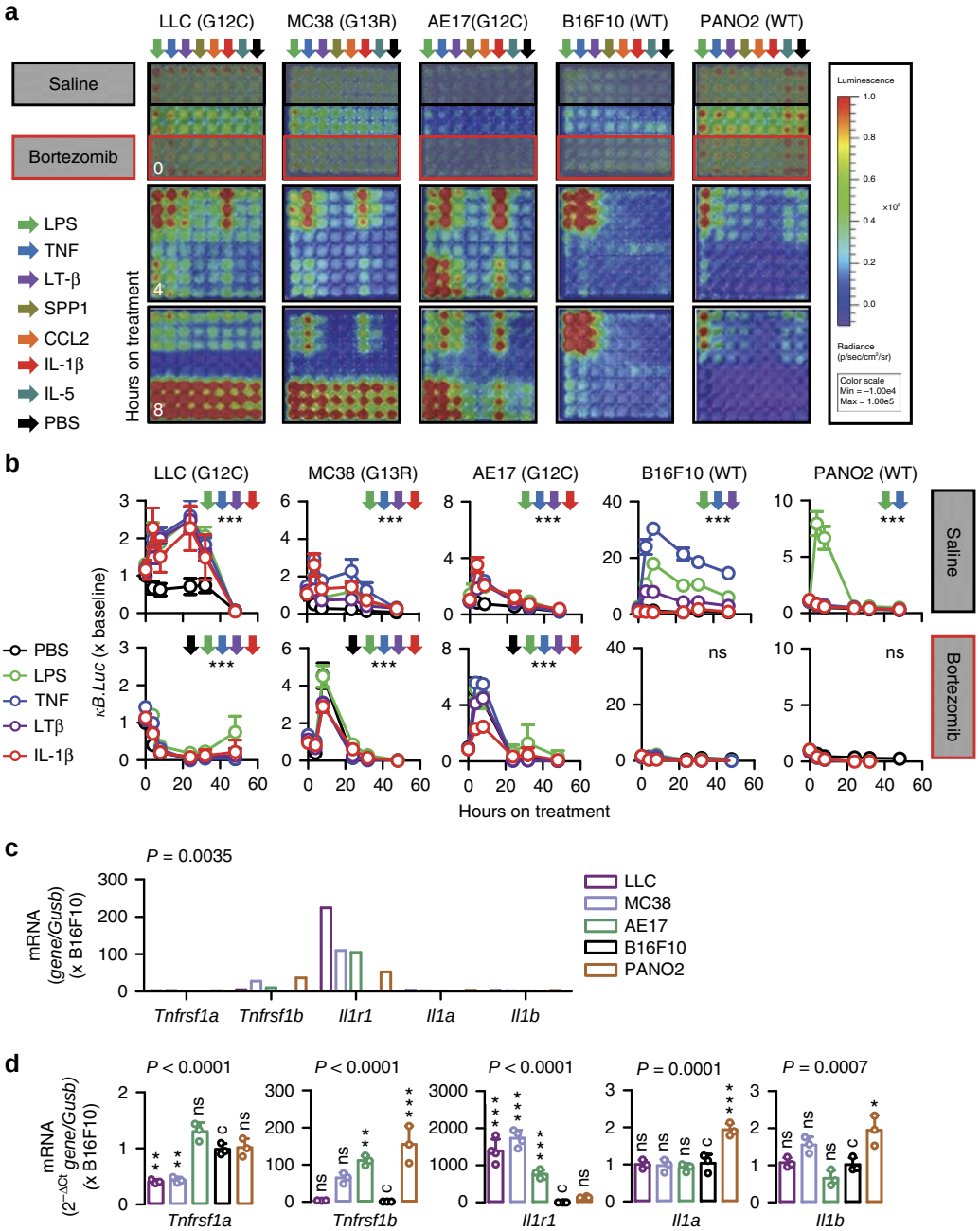

Fig. 2 *Kras*-mutant tumor cells possess IL-1β-inducible NF-κB activity. Five different *C57BL/6* mouse tumor cell lines with (LLC, MC38, AE17) or without (B16F10, PANO2) *Kras* mutations were assessed for inducible NF-κB activation in response to exogenous stimuli and for the expression of relevant receptors in vitro. **a**, **b** Representative bioluminescent images (**a**; shown are $n = 3$ replicates/data-point) and data summary (**b**; mean ± s.d. of $n = 3$ independent experiments) of cells stably expressing p*NGL* and pretreated with saline or 1 μM bortezomib at different time points after addition of 1 nM of the indicated NF-κB ligands (arrows in **a** and legend in **b**). Note NF-κB inducibility by IL-1β and bortezomib exclusively in $Kras^{MUT}$ cells. ns and *** $P > 0.05$ and $P < 0.001$, respectively, for comparison between ligands indicated by colored arrows and PBS at 4 and 8 h on treatment by two-way ANOVA with Bonferroni post-tests. **c**, **d** *Tnfrsf1a*, *Tnfrsf1b*, *Il1r1*, *Il1a*, and *Il1b* mRNA expression relative to *Gusb* by microarray (**c**) and qPCR (**d**). Shown are mean (**c**) and mean ± s.d. (**d**) of $n = 5$ independent technical replicates of one biologic sample. *P*, probability of no difference between cell lines by two-way (**c**) or one-way (**d**) ANOVA. ns, single, double, and triple asterisks (*, **, and ***): $P > 0.05$, $P < 0.05$, $P < 0.01$, and $P < 0.001$, respectively, for comparison with B16F10 cells (**c**) by Bonferroni post-tests

activation (Fig. 7a–d; Supplementary Table 3). Host-provided IL-1β was of myeloid origin, since bone marrow (BM) transplants[34,35] from *C57BL/6* and *Tnf*−/−, but not *Il1b*−/− donors, to lethally irradiated *Il1b*−/− recipients unable to foster MPE rendered LLC cells MPE proficient (Fig. 7e, f; Supplementary Table 3). To define which myeloid cells provide the bulk of IL-1β to fuel tumor cell NF-κB activity, we isolated BM cells from *C57BL/6* mice and drove them toward monocyte and neutrophil differentiation by macrophage colony-stimulating factor (M-CSF) and granulocyte-colony-stimulating factor (G-CSF culture, respectively. Both BM-derived monocytes and neutrophils secreted IL-1β upon 24-hour treatment with cell-free LLC supernatants as measured by ELISA, but monocytes secreted ~200 times higher cytokine levels than undifferentiated BM cells

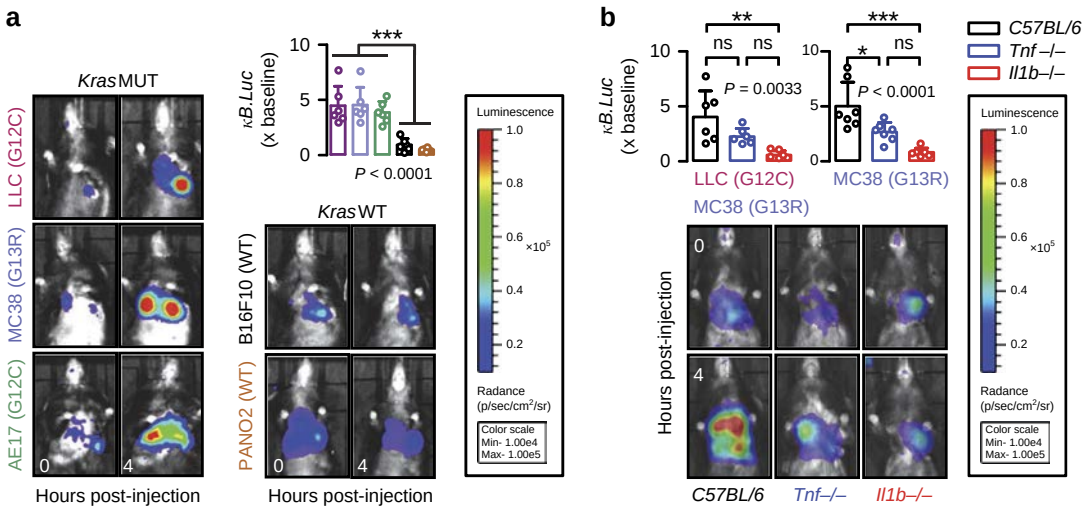

Fig. 3 Pleural IL-1β activates NF-κB in *Kras*-mutant tumor cells in vivo. Five different *C57BL/6* mouse tumor cell lines with (LLC, MC38, AE17) or without (B16F10, PANO2) *Kras* mutations were assessed for inducible NF-κB activation in response to the pleural environment in vivo. **a** Representative bioluminescent images and data summary ($n = 6$ mice/cell line) of *C57BL/6* mice at 0 and 4 h after intrapleural injection of a million mouse tumor cells stably expressing *pNGL*. Note the marked induction of the bioluminescent signal emitted specifically by $Kras^{MUT}$ cells after 4 h. Note also the diminishing signal emitted by $Kras^{WT}$ cells. **b** Representative bioluminescent images and data summary (LLC: $n = 6$ mice/genotype; MC38: $n = 7$ mice/genotype) of *C57BL/6*, *Tnf–/–* and *Il1b–/–* mice at 0 and 4 h after intrapleural injection of LLC or MC38 cells stably expressing *pNGL*. Note the marked induction of the bioluminescent signal in *C57BL/6* mice, the borderline reduction of its inducibility in *Tnf–/–* mice, and the disappearance of signal inducibility in *Il1b–/–* mice. Data are presented as mean ± s.d. *P*, probability of no difference between cell lines or genotypes by one-way ANOVA. ns, single, double, and triple asterisks (*, **, and ***): $P > 0.05$, $P < 0.05$, $P < 0.01$, and $P < 0.001$, respectively, for the indicated comparisons by Bonferroni post-tests

and neutrophils (Fig. 7g). These data clearly show that the main source of IL-1β in the pleural space during MPE development likely are recruited myeloid monocyte cells.

Mutant *KRAS*-IKKα addiction promotes MPE via CXCL1 secretion. To identify the MPE effectors and transcriptional signatures of IL-1β/*KRAS*/IKKα-addicted tumor cells, we subjected KRAS-silenced, IKKα-silenced, and IL-1β-challenged LLC and MC38 cells to microarray analyses, seeking for transcripts altered heterodirectionally by silencing/challenge. Thirty transcripts fulfilled these criteria in LLC (including *Ppbp*, encoding pro-platelet basic protein, PPBP, and *Cxcl1*, encoding CXCL1) and 20 in MC38 (including *Cxcl1*) cells, with *Cxcl1* being the only common gene of these two signatures (Fig. 8a, b; Supplementary Tables 4, 5). *Cxcl1* microarray results were validated by quantitative PCR (qPCR) and ELISA (Fig. 8c–e). Furthermore, chromatin immunoprecipitation (ChIP) was performed in LLC cells treated with phosphate-buffered saline (PBS) or IL-1β in order to specify whether and which NF-κB component directly binds to the promoter region of *Cxcl1*. The data indicate that only *Rel*B and IKKα bind to the NF-κB element in the *Cxcl1* promoter and that IL-1β significantly strengthens this binding (Fig. 8f). These findings are consistent with the enhanced transcriptional induction of *Cxcl1*. Moreover, *Cxcl1* and *Ppbp* expression was pivotal for MPE induction by IL-1β/*KRAS*/IKKα-addicted LLC cells, since these were MPE incompetent in both C-X-C chemokine motif receptor 1 (CXCR1) and CXCR2 gene-deficient mice[36,37] that lack the genes encoding CXCL1/PPBP-cognate CXCR1 and CXCR2 receptors[38] (Fig. 8g; Supplementary Table 3). Notably, in MPEs from CXCR1 and CXCR2 gene-deficient mice the predominant cell population was monocytes, whereas in MPEs from CCR2 gene-deficient mice[11] the prevalent cell type was neutrophils. This result was not unexpected since the majority of myeloid cells recruited in the pleural space during MPE development in *C57BL/6* mice consist of both neutrophils and monocytes (Fig. 8h). Of note, the monocyte population is the most prevalent during MPE development.

Combined targeting of *KRAS*/IKKα is effective against MPE. To explore the therapeutic implications of the proposed mechanism, we examined potential synergy of the KRAS inhibitor deltarasin[39] with the IKKβ-specific inhibitor IMD-0354 or the HSP90/IKKα/IKKβ inhibitor 17-DMAG using TNF- or IL-1β-stimulated LLC murine and A549 human lung adenocarcinoma cells expressing p*NGL* (Fig. 9a, b). Interestingly, all inhibitors alone or in combination failed to block TNF-inducible NF-κB activation in both cell lines. In addition, all standalone drugs failed to inhibit IL-1β-inducible NF-κB activation in both cell lines, except from partial effects observed in A549 cells by 17-DMAG. However, deltarasin/17-DMAG but not deltrarasin/IMD-0354 combination treatment completely abolished IL-1β-induced NF-κB activation in both cell types to unstimulated levels (Fig. 9a, b), indicating that drugging the *KRAS*/IKKα axis can halt IL-1β responsiveness. To determine the potential efficacy of this approach against MPE, standalone or combined deltarasin, and 17-DMAG treatments (both 15 mg/Kg) were delivered to mice with established pleural tumors. For this, *C57BL/6* mice received pleural LLC cells and treatments commenced after 5 days to allow initial pleural tumor implantation[11]. At day 13 post-tumor cells, standalone deltarasin and 17-DMAG-treated mice had significantly decreased MPE volume compared with saline-treated controls (40% reductions for both groups; $P < 0.05$; one-way analysis of variance (ANOVA) with Bonferroni post-tests). However, combination-treated mice were markedly protected from MPE development (57% incidence) and progression (65% volume reduction; $P < 0.001$; one-way ANOVA with Bonferroni post-tests) (Fig. 9c; Supplementary Table 3). Hence combined targeting of mutant *KRAS* and IKKα is effective in halting oncogenic NF-κB activation and MPE in mice.

IL-1β-inducible NF-κB activity in human *KRAS*-mutant cells. To assess whether our findings are relevant to human cancer, we screened nine human cancer cell lines of known *KRAS* mutation status[40] for *Rel*-binding activity of nuclear extracts. In accord with murine data, $KRAS^{MUT}$ cells displayed enhanced nuclear *Rel*B

compared with *Rel*A binding (Fig. 10a). In addition, A549 (*KRAS*^{G12S}) and NCI-H23 (*KRAS*^{G12C}) cells displayed IL-1β-induced NF-κB activation, as opposed to HT-29 and SKMEL2 cells (both *KRAS*^{WT}). Importantly, stable p*Kras*^{G12C} expression in SKMEL2 cells rendered them responsive to IL-1β (Fig. 10b, c).

In summary, *KRAS* mutations alter NF-κB signaling in tumor cells. *KRAS*^{WT} cells preferentially utilize intrinsically or exogenously (i.e., by LPS, TNF) stimulated IKKβ-mediated NF-κB signaling, display sensitivity to IKKβ inhibition, poor CXCR1/2 ligand secretion, and MPE incompetence. *KRAS*^{MUT} cells

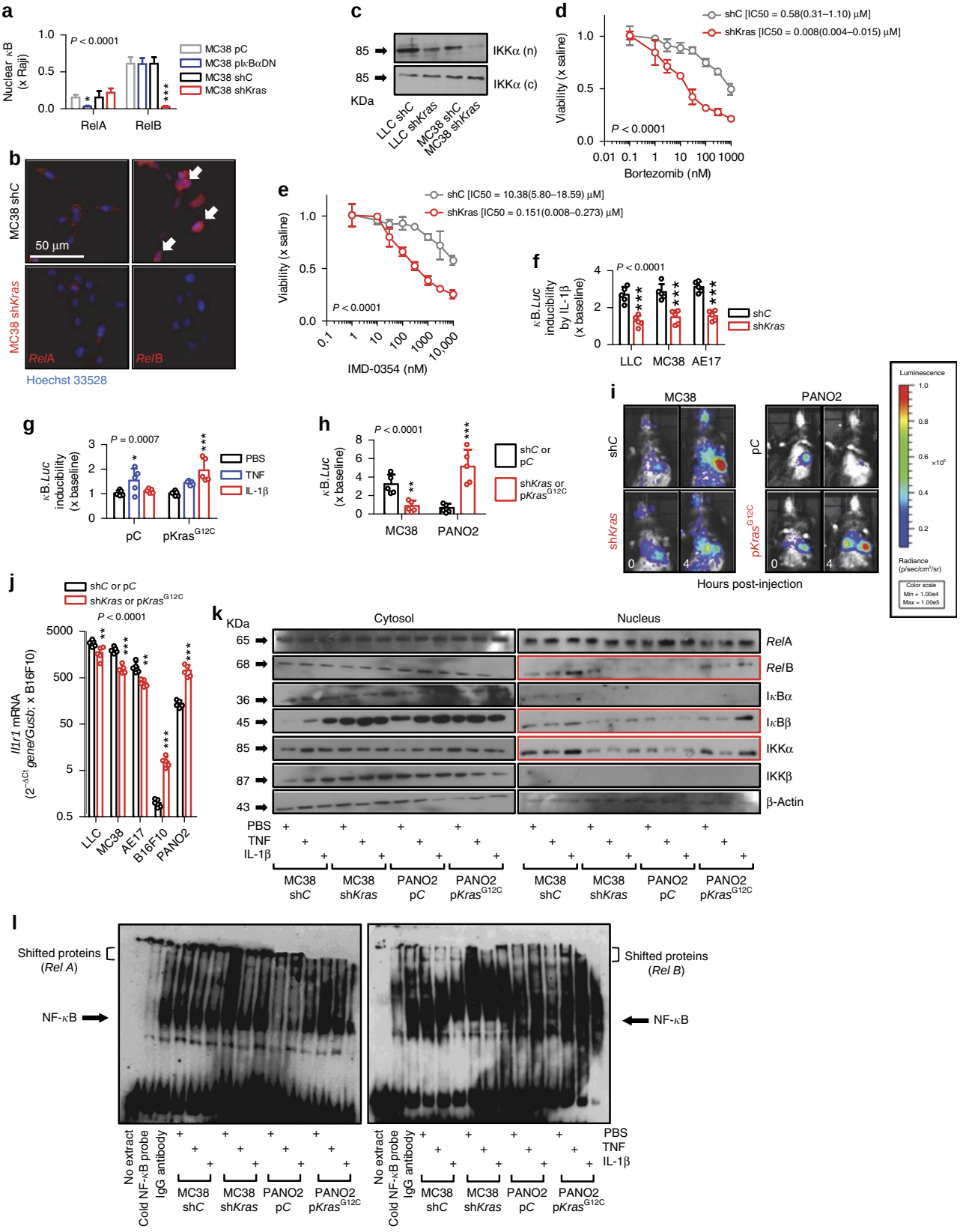

predominantly use IKKα-mediated non-canonical NF-κB signaling at resting state and in response to myeloid IL-1β, display enhanced CXCR1/2 ligand secretion and MPE proficiency, and are addicted to sustained IKKα activity evident as resistance to IKKβ inhibitors.

Discussion

We provide a novel paradigm of how an oncogene can co-opt the host environment to foster addiction with a perturbed signaling pathway. *KRAS*-mutant cancer cells are shown to respond to host provided IL-1β in the pleural space by increasing non-canonical IKKα-RelB pathway activity. The co-existence of mutant *KRAS* and elevated IKKα-mediated non-canonical NF-κB signaling in the cancer cell, relentlessly driven by host IL-1β, leads to two important consequences. First, to enhanced transcription of CXCL1/PPBP chemokines, recruitment of CXCR1+ and CXCR2+ myeloid cells, and frank escalation of inflammatory MPE development. Second, to oncogenic addiction between mutant *KRAS* and IKKα that culminates in drug resistance. Using immunocompetent mouse models of MPE, we show how IL-1β, mutant *KRAS*, and IKKα interplay to mediate non-canonical NF-κB activation, resistance to proteasome and IKKβ inhibitors, CXCL1/PPBP secretion, and MPE. Finally, we show that this partnership can be annihilated by combined inhibition of *KRAS* together with IKKα but not alone.

Although cell-autonomous pro-tumorigenic functions of mutant *KRAS* are well charted[41–43], mechanisms utilized by the oncogene to co-opt host cells from the tumor microenvironment in order to favor tumor progression have only recently begun to be elucidated. In this regard, mutant *KRAS* was first shown to promote chemokine secretion by tumor-initiated cells, thereby promoting tumor-associated inflammation[44,45]. Along similar lines, we recently showed that the oncogene is responsible for CCL2 secretion by pleural metastatic cancer cells, fostering inflammatory MPE formation[11]. Our present findings expand the paradigm of how mutant *KRAS* impacts tumor–host interactions: it renders tumor cells capable of sensing inflammatory IL-1β signals originating from the CCL2-recruited monocytes. The increased *Il1r1* expression in these cells could be a result of IL-1β -induced phosphorylation by nuclear IKKa of Ser10 in histone H3 that could be especially important for subsequent modifications in a variety of genes, including *Il1r1*. Moreover, integrated by IKKα-mediated non-canonical NF-κB activity, IL-1β signaling culminates in enhanced CXCL1/PPBP expression and secretion that function to escalate tumor-associated inflammation required for MPE. Hence, in addition to directly promoting chemokine expression, mutant *KRAS* is shown here to amplify host-originated inflammatory signals in order to escalate MPE-promoting inflammation.

Mutant *KRAS* is known to enhance oncogenic NF-κB activity; however, it was mainly linked to IKKβ, IKKε, and TBK1 function[12,14,17,18,21,23,24,43], and only two studies identified IKKα as an accessory to IKKβ in *KRAS*-mutant lung adenocarcinoma[22] and epidermal growth factor receptor-driven head and neck cancers[19]. Here we show for the first time that *KRAS*-mutant cancer cells display altered NF-κB utilization in resting and stimulated states, a phenomenon previously identified in pancreatic β cells[46]. Indeed, *KRAS*-mutant cancer cells displayed non-canonical endogenous NF-κB activity evident by enhanced nuclear localization and/or DNA-binding activity of *Rel*B, IκBβ, and IKKα, which was further inducible by exogenous IL-1β. Importantly, non-canonical NF-κB utilization by *KRAS*-mutant cancer cells was IKKα driven, involved RelB activation, and was required for MPE. Nuclear IKKα functions have been identified previously, including histone 3 modifications augmenting TNF and receptor activator of NF-κB ligand-induced gene expression and repression of maspin, a metastasis gate-keeper[47–49]. Our work links IKKα function with IL-1β-induced RelB activation and CXCL1/PPBP transcription. Moreover, we provide novel evidence that mutant *KRAS* is indirectly responsible for non-canonical NF-κB activation, which is IKKa and RelB based, via sensitization of cancer cells to host IL-1β. Finally, IKKα is found to be responsible for MPE, an important metastatic manifestation of various cancers. The findings concur with previous reports of a combined requirement for IKKα and IKKβ for oncogenic NF-κB activation[19,22], as well as with human observations of predominant non-canonical NF-κB activity of tumors with high incidence of *KRAS* mutations, such as lung adenocarcinoma[50]. However, we demonstrate an isolated requirement for IKKα in *KRAS*-driven MPE, an important cancer phenotype.

In recent years, inflammation was established as a conditional tumor promoter[51]. IL-1α/β are important components of the tumor microenvironment that stimulate tumor invasiveness and angiogenesis[52]. Myeloid-derived IL-1β is implicated in the resistance to NF-κB inhibitors and IL-1β antagonism yielded beneficial effects in a mouse model of *KRAS*-mutant pancreatic cancer[53,54]. We found previously that IL-1α/β are present in human and experimental MPE and that MPE-competent adenocarcinomas trigger myeloid cells to secrete IL-1β[35]. Here the mechanism of pleural IL-1β function in MPE promotion is elucidated: CCL2-attracted monocyte-released IL-1β fosters NF-κB activation of MPE-prone *KRAS*-mutant carcinomas by potentiating non-canonical NF-κB signaling via IKKα. Undoubtedly, IL-1β is not the sole NF-κB ligand expressed in the malignancy-affected pleural space: TNF, a known stimulator of canonical NF-κB signaling, is present in MPE and promotes disease progression[9]. However, TNF likely originates from tumor cells in MPE[9] and non-specifically triggers NF-κB activation in any tumor type irrespective of its *KRAS* status and MPE competence, suggesting

Fig. 4 Mutant *Kras* drives basal and IL-1β-induced non-canonical NF-κB signaling and drug resistance. **a** *Rel*A and *Rel*B binding of nuclear extracts of MC38 cells stably expressing a control plasmid (pC), a mutant dominant-negative form of IκBα (p*IκBα*DN), control shRNA (shC), or anti-*Kras* shRNA (sh*Kras*) relative to Raji leukemia cells by NF-κB ELISA ($n = 3$ experiments). **b** Immunofluorescent detection of *Rel*A and *Rel*B in MC38 cells showing increased nuclear *Rel*B (arrows) and its disappearance in cells expressing sh*Kras*. **c** IKKα immunoblots of cytoplasmic and nuclear extracts of LLC and MC38 cells expressing shC or sh*Kras*. ($n = 3$ experiments). **d**, **e** MTT data ($n = 3$ replicates/data-point) and mean (95% CI) IC_{50} values ($n = 3$ experiments) of MC38 cells stably expressing shC or sh*Kras* treated with bortezomib (**d**) or IMD-0354 (**e**) for 72 h. *P*, probability of no difference between cell lines by extra sum-of-squares *F* test. **f**, **g** Bioluminescent detection of NF-κB activity in $Kras^{MUT}$ (**f**) and $Kras^{WT}$ (**g**) cells stably expressing p*NGL* and the indicated vectors during 4-h incubation with PBS or 1 nM TNF or IL-1β ($n = 3$ experiments). **h**, **i** Data summary (**h**; $n = 6$ mice/group) and images (**i**) of *C57BL/6* mice at 0 and 4 h after intrapleural injection of MC38 or PANO2 cells stably expressing *pNGL* and the indicated vectors. **j** *Il1r1* mRNA expression by qPCR of $Kras^{MUT}$ and $Kras^{WT}$ cells stably expressing the indicated vectors. **k** Immunoblots of protein extracts of MC38 and PANO2 cells stably expressing the indicated vectors for NF-κB members after 4-h incubation with PBS or 1 nM TNF or IL-1β ($n = 3$ experiments). **l** The above extracts were subjected to EMSA. Super-shift EMSA was performed with the indicated antibodies. IgG antibody served as negative control. Data are presented as mean ± s.d. *P*, probability of no difference between cell lines by two-way ANOVA. Single, double, and triple asterisks (*, **, and ***): $P < 0.05$, $P < 0.01$, and $P < 0.001$, respectively, for comparison with pC or shC (**a**, **f**, **h**, **j**) or with PBS (**g**) by Bonferroni post-tests

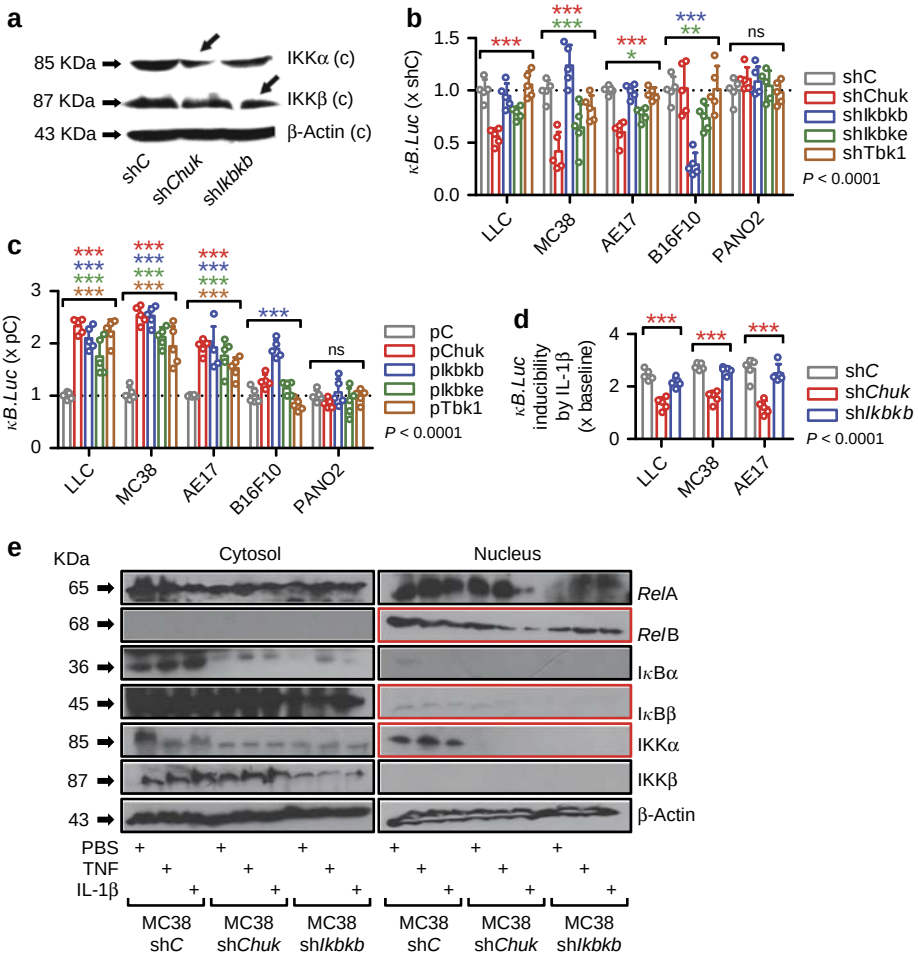

Fig. 5 IL-1β-induced NF-κB signaling of *KRAS*-mutant cells is IKKα dependent. Five different *C57BL/6* mouse tumor cell lines with (LLC, MC38, AE17) or without (B16F10, PANO2) *Kras* mutations were stably transfected with p*NGL* NF-κB reporter and any of the following: control shRNA (sh*C*) or shRNA targeting IKKα (sh*Chuk*), IKKβ (sh*Ikbkb*), IKKε (sh*Ikbke*), or TBK1 (sh*Tbk1*) transcripts; control plasmid (p*C*); or overexpression vectors encodong IKKα (p*Chuk*), IKKβ (p*Ikbkb*), IKKε (p*Ikbke*), or TBK1 (p*Tbk1*) transcripts. **a** Immunoblot of cytoplasmic protein extracts from LLC cells stably expressing sh*C*, sh*Chuk*, or sh*Ikbkb* for IKKα and IKKβ relative to β-actin (representative of $n = 3$ independent experiments). **b** Bioluminescent quantification of NF-κB reporter activity of p*NGL* cell lines stably expressing sh*C*, sh*Chuk*, sh*Ikbkb*, sh*Ikbke*, and sh*Tbk1*, ($n = 3$ independent experiments). **c** Bioluminescent quantification of NF-κB reporter activity of p*NGL* cell lines stably expressing p*C*, p*Chuk*, p*Ikbkb*, p*Ikbke*, and p*Tbk1*, ($n = 3$ independent experiments). **d** Bioluminescent detection of NF-κB reporter activity in LLC, MC38, and AE17 cells ($Kras^{MUT}$) stably expressing p*NGL* and sh*C*, sh*Chuk*, or sh*Ikbkb* ($n = 3$ independent experiments) during 4-h incubation with 1 nM IL-1β. Note IL-1β-induced NF-κB activity of sh*C* and sh*Ikbkb* cells that is silenced in sh*Chuk* cells. **e** Immunoblots of cytoplasmic and nuclear protein extracts of MC38 cells stably expressing p*NGL* and sh*C*, sh*Chuk*, or sh*Ikbkb* after 4-h treatment with PBS, TNF, and IL-1β for various NF-κB pathway members and β-actin ($n = 3$). Data are presented as mean ± s.d. of $n = 3$ independent experiments. *P*, probability of no difference between cell lines by two-way ANOVA. ns, single, double, and triple asterisks (*, **, and ***): $P > 0.05$, $P < 0.05$, $P < 0.01$, and $P < 0.001$, respectively, for comparison of color-coded sh or p with control sh or p within each cell line by Bonferroni post-tests

it functions as an autocrine growth factor across tumor types. On the contrary, IL-1α/β selectively fostered MPE competence of *KRAS*-mutant carcinomas, in agreement with previous reports of IL-1β-induced NF-κB activation independent from IKKβ[55]. Our findings explain how the tumor microenvironment fuels tumor NF-κB activity[56] and link the pro-tumorigenic functions of IL-1β with *KRAS* mutations, setting a rationale for genotype-stratified future investigations on IL-1β functions and therapies in cancer.

Unbiased analyses identified cancer-elaborated CXCL1/PPBP, potent myeloid cell chemoattractants that drive inflammation and metastasis via CXCR1/CXCR2 on host cells[57,58], as the transcriptional targets of IL-1β-fostered *KRAS*-IKKα addiction. Indeed, *Cxcl1* expression was downregulated by *Kras* or *Chuk* silencing and IL-1β induced *Cxcl1* expression by two different cancer cell lines and *Ppbp* by LLC cells (MC38 cells do not express *Ppbp*[25]). Our experiments using CXCR1- and CXCR2-deficient mice support that pleural tumor cell-secreted CXCL1/PPBP is cardinal for MPE and are in line with a previous study demonstrating increased production of CXCL1 by tumor cells during human MPE development that mobilizes regulatory T cells[59].

In addition to the mechanistic insights into host environment-fostered co-option of IKKα activity by mutant *KRAS*, our data bear therapeutic implications for KRAS inhibitors[39]. *KRAS* is notoriously undruggable, and proteasome and IKKβ inhibitors have yielded suboptimal results in mice and men with cancer. Focusing on lung cancer, a tumor with high *KRAS* mutation frequency[60], bortezomib has shown poor efficacy in clinical trials[61]. In animal models of lung cancer, bortezomib and IKKβ inhibitors caused resistance or paradoxical tumor promotion via development of secondary mutations, NF-κB inhibition in myeloid cells, or enhanced IL-1β secretion by tumor-associated

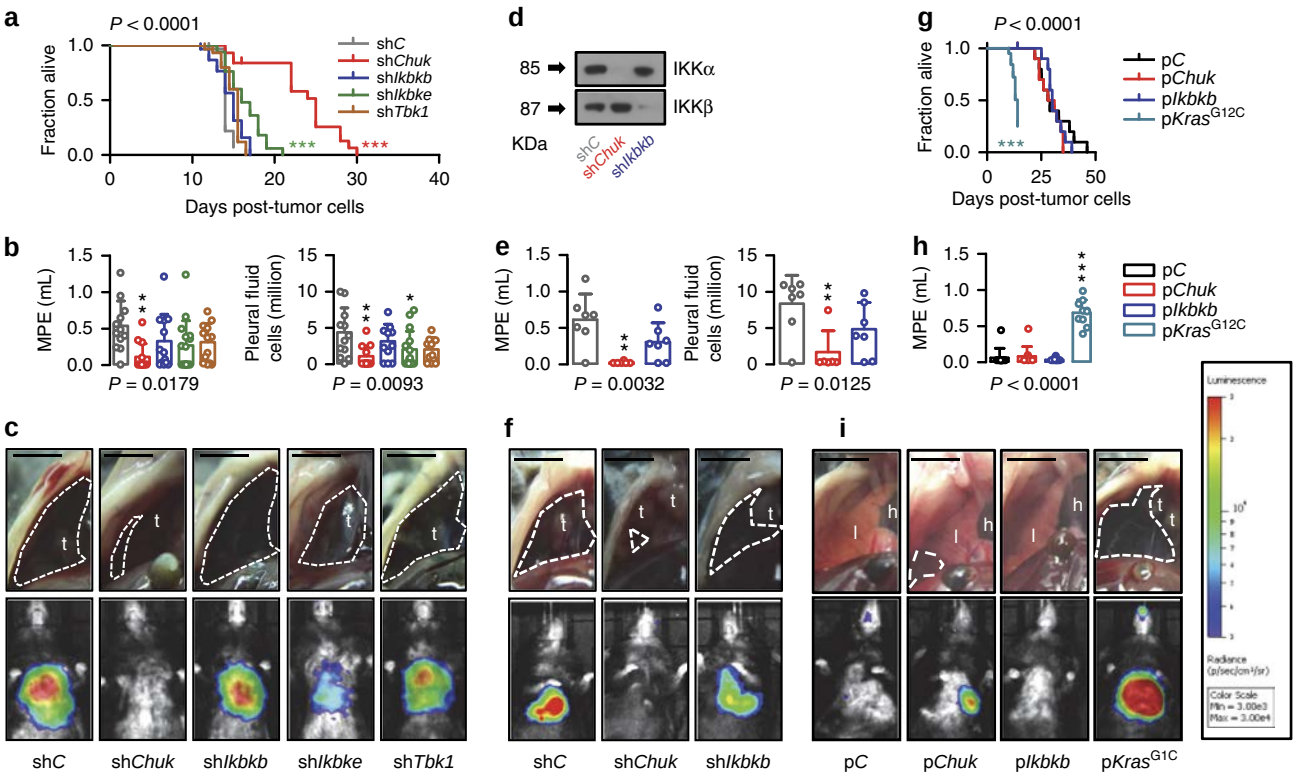

Fig. 6 IKKα is required for mutant *KRAS*-induced malignant pleural effusion. **a**–**c** Malignant pleural disease induced by LLC cells ($Kras^{G12C}$) stably expressing p*NGL* NF-κB reporter and control shRNA (sh*C*) or shRNA targeting IKKα (sh*Chuk*), IKKβ (sh*Ikbkb*), IKKε (sh*Ikbke*), or TBK1 (sh*Tbk1*) transcripts (*n* is given in Table 3). Shown are Kaplan–Meier survival plot (**a**), data summaries of effusion volume and pleural fluid cells (**b**), and representative images of effusions (dashed lines) and pleural tumors (t) as well as bioluminescent images at day 13 after pleural injections of the indicated tumor cells (**c**). **d**–**f** Malignant pleural disease induced by MC38 cells ($Kras^{G13R}$) stably expressing p*NGL* NF-κB reporter and sh*C*, sh*Chuk*, or sh*Ikbkb* (*n* is given in Supplementary Table 3). Shown are immunoblots of cytoplasmic extracts (**d**), data summaries of effusion volume and pleural fluid cells (**e**), and representative images of effusions (dashed lines) and pleural tumors (t) as well as representative bioluminescent images at day 13 after pleural injections of the indicated tumor cells (**f**). **g**–**i** Malignant pleural disease induced by PANO2 cells ($Kras^{WT}$) stably expressing p*NGL* NF-κB reporter and control plasmid (sh*C*) or plasmid encoding IKKα (p*Chuk*), IKKβ (p*Ikbkb*), or mutant (p$Kras^{G12C}$) transcripts (*n* is given in Supplementary Table 3). Shown are Kaplan–Meier survival plot (**g**), data summary of effusion volume (**h**), and representative images of effusions (dashed lines) and pleural tumors (t), hearts (h), and lungs (l), as well as representative bioluminescent images at day 14 after pleural injections of the indicated tumor cells (**i**). Data are presented as mean ± s.d. *P*, probability of no difference between cell lines by overall log-rank test (**a**, **g**) or one-way ANOVA (**b**, **e**, **h**). ns, single, double, and triple asterisks (*, **, and ***): $P > 0.05$, $P < 0.05$, $P < 0.01$, and $P < 0.001$, respectively, for the indicated comparisons with control cells by Bonferroni post-tests. Scale bars, 0.5 cm

neutrophils through an unknown mechanism[15,16,53]. We show how *KRAS*-mutant cancer cells utilize myeloid-IL-1β in order to activate IKKα and alternative NF-κB signaling and to by-pass IKKβ canonical NF-κB dependence. We provide proof-of-concept data that *KRAS*-mutant cancer cells can be targeted by combined inhibition of KRAS and HSP90/IKKα/IKKβ signaling, a strategy that blocks IL-1β-inducible oncogenic NF-κB activation and in vivo MPE development, a cancer phenotype that requires mutant *KRAS*-potentiated, IL-1β-induced IKKα activity. These results challenge the prevailing focus on IKKβ for the development of anti-tumor drugs and establish IL-1β and IKKα as important targets in *KRAS*-mutant tumors.

In conclusion, we show that *KRAS*-mutant cancer cells use host IL-1β to sustain IKKα-mediated non-canonical NF-κB activity responsible for MPE development and primary drug resistance. We identify CXCL1/PPBP as effectors of MPE downstream of *KRAS*/IKKα addiction. Finally, we provide proof-of-concept data suggesting that *KRAS*/IKKα addiction may occur in human cancers and may be targeted by combined *KRAS*/IKKα inhibition.

Methods

Study approval. All mouse experiments were prospectively approved by the Veterinary Administration of Western Greece (approval # 276134/14873/2) and were conducted according to Directive 2010/63/EU (http://eur-lex.europa.eu/legal-content/EN/TXT/?uri=celex%3A32010L0063).

Reagents. D-Luciferin was from Gold Biotechnology (St. Louis, MO); lentiviral shRNA and puromycin from Santa Cruz (Dallas, TX); 3-(4,5-dimethylthiazol-2-yl)-2,5-diphenyltetrazolium bromide (MTT) assay and Hoechst 33528 from Sigma-Aldrich (St. Louis, MO); mouse gene ST2.0 microarrays and relevant reagents from Affymetrix (Santa Clara, CA); recombinant cytokines and growth factors from Immunotools (Friesoythe, Germany); NF-κB-binding ELISA from Active Motif (La Hulpe, Belgium); bortezomib, IMD-0354, 17-DMAG, and deltarasin from Selleckchem (Houston, TX); G418 from Applichem (Darmstadt, Germany); IL-1β and CXCL1 ELISA from Peprotech (London, UK); and primers from VBC Biotech (Vienna, Austria). Primers, antibodies, and lentiviral shRNA pools are listed in Supplementary Tables 6–8.

Cells. LLC, B16F10, PANO2, and A549 cells were from the National Cancer Institute Tumor Repository (Frederick, MD); MC38 cells were a gift from Dr. Barbara Fingleton (Vanderbilt University, Nashville, TN)[34,35], and AE17 cells from Dr. YC Gary Lee (University of Western Australia, Perth, Australia)[11,25]. All cell lines were cultured at 37 °C in 5% CO_2–95% air using Dulbecco's modified Eagle's medium (DMEM) containing 10% fetal bovine serum, 2 mM L-glutamine, 1 mM pyruvate, 100 U/mL penicillin, and 100 mg/mL streptomycin. Cell lines were tested annually for identity by short tandem repeats and for *Mycoplasma*Spp. by PCR. For in vivo injections, cells were harvested using trypsin, incubated with Trypan blue, counted in a hemocytometer, and 95% viable cells were injected intrapleurally[8,11,34,35].

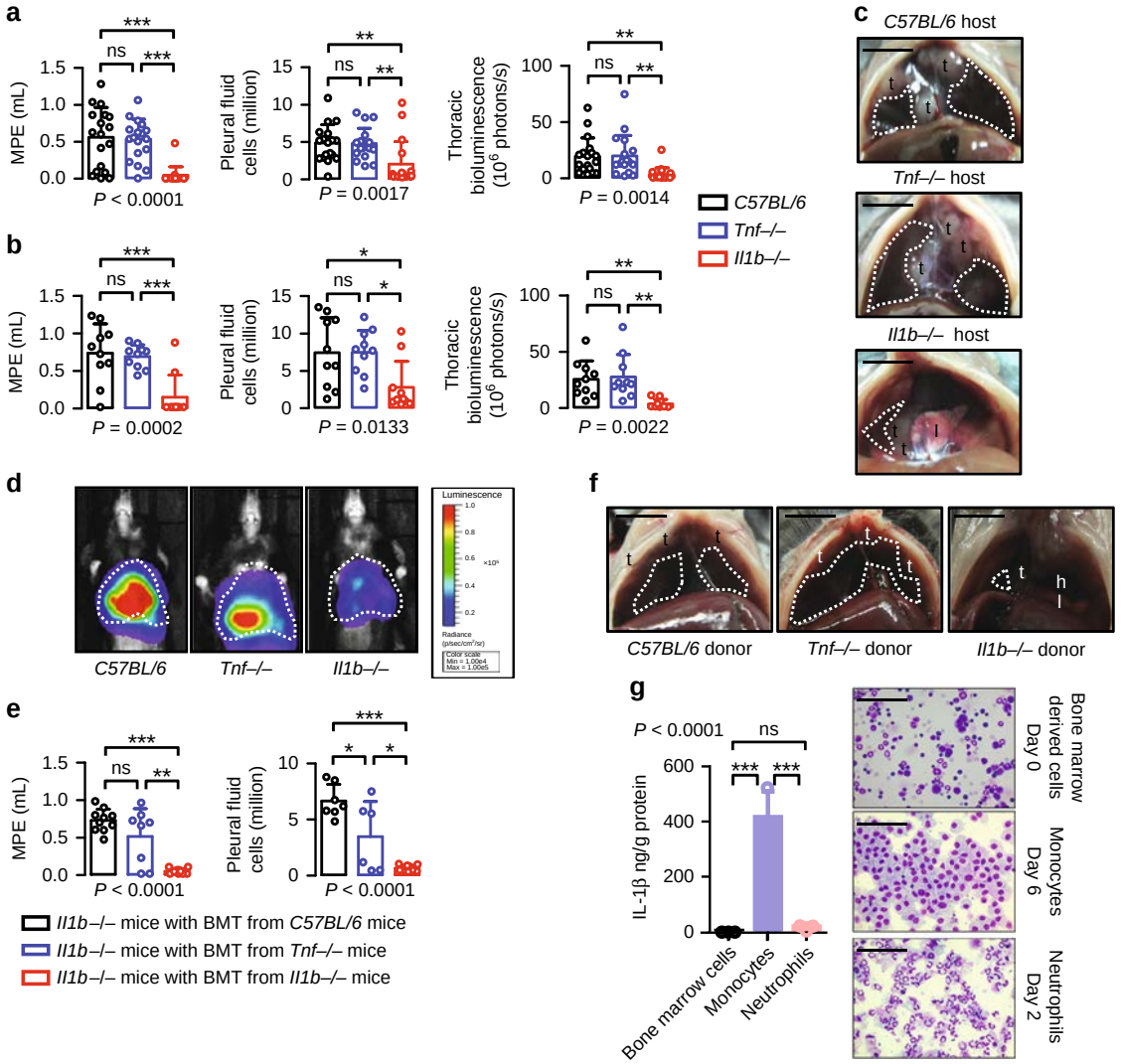

Fig. 7 Myeloid cell-derived IL-1β drives mutant *KRAS*-IKKα addiction in malignant pleural effusion. **a** Malignant pleural disease induced by LLC cells (*Kras*^{G12C}) stably expressing p*NGL* NF-κB reporter plasmid in wild-type *C57BL/6* mice (black) and TNF (blue) and IL-1β (red)-deficient mice (*Tnf–/–* and *Il1b–/–*, respectively; both *C57BL/6* background; *n* is given in Supplementary Table 3). Shown are data summaries of effusion volume, pleural fluid cells, and NF-κB-dependent thoracic bioluminescent signal. **b**–**d** Malignant pleural disease induced by MC38 cells (*Kras*^{G13R}) stably expressing p*NGL* NF-κB reporter plasmid in wild-type *C57BL/6* (black), *Tnf–/–* (blue), and *Il1b–/–* (red) mice (all *C57BL/6* background; *n* is given in Supplementary Table 3). Shown are data summaries of effusion volume, pleural fluid cells, and NF-κB-dependent thoracic bioluminescent signal (**b**), representative images of effusions (dashed lines), pleural tumors (t), and lungs (l) (**c**), as well as representative bioluminescent images at day 13 after pleural injections of the indicated tumor cells (**d**). **e**, **f** Malignant pleural disease induced by LLC cells in *Il1b–/–* mice (*C57BL/6* background; *n* is given in Supplementary Table 3) that received total body irradiation (1100 Rad), same-day bone marrow transplants (10 million cells) from *C57BL/6* (black), *Tnf–/–* (blue), or *Il1b–/–* (red) donors, and pleural tumor cells after 1 month. Shown are data summaries of effusion volume and pleural fluid cells (**e**) and representative images of effusions (dashed lines), pleural tumors (t), lungs (l), and hearts (h) (**f**). **g** IL-1β protein secretion by *C57BL/6* mouse bone marrow-isolated myeloid cells 24 h after treatment with LLC supernatants; undifferentiated cells (day 0), neutrophils (day 2 after addition of 20 ng/ml G-CSF), and macrophages (day 6 after addition of 20 ng/ml M-CSF; $n = 3$ independent experiments). Data are presented as mean ± s.d. *P*, probability of no difference by one-way ANOVA. ns, single, double, and triple asterisks (*, **, and ***): $P > 0.05$, $P < 0.05$, $P < 0.01$, and $P < 0.001$, respectively, for the indicated comparisons by Bonferroni post-tests. Scale bars, 1 cm (**c**, **f**) and 100 μM (**g**)

Mouse models and drug treatments. *C57BL/6* (#000664), B6.129P2-*Cxcr1*^{tm1Dgen}/J (*Cxcr1–/–*; #005820[36]), B6.129 S2(C)-*Cxcr2*^{tm1Mwm}/J (*Cxcr2*$^{+/–}$; #006848[37]), B6;129S-*Tnf*^{tm1Gkl}/J (*Tnf–/–*; #003008[32]) (Jackson Laboratory, Bar Harbor, ME), and *Il1b*^{tm1Yiw} (*Il1b–/–*; MGI #2157396[31]) mice were bred at the Center for Animal Models of Disease of the University of Patras. Male and female experimental mice and littermate controls were sex, weight (20–25 g), and age (6–12 weeks) matched. For MPE induction, mice received 150,000 cancer cells in 100 μL PBS intrapleurally. Mice were observed continuously till recovery and daily thereafter and were sacrificed when moribund (13–14 days post-tumor cells) for survival and pleural fluid analyses. Mice with pleural fluid volume ≥100 μL were judged to have a MPE and were subjected to pleural fluid aspiration, whereas animals with pleural fluid volume <100 μL were judged not to have a MPE and were subjected to pleural lavage. Injection, harvest, and sample handling are described elsewhere[8–11,34,35]. Drug treatments were initiated 5 days post-tumor cells and consisted of daily intraperitoneal injections of 100 μL PBS containing no drug, deltarasin[39], 17-DMAG[28], or both at 15 mg/kg.

Constructs. p*NGL*, p*IκBα*DN, and p*CAG.LUC* (#74409) have been described elsewhere[8,25,33]. Lentiviral shRNA pools (Santa Cruz) are described in Supplementary Table 8. A p*MIGR1*-based (#27490) bicistronic retroviral expression vector was generated by replacing *eGFP* sequences with puromycin resistance gene (#58250). *Kras*^{G12C},*Chuk*, *Ikbkb*, *Ikbke*, and *Tbk1* cDNAs were cloned via reverse transcriptase-PCR (RT-PCR) from LLC or MC38 RNA using specific primers

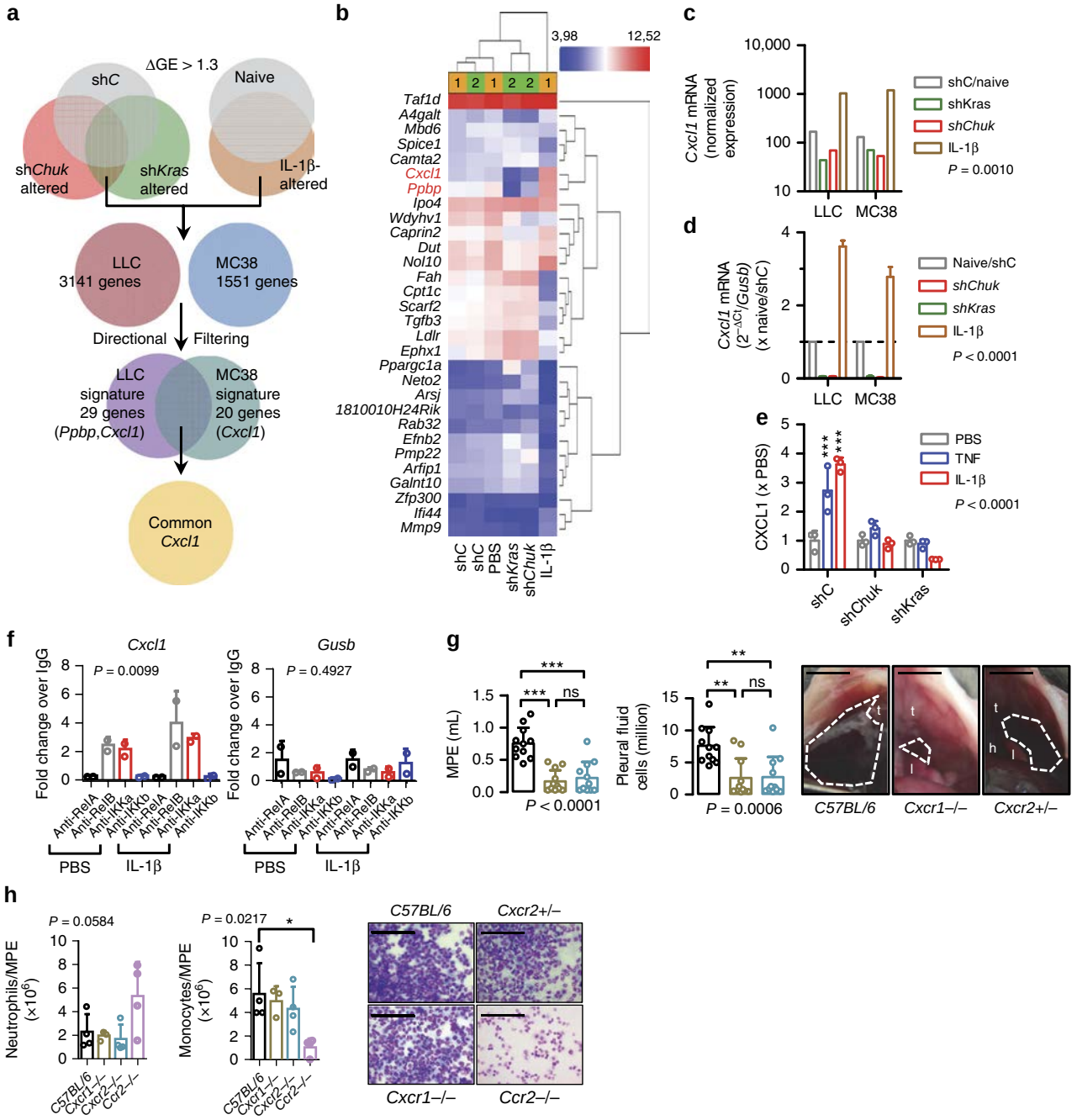

Fig. 8 CXCL1/PPBP are the downstream effectors of KRAS/IL-1β/IKKα signaling in malignant pleural effusion. **a**–**c** LLC and MC38 cells were stably transfected with shC or sh*Kras* or shChuk or were stimulated with 1 nM IL-1β for 4 h, and total cellular RNA was examined by Affymetrix mouse gene ST2.0 microarrays. **a** Venn diagram of analytic strategy employed: transcripts altered >1.3-fold in one direction by sh*Kras* and sh*Chuk* and in the other by IL-1β were filtered for each cell line and are given in Supplementary Tables S1–S2. These gene sets, coined KRAS/IL-1β/IKKα signatures, were crossexamined and only *Cxcl1* was common to both. **b** Unsupervised hierarchical clustering of LLC cell results by the 29-gene KRAS/IL-1β/IKKα signature accurately clustered three control samples together, sh*Kras* and sh*Chuk* samples together, and IL-1β-stimulated cells apart. **c** *Cxcl1* mRNA normalized expression levels by microarray ($n = 2$ independent experiments). **d** *Cxcl1* mRNA expression by qPCR relative to *Gusb* ($n = 3$ independent experiments). **e** CXCL1 protein secretion by LLC cells stably expressing shC, sh*Chuk*, or sh*Kras* after 24 h of stimulation with PBS or 1 nM TNF or IL-1β ($n = 3$ independent experiments). **f** Chromatin immunoprecipitation (ChIP) was performed in PBS- or IL-1β-treated LLC cells, followed by immunoprecipitation with the indicated antibodies. The immunoprecipitates were then detected by qPCR. Data are shown as fold enrichment of *Cxcl1* or *Gusb* promoter in each antibody immunoprecipitate over control IgG immunoprecipitate. **g** Malignant pleural disease induced by LLC cells in *C57BL/6*, *Cxcr*$^{+/-}$, and *Cxcr2*$^{+/-}$ mice (*n* is given in Supplementary Table 3). Shown are data summaries of effusion volume and pleural fluid cells, as well as representative images of effusions (dashed lines), pleural tumors (t), lungs (l), and hearts (h). **h** Data summaries of *C57BL/6*, *Cxcr1*$^{-/-}$, *Cxcr2*$^{+/-}$ and *Ccr2*$^{-/-}$ pleural neutrophils and monocytes, accompanied by microphotographs. Data are presented as mean ± s.d. *P*, probability of no difference by two-way (**c**–**e**) or one-way (**f**–**h**) ANOVA. ns, single, double, and triple asterisks (** and ***): $P > 0.05$, $P < 0.05$, $P < 0.01$, and $P < 0.001$, respectively, for comparison with PBS (**e**) or indicated (**g**, **h**) by Bonferroni post-tests. Scale bars 1 cm (**g**) and 200 μM (**h**)

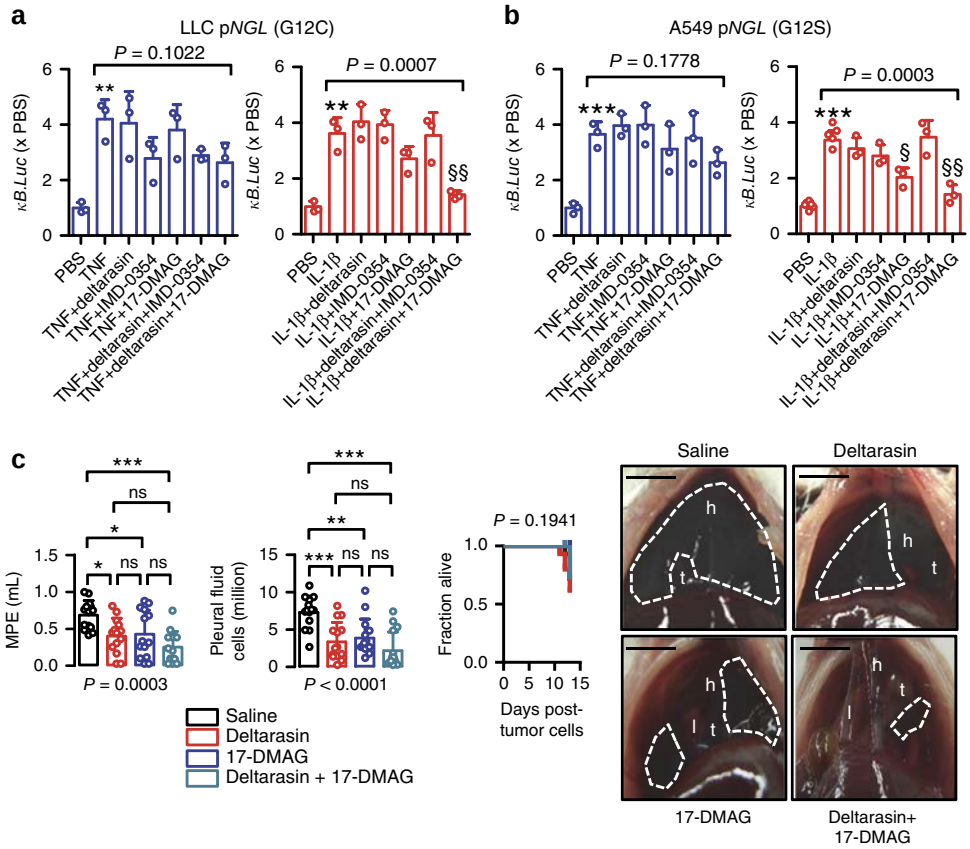

Fig. 9 Combined targeting of mutant *KRAS* and IKKα abolishes IL-1β-induced NF-κB activation and malignant pleural effusion development. **a**, **b** Bioluminescent detection of NF-κB reporter activity in LLC (**a**; *C57BL/6* Lewis lung carcinoma, *Kras*^{G12C}) and A549 (**b**; human lung adenocarcinoma, *Kras*^{G12S}) cells stably expressing p*NGL* under PBS or 1 nM TNF- or IL-1β-stimulated conditions (4 h), with or without pretreatment with 1 μM deltarasin, IMD-0354, or 17-DMAG alone or in combination ($n = 3$ independent experiments). Note four-fold induction of NF-κB reporter activity by both TNF and IL-1β. Note also inability of any treatment to block TNF-induced NF-κB activation and of any standalone treatment except 17-DMAG to inhibit IL-1β-induced NF-κB activation. Finally, note complete abrogation of IL-1β-induced NF-κB activation in both cell lines by deltarasin/17-DMAG combination. Data are presented as mean ± s.d. *P*, probability of no difference by one-way ANOVA (PBS group excluded). Double and triple asterisks (** and ***): $P < 0.01$ and $P < 0.001$, respectively, for comparison with PBS by Student's *t*-tests. Single and double section symbols (§ and §§): $P < 0.05$ and $P < 0.01$, respectively, for comparison with TNF or IL-1β by Bonferroni post-tests. **c** Malignant pleural disease induced by LLC cells in wild-type *C57BL/6* mice treated with deltarasin and/or 17-DMAG. Mice received pleural LLC cells, were allowed 5 days for pleural tumor development, and were randomized to daily intraperitoneal treatments with saline (100 μL), deltarasin, 17-DMAG, or both (both at 15 mg/Kg in 100 μL saline; *n* is given in Supplementary Table 3). Shown are data summaries of effusion volume and pleural fluid cells and Kaplan–Meier survival plot, as well as representative images of effusions (dashed lines), pleural tumors (t), lungs (l), and hearts (h). Data are presented as mean ± s.d. *P*, probability of no difference by one-way ANOVA or log-rank test. ns, single, double, and triple (*, **, and ***): $P > 0.05$, $P < 0.05$, $P < 0.01$, and $P < 0.001$, respectively, for the indicated comparisons by Bonferroni post-tests. Scale bars, 1 cm

(Supplementary Table 6) and were subcloned into peGFP-C1 (Takara, Mountain View, CA). *eGFP*, *eGFP.Kras*^{G12C}, *eGFP.Chuk*, *eGFP.Ikbkb*, *eGFP.Ikbke*, and *eGFP.Tbk1* cDNAs were subcloned into the new retroviral expression vector (#58249, #64372,# 87033, #58251, #87444, and #87443, respectively). Retroviral particles were obtained by co-transfecting HEK293T cells with retroviral vectors, *pMD2.G* (#12259), and *pCMV-Gag-Pol* (Cell Biolabs, San Diego, CA) at 1.5:1:1 stoichiometry using $CaCl_2$/BES. After 2 days, culture media were collected and applied to cancer cells. After 48 h, media were replaced by selection medium containing 2–10 μg/mL puromycin. Stable clones were selected and subcultured[11]. For stable plasmid/shRNA transfection, 10^5 tumor cells in six-well culture vessels were transfected with 5 μg DNA using Xfect (Takara), and clones were selected by G418 (400–800 μg/mL) or puromycin (2–10 μg/mL).

Cellular assays. In vitro cancer cell proliferation was determined using MTT assay. Nuclear extracts were assayed for *Rel*A, *Rel*B, c-*Rel*, P50, and P52 DNA-binding activity using a commercially available ELISA kit (Transam, Active Motif, Belgium). All cellular experiments were independently repeated at least thrice.

Bioluminescence imaging. Living cells and mice were imaged 0, 4, 8, 24, and 48 h after cellular treatments and 0 h, 4 h, and 12–14 days after pleural delivery of p*NGL*-expressing cells on a Xenogen Lumina II (Perkin-Elmer, Waltham, MA) after addition of 300 μg/mL D-luciferin to culture media or isoflurane anesthesia and delivery of 1 mg intravenous D-luciferin to the retro-orbital veins[8–11,16,25,34,35]. Data were analyzed using Living Image v.4.2 (Perkin-Elmer).

qPCR and microarray. RNA was isolated using Trizol (Invitrogen, Carlsbad, CA) and RNAeasy (Qiagen, Hilden, Germany) was reverse transcribed using Superscript III (Invitrogen), and RT-PCR or qPCR was performed using SYBR Green Master Mix in a StepOnePlus (Applied Biosystems, Carlsbad, CA) and specific primers (Supplementary Table 6). Ct values from triplicate qPCR reactions were analyzed by the $2^{-\Delta\Delta CT}$ method[62] relative to *Gusb* mRNA levels. For microarray, RNA was extracted from triplicate cultures of 10^6 cells. Five micrograms pooled total RNA were quality tested on an ABI 2000 (Agilent Technologies, Sta. Clara, CA), labeled, and hybridized to GeneChip Mouse Gene 2.0 ST arrays (Affymetrix, St. Clara, CA). For analysis of differential gene expression (ΔGE) and unsupervised hierarchical clustering, Affymetrix Expression and Transcriptome Analysis Consoles were used.

Chromatin immunoprecipitation. LLC cells were treated with PBS or 1 nM IL-1β, and 30 min later, cells were fixed sequentially with 2 mM di(N-succinimidyl) glutarate (Sigma) and 1% formaldehyde (Sigma) and quenched with 0.125 M glycine, followed by lysis with 1% sodium dodecyl sulfate (SDS), 10 mM EDTA,

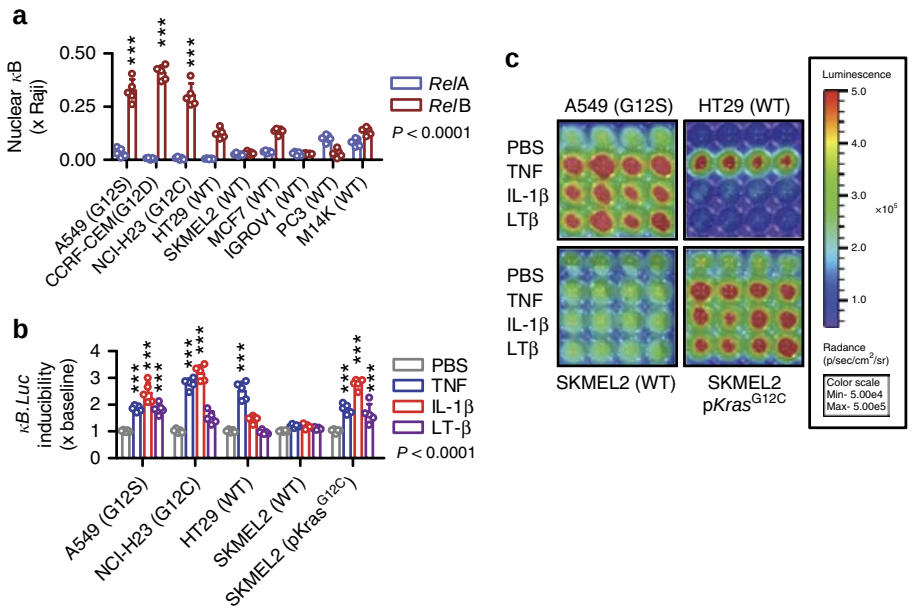

Fig. 10 Non-canonical endogenous and IL-1β-inducible NF-κB activation of *KRAS*-mutant human tumor cells. Different human cancer cell lines with (*KRAS*^{MUT}: A549, *KRAS*^{G12S}; CCRF-CEM, *KRAS*^{G12D}; NCI-H23, *KRAS*^{G12C}) or without (*KRAS*^{WT}; HT29, SKMEL2, MCF7, IGROV1, PC3, and M14K) *KRAS* mutations were assessed for NF-κB activation at resting and stimulated conditions in vitro. **a** Data summary ($n = 5$ independent experiments) of DNA NF-κB motif-binding activity of nuclear extracts by NF-κB ELISA relative to nuclear extracts of Raji leukemia cells. Note increased nuclear *Rel*B and P52 binding activity of *KRAS*^{MUT} compared with *KRAS*^{WT} cells. **b**, **c** Bioluminescent detection of NF-κB reporter activity in A549, NCI-H23, HT29, and SKMEL2 cells stably expressing p*NGL*, as well as in SKMEL2 cells stably expressing p*NGL* and p*Kras*^{G12C} (**b**; data summary of $n = 5$ independent experiments; **c**: representative bioluminescent images) during 4-h incubation with PBS or 1 nM TNF, IL-1β, or lymphotoxin (LT)-β. Note IL-1β-induced NF-κB activity of *KRAS*^{MUT} but not of *KRAS*^{WT} cells. Note also instalment of IL-1β-induced NF-κB activation in SKMEL2 cells by p*Kras*^{G12C} (SKMEL2 cells expressing p*C* behaved exactly as parental cells). Data are presented as mean ± s.d. *P*, probability of no difference by two-way ANOVA. Triple astrisks (***): $P < 0.001$ for comparison with *Rel*A (**a**) or PBS (**b**) by Bonferroni post-tests

and 50 mM Tris pH 8. Sonication was performed in a Bioruptor (Diagenode) for 40 cycles (30 s on/off) power settings high), using 3×10^6 cells; 20 µg of chromatin was precipitated with 5 µg of *Rel*A, *Rel*B, IKKα, or IKKβ antibody or a mouse control immunoglobulin G (IgG). Immunoprecipitates were retrieved with 50 µl of magnetic Dynabeads conjugated to protein G (Invitrogen) and subjected to quantitative real-time PCR (Applied Biosystems StepOne), using the Kapa SYBR Fast qPCR Kit (KapaBiosystems, KK4605) for amplification of the *Cxcl1* promoter or *Gusb* as control. The sequences of the primers used for Cxcl1 promoter are: 5′-ATA-CAGCAGGGTAGGGATGC, 3′-TTGCCAACTGTTTTTGTGG. The sequences of the primers used for Gusb are: 5′-TTACTTTAAGACGCTGATCACC, 3′-ACCTCCAAATGCCCATAGTC.

BM cell derivation and transfer. For adoptive BM replacement, *Il1β*−/− mice (*C57BL/6* background) received 10 million BM cells flushed from the femurs and tibias of *C57BL/6*, *Tnf*−/−, or *Il1β*−/− donors (*C57BL/6* background) intravenously 12 h after total-body irradiation (1100 Rad)[11,25,34,35]. One mouse in each experiment was not engrafted (sentinel) and was observed till moribund between days 5 and 15 post-irradiation. The mice were left to be engrafted for 1 month, when full BM reconstitution is complete, before experimental induction of pleural carcinomatosis via intrapleural injection of LLC cells. For BM cell retrieval, BM cells were flushed from *C57BL/6* femurs and tibias using full DMEM and were simply cultured in full culture media (the same used for cancer cell line cultures), supplemented with 20 ng/ml M-CSF or G-CSF in order for cells to differentiate to monocytes or neutrophils, respectively. Supernatants and cytocentrifugal specimens were obtained at day 0 for undifferentiated cells, day 2 for neutrophils, and at day 6 for monocytes/macrophages.

Immunoblotting. Nuclear and cytoplasmic extracts were prepared using the NE-PER Extraction Kit (Thermo, Waltham, MA), separated by 12% SDS polyacrylamide gel electrophoresis, and electroblotted to polyvinylidene difluoride membranes (Merck Millipore, Darmstadt, Germany). Membranes were probed with specific antibodies (Supplementary Table 7) and were visualized by film exposure after incubation with enhanced chemiluminescence substrate (Merck Millipore, Darmstadt, Germany).

Electrophoretic mobility shift assay (EMSA). Nuclear extracts were prepared using the NE-PER Extraction Kit. Proteins (10 µg) were incubated with NF-κB biotin-labeled probe using a commercially available non-radioactive EMSA Kit (Signosis Inc, Santa Clara, USA). DNA–protein complexes were electrophoresed in a prerinsed 6.5% polyacrylamide gel, transferred to a positively charged nylon membrane, and were visualized by film exposure after incubation with enhanced chemiluminescence substrate. For gel shift reactions, proteins were incubated with the specific antibody for 1 h at 4 °C before probe incubation. The antibodies used for observing the supershifted bands were *Rel*A and *Rel*B. IgG antibody served as negative control for super-shift assays.

Immunofluorescence. For immunofluorescence, cells were fixed in 4% paraformaldehyde overnight at 4 °C and were labeled with the indicated primary antibodies (Supplementary Table 7) followed by incubation with fluorescent secondary antibodies (Invitrogen, Waltham, MA; Supplementary Table 7). Cells were then counterstained with Hoechst 33258 (Sigma-Aldrich, St. Louis, MO) and mounted with Mowiol 4-88 (Calbiochem, Gibbstown, NJ). For isotype control, the primary antibody was omitted. Fluorescent microscopy was carried out on an AxioObserver.D1 inverted microscope (Zeiss, Jena, Germany) connected to an AxioCam ERc 5 s camera (Zeiss), and digital images were processed with the Fiji academic imaging freeware[63].

Statistics. Sample size was calculated using G*power (http://www.gpower.hhu.de/)[64] assuming $\alpha = 0.05$, $\beta = 0.05$, and $d = 1.5$, tailored to detect 30% differences between means with 20–30% SD spans, yielding $n = 13$/group. Animals were allocated to groups by alternation (treatments or cells) or case–control-wise (transgenic animals). Data acquisition was blinded on samples coded by non-blinded investigators. No data were excluded. All data were examined for normality by Kolmogorov–Smirnof test and were normally distributed. Values are given as mean ± SD. Sample size (n) refers to biological replicates. Differences in means were examined by t-test and one-way or two-way ANOVA with Bonferroni post-tests, in frequencies by Fischer's exact or χ^2 tests, and in Kaplan–Meier survival estimates by log-rank test, as appropriate. P-values are two-tailed. $P < 0.05$ was considered significant. Analyses and plots were done on Prism v5.0 (GraphPad, La Jolla, CA).

Data availability. All new plasmids have been deposited at the Addgene plasmid repository (https://www.addgene.org/search/advanced/?q=stathopoulos) and their IDs (#) are given in the text. Microarray data are available at the GEO (http://www.ncbi.nlm.nih.gov/geo/; Accession IDs: GSE93369 and GSE93370). The authors declare that all the other data supporting the findings of this study are available

within the article and its supplementary information files and from the corresponding authors upon reasonable request.

Received: 8 April 2017 Accepted: 15 January 2018
Published online: 14 February 2018

References

1. Clive, A. O. et al. Predicting survival in malignant pleural effusion: development and validation of the LENT prognostic score. *Thorax* **69**, 1098–1104 (2014).
2. Taghizadeh, N., Fortin, M. & Tremblay, A. USA hospitalizations for malignant pleural effusions - data from the 2012 national inpatient sample. *Chest* **19**, https://doi.org/10.1016/j.chest.2016.11.010 (2016).
3. Wu, S. G. et al. Survival of lung adenocarcinoma patients with malignant pleural effusion. *Eur. Respir. J.* **41**, 1409–1418 (2013).
4. Tanrikulu, A. C. et al. A clinical, radiographic and laboratory evaluation of prognostic factors in 363 patients with malignant pleural mesothelioma. *Respiration* **80**, 480–487 (2010).
5. Burgers, J. A. et al. Pleural drainage and pleurodesis: implementation of guidelines in four hospitals. *Eur. Respir. J.* **32**, 1321–1327 (2008).
6. Rintoul, R. C. et al. Efficacy and cost of video-assisted thoracoscopic partial pleurectomy versus talc pleurodesis in patients with malignant pleural mesothelioma (MesoVATS): an open-label, randomised, controlled trial. *Lancet* **384**, 1118–1127 (2014).
7. Stathopoulos, G. T. & Kalomenidis, I. Malignant pleural effusion: tumor-host interactions unleashed. *Am. J. Respir. Crit. Care Med.* **186**, 487–492 (2012).
8. Stathopoulos, G. T. et al. Nuclear factor-kappaB affects tumor progression in a mouse model of malignant pleural effusion. *Am. J. Respir. Cell Mol. Biol.* **34**, 142–150 (2006).
9. Stathopoulos, G. T. et al. Tumor necrosis factor-alpha promotes malignant pleural effusion. *Cancer Res.* **67**, 9825–9834 (2007).
10. Psallidas, I. et al. Specific effects of bortezomib against experimental malignant pleural effusion: a preclinical study. *Mol. Cancer* **9**, 56 (2010).
11. Agalioti, T. et al. Mutant KRAS promotes malignant pleural effusion formation. *Nat. Commun.* **16**, 15205 (2017).
12. Meylan, E. et al. Requirement for NF-kappaB signalling in a mouse model of lung adenocarcinoma. *Nature* **462**, 104–107 (2009).
13. Stathopoulos, G. T. et al. Epithelial NF-kappaB activation promotes urethane-induced lung carcinogenesis. *Proc. Natl. Acad. Sci. USA* **104**, 18514–18519 (2007).
14. Ling, J. et al. KrasG12D-induced IKK2/β/NF-κB activation by IL-1α and p62 feedforward loops is required for development of pancreatic ductal adenocarcinoma. *Cancer Cell* **21**, 105–120 (2012).
15. Xue, W. et al. Response and resistance to NF-κB inhibitors in mouse models of lung adenocarcinoma. *Cancer Discov.* **1**, 236–247 (2011).
16. Karabela, S. P. et al. Opposing effects of bortezomib-induced nuclear factor-κB inhibition on chemical lung carcinogenesis. *Carcinogenesis* **33**, 859–867 (2012).
17. Daniluk, J. et al. An NF-κB pathway-mediated positive feedback loop amplifies Ras activity to pathological levels in mice. *J. Clin. Invest.* **122**, 1519–1528 (2012).
18. Seguin, L. et al. An integrin β_3-KRAS-RalB complex drives tumour stemness and resistance to EGFR inhibition. *Nat. Cell Biol.* **16**, 457–468 (2014).
19. Nottingham, L. K. et al. Aberrant IKKα and IKKβ cooperatively activate NF-κB and induce EGFR/AP1 signaling to promote survival and migration of head and neck cancer. *Oncogene* **33**, 1135–1147 (2014).
20. Xia, Y. et al. Reduced cell proliferation by IKK2 depletion in a mouse lung-cancer model. *Nat. Cell Biol.* **14**, 257–265 (2012).
21. Maier, H. J. et al. Requirement of NEMO/IKKγ for effective expansion of KRAS-induced precancerous lesions in the pancreas. *Oncogene* **32**, 2690–2695 (2013).
22. Bassères, D. S., Ebbs, A., Cogswell, P. C. & Baldwin, A. S. IKK is a therapeutic target in KRAS-induced lung cancer with disrupted p53 activity. *Genes Cancer* 5, 41–55 (2014).
23. Barbie, D. A. et al. Systematic RNA interference reveals that oncogenic KRAS-driven cancers require TBK1. *Nature* **462**, 108–112 (2009).
24. Rajurkar, M. et al. IKBKE is required during KRAS-induced pancreatic tumorigenesis. *Cancer Res.* **77**, 320–329 (2017).
25. Giannou, A. D. Mutant *NRAS* destines tumor cells to the lungs. *EMBO Mol. Med* **9**, 672–686, (2017).
26. Sunwoo, J. B. et al. Novel proteasome inhibitor PS-341 inhibits activation of nuclear factor-kappa B, cell survival, tumor growth, and angiogenesis in squamous cell carcinoma. *Clin. Cancer Res.* **7**, 1419–1428 (2001).
27. Fan, M., Ahmed, K. M., Coleman, M. C., Spitz, D. R. & Li, J. J. Nuclear factor-kappaB and manganese superoxide dismutase mediate adaptive radioresistance in low-dose irradiated mouse skin epithelial cells. *Cancer Res.* **67**, 3220–3228 (2007).
28. Rastelli, G., Tian, Z. Q., Wang, Z., Myles, D. & Liu, Y. Structure-based design of 7-carbamate analogs of geldanamycin. *Bioorg. Med. Chem. Lett.* **15**, 5016–5021 (2005).
29. Hertlein, E. et al. 17-DMAG targets the nuclear factor-kappaB family of proteins to induce apoptosis in chronic lymphocytic leukemia: clinical implications of HSP90 inhibition. *Blood* **116**, 45–53 (2010).
30. Pahl, H. L. Activators and target genes of Rel/NF-kappaB transcription factors. *Oncogene* **18**, 6853–6866 (1999).
31. Horai, R. et al. Production of mice deficient in genes for interleukin (IL)-1alpha, IL-1beta, IL-1alpha/beta, and IL-1 receptor antagonist shows that IL-1beta is crucial in turpentine-induced fever development and glucocorticoid secretion. *J. Exp. Med.* **187**, 1463–1475 (1998).
32. Keffer, J. et al. Transgenic mice expressing human tumour necrosis factor: a predictive genetic model of arthritis. *EMBO J.* **10**, 4025–4031 (1991).
33. Stathopoulos, G. T. et al. Use of bioluminescent imaging to investigate the role of nuclear factor-kappaBeta in experimental non-small cell lung cancer metastasis. *Clin. Exp. Metastasis* **25**, 43–51 (2008).
34. Marazioti, A. et al. Beneficial impact of CCL2 and CCL12 neutralization on experimental malignant pleural effusion. *PLoS ONE* **8**, e71207 (2013).
35. Giannou, A. D. et al. Mast cells mediate malignant pleural effusion formation. *J. Clin. Invest.* **125**, 2317–2334 (2015).
36. Sakai, N. et al. CXCR1 deficiency does not alter liver regeneration after partial hepatectomy in mice. *Transplant. Proc.* **43**, 1967–1970 (2011).
37. Cacalano, G. et al. Neutrophil and B cell expansion in mice that lack the murine IL-8 receptor homolog. *Science* **265**, 682–684 (1994).
38. Zlotnik, A. & Yoshie, O. The chemokine superfamily revisited. *Immunity* **36**, 705–716 (2012).
39. Zimmermann, G. et al. Small molecule inhibition of the KRAS-PDEδ interaction impairs oncogenic KRAS signalling. *Nature* **497**, 638–642 (2013).
40. Ikediobi, O. N. et al. Mutation analysis of 24 known cancer genes in the NCI-60 cell line set. *Mol. Cancer Ther.* **5**, 2606–2612 (2006).
41. Schubbert, S., Shannon, K. & Bollag, G. Hyperactive Ras in developmental disorders and cancer. *Nat. Rev. Cancer* **7**, 295–308 (2007).
42. Stephen, A. G., Esposito, D., Bagni, R. K. & McCormick, F. Dragging ras back in the ring. *Cancer Cell* **25**, 272–281 (2014).
43. Starczynowski, D. T. et al. TRAF6 is an amplified oncogene bridging the RAS and NF-κB pathways in human lung cancer. *J. Clin. Invest.* **121**, 4095–4105 (2011).
44. Sparmann, A. & Bar-Sagi, D. Ras-induced interleukin-8 expression plays a critical role in tumor growth and angiogenesis. *Cancer Cell* **6**, 447–458 (2004).
45. Ji, H. et al. K-ras activation generates an inflammatory response in lung tumors. *Oncogene* **25**, 2105–2112 (2006).
46. Ortis, F. et al. Differential usage of NF-κB activating signals by IL-1β and TNF-α in pancreatic beta cells. *FEBS Lett.* **586**, 984–989 (2012).
47. Anest, V. et al. A nucleosomal function for IkappaB kinase-alpha in NF-kappaB-dependent gene expression. *Nature* **423**, 659–663 (2003).
48. Yamamoto, Y., Verma, U. N., Prajapati, S., Kwak, Y. T. & Gaynor, R. B. Histone H3 phosphorylation by IKK-alpha is critical for cytokine-induced gene expression. *Nature* **423**, 655–659 (2003).
49. Luo, J. L. et al. Nuclear cytokine-activated IKKalpha controls prostate cancer metastasis by repressing Maspin. *Nature* **446**, 690–694 (2007).
50. Giopanou, I. et al. Comprehensive evaluation of nuclear factor-κB expression patterns in non-small cell lung cancer. *PLoS ONE* **10**, e0132527 (2015).
51. Shalapour, S. & Karin, M. Immunity, inflammation, and cancer: an eternal fight between good and evil. *J. Clin. Invest.* **125**, 3347–3355 (2015).
52. Voronov, E. et al. IL-1 is required for tumor invasiveness and angiogenesis. *Proc. Natl. Acad. Sci. USA* **100**, 2645–2650 (2003).
53. McLoed, A. G. et al. Neutrophil-derived IL-1β impairs the efficacy of NF-κB inhibitors against lung cancer. *Cell. Rep.* **16**, 120–132 (2016).
54. Zhuang, Z. et al. IL1 receptor antagonist inhibits pancreatic cancer growth by abrogating NF-κB activation. *Clin. Cancer Res.* **22**, 1432–1444 (2016).
55. Solt, L. A., Madge, L. A., Orange, J. S. & May, M. J. Interleukin-1-induced NF-kappaB activation is NEMO-dependent but does not require IKKbeta. *J. Biol. Chem.* **282**, 8724–8733 (2007).
56. Dong, G., Chen, Z., Kato, T. & Van Waes, C. The host environment promotes the constitutive activation of nuclear factor-kappaB and proinflammatory cytokine expression during metastatic tumor progression of murine squamous cell carcinoma. *Cancer Res.* **59**, 3495–3504 (1999).
57. Ginestier, C. et al. CXCR1 blockade selectively targets human breast cancer stem cells in vitro and in xenografts. *J. Clin. Invest.* **120**, 485–497 (2010).
58. Jamieson, T. et al. Inhibition of CXCR2 profoundly suppresses inflammation-driven and spontaneous tumorigenesis. *J. Clin. Invest.* **122**, 3127–3144 (2012).
59. Lv, M. et al. miR141-CXCL1-CXCR2 signaling-induced Treg recruitment regulates metastases and survival of non-small cell lung cancer. *Mol. Cancer Ther.* **13**, 3152–3162 (2014).

60. Cancer Genome Atlas Research Network. Comprehensive molecular profiling of lung adenocarcinoma. *Nature* **511**, 543–550 (2014).
61. Lilenbaum, R. et al. Randomized phase II trial of docetaxel plus cetuximab or docetaxel plus bortezomib in patients with advanced non-small-cell lung cancer and a performance status of 2: CALGB 30402. *J. Clin. Oncol.* **27**, 4487–4491 (2009).
62. Pfaffl, M. W. A new mathematical model for relative quantification in real-time RT-PCR. *Nucleic Acids Res.* **29**, e45 (2001).
63. Schindelin, J. et al. Fiji: an open-source platform for biological-image analysis. *Nat. Methods* **9**, 676–682 (2012).
64. Faul, F., Erdfelder, E., Lang, A. G. & Buchner, A. G*Power 3: a flexible statistical power analysis program for the social, behavioral, and biomedical sciences. *Behav. Res. Methods* **39**, 175–191 (2007).

Acknowledgements

This work was supported by European Research Council 2010 Starting Independent Investigator and 2015 Proof of Concept Grants (260524 and 679345, to GTS), by European Respiratory Society 2013 Romain Pauwels Research Award (to G.T.S.), by a Hellenic Association for Molecular Cancer Research Award 2015 (to A.M.), by a Hellenic Thoracic Society Research Award 2014 (to M.V.), and by an Immunotools Award 2014 (to A.D.G.). The authors thank the University of Patras Center for Animal Models of Disease for experimental support.

Author contributions

A.M. designed and performed NF-κB ELISA, immunoblotting, EMSA, drug testing, transfections, reporter assays, and most in vivo experiments, quantified and analyzed the data, provided critical intellectual input, and wrote the paper draft; I.L. isolated BMMCs; M.V. designed and performed reporter assays and in vivo experiments including bioluminescent imaging, quantified and analyzed the data, and provided critical intellectual input; H.A. and A.D.G. performed pNGL induction studies, mutant KRAS and IKK silencing/overexpression and relevant in vitro assays, and drug testing; A.K. performed CHIP experiments; I.G. did qPCR experiments; G.A.G. and A.C.K. performed in vivo deltarasin/17-DMAG treatment experiments; M.I. did pleural fluid cell counts; N.I.K. analyzed microarray; T.A. cloned eukaryotic expression vectors; C.J.-P. performed NF-κB ELISA; Y.I. provided analytical tools and critical intellectual input; D.K. performed total body irradiation; T.S.B. provided pNGL and critical intellectual input; S.T. provided analytical tools and critical intellectual input; M.S. performed immunofluorescence; G.T.S. conceived the idea and supervised the study, designed experiments, analyzed the data, wrote the paper, and is the guarantor of the study's integrity. All authors reviewed, edited, and concur with the submitted manuscript.

Additional information

Supplementary Information accompanies this paper at https://doi.org/10.1038/s41467-018-03051-z.

Competing interests: The authors declare no competing financial interests.

Reprints and permission information is available online at http://npg.nature.com/reprintsandpermissions/

Publisher's note: Springer Nature remains neutral with regard to jurisdictional claims in published maps and institutional affiliations.

ONLINE SUPPLEMENTARY INFORMATION

Myeloid-derived IL-1β drives oncogenic *KRAS*-NF-κB addiction in malignant pleural effusion

Marazioti et al.

Supplementary Figure 1. Full unedited blots for **Fig. 1f**. Dashed lines indicate blot areas shown in the main Figure.

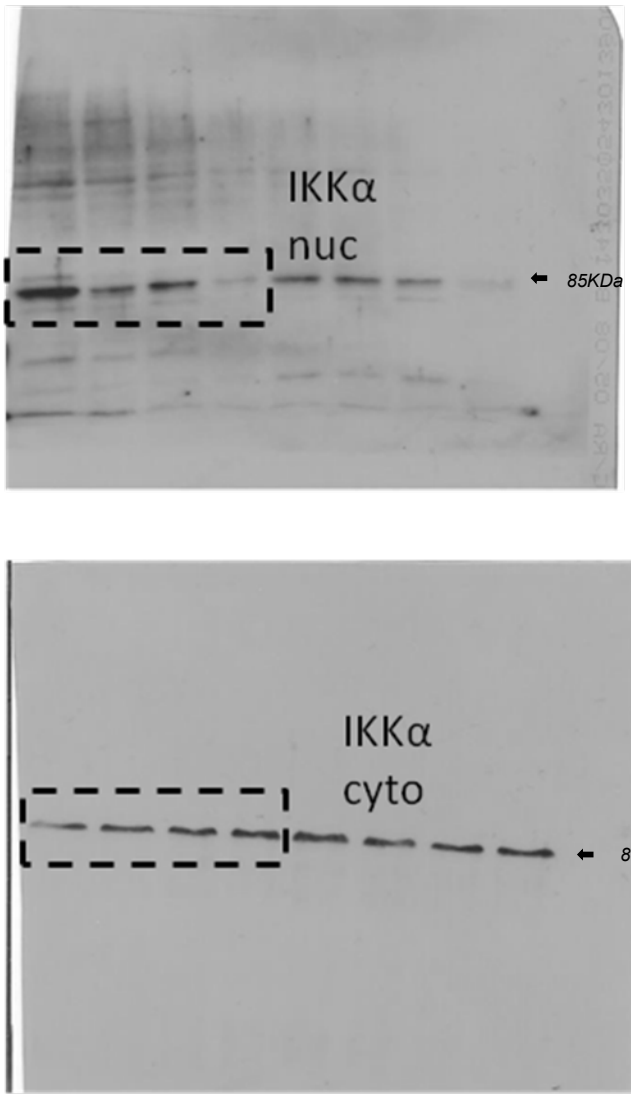

Supplementary Figure 2. Full unedited blots for **Fig. 4c**. Dashed lines indicate blot areas shown in the main Figure.

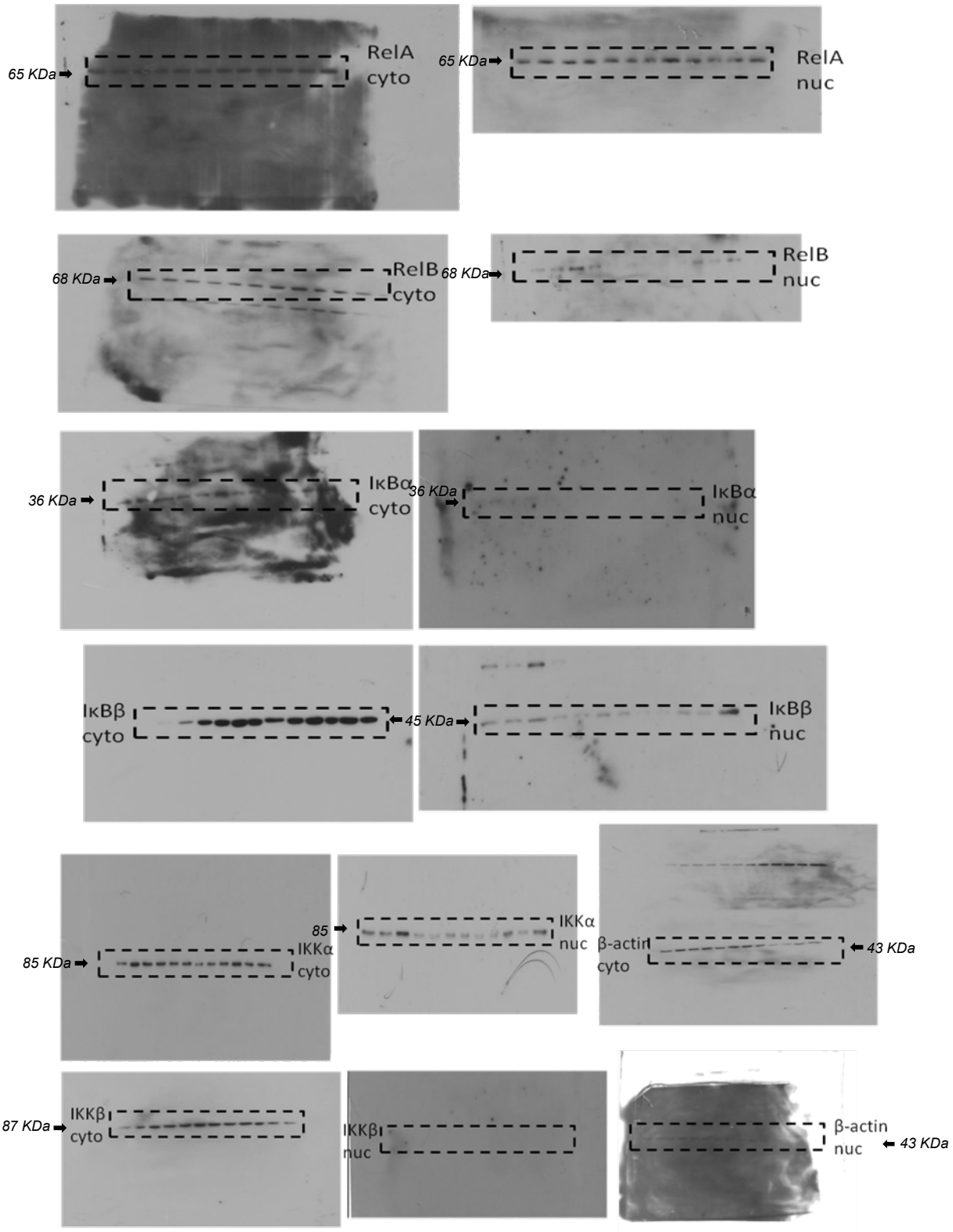

Supplementary Figure 3. Full unedited blots for **Fig. 4k**. Dashed lines indicate blot areas shown in the main Figure.

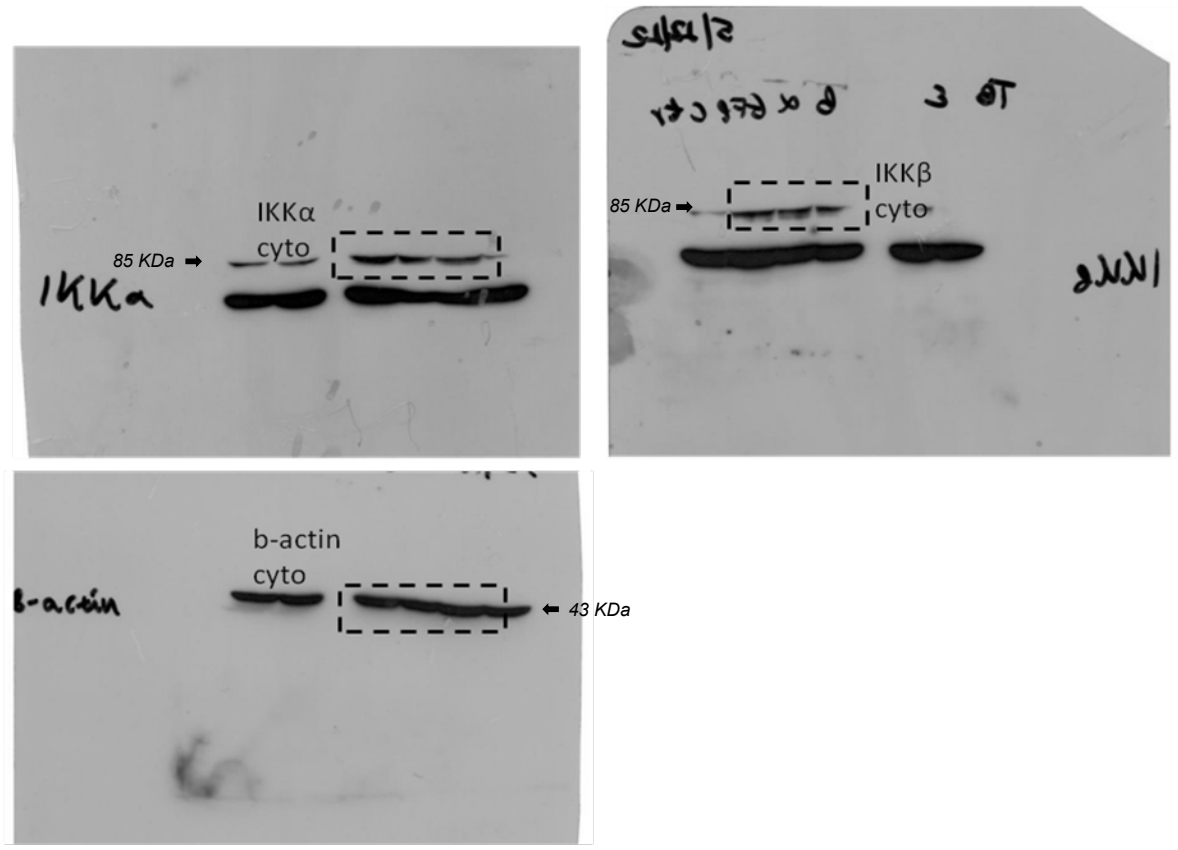

Supplementary Figure 4. Full unedited blots for **Fig. 5a**. Dashed lines indicate blot areas shown in the main Figure.

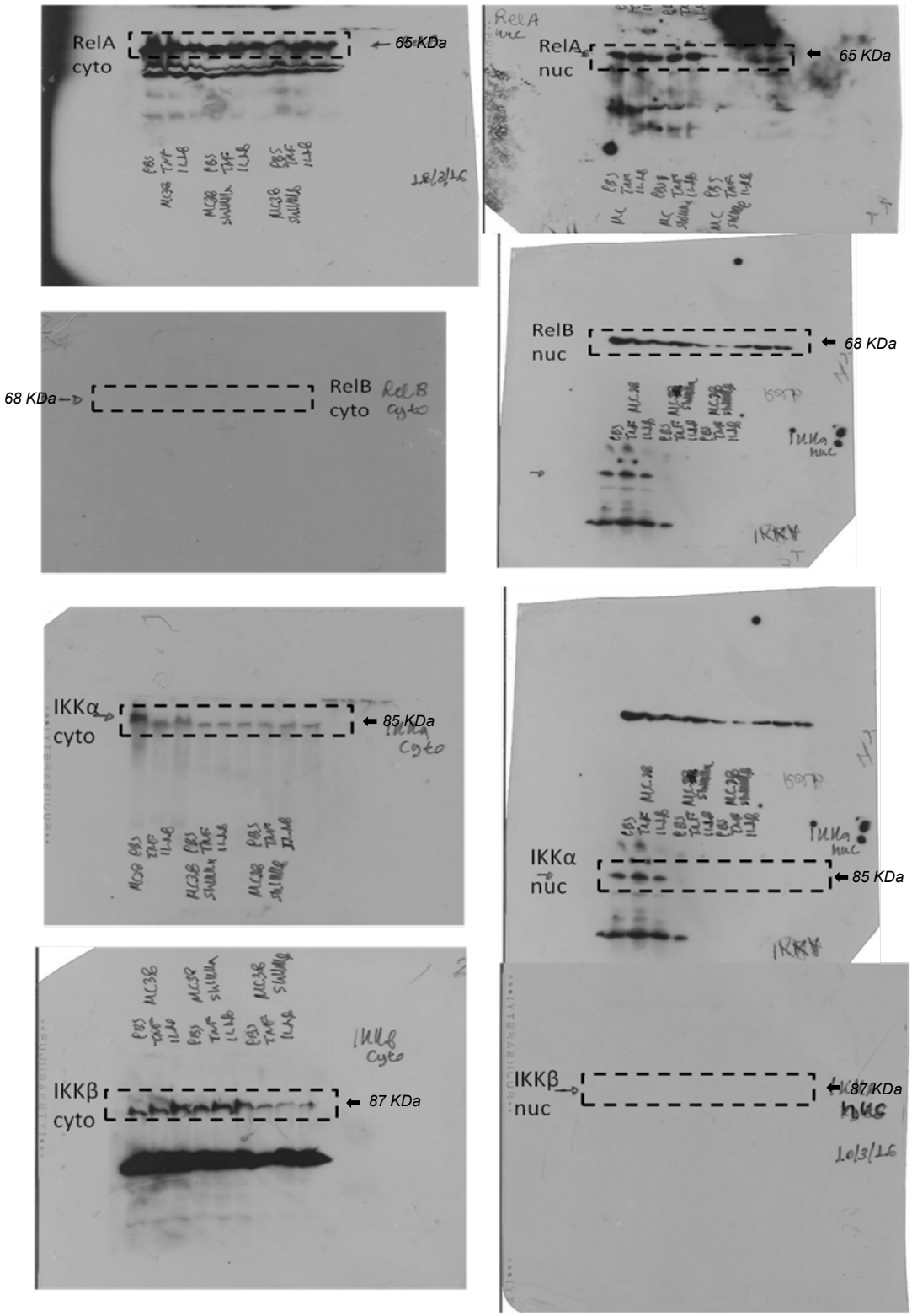

Supplementary Figure 5. Full unedited blots for **Fig. 5e**. Dashed lines indicate blot areas shown in the main Figure.

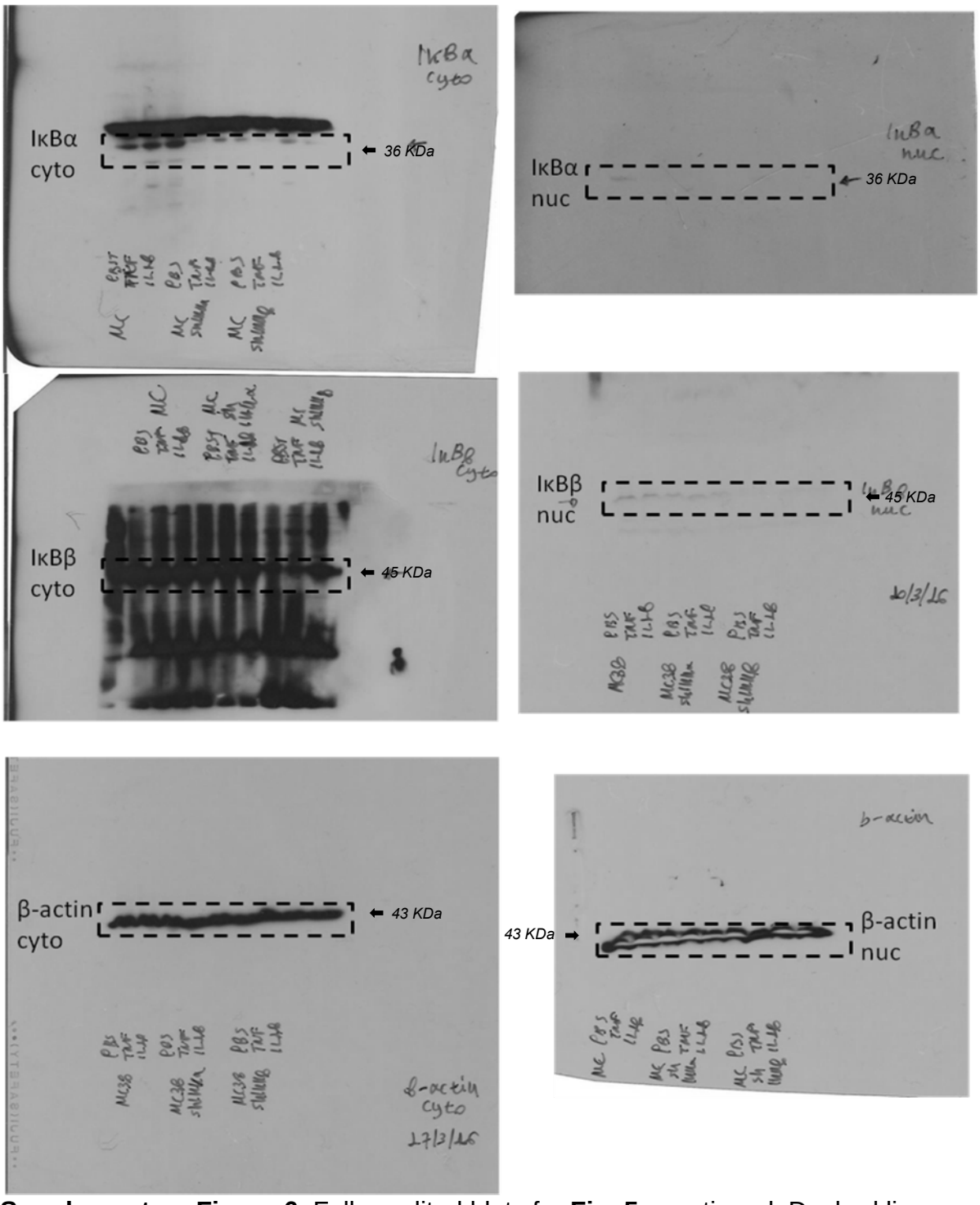

Supplementary Figure 6. Full unedited blots for **Fig. 5e** continued. Dashed lines indicate blot areas shown in the main Figure.

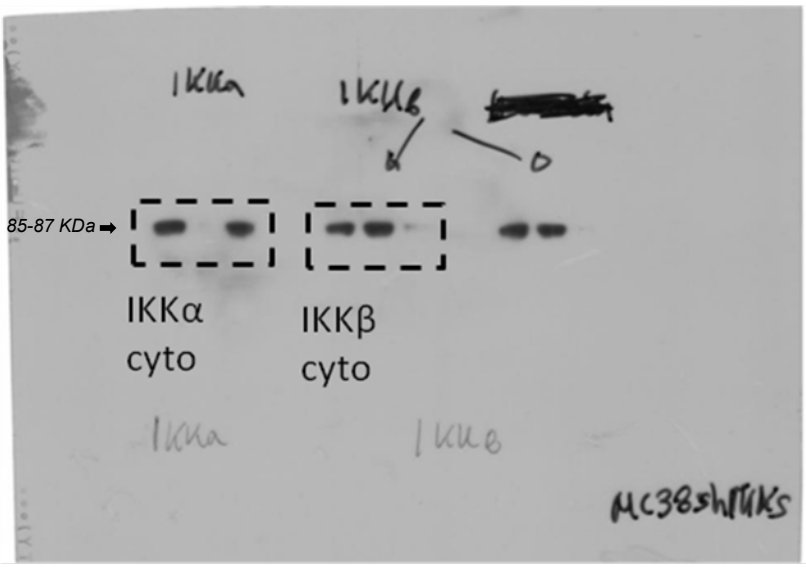

Supplementary Figure 7. Full unedited blots for **Fig. 6d**. Dashed lines indicate blot areas shown in the main Figure.

Supplementary Table 1. Inhibitory activity of the proteasome inhibitor bortezomib, the IKKβ-specific inhibitor IMD-0354, and the HSP90 and dual IKKα/IKKβ inhibitor 17-DMAG on NF-κB reporter activity and cellular proliferation of *KRAS*-mutant and *KRAS*-wild-type murine cell lines A detailed description of the experiments is given in Fig.1.

	LLC (*KRAS*^{G12C})	**MC38** (*KRAS*^{G13R})	**AE17** (*KRAS*^{G12C})	**B16F10** (*KRAS*^{WT})[a]	**PANO2** (*KRAS*^{WT})[a]	
	NF-κB IC50[b] [μM; n = 3; mean(95%CI)]					***P*** [d]
bortezomib	nd	nd	nd	0.12 (0.05-0.16)	0.23 (0.10-0.43)	nd
IMD-0354	27.55 (13.38-56.73)	9.21 (6.53-13.00)	4.04 (3.01-5.43)	0.03 (0.02-0.03)	0.03 (0.01-0.08)	< 0.0001
17-DMAG	0.13 (0.07-0.24)	0.57 (0.29-1.11)	0.06 (0.03-0.10)	0.04 (0.00-0.06)	0.23 (0.16-0.33)	< 0.0001
	MTT IC50[c] [μM; n = 3-4; mean(95%CI)]					
bortezomib	1.89 (1.21-2.94)	1.29 (0.86-1.94)	1.05 (0.75-1.47)	0.14 (0.09-0.20)	0.33 (0.20-0.53)	< 0.0001
IMD-0354	10.37 (5.66-19.00)	29.35 (11.02-78.18)	54.68 (25.08-119.20)	0.06 (0.04-0.10)	0.65 (0.33-1.26)	< 0.0001
17-DMAG	1.94 (0.79-4.73)	2.57 (0.86-7.73)	4.65 (2.13-10.18)	11.85 (3.50-40.18)	20.82 (8.87-48.9)	0.0042

[a] WT, wild-type.
[b] NF-κB IC_{50}, 50% inhibitory concentration of p*NGL* NF-κB reporter activity by bioluminescence imaging of live cells.
[c] MTT IC_{50}, 50% inhibitory concentration of 3-(4,5-dimethylthiazol-2-yl)-2,5-diphenyltetrazolium bromide reduction capacity.
[d] *P*, probability of no difference between cell lines by extra sum-of-squares F test.
LLC, *C57BL/6* Lewis lung carcinoma; MC38, *C57BL/6* colon adenocarcinoma; AE17, *C57BL/6* malignant pleural mesothelioma; B16F10, *C57BL/6* malignant skin melanoma; PANO2, *C57BL/6* pancreatic adenocarcinoma.

Supplementary Table 2. Inducibility of NF-κB reporter activity of *KRAS*-mutant and *KRAS*-wild-type murine cell lines by 60 different candidate ligands A detailed description of the experiments is given in Fig. 2.

CCL11	-	**IGF**	-	**IL-31**	-
CCL19	-	**IL-10**	-	**IL-33**	-
CCL2	-	**IL-11**	-	**IL-4**	-
CCL20	-	**IL-13**	-	**IL-5**	-
CCL3	-	**IL-15**	-	**IL-6**	-
CCL4	-	**IL-16**	-	**IL-7**	-
CCL5	-	**IL-17A**	-	**IL-9**	-
CD135	-	**IL-17C**	-	**LIF**	-
CD40L	-	**IL-17F**	-	**LPS**	LMABP
CXCL1	-	**IL-18**	-	**LTβ**	LMAB
CXCL10	-	**IL-19**	-	**MCSF**	-
CXCL12a	-	**IL-1α**	LMA	**NGF**	-
CXCL12b	-	**IL-1β**	LMA	**PDGFaa**	-
CXCL2	-	**IL-2**	-	**PDGFbb**	-
EGF	-	**IL-20**	-	**SCF**	-
FGF1	-	**IL-21**	-	**SPP1**	-
FGF2	-	**IL-22**	-	**TGF**	-
GCSF	-	**IL-25**	-	**TNF**	LMABP
GMCSF	-	**IL-27**	-	**TPO**	-
IFN-γ	-	**IL-3**	-	**VEGF**	-

L, induced > 2-fold in Lewis lung canrcinoma (LLC) cells (*Kras*^{G12C} mutant).
M, induced > 2-fold in MC38 colon adenocarcinoma cells (*Kras*^{G13R} mutant).
A, induced > 2-fold in AE17 malignant pleural mesothelioma cells (*Kras*^{G12C} mutant).
B, induced > 2-fold in B16F10 malignant skin melanoma cells (*Kras* wild-type).
P, induced > 2-fold in PANO2 pancreatic adenocarcinoma cells (*Kras* wild-type).

CCL; C-C motif chemokine ligand; CXCL, C-X-C motif chemokine ligand; EGF, epidermal growth factor; FGF1, fibroblast growth factor; GCSF, granulocyte colony stimulating factor; GMCSF, granulocyte-macrophage colony stimulating factor; IFN, interferon; IGF, insulin growth factor; IL, interleukin; LIF, leukemia inhibitory factor; LTβ, lymphotoxin β; MCSF, macrophage colony stimulating factor; NGF, nerve growth factor; PDGF, platelet-derived growth factor; SCF, stem cell factor; SPP, secreted phosphoprotein; TGF, transforming growth factor; TNF, tumor necrosis factor; TPO, thyroid peroxidase; VEGF, vascular endothelial growth factor.

Supplementary Table 3. Incidence of experimental malignant pleural effusions (MPE) MPE incidence in *in vivo* experiments from Figures 6-9. Shown are numbers of mice (*n*) and probability (*P*) for comparison with controls (top row of each experiment) by Fischer's exact test or for overall comparison within each experiment by χ^2 tests.

	Groups	No MPE	MPE	*P*
Experiment from Figs. 6A-C **LLC**-induced MPE. Cells stably expressing control or anti-IKK-specific shRNAs.	sh*C*	1	18	1.0000
	sh*Chuk*	10	6	0.0006
	sh*Ikbkb*	3	12	0.2994
	sh*Ikbke*	8	10	0.0078
	sh*Tbk1*	3	12	0.2994
				χ^2 *P* = 0.0021
Experiment from Figs. 6D-F **MC38**-induced MPE. Cells stably expressing control or anti-IKK-specific shRNAs.	sh*C*	1	7	1.0000
	sh*Chuk*	6	2	0.0406
	sh*Ikbkb*	2	6	1.0000
				χ^2 *P* = 0.0239
Experiment from Figs. 6G-I **PANO2**-induced MPE. Cells stably expressing control or IKKα, IKKβ, or mutant *Kras*^{G12C} expression plasmids.	p*C*	9	1	1.0000
	p*Chuk*	9	1	1.0000
	p*Ikbkb*	10	0	1.0000
	p*Kras*^{G1C}	0	10	0.0001
				χ^2 *P* = 0.0239
Experiment from Fig. 7A **LLC**-induced MPE. Wild-type (*C57BL/6*), TNF (*Tnf-/-*), and IL-1β (*Il1b-/-*) deficient mice.	*C57BL/6*	4	14	1.0000
	Tnf-/-	1	17	0.3377
	Il1b-/-	17	1	< 0.0001
				χ^2 *P* < 0.0001
Experiment from Fig7B **MC38**-induced MPE. Wild-type (*C57BL/6*), TNF (*Tnf-/-*), and IL-1β (*Il1b-/-*) deficient mice.	*C57BL/6*	1	9	1.0000
	Tnf-/-	0	10	1.0000
	Il1b-/-	8	2	0.0055
				χ^2 *P* = 0.0001
Experiment from Fig. 7E **LLC**-induced MPE. *Il1b-/-* mice transplanted with bone marrow from wild-type, *Tnf-/-*, and *Il1b-/-* donors.	*C57BL/6*	0	10	1.0000
	Tnf-/-	2	6	0.1830
	Il1b-/-	9	2	0.0002
				χ^2 *P* = 0.0004
Experiment from Fig. 8F **LLC**-induced MPE. Wild-type (*C57BL/6*), CXCR1 (*Cxcr1-/-*), and CXCR2 (*Cxcr2+/-*)-deficient mice.	*C57BL/6*	0	11	1.0000
	Cxcr1-/-	5	6	0.0351
	Cxcr2+/-	5	6	0.0351
				χ^2 *P* = 0.0277
Experiment from Fig. 9C **LLC**-induced MPE. *C57BL/6* mice treated with daily intraperitoneal PBS, deltarasin, 17-DMAG, or deltarasin/17-DMAG (all at 15 mg/Kg in 100 µL PBS).	PBS	0	14	1.0000
	deltarasin	2	12	0.4815
	17-DMAG	2	12	0.4815
	Deltarasin + 17-DMAG	6	8	0.0159
				χ^2 *P* = 0.0261

LLC, *C57BL/6* Lewis lung carcinoma; IKK, IκB kinase; MC38, *C57BL/6* colon adenocarcinoma; Tnf, tumor necrosis factor; Il, interleukin; CXCR, C-X-C-motif chemokine receptor.

Supplementary Table 4. Microarray results from LLC cells Thirty transcripts altered more than 1.3-fold in Lewis lung adenocarcinoma cells treated with 20 ng/mL rmIL-1β (in one direction) and in Lewis lung carcinoma cells stably expressing anti-*Kras* or anti-*Chuk* shRNA (in the other direction), as assessed by microarray (mouse Gene ST2.0, Affymetrix, Sta.Clara, CA). A positive ΔGE indicates induction and a negative ΔGE suppression of a gene transcript. Gene symbols in red font were further examined in this study. A detailed description of the experiment is given in Figure 8A.

Gene symbol	Gene name	*Δ*GE[a] IL-1β	*Δ*GE[a] sh*Kras*	*Δ*GE[a] sh*Chuk*
Ppbp	pro-platelet basic protein	1,81	-3,00	-1,31
Cxcl1	chemokine (C-X-C motif) ligand 1	2,40	-1,93	-1,28
A4galt	alpha 1,4-galactosyltransferase	0,74	-1,08	-1,22
Wdyhv1	WDYHV motif containing 1	0,59	-0,58	-1,72
Taf1d	Tbp-associated factor, RNA polymerase I, D	0,96	-0,83	-1,08
Ifi44	interferon-induced protein 44	0,75	-0,94	-0,86
Nol10	nucleolar protein 10	1,40	-0,60	-0,41
Mmp9	matrix metallopeptidase 9	0,90	-0,45	-0,95
Caprin2	caprin family member 2	1,04	-0,58	-0,57
Dut	deoxyuridine triphosphatase	0,40	-0,54	-0,75
Fam160a1	family with sequence similarity 160, A1	-0,46	0,71	0,55
Ipo4	importin 4	-0,57	0,58	0,66
1810010H24Rik	RIKEN cDNA 1810010H24 gene	-0,61	0,83	0,49
Zfp300	zinc finger protein 300	-1,11	0,45	0,48
Camta2	calmodulin binding transcription activator 2	-0,66	0,64	0,77
Mbd6	methyl-CpG binding domain protein 6	-0,63	1,12	0,44
Spice1	spindle and centriole associated protein 1	-1,16	0,67	0,43
Scarf2	scavenger receptor class F, member 2	-1,01	0,68	0,65
Ldlr	low density lipoprotein receptor	-0,47	1,01	0,93
Rab32	RAB32, member RAS oncogene family	-0,92	0,56	1,00
Tgfb3	transforming growth factor, beta 3	-1,65	0,53	0,43
Galnt10	UDP-N-ac-α-D-galactosamine:polypeptide N-acetylgalactosaminyltransferase 10	-1,42	0,68	0,57
Neto2	neuropilin (NRP) and tolloid (TLL)-like 2	-1,06	0,44	1,74
Cpt1c	carnitine palmitoyltransferase 1c	-2,09	0,55	0,69
Arsj	arylsulfatase J	-1,82	1,00	0,87
Pmp22	peripheral myelin protein 22	-1,33	0,90	1,62
Fah	fumarylacetoacetate hydrolase	-2,04	0,91	1,12
Ephx1	epoxide hydrolase 1, microsomal	-0,96	1,62	1,52
Efnb2	ephrin B2	-2,63	1,39	0,65
Ppargc1a	peroxisome proliferative activated receptor, gamma, coactivator 1 alpha	-1,58	3,30	1,64

[a] *Δ*GE, difference in gene expression.

Supplementary Table 5. Microarray results from MC38 cells Twenty transcripts altered more than 1.3-fold in MC38 colon adenocarcinoma cells treated with 20 ng/mL rmIL-1β (in one direction) and in Lewis lung carcinoma cells stably expressing anti-*Kras* or anti-*Chuk* shRNA (in the other direction), as assessed by microarray (mouse Gene ST2.0, Affymetrix, Sta.Clara, CA). A positive ΔGE indicates induction and a negative ΔGE suppression of a gene transcript. Gene symbols in red font were further examined in this study. A detailed description of the experiment is given in Figure 8A.

Gene symbol	Gene name	*Δ*GE[a] IL-1β	*Δ*GE[a] sh*Kras*	*Δ*GE[a] sh*Chuk*
Cxcl1	chemokine (C-X-C motif) ligand 1	3,19	-0,87	-1,29
Grem1	gremlin 1	0,50	-1,79	-1,48
Mmp3	matrix metallopeptidase 3	1,92	-1,27	-0,47
Mmp13	matrix metallopeptidase 13	0,46	-0,72	-2,09
Alcam	activated leukocyte cell adhesion molecule	0,73	-1,41	-1,02
Hgf	hepatocyte growth factor	1,16	-0,86	-1,11
Creb5	cAMP responsive element binding protein 5	0,74	-1,55	-0,80
Adamts7	a disintegrin-like and metallopeptidase (reprolysin type) with thrombospondin type 1 motif, 7	0,44	-1,23	-1,01
Sema6d	sema domain, transmembrane domain (TM), and cytoplasmic domain, (semaphorin) 6D	0,45	-1,29	-0,71
Rin2	Ras and Rab interactor 2	0,41	-0,86	-1,12
Syne1	spectrin repeat containing, nuclear envelope 1	-1,31	-1,05	-2,39
Procr	protein C receptor, endothelial	0,66	-0,41	-0,86
Dgkh	diacylglycerol kinase, eta	0,56	-0,51	-0,41
LOC101056159	uncharacterized LOC101056159	-0,41	0,54	0,82
Olfr1251	olfactory receptor 1251	-0,64	0,45	0,71
H2-Q5	histocompatibility 2, Q region locus 5	-0,62	0,43	0,92
Eif4a2	eukaryotic translation initiation factor 4A2	-0,43	0,42	1,39
LOC102633783	sp110 nuclear body protein-like	-1,20	0,42	1,10
Lgals9	lectin, galactose binding, soluble 9	-1,43	1,52	1,03
Apol9b	apolipoprotein L 9b	-2,52	1,48	0,52

[a] *Δ*GE, difference in gene expression.

Supplementary Table 6. PCR primers used for these studies.

Method[a]	Primer	Sequence	Amplicon (bp)
qPCR	Tnfrsf1aF	CAACGTCCTGACAATGCAGA	129
qPCR	Tnfrsf1aR	CTGCATCTCCAGCCTCTCGA	
qPCR	Il1r1F	TGGAAGTCTTGTGTGCCCTT	150
qPCR	Il1r1R	GCCACATTCCTCACCAACAG	
qPCR	Il1βF	TTTGACAGTGATGAGAATGACC	162
qPCR	Il1βR	AATGAGTGATACTGCCTGCC	
qPCR	Cxcl1F	CTTGACCCTGAAGCTCCCTT	127
qPCR	Cxcl1R	GTTGTCAGAAGCCAGCGTTC	
qPCR	GusbF	TTACTTTAAGACGCTGATCACC	165
qPCR	GusbR	ACCTCCAAATGCCCATAGTC	
PCR	Mycoplasma Spp.F	GGGAGCAAACAGGATTAGATACCCT	270
PCR	Mycoplasma Spp.R	TGCACCATCTGTCACTCTGTTAACCTC	
CL	mKrasF	GGAGATCTATGACTGAGTATAAACTTGTGGTGG	583
CL	mKrasR	GGGAATTCTCACATAACTGTACACCTTGTCCTT	
CL	ChukF	ATGGGCGGCCCCCGGGGCTGCGGC	2238
CL	ChukR	TCATTCTGCTAACCAACTCCAATC	
CL	IkbkbF	ATGAGCTGGTCACCGTCCCTCCCAACCC	2274
CL	IkbkbR	TCAGTCACAGGCCTGCTCCAGGC	
CL	IkbkeF	ATGCAGAGTACCACTAACTACCTGTGGC	1900
CL	IkbkeR	TCAGACATCTGGTGCCGATGGAA	
CL	Tbk1F	ATGCAGAGCACCTCCAACCATCTGTGGC	2191
CL	Tbk1R	CTAAAGACAGTCCACATTGCGAAGGCCA	

[a]Application: PCR, DNA polymerase chain reaction; qPCR, quantitative (real-time) PCR. CL, cloning.
Provider: VBC Biotech, Vienna, Austria.

Supplementary Table 7. Antibodies used for these studies

Method[a]	Target	Provider[b]	Catalog #	Dilution	Conjugate[c]
IF,WIB	*Rel*A	Santa Cruz	Sc-372	1:200, 1:500	-
IF, WIB	*Rel*B	Santa Cruz	Sc-30887	1:200, 1:500	-
WIB	IKKα	Cell Signaling	2682	1:1000	-
WIB, ChIP	IKKβ	Cell Signaling	2684	1:1000	-
WIB	IKKε	Cell Signaling	2690	1:1000	-
WIB	TBK1	Cell Signaling	3013	1:1000	-
WIB	IκBα	Santa Cruz	Sc-371	1:500	-
WIB	IκBβ	Santa Cruz	Sc-9130	1:500	-
WIB	β-actin	Santa Cruz	sc-47778	1:500	-
WIB	Goat anti-rabbit IgG	Southern Biotech	4030-05	1:8000	HRP
WIB	Goat anti-mouse IgG	Southern Biotech	1030-05	1:8000	HRP
IF	donkey anti-rabbit & anti-mouse IgG	Invitrogen	A21206 A21202	1:1000	Alexa 488
IF	donkey anti-rabbit & anti-mouse IgG	Invitrogen	A10042 A10037	1:1000	Alexa 568
ChIP, EMSA	*Rel*A	Santa Cruz	Sc-372 X	1:60	-
ChIP, EMSA	*Rel*B	Santa Cruz	Sc-226 X	1:60	-
ChIP	IKKα	Santa Cruz	Sc-7606 X	1:60	-

[a]Application: IF, immunofluorescence; WIB, Western immunoblotting; ChIP, Chromatin Immunoprecipitation; EMSA; electrophoretic mobility shift assay
[b]Providers*:* Cell Signaling, Danvers MA, USA; Santa Cruz Biotechnology, Dallas, TX; Southern Biotech, Birmingham, AL; Invitrogen, Carlsbad, CA.
[c]Conjugates*:* HRP, horse radish peroxidase.

Supplementary Table 8. Lentiviral shRNA pools used for these studies.

Target	Abbreviation	Catalog #	Target Sequences
random	sh*C*	sc-108080-V	target sequence proprietary
Chuk	sh*Chuk*	sc-29366-V	CCATGGTGTTTGAATGTATTT CTCTCAGTGTGTTCTAGATTT GCAAGCAGAAGATTATTGATT
Ikbkb	sh*Ikbkb*	sc-35645-V	GATGACATCTTGAACTTGATT CTGCACATTTGAATCTGTATT CAGCTCTCTTAGACAGTTATT
Ikbke	sh*Ikbke*	sc-39057-V	GAGATCATGTACAGAATCATT CAGTGTTGTTTGGACAAGATT CCAACAAACTAGCATTACTTT
Tbk1	sh*Tbk1*	sc-39059-V	GTAGGACTGAGATATGAAATT GCATCACAGAGATTTACTATT GAAGTTCTAGTTTGCACAATT
Kras	sh*Kras*	sc-43876-V	CTACAGGAAACAAGTAGTA GAACAGTAGACACGAAACA CCATTCAGTTTCCATGTTA

Provider: Santa Cruz Biotechnology, Dallas, TX.

6. Discussion, conclusions, and unpublished observations

In this work, we valorized our previous development of mouse models of MPE to identify a causative inflammatory circuitry initiated by mutant KRAS in tumor cells and perpetuated by myeloid cells that home to the pleura and sustain a proinflammatory tumor microenvironment. This MPE-associated inflammation is critical for frank fluid extravasation and for active pleural fluid accumulation in the chest. This work set a rational framework for a shift of the paradigm of MPE treatment: currently this is anatomic and aims at the elimination of the pleural fluid or pleural space altogether. Based on our work, targeted, immune, or precision therapies may be applied in the future to patients with MPE. One clinical trial of zoledronic acid was already done inspired by our studies (Clive et al., 2015). Although underpowered and negative, this was the first attempt to apply mechanistically targeted therapy to this patient population.

In more detail, we found that *KRAS*-mutant cancer cells secret CCL2 to chemoattract myeloid cells of the macrophage and mast cell lineage upon their homing to the pleural space. At the same time, they secret SPP1 and VCAN to activate these cells via cognate receptors. In turn, myeloid cells release IL-1β and TPSAB1 into the pleural tumor microenvironment to increase vascular permeability and to drive IKKα-mediated NF-κB activation in cancer cells, which leads to further chemokine secretion and neutrophil accumulation. All the mediators above also activate endothelial cells to augment angiogenesis and vascular leakage, culminating in r accumulation of protein and cell-rich exudate in the pleural space, also known as MPE. The above findings are reported in the three publications included in this thesis report (Figure 4).

In addition, we have identified further targets for therapy and have gathered a multitude of unpublished results from this work, which we intend to publish soon. These include but are not restricted to findings related to the role of mesothelial KRAS mutations in the pathogenesis of malignant pleural mesothelioma in mice and humans (Marazioti et al., manuscript submitted), as well as to the role of tumor-derived versican in triggering TLR2-mediated IKKβ acivation in MPE-associated macrophages, in turn leading to enhanced IL-1β secretion into MPE and enhanced effusion development and progression (Spella et al., manuscript submitted).

Taken together, here we describe how mouse models of MPE were developed and used to map the mechanisms of its formation and to identified potential targets for therapy. We found such to be mast cells and macrophages, tumor cell IKKα and myeloid cell IKKβ, tumor cell IL1R1 and myeloid cell IL-1β, among others, as well as tumor cell mutant KRAS oncoprotein, a cardinal culprit and driver of MPE development and progression.

The project yielded the publications described herein and additional publications related to the topic (some of which are included and highlighted in bold in the reference list), one European Research Council Starting and one Proof-of-Concept Grants, and one Maurizio Vignola and one Romain Pauwels Awards by the European Respiratory Society. In addition, this work yielded more than 25 graduate scientists with significant clinical and experimental expertise in malignant pleural diseases, which are serving today at the different ranks of academia and industry.

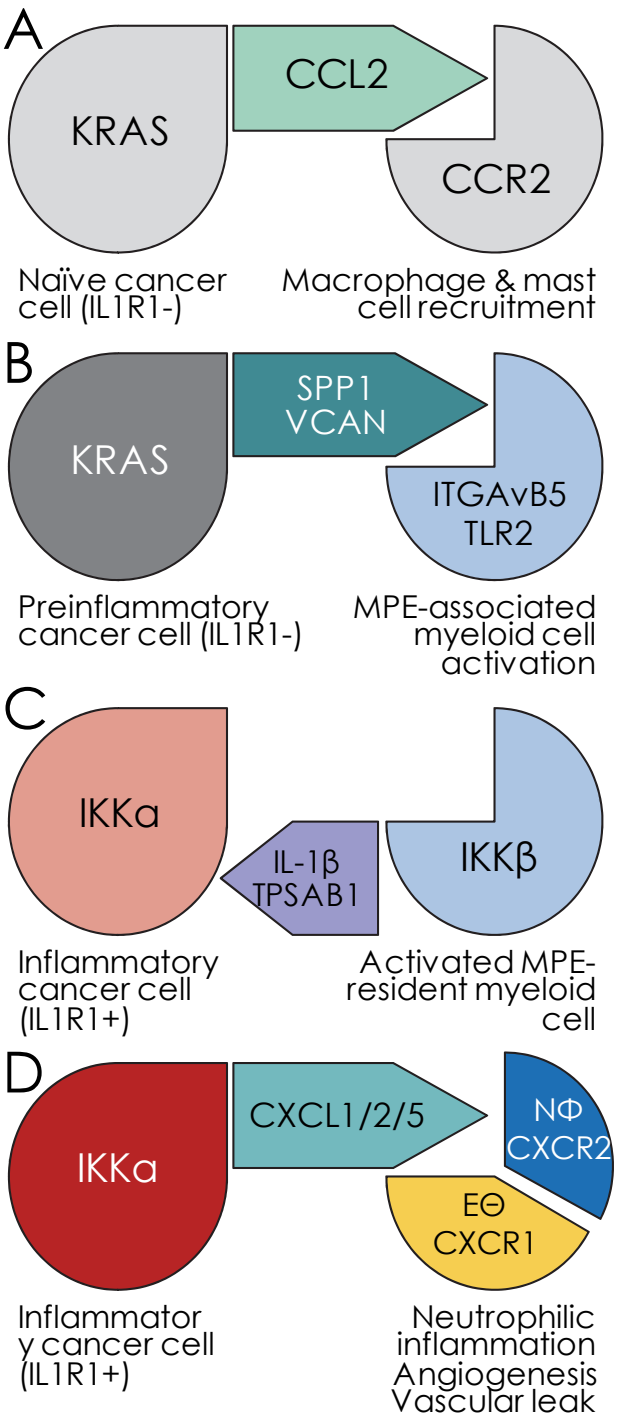

Figure 4. Cascade of events leading to malignant pleural effusion (MPE) development after pleural homing of cancer cells that harbor mutant *KRAS* alleles.

(A) KRAS proto-oncogene GTPase (KRAS)-mutant cancer cells secret C-C-motif chemokine ligand 2 (CCL2) that chemoattracts myeloid cells of the macrophage and mast cell lineage.

(B) KRAS-mutant cancer cells secret osteopontin (secreted phosphoprotein 1, SPP1) and versican (VCAN), which bind to integrin (ITG) avβ5 and toll-like receptor 2 (TLR2) to activate myeloid cells.

(C) Activated myeloid cells release interleukin (IL)-1β and tryptase AB1 (TPSAB1) into the pleural tumor microenvironment. While TPSAB1 acts to increase vascular permeability, IL-1β activates interleukin 1 receptor 1 (IL1R1), which is specifically overexpressed by KRAS-mutant cancer cells.

(D) KRAS-mutant cancer cells respond to myeloid-derived IL-1β with inhibitor of NF-κB kinase (IKK) α -mediated activation of nuclear factor kappa B (NF-κB), which leads to further C-X-C motif chemokine ligand (CXCL) secretion. The latter chemorecruit further myeloid cells of the neutrophil lineage (NΦ) via C-X-C motif chemokine receptoer (CXCR) 2, but also bind to CXCR2 on endothelial cells (EΘ) to augment angiogenesis and vascular leakage. These inflammatory and vasoactive phenomena are responsible for accumulation of protein and cell-rich exudate in the pleural space, also known as MPE.

7. References

Agalioti T, Giannou AD, Krontira AC, Kanellakis NI, Kati D, Vreka M, Pepe M, Spella M, Lilis I, Zazara DE, Nikolouli E, Spiropoulou N, Papadakis A, Papadia K, Voulgaridis A, Harokopos V, Stamou P, Meiners S, Eickelberg O, Snyder LA, Antimisiaris SG, Kardamakis D, Psallidas I, Marazioti A, Stathopoulos GT. Mutant KRAS promotes malignant pleural effusion formation. Nat Commun. 2017 May 16;8:15205. doi: 10.1038/ncomms15205.

Antony VB, Loddenkemper R, Astoul P, Boutin C, Goldstraw P, Hott J, Rodriguez Panadero F, Sahn SA. Management of malignant pleural effusions. Eur Respir J. 2001 Aug;18(2):402-19. doi: 10.1183/09031936.01.00225601.

Antunes G, Neville E, Duffy J, Ali N; Pleural Diseases Group, Standards of Care Committee, British Thoracic Society. BTS guidelines for the management of malignant pleural effusions. Thorax. 2003 May;58 Suppl 2(Suppl 2):ii29-38. doi: 10.1136/thorax.58.suppl_2.ii29.

Balkwill FR, Mantovani A. Cancer-related inflammation: common themes and therapeutic opportunities. Semin Cancer Biol. 2012 Feb;22(1):33-40. doi: 10.1016/j.semcancer.2011.12.005.

Barbie DA, Tamayo P, Boehm JS, Kim SY, Moody SE, Dunn IF, Schinzel AC, Sandy P, Meylan E, Scholl C, Fröhling S, Chan EM, Sos ML, Michel K, Mermel C, Silver SJ, Weir BA, Reiling JH, Sheng Q, Gupta PB, Wadlow RC, Le H, Hoersch S, Wittner BS, Ramaswamy S, Livingston DM, Sabatini DM, Meyerson M, Thomas RK, Lander ES, Mesirov JP, Root DE, Gilliland DG, Jacks T, Hahn WC. Systematic RNA interference reveals that oncogenic KRAS-driven cancers require TBK1. Nature. 2009 Nov 5;462(7269):108-12. doi: 10.1038/nature08460.

Basak SK, Veena MS, Oh S, Huang G, Srivatsan E, Huang M, Sharma S, Batra RK. The malignant pleural effusion as a model to investigate intratumoral heterogeneity in lung cancer. PLoS One. 2009 Jun 12;4(6):e5884. doi: 10.1371/journal.pone.0005884.

Bassères DS, Ebbs A, Cogswell PC, Baldwin AS. IKK is a therapeutic target in KRAS-Induced lung cancer with disrupted p53 activity. Genes Cancer. 2014 Apr;5(1-2):41-55. doi: 10.18632/genesandcancer.5.

Blair RJ, Meng H, Marchese MJ, Ren S, Schwartz LB, Tonnesen MG, Gruber BL. Human mast cells stimulate vascular tube formation. Tryptase is a novel, potent angiogenic factor. J Clin Invest. 1997 Jun 1;99(11):2691-700. doi: 10.1172/JCI119458.

Burgers JA, Kunst PW, Koolen MG, Willems LN, Burgers JS, van den Heuvel M. Pleural drainage and pleurodesis: implementation of guidelines in four hospitals. Eur Respir J. 2008 Nov;32(5):1321-7. doi: 10.1183/09031936.00165607.

Chen R, Ning G, Zhao ML, Fleming MG, Diaz LA, Werb Z, Liu Z. Mast cells play a key role in neutrophil recruitment in experimental bullous pemphigoid. J Clin Invest. 2001 Oct;108(8):1151-8. doi: 10.1172/JCI11494.

Clive AO, Kahan BC, Hooper CE, Bhatnagar R, Morley AJ, Zahan-Evans N,

Bintcliffe OJ, Boshuizen RC, Fysh ET, Tobin CL, Medford AR, Harvey JE, van den Heuvel MM, Lee YC, Maskell NA. Predicting survival in malignant pleural effusion: development and validation of the LENT prognostic score. Thorax. 2014 Dec;69(12):1098-104. doi: 10.1136/thoraxjnl-2014-205285.

Clive AO, Hooper CE, Edey AJ, Morley AJ, Zahan-Evans N, Hall D, Lyburn I, White P, Braybrooke JP, Sequeiros I, Lyen SM, Milton T, Kahan BC, Maskell NA. A randomised controlled trial of intravenous zoledronic acid in malignant pleural disease: a proof of principle pilot study. PLoS One. 2015 Mar 17;10(3):e0118569. doi: 10.1371/journal.pone.0118569.

Coussens LM, Pollard JW. Leukocytes in mammary development and cancer. Cold Spring Harb Perspect Biol. 2011 Mar 1;3(3):a003285. doi: 10.1101/cshperspect.a003285.

Dalton DK, Noelle RJ. The roles of mast cells in anticancer immunity. Cancer Immunol Immunother. 2012 Sep;61(9):1511-20. doi: 10.1007/s00262-012-1246-0.

Daniluk J, Liu Y, Deng D, Chu J, Huang H, Gaiser S, Cruz-Monserrate Z, Wang H, Ji B, Logsdon CD. An NF-κB pathway-mediated positive feedback loop amplifies Ras activity to pathological levels in mice. J Clin Invest. 2012 Apr;122(4):1519-28. doi: 10.1172/JCI59743.

Dudeck A, Dudeck J, Scholten J, Petzold A, Surianarayanan S, Köhler A, Peschke K, Vöhringer D, Waskow C, Krieg T, Müller W, Waisman A, Hartmann K, Gunzer M, Roers A. Mast cells are key promoters of contact allergy that mediate the adjuvant effects of haptens. Immunity. 2011 Jun 24;34(6):973-84. doi: 10.1016/j.immuni.2011.03.028.

Feyerabend TB, Weiser A, Tietz A, Stassen M, Harris N, Kopf M, Radermacher P, Möller P, Benoist C, Mathis D, Fehling HJ, Rodewald HR. Cre-mediated cell ablation contests mast cell contribution in models of antibody- and T cell-mediated autoimmunity. Immunity. 2011 Nov 23;35(5):832-44. doi: 10.1016/j.immuni.2011.09.015.

Floor SL, Dumont JE, Maenhaut C, Raspe E. Hallmarks of cancer: of all cancer cells, all the time? Trends Mol Med. 2012 Sep;18(9):509-15. doi: 10.1016/j.molmed.2012.06.005.

Galli SJ, Kalesnikoff J, Grimbaldeston MA, Piliponsky AM, Williams CM, Tsai M. Mast cells as "tunable" effector and immunoregulatory cells: recent advances. Annu Rev Immunol. 2005;23:749-86. doi: 10.1146/annurev.immunol.21.120601.141025.

Giannou AD, Marazioti A, Spella M, Kanellakis NI, Apostolopoulou H, Psallidas I, Prijovich ZM, Vreka M, Zazara DE, Lilis I, Papaleonidopoulos V, Kairi CA, Patmanidi AL, Giopanou I, Spiropoulou N, Harokopos V, Aidinis V, Spyratos D, Teliousi S, Papadaki H, Taraviras S, Snyder LA, Eickelberg O, Kardamakis D, Iwakura Y, Feyerabend TB, Rodewald HR, Kalomenidis I, Blackwell TS, Agalioti T, Stathopoulos GT. Mast cells mediate malignant pleural effusion formation. J Clin Invest. 2015 Jun;125(6):2317-34. doi: 10.1172/JCI79840.

Han HS, Eom DW, Kim JH, Kim KH, Shin HM, An JY, Lee KM, Choe KH, Lee KH, Kim ST, Koo JH, Lee HC, Lee OJ. EGFR mutation status in primary lung adenocarcinomas and corresponding metastatic lesions: discordance in pleural

metastases. Clin Lung Cancer. 2011 Nov;12(6):380-6. doi: 10.1016/j.cllc.2011.02.006.

Hanahan D, Weinberg RA. Hallmarks of cancer: the next generation. Cell. 2011 Mar 4;144(5):646-74. doi: 10.1016/j.cell.2011.02.013.

Jackaman C, Bundell CS, Kinnear BF, Smith AM, Filion P, van Hagen D, Robinson BW, Nelson DJ. IL-2 intratumoral immunotherapy enhances CD8+ T cells that mediate destruction of tumor cells and tumor-associated vasculature: a novel mechanism for IL-2. J Immunol. 2003 Nov 15;171(10):5051-63. doi: 10.4049/jimmunol.171.10.5051.

Ji H, Houghton AM, Mariani TJ, Perera S, Kim CB, Padera R, Tonon G, McNamara K, Marconcini LA, Hezel A, El-Bardeesy N, Bronson RT, Sugarbaker D, Maser RS, Shapiro SD, Wong KK. K-ras activation generates an inflammatory response in lung tumors. Oncogene. 2006 Mar 30;25(14):2105-12. doi: 10.1038/sj.onc.1209237.

Kang JY, Park CK, Yeo CD, Lee HY, Rhee CK, Kim SJ, Kim SC, Kim YK, Park MS, Yim HW. Comparison of PNA clamping and direct sequencing for detecting KRAS mutations in matched tumour tissue, cell block, pleural effusion and serum from patients with malignant pleural effusion. Respirology. 2015 Jan;20(1):138-46. doi: 10.1111/resp.12413.

Karabela SP, Psallidas I, Sherrill TP, Kairi CA, Zaynagetdinov R, Cheng DS, Vassiliou S, McMahon F, Gleaves LA, Han W, Stathopoulos I, Zakynthinos SG, Yull FE, Roussos C, Kalomenidis I, Blackwell TS, Stathopoulos GT. Opposing effects of bortezomib-induced nuclear factor-κB inhibition on chemical lung carcinogenesis. Carcinogenesis. 2012 Apr;33(4):859-67. doi: 10.1093/carcin/bgs024.

Kimura H, Fujiwara Y, Sone T, Kunitoh H, Tamura T, Kasahara K, Nishio K. EGFR mutation status in tumour-derived DNA from pleural effusion fluid is a practical basis for predicting the response to gefitinib. Br J Cancer. 2006 Nov 20;95(10):1390-5. doi: 10.1038/sj.bjc.6603428.

Kraus-Berthier L, Jan M, Guilbaud N, Naze M, Pierré A, Atassi G. Histology and sensitivity to anticancer drugs of two human non-small cell lung carcinomas implanted in the pleural cavity of nude mice. Clin Cancer Res. 2000 Jan;6(1):297-304. PMID: 10656461

Lee YC, Wilkosz S. Malignant pleural effusions: fixing the leaky faucet. Am J Respir Crit Care Med. 2008 Jul 1;178(1):3-5. doi: 10.1164/rccm.200804-616ED.

Li Y, Li Y, Yang T, Wei S, Wang J, Wang M, Wang Y, Zhou Q, Liu H, Chen J. Clinical significance of EML4-ALK fusion gene and association with EGFR and KRAS gene mutations in 208 Chinese patients with non-small cell lung cancer. PLoS One. 2013;8(1):e52093. doi: 10.1371/journal.pone.0052093.

Ling J, Kang Y, Zhao R, Xia Q, Lee DF, Chang Z, Li J, Peng B, Fleming JB, Wang H, Liu J, Lemischka IR, Hung MC, Chiao PJ. KrasG12D-induced IKK2/β/NF-κB activation by IL-1α and p62 feedforward loops is required for development of pancreatic ductal adenocarcinoma. Cancer Cell. 2012 Jan 17;21(1):105-20. doi: 10.1016/j.ccr.2011.12.006.

Maier HJ, Wagner M, Schips TG, Salem HH, Baumann B, Wirth T. Requirement of NEMO/IKKγ for effective expansion of KRAS-induced precancerous lesions in the pancreas. Oncogene. 2013 May 23;32(21):2690-5. doi: 10.1038/onc.2012.272.

Mantovani A, Allavena P, Sica A, Balkwill F. Cancer-related inflammation. Nature. 2008;454:436-444. doi:10.1038/nature07205

Marazioti A, Kairi CA, Spella M, Giannou AD, Magkouta S, Giopanou I, Papaleonidopoulos V, Kalomenidis I, Snyder LA, Kardamakis D, Stathopoulos GT. Beneficial impact of CCL2 and CCL12 neutralization on experimental malignant pleural effusion. PLoS One. 2013 Aug 14;8(8):e71207. doi: 10.1371/journal.pone.0071207.

Marazioti A, Lilis I, Vreka M, Apostolopoulou H, Kalogeropoulou A, Giopanou I, Giotopoulou GA, Krontira AC, Iliopoulou M, Kanellakis NI, Agalioti T, Giannou AD, Jones-Paris C, Iwakura Y, Kardamakis D, Blackwell TS, Taraviras S, Spella M, Stathopoulos GT. Myeloid-derived interleukin-1β drives oncogenic KRAS-NF-κB addiction in malignant pleural effusion. Nat Commun. 2018 Feb 14;9(1):672. doi: 10.1038/s41467-018-03051-z.

Meylan E, Dooley AL, Feldser DM, Shen L, Turk E, Ouyang C, Jacks T. Requirement for NF-kappaB signalling in a mouse model of lung adenocarcinoma. Nature. 2009 Nov 5;462(7269):104-7. doi: 10.1038/nature08462.

Nottingham LK, Yan CH, Yang X, Si H, Coupar J, Bian Y, Cheng TF, Allen C, Arun P, Gius D, Dang L, Van Waes C, Chen Z. Aberrant IKKα and IKKβ cooperatively activate NF-κB and induce EGFR/AP1 signaling to promote survival and migration of head and neck cancer. Oncogene. 2014 Feb 27;33(9):1135-47. doi: 10.1038/onc.2013.49.

Pittoni P, Colombo MP. The dark side of mast cell-targeted therapy in prostate cancer. Cancer Res. 2012 Feb 15;72(4):831-5. doi: 10.1158/0008-5472.CAN-11-3110.

Psallidas I, Karabela SP, Moschos C, Sherrill TP, Kollintza A, Magkouta S, Theodoropoulou P, Roussos C, Blackwell TS, Kalomenidis I, Stathopoulos GT. Specific effects of bortezomib against experimental malignant pleural effusion: a preclinical study. Mol Cancer. 2010 Mar 10;9:56. doi: 10.1186/1476-4598-9-56.

Rajurkar M, Dang K, Fernandez-Barrena MG, Liu X, Fernandez-Zapico ME, Lewis BC, Mao J. IKBKE Is Required during KRAS-Induced Pancreatic Tumorigenesis. Cancer Res. 2017 Jan 15;77(2):320-329. doi: 10.1158/0008-5472.CAN-15-1684.

Raparia K, Villa C, Raj R, Cagle PT. Peripheral lung adenocarcinomas with KRAS mutations are more likely to invade visceral pleura. Arch Pathol Lab Med. 2015 Feb;139(2):189-93. doi: 10.5858/arpa.2013-0759-OA.

Renaud S, Seitlinger J, Falcoz PE, Schaeffer M, Voegeli AC, Legrain M, Beau-Faller M, Massard G. Specific KRAS amino acid substitutions and EGFR mutations predict site-specific recurrence and metastasis following non-small-cell lung cancer surgery. Br J Cancer. 2016 Jul 26;115(3):346-53. doi: 10.1038/bjc.2016.182.

Rintoul RC, Ritchie AJ, Edwards JG, Waller DA, Coonar AS, Bennett M, Lovato E, Hughes V, Fox-Rushby JA, Sharples LD; MesoVATS Collaborators. Efficacy and cost of

video-assisted thoracoscopic partial pleurectomy versus talc pleurodesis in patients with malignant pleural mesothelioma (MesoVATS): an open-label, randomised, controlled trial. Lancet. 2014 Sep 20;384(9948):1118-27. doi: 10.1016/S0140-6736(14)60418-9.

Roscilli G, De Vitis C, Ferrara FF, Noto A, Cherubini E, Ricci A, Mariotta S, Giarnieri E, Giovagnoli MR, Torrisi MR, Bergantino F, Costantini S, Fenizia F, Lambiase M, Aurisicchio L, Normanno N, Ciliberto G, Mancini R. Human lung adenocarcinoma cell cultures derived from malignant pleural effusions as model system to predict patients chemosensitivity. J Transl Med. 2016 Feb 29;14:61. doi: 10.1186/s12967-016-0816-x.

Ryu JS, Ryu HJ, Lee SN, Memon A, Lee SK, Nam HS, Kim HJ, Lee KH, Cho JH, Hwang SS. Prognostic impact of minimal pleural effusion in non-small-cell lung cancer. J Clin Oncol. 2014 Mar 20;32(9):960-7. doi: 10.1200/JCO.2013.50.5453.

Seguin L, Kato S, Franovic A, Camargo MF, Lesperance J, Elliott KC, Yebra M, Mielgo A, Lowy AM, Husain H, Cascone T, Diao L, Wang J, Wistuba II, Heymach JV, Lippman SM, Desgrosellier JS, Anand S, Weis SM, Cheresh DA. An integrin β_3-KRAS-RalB complex drives tumour stemness and resistance to EGFR inhibition. Nat Cell Biol. 2014 May;16(5):457-68. doi: 10.1038/ncb2953.

Sinnamon MJ, Carter KJ, Sims LP, Lafleur B, Fingleton B, Matrisian LM. A protective role of mast cells in intestinal tumorigenesis. Carcinogenesis. 2008 Apr;29(4):880-6. doi: 10.1093/carcin/bgn040.

Smits AJ, Kummer JA, Hinrichs JW, Herder GJ, Scheidel-Jacobse KC, Jiwa NM, Ruijter TE, Nooijen PT, Looijen-Salamon MG, Ligtenberg MJ, Thunnissen FB, Heideman DA, de Weger RA, Vink A. EGFR and KRAS mutations in lung carcinomas in the Dutch population: increased EGFR mutation frequency in malignant pleural effusion of lung adenocarcinoma. Cell Oncol (Dordr). 2012 Jun;35(3):189-96. doi: 10.1007/s13402-012-0078-4.

Soucek L, Lawlor ER, Soto D, Shchors K, Swigart LB, Evan GI. Mast cells are required for angiogenesis and macroscopic expansion of Myc-induced pancreatic islet tumors. Nat Med. 2007 Oct;13(10):1211-8. doi: 10.1038/nm1649.

Sparmann A, Bar-Sagi D. Ras-induced interleukin-8 expression plays a critical role in tumor growth and angiogenesis. Cancer Cell. 2004;6(5):447-458. doi:10.1016/j.ccr.2004.09.028

Stathopoulos GT, Zhu Z, Everhart MB, Kalomenidis I, Lawson WE, Bilaceroglu S, Peterson TE, Mitchell D, Yull FE, Light RW, Blackwell TS. Nuclear factor-kappaB affects tumor progression in a mouse model of malignant pleural effusion. Am J Respir Cell Mol Biol. 2006 Feb;34(2):142-50. doi: 10.1165/rcmb.2005-0130OC.

Stathopoulos GT, Kollintza A, Moschos C, Psallidas I, Sherrill TP, Pitsinos EN, Vassiliou S, Karatza M, Papiris SA, Graf D, Orphanidou D, Light RW, Roussos C, Blackwell TS, Kalomenidis I. Tumor necrosis factor-alpha promotes malignant pleural effusion. Cancer Res. 2007 Oct 15;67(20):9825-34. doi: 10.1158/0008-5472.CAN-07-1064.

Stathopoulos GT, Sherrill TP, Cheng DS, Scoggins RM, Han W, Polosukhin VV, Connelly L, Yull FE, Fingleton B, Blackwell TS. Epithelial NF-kappaB activation

promotes urethane-induced lung carcinogenesis. Proc Natl Acad Sci U S A. 2007 Nov 20;104(47):18514-9. doi: 10.1073/pnas.0705316104.

Stathopoulos GT, Moschos C, Loutrari H, Kollintza A, Psallidas I, Karabela S, Magkouta S, Zhou Z, Papiris SA, Roussos C, Kalomenidis I. Zoledronic acid is effective against experimental malignant pleural effusion. Am J Respir Crit Care Med. 2008 Jul 1;178(1):50-9. doi: 10.1164/rccm.200710-1513OC.

Stathopoulos GT, Psallidas I, Moustaki A, Moschos C, Kollintza A, Karabela S, Porfyridis I, Vassiliou S, Karatza M, Zhou Z, Joo M, Blackwell TS, Roussos C, Graf D, Kalomenidis I. A central role for tumor-derived monocyte chemoattractant protein-1 in malignant pleural effusion. J Natl Cancer Inst. 2008 Oct 15;100(20):1464-76. doi: 10.1093/jnci/djn325.

Stathopoulos GT, Sherrill TP, Han W, Sadikot RT, Yull FE, Blackwell TS, Fingleton B. Host nuclear factor-kappaB activation potentiates lung cancer metastasis. Mol Cancer Res. 2008 Mar;6(3):364-71. doi: 10.1158/1541-7786.MCR-07-0309.

Stathopoulos GT, Kalomenidis I. Malignant pleural effusion: tumor-host interactions unleashed. Am J Respir Crit Care Med. 2012 Sep 15;186(6):487-92. doi: 10.1164/rccm.201203-0465PP.

Sugiura S, Ando Y, Minami H, Ando M, Sakai S, Shimokata K. Prognostic value of pleural effusion in patients with non-small cell lung cancer. Clin Cancer Res. 1997 Jan;3(1):47-50. PMID: 9815536.

Swamy M, Jamora C, Havran W, Hayday A. Epithelial decision makers: in search of the 'epimmunome'. Nat Immunol. 2010 Aug;11(8):656-65. doi: 10.1038/ni.1905.

Fortin M, Taghizadeh N, Tremblay A. Procedures Performed during Hospitalizations for Malignant Pleural Effusions: Data from the 2012 National Inpatient Sample. Respiration. 2018;95(4):228-234. doi: 10.1159/000485934.

Takai Y, Sasaki T, Matozaki T. Small GTP-binding proteins. Physiol Rev. 2001;81(1):153-208. doi:10.1152/physrev.2001.81.1.153

Tanrikulu AC, Abakay A, Kaplan MA, Küçüköner M, Palanci Y, Evliyaoglu O, Sezgi C, Sen H, Carkanat Aİ, Kirbas G. A clinical, radiographic and laboratory evaluation of prognostic factors in 363 patients with malignant pleural mesothelioma. Respiration. 2010;80(6):480-7. doi: 10.1159/000321370.

Theoharides TC, Kempuraj D, Tagen M, Conti P, Kalogeromitros D. Differential release of mast cell mediators and the pathogenesis of inflammation. Immunol Rev. 2007 Jun;217:65-78. doi: 10.1111/j.1600-065X.2007.00519.x.

Theoharides TC. Mast cells and pancreatic cancer. N Engl J Med. 2008 Apr 24;358(17):1860-1. doi: 10.1056/NEJMcibr0801519.

Tsai MF, Chang TH, Wu SG, Yang HY, Hsu YC, Yang PC, Shih JY. EGFR-L858R mutant enhances lung adenocarcinoma cell invasive ability and promotes malignant pleural effusion formation through activation of the CXCL12-CXCR4 pathway. Sci Rep. 2015 Sep 4;5:13574. doi: 10.1038/srep13574.

Tsai TH, Su KY, Wu SG, Chang YL, Luo SC, Jan IS, Yu CJ, Yu SL, Shih JY, Yang PC. RNA is favourable for analysing EGFR mutations in malignant pleural effusion of lung cancer. Eur Respir J. 2012 Mar;39(3):677-84. doi: 10.1183/09031936.00043511.

Tsai TH, Wu SG, Hsieh MS, Yu CJ, Yang JC, Shih JY. Clinical and prognostic implications of RET rearrangements in metastatic lung adenocarcinoma patients with malignant pleural effusion. Lung Cancer. 2015 May;88(2):208-14. doi: 10.1016/j.lungcan.2015.02.018.

Wu SG, Gow CH, Yu CJ, Chang YL, Yang CH, Hsu YC, Shih JY, Lee YC, Yang PC. Frequent epidermal growth factor receptor gene mutations in malignant pleural effusion of lung adenocarcinoma. Eur Respir J. 2008 Oct;32(4):924-30. doi: 10.1183/09031936.00167407.

Wu SG, Yu CJ, Tsai MF, Liao WY, Yang CH, Jan IS, Yang PC, Shih JY. Survival of lung adenocarcinoma patients with malignant pleural effusion. Eur Respir J. 2013 Jun;41(6):1409-18. doi: 10.1183/09031936.00069812.

Xia Y, Yeddula N, Leblanc M, Ke E, Zhang Y, Oldfield E, Shaw RJ, Verma IM. Reduced cell proliferation by IKK2 depletion in a mouse lung-cancer model. Nat Cell Biol. 2012 Feb 12;14(3):257-65. doi: 10.1038/ncb2428.

Xue W, Meylan E, Oliver TG, Feldser DM, Winslow MM, Bronson R, Jacks T. Response and resistance to NF-κB inhibitors in mouse models of lung adenocarcinoma. Cancer Discov. 2011 Aug;1(3):236-47. doi: 10.1158/2159-8290.CD-11-0073.

Yang J, Pan WH, Clawson GA, Richmond A. Systemic targeting inhibitor of kappaB kinase inhibits melanoma tumor growth. Cancer Res. 2007 Apr 1;67(7):3127-34. doi: 10.1158/0008-5472.CAN-06-3547.

Zimmermann G, Papke B, Ismail S, Vartak N, Chandra A, Hoffmann M, Hahn SA, Triola G, Wittinghofer A, Bastiaens PI, Waldmann H. Small molecule inhibition of the KRAS-PDEδ interaction impairs oncogenic KRAS signalling. Nature. 2013 May 30;497(7451):638-42. doi: 10.1038/nature12205.